TU Delft

Delft University of Technology

Document Version
Final published version

Citation (APA)
Bangalore Govindaraju, S. (2026). *Microbial Growth in Microcompartments: Applications in Biotechnology and Ecology*. [Dissertation (TU Delft), Delft University of Technology]. https://doi.org/10.4233/uuid:ef1255cf-e75f-459a-80e8-b8f2432c31c6

Important note
To cite this publication, please use the final published version (if applicable).
Please check the document version above.

Copyright
In case the licence states “Dutch Copyright Act (Article 25fa)”, this publication was made available Green Open Access via the TU Delft Institutional Repository pursuant to Dutch Copyright Act (Article 25fa, the Taverne amendment). This provision does not affect copyright ownership.
Unless copyright is transferred by contract or statute, it remains with the copyright holder.

Sharing and reuse
Other than for strictly personal use, it is not permitted to download, forward or distribute the text or part of it, without the consent of the author(s) and/or copyright holder(s), unless the work is under an open content license such as Creative Commons.

Takedown policy
Please contact us and provide details if you believe this document breaches copyrights.
We will remove access to the work immediately and investigate your claim.

This work is downloaded from Delft University of Technology.

Microbial Growth in Microcompartments

Applications in Biotechnology and Ecology

Sagarika Bangalore Govindaraju

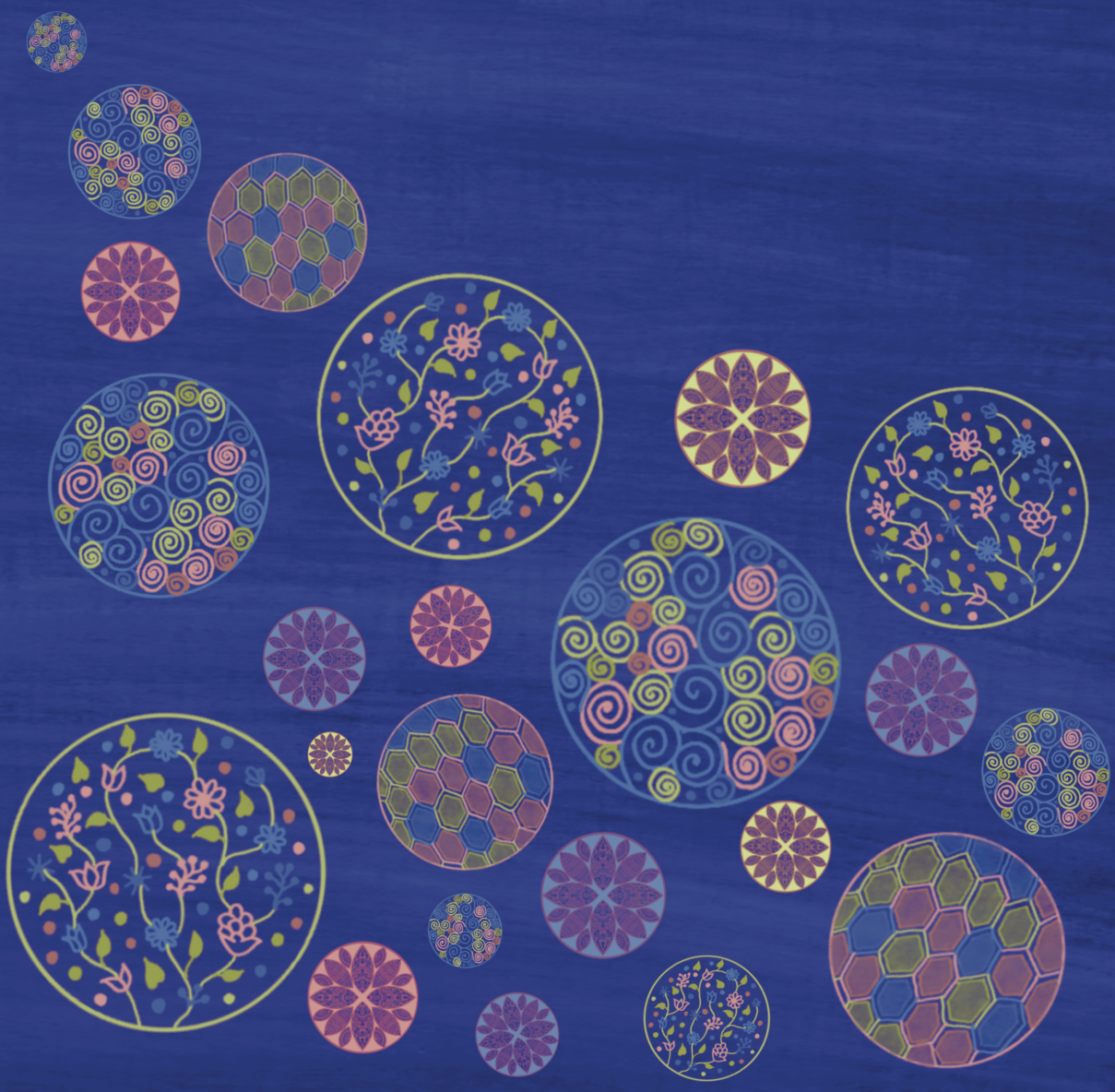

Microbial Growth in Microcompartments: Applications in Biotechnology and Ecology

Dissertation

for the purpose of obtaining the degree of doctor

at Delft University of Technology

by the authority of the Rector Magnificus Prof. dr. ir. H. Bijl,

Chair of the Board for Doctorates

to be defended publicly on

31 March 2026 at 12:30

by

Sagarika BANGALORE GOVINDARAJU

This dissertation has been approved by the promotors.

Composition of the doctoral committee:

Rector Magnificus	Chairperson
Prof. dr. J.T. Pronk	Delft University of Technology, promotor
dr. ir. R.J. van Tatenhove-Pel	Delft University of Technology, copromotor

Independent members:

Prof. dr. P.A.S Daran-Lapujade	Delft University of Technology
Prof. dr. H. Bachmann	Vrije Universiteit Amsterdam
dr.ir. V. van Steijn	Delft University of Technology
dr.ir. M.G.J. de Vos	University of Groningen
dr.ir. N.N.M.E. van Peij	dsm-firmenich
Prof. dr. F. Hollmann	Delft University of Technology, reserve member

The research presented in this thesis was performed at the Industrial Microbiology Section, Department of Biotechnology, Faculty of Applied Sciences, Delft University of Technology, The Netherlands.

Cover:	P. Padmanabhan & R. I. Wouters
Layout:	S.B. Govindaraju
Printed by:	Ridderprint, The Netherlands
ISBN:	978-94-6537-245-7

© 2025 Sagarika Bangalore Govindaraju
All rights reserved. No part of this publication may be reproduced, stored in a retrieval system, or transmitted, in any form or by any means, electronically, mechanically, by photo-copying, recording or otherwise, without prior written permission of the author.

Table of Contents

Summary 7

Samenvatting 11

Chapter 1 15

General Introduction

Chapter 2 45

Development of a high-throughput label-free method for enrichment of antimetabolite-resistant yeast strains using pico-litre agarose beads.

Chapter 3 77

Saccharomyces cerevisiae mutants selected by propagation in water-in-oil emulsion cultures exhibit increased biomass and cell number yields on glucose in aerobic batch cultures.

Chapter 4 111

Deciphering microbial interactions using a label-free microbead sorting approach.

Chapter 5 153

Unlocking the potential of defined co-cultures for industrial biotechnology: opportunities and challenges.

Outlook and valorisation 185

Acknowledgements 193

Curriculum vitae 197

List of publications 198

Selected conference contributions 199

Summary

In natural ecosystems, spatially structured growth of microorganisms is ubiquitous, from biofilms in aquatic natural environments to aggregates in dairy products. These spatial structures influence how microorganisms behave; they shape colonisation patterns, mediate interactions such as nutrient exchange or competition, and provide protection that helps communities remain robust in changing environments. To better understand spatially structured growth and translate the insights into applications, researchers have developed laboratory systems that mimic these environments. Apart from revealing how spatial organisation affects microbial fitness and interactions, such systems also enable the coupling of individual cells or communities to their performance. Among these tools, microdroplet-based platforms have gained prominence. Microdroplets provide isolated environments for microorganisms to grow, interact, and evolve. Microdroplet-based platforms also offer a high-throughput approach to discover and select unique microbial properties that are challenging to access with conventional methods. This thesis explores how compartmentalised microbial growth in microdroplets can be harnessed for application in biotechnology and ecology.

Microdroplets are generated by mixing an aqueous phase, which contains nutrients for microbial growth, with an oil phase containing an oil-soluble surfactant that prevents coalescence of droplets. The oil phase serves as a diffusion barrier for nutrients between microdroplets, ensuring that each droplet functions as an isolated compartment. In addition, millions of microdroplets are generated in a small volume, facilitating high-throughput cultivation. The introduction (**Chapter 1)** of this thesis summarises the biotechnological and ecological applications of microdroplet-based technologies for high-throughput cultivation, selection, and screening of microbial cells and communities. This chapter highlights studies where selecting certain microbial phenotypes is particularly challenging to achieve using conventional techniques, but where microdroplets offer unique solutions. **Chapter 1** discusses technical and practical aspects, including microdroplet types, microdroplet generation, encapsulation, and distribution of cells between microdroplets, and constraints for growth in microdroplets.

Alongside the ability to generate millions of microdroplets, they offer the advantage of requiring small volumes of aqueous phase—often less than a millilitre—thereby reducing costs of large-scale screening efforts. **Chapter 2** proposes a microdroplet-

based approach for low-volume, label-free, and high-throughput screening of *Saccharomyces cerevisiae* strains resistant to costly antimetabolites, a common strategy for selecting metabolite overproducers and carbon-de-repressed enzymes. Using this method, 16,000-fold enrichment of an antibiotic-resistant strain and a 600-fold enrichment of a glucose-analogue-resistant strain were achieved in a single round of selection.

Microdroplets can also be applied to select for increased biomass yield on glucose. Such selection for high-biomass-yield strategies can provide insights into metabolic strategies and constraints imposed by cellular regulations and metabolism. By physically separating cells into individual droplets, microdroplet cultivation eliminates competition for glucose between cells in different droplets, enabling the selection of cells with higher cell-number yield on glucose. A higher cell-number yield can, but not necessarily, translate to a higher biomass yield on glucose. In *S. cerevisiae,* increased biomass yield on glucose often corresponds to a metabolic shift from less energetically efficient (respiro)fermentation toward more efficient respiration. In a previous study, *S. cerevisiae* mutants were propagated in emulsion with glucose as the sole carbon source, resulting in enrichment of mutants with increased biomass yield. In **Chapter 3**, these *S. cerevisiae* mutants were further characterised. Experiments showed that, in addition to an increased cell-number yield, the mutants also showed increased biomass yields on glucose. These increased yields coincided with a decrease in ethanol yield on glucose, which is consistent with a shift in metabolism from (respiro)fermentation toward respiration. Among other mutations, these emulsion-propagated isolates showed amino-acid substitutions in hexokinase 2, which catalyses the first reaction of glycolysis. In **Chapter 3**, these mutations were reverse-engineered into the parental strain of the emulsion-propagated isolates as well as into another commonly used laboratory strain of *S. cerevisiae*. Despite strain-dependent differences in phenotype, the reverse-engineered strains exhibited higher biomass yields and lower ethanol yields on glucose. Further experiments showed that this phenotype is most likely due to a loss of catalytic activity caused by the mutations.

Building on the above mentioned work with single-strain selection in microdroplets, the last two chapters of the thesis shift focus to microbial communities. In nature, microbial growth often occurs in communities, where interactions shape the overall community function and stability. Deciphering these interactions is crucial for understanding microbial communities. Microdroplets are promising for this purpose as they enable high-throughput parallel cultivation of sub-communities. However, existing microdroplet-based approaches require cumbersome or sometimes infeasible steps, such as isolation of community members and labelling cell types with fluorescent markers via genetic engineering. **Chapter 4** proposes a microdroplet-based, label-free, and isolation-independent approach to decipher microbial pairwise interactions. In this approach, sub-communities were sorted based on growth, and through a combination of experimental data and probabilistic modelling of experimental steps, it was demonstrated that pairwise interactions can be deciphered

in three-member *Lactococcus cremoris* consortia. Furthermore, this approach was computationally validated to decipher pairwise interactions in larger consortia.

Understanding microbial interactions opens possibilities to design robust microbial co-cultures for industrial applications. Currently, industrial biotechnological processes are largely dominated by monocultures with rare examples of co-cultures. **Chapter 5** of this thesis reviews studies that explore potential advantages of co-cultures over monocultures, with special attention to studies that provide quantitative data to enable reliable comparisons with monocultures. This chapter also outlines the key challenges that currently limit the implementation of co-cultures in industrial processes.

The thesis is concluded by reflecting on the future broader implications of microdroplet-based approaches for biotechnological applications and the study of microbial ecology.

Samenvatting

Translated by Miriam Cammaert and Rosalie Wouters.

Ruimtelijk gestructureerde groei van micro-organismen is alom aanwezig in de natuur, van biofilms in waterrijke natuurlijke milieus tot aggregaten in zuivelproducten. Ruimtelijke rangschikking beïnvloedt het gedrag van micro-organismen; ze geeft vorm aan de patronen van kolonisatie, bepaalt interacties zoals uitwisseling van voedingsstoffen of competitie, en biedt bescherming die de microbiële consortia robuust houdt in dynamische omgevingen. Om ruimtelijk gestructureerde groei beter te begrijpen en dit begrip te gebruiken voor (industriële) toepassingen hebben onderzoekers technieken ontwikkeld die dergelijke ecosystemen nabootsen. Naast het begrijpen van de impact van ruimtelijke organisatie op microbiële groei, “fitness” en interacties maken deze technieken ook het koppelen van individuele cellen of microbiële consortia aan de prestaties van de micro-organismen mogelijk. Een opkomende techniek is het onderzoeken van microbiële groei in microdruppels. Microdruppels bieden micro-organismen geïsoleerde omgevingen om te groeien, interacties te hebben en te evolueren. Studies gebaseerd op microdruppels bieden een snelle manier om unieke microbiële eigenschappen te ontdekken en ervoor te selecteren die met conventionele laboratoriumtechnieken lastig is te evenaren. Dit proefschrift verkent hoe gecompartimentaliseerde microbiële groei in microdruppels kan worden ingezet binnen de biotechnologie en ecologie.

Microdruppels worden gemaakt door een waterfase, die voedingstoffen voor de micro-organismen bevat, te mengen met een oliefase die een olie-oplosbare oppervlakte-actieve stof bevat om samenklontering van de druppels te voorkomen. De oliefase vormt een barrière voor diffusie tussen de microdruppels en zorgt ervoor dat elke druppel een geïsoleerd compartiment is. Omdat er miljoenen microdruppels gemaakt worden in een klein volume, kunnen op deze manier grote aantallen micro-culturen parallel worden bestudeerd. De introductie (**Hoofdstuk 1**) van dit proefschrift vat de biotechnologische en ecologische toepassingen van op microdruppels gebaseerde technologieën voor de kweek, de selectie en het testen van microbiële cellen en consortia samen. Dit hoofdstuk belicht studies waarin verrijking van een specifiek fenotype lastig te realiseren is met conventionele technieken, maar goed haalbaar is met microdruppels. **Hoofdstuk 1** beschrijft technische en praktische afwegingen zoals het type microdruppel, het maken van microdruppels, inkapseling en verdeling van cellen over microdruppels, en groeibeperkingen binnen microdruppels.

Naast het feit dat microdruppels in grote aantallen gemaakt kunnen worden, bieden ze ook het voordeel van een minimaal volume voor de waterfase (vaak minder dan een milliliter), hetgeen de kosten van grootschalig testen reduceert. Metaboliet-analogen worden veelvoudig toegepast in de industrie en de wetenschap om te selecteren voor mutanten die een hoge productiecapaciteit hebben omdat sleutelenzymen niet langer gevoelig zijn voor remming. **Hoofdstuk 2** stelt voor om microdruppels te gebruiken als een methode voor het screenen van resistentie tegen metaboliet-analogen in stammen van de gist *Saccharomyces cerevisiae*. Deze methode is snel, labelvrij en kan in een klein volume worden uitgevoerd. Met behulp van deze methode is in één enkele ronde van selectie een 16000-maal verrijking van een antibioticaresistente stam en een 600-maal verrijking van een glucose-analoog-resistente stam bereikt.

Microdruppels kunnen ook gebruikt worden voor het selecteren voor een verhoogde biomassa-opbrengst op glucose. Strategieën die leiden tot een verhoogde biomassa-opbrengst kunnen inzicht verschaffen in stofwisselingsstrategieën en grenzen die zijn opgelegd door cellulaire stofwisseling en regelprocessen. Door cellen fysiek van elkaar te scheiden in individuele microdruppels wordt competitie voor glucose geëlimineerd. Hierdoor kan geselecteerd worden voor cellen die een groter aantal cellen maken per hoeveelheid geconsumeerde glucose. Zo'n hogere opbrengst van cellen kan, tenzij deze alleen voortkomt uit een kleinere celgrootte, gepaard gaan met een hogere biomassa-opbrengst op glucose. In micro-organismen die zowel kunnen gisten (fermenteren) als ademhalen, gaat een hogere biomassa-opbrengst op glucose vaak samen met een verschuiving in de suikerstofwisseling van het energetisch minder efficiënte fermenteren naar het efficiëntere ademhalen. Een eerder onderzoek liet zien dat langdurig kweken van *S. cerevisiae*-mutanten in microdruppels, met glucose als de enige koolstofbron, leidde tot het verrijken van mutanten met een verhoogde biomassa-opbrengst. In **hoofdstuk 3** werden deze *S. cerevisiae*-mutanten nader gekarakteriseerd. Dit onderzoek liet zien dat de mutanten naast een hogere biomassa-opbrengst, ook op basis van aantal cellen een hogere opbrengst op glucose vertoonden. Deze veranderingen in groei-efficiëntie gingen gepaard met een afname van de ethanol-opbrengst per glucose, hetgeen consistent is met een verschuiving van de stofwisseling van (respiro)fermentatie naar ademhaling. Naast andere mutaties vertoonden de in microdruppels geselecteerde *S. cerevisiae*-mutanten aminozuurwijzigingen in het enzym hexokinase 2, dat de eerste reactie in de glycolyse katalyseert. In **hoofdstuk 3** zijn deze mutaties ingebracht in de oorspronkelijke *S. cerevisiae*-stam waarmee de selectie in microdruppels werd gestart, en daarnaast ook in een andere laboratoriumstam van deze gist. Ondanks stam-afhankelijke verschillen vertoonden de stammen met de ingebrachte mutaties een hogere biomassa-opbrengst en lagere ethanol-opbrengst op glucose. Verdere experimenten lieten zien dat de verschillende mutaties in het hexokinase-2-enzym zeer waarschijnlijk leidden tot verlies van katalytische activiteit.

Voortbouwend op het bovengenoemde onderzoek aan selectie van één stam in microdruppels, werd in de laatste twee hoofdstukken van dit proefschrift de aandacht verlegd naar microbiële consortia, ofwel co-culturen. In de natuur groeien

micro-organismen meestal in consortia, waarbinnen interacties de functionaliteit en de stabiliteit van het consortium als geheel dicteren. Het ontrafelen van deze interacties is cruciaal voor het begrijpen van microbiële consortia. Groeistudies in microdruppels bieden unieke mogelijkheden voor onderzoek hieraan, omdat microdruppels het mogelijk maken om sub-consortia snel en in grote aantallen parallel te kweken. Echter, analyse van interacties vereiste tot nu toe omslachtige of zelfs onhaalbare stappen, zoals het isoleren van micro-organismen uit het consortium en het labelen van verschillende celtypes met fluorescente markers via genetische modificatie. **Hoofdstuk 4** presenteert een methode gebaseerd op microdruppels voor het ontrafelen van paarsgewijze microbiële interacties op een labelvrije en isolatie-onafhankelijke manier. Deze methode werd gebruikt voor het sorteren van sub-consortia op basis van groei. Door een combinatie van experimentele data en probabilistische modellen werd aangetoond dat paarsgewijze interacties kunnen worden ontcijferd in consortia van drie verschillende stammen van de melkzuurbacterie *Lactococcus cremoris*. Bovendien werd toepasbaarheid van de methode voor het ontcijferen van paarsgewijze interacties in grotere consortia met behulp van computersimulaties gevalideerd.

Huidige biotechnologische processen worden grotendeels uitgevoerd met monoculturen. Beter begrip van microbiële consortia vergroot de kansen voor het succesvol ontwerpen van robuuste co-culturen voor industriële toepassingen. **Hoofdstuk 5** van dit proefschrift bespreekt recente studies waarin potentiële voordelen van co-culturen ten opzichte van monoculturen zijn onderzocht. De nadruk ligt hierbij op onderzoeken die kwantitatieve data presenteren om zo een betrouwbare vergelijking met monoculturen te maken. Dit hoofdstuk benoemt daarnaast de belangrijkste uitdagingen die op dit moment het daadwerkelijk gebruik van co-culturen in industriële processen beperken.

Dit proefschrift eindigt met een beschrijving van de impact van microdruppel-gebaseerde kweektechnieken op biotechnologische toepassingen en op het bestuderen van microbiële ecologie.

Chapter 1

General Introduction

1. Microbial growth in compartments

Microbial growth in nature often occurs within spatially structured communities, which play essential roles in microbial ecology, health, and biogeochemical processes (1–3). One of the earliest documented observations of such spatially organised microbial growth dates to 1683 in Delft, when Antonie van Leeuwenhoek examined the material scraped from his teeth under a magnifying lens. The tiny “animals” he described were among the first documented microbial communities (4). Today, we know that what he observed was dental plaque, a classic example of a spatially organised biofilm formed through sequential microbial colonisation. These structured communities are now known to be closely associated with the development of periodontal disease (2).

Beyond the human body, spatially organised microbial communities also play key roles in natural ecosystems. Cyanobacteria are photosynthetic prokaryotes that serve as primary producers in various terrestrial and marine environments, crucial for nutrient cycling, often growing in microbial mats alongside other prokaryotes (5). These microbial mats are composed of extracellular polymeric substances and not only provide physical protection and nutrients but also facilitate cell-to-cell interactions and horizontal gene transfer (5). In deep-sea sediments, methanotrophic archaea form aggregates with sulfate-reducing bacteria and an intimate spatial organisation that enables efficient cross-feeding of electrons and fixed nitrogen (2). This syntrophic interaction is essential for methane oxidation, which accounts for up to 80% of methane consumption in these environments (2).

Together, these examples illustrate how spatial structure is a defining feature of natural microbial communities and central to their ecological roles. Understanding microbial growth in such contexts is essential for studying ecological dynamics and developing biotechnological applications. The following sections highlight the successful valorisation of spatial organisation in biotechnology and efforts to achieve, and study compartmentalised microbial growth under controlled laboratory conditions.

2. Compartmentalised growth in biotechnology

Beyond its ecological relevance, the spatial structuring of microbial communities has been successfully applied in various industrial settings, thereby enabling complex multi-step processes that would be difficult to achieve in well-mixed systems.

A well-established example is the use of aerobic granular sludge in wastewater treatment. These granules consist of microbial aggregates with spatially distinct zones. The outer aerobic layer contains nitrifying bacteria, which use oxygen to oxidise ammonia to nitrite and/or nitrate, and heterotrophic bacteria that degrade organic matter. Due to oxygen consumption in the outer layer and diffusion limitation, the inner layer is anaerobic. In the inner layer, denitrifying bacteria convert nitrate to nitrogen gas. This spatial separation of metabolic functions enables the simultaneous removal of multiple pollutants, contributing to the overall efficiency of biological wastewater

treatment systems. (6)

Another industrial example of microbial growth in spatially structured environments is found in food biotechnology. Kefir grains are composed mainly of lactic acid bacteria and acetic acid bacteria. These grains serve as a spatially structured inoculum or “basecamp”, from which microorganisms colonise the milk. As fermentation progresses, the colonising microbial community changes dynamically. More importantly, the structure of the grains supports the survival of microbial species that would otherwise be poorly suited to the milk environment. (7)

3. Compartmentalised growth in laboratory set-ups

While many natural microbial communities grow in spatially structured environments, and this principle is successfully applied in industrial settings, laboratory studies of microorganisms predominantly rely on well-mixed liquid cultures. These laboratory setups serve a key purpose: they physically separate strains or mutants to prevent competition and enable the linking of genotypes to phenotypes, such as growth rate, substrate uptake, or product formation.

Among the laboratory-based setups, microdroplet-based systems have emerged as particularly powerful spatially structured models for studying microbial growth. They enable high-throughput cultivation, screening, and selection, especially of industrially relevant phenotypes that are challenging to isolate in suspension cultures (8). Moreover, microdroplets allow researchers to study microbial interactions and spatial dynamics in both monocultures and co-cultures (8,9). They facilitate the localisation of sub-communities, making it possible to study emergent properties that are often masked in bulk suspensions (9,10).

The research described in this thesis aims to further explore the potential of microdroplets as a platform for studying microbial growth and interactions, thereby enabling the enrichment of mono- and co-cultures for both ecological understanding and biotechnological applications. Before exploring these applications, key concepts and practical aspects of microbial growth in microdroplets will be discussed.

4. Microbial growth in microdroplets

Microdroplets generated in water-in-oil emulsions have been used since the 1990s as microcompartments for studying microbial growth at the single-cell level (11,12). Each microdroplet consists of an aqueous phase, in which microorganisms can grow, encapsulated within a continuous oil phase. The emulsion is stabilised by surfactants that prevent droplet coalescence (Figure 1).

4.1. Generation of microdroplets

Microdroplets are generated by mixing an aqueous phase—containing cells, carbon

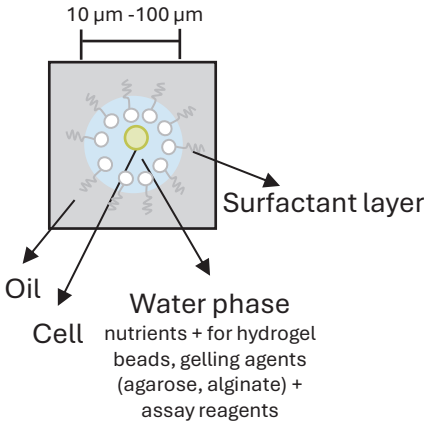

Figure 1: Microbial cell compartmentalised in a microdroplet (containing a water phase) surrounded by an oil phase that acts as a barrier for diffusion of key substrates, nutrients, products, and other components of the water phase. The water-in-oil emulsions are stabilised by an oil-soluble surfactant that prevents the coalescence of microdroplets.

source, and nutrients—with an immiscible oil phase and an oil-soluble surfactant (Figure 1). Water-in-oil emulsions can be generated by simple mixing methods such as vortexing or homogenization, which yield polydisperse emulsions (Figure 2). Such approaches are high throughput, enabling the production of 10^6 to 10^{10} droplets per hour (8). However, differences in droplet sizes introduce heterogeneity in phenotypic readouts such as cell concentration or product titres, which makes it challenging to quantitatively assess small phenotypic differences. Alternatively, monodisperse emulsions can be generated by using microfluidic devices (Figure 2) that offer precise control over droplet sizes. These microdroplets exhibit only a ~3% variation in volume, thereby enhancing the accuracy of screening (13). However, generating monodisperse emulsions requires specialised microfluidic equipment (8).

To enable compatibility with fluorescence-activated cell sorting (FACS) or microfluidics-based on-chip sorting, microdroplets must be suspended in an aqueous phase (Figure 2). This can be achieved by incorporating agarose or alginate into the aqueous phase (8). Upon cooling, the agarose or alginate solidifies, forming microbeads that retain their structure and can be easily separated into an aqueous source. Alternatively, water-in-oil-in-water double emulsions (w/o/w) can be applied, which are generated by re-emulsifying the water-in-oil emulsions with an aqueous phase that contains a water-soluble surfactant (8). This generates microcompartments already surrounded by an aqueous phase, which can be directly screened using FACS/ on-chip sorting (Figure 2).

4.2. Distribution of cells between microdroplets

During the generation of microdroplets, cells are disturbed among individual droplets according to a Poisson distribution (Figure 3A and B), where the probability of a droplet containing x cells is given by:

$$P(x) = \frac{\left(e^{-\lambda}\lambda^{x}\right)}{x!}$$

where λ is the average number of cells per droplet.

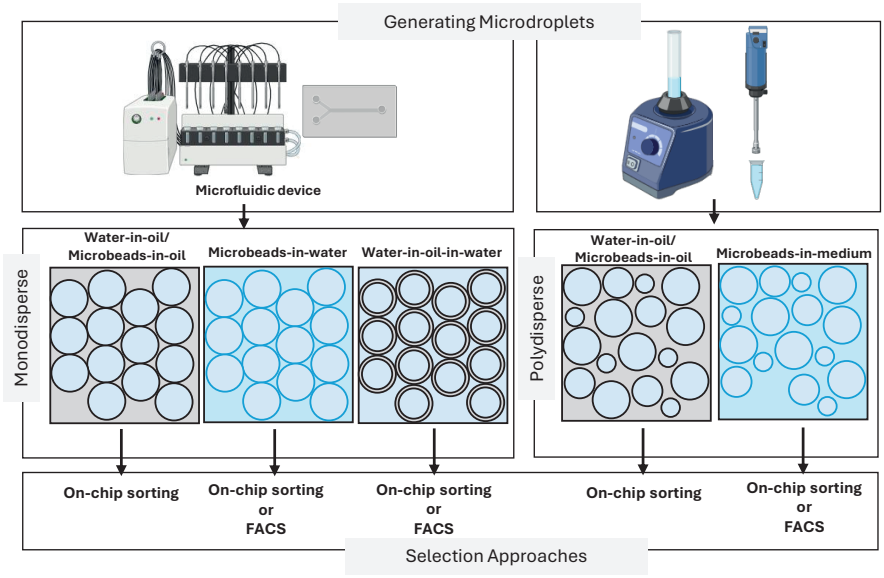

Figure 2: Microdroplets can be generated either via microfluidic devices, producing monodisperse emulsions, or by vortexing/homogenising, resulting in polydisperse emulsions. Emulsion types include water-in-oil, microbeads-in-oil (when the aqueous phase contains agarose or alginate), microbeads-in-water and water-in-oil-in-water. Microdroplets or microbeads suspended in an aqueous phase are compatible with high-throughput analysis and sorting using FACS or on-chip microfluidic sorting. In contrast, microdroplets suspended in oil can only be sorted using on-chip microfluidic systems. Clip art from Biorender (https://BioRender.com/lf23uka).

The λ-value of the Poisson distribution defines the average number of cells per microdroplet for a given droplet size. The λ-value is controlled by adjusting the cell concentration in the inoculum. Increasing λ increases the average number of cells per microdroplet and the fraction of filled microdroplets (Figure 3B).

At a λ-value of 0.1, 10% of the inoculated microdroplets contain a cell, and of these microdroplets 95% contain a single cell. Therefore, a λ-value of 0.1 is generally used to achieve single-strain encapsulation (14,15). Complete single-cell encapsulation can be achieved at lower λ-values (at λ = 0.02, 99% of inoculated microdroplets contain 1 cell). However, this leaves a large fraction of the microdroplets empty (98% at λ = 0.02), which reduces the throughput of screening experiments (Figure 3B). To “beat Poisson” and ensure that all microdroplets are filled with a single cell, acoustic waves or inertial focusing can be used (16,17). Alternately, diamagnetic separation of single-cell and empty droplets can be employed (16,17).

Co-encapsulation strategies of multiple microorganisms require a careful choice of the average droplet occupancy (λ). This is particularly important when co-encapsulating a cell-based biosensor with a mutant strain that produces a target compound. In such cases, the biosensor serves to detect the product secreted by the producer strains, and the likelihood of both cells being present in the same droplet—and therefore of product detection—depends on the chosen average droplet occupancy (λ).

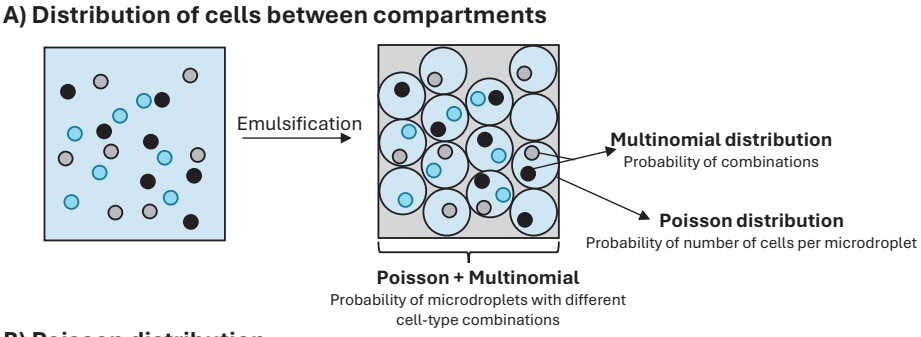

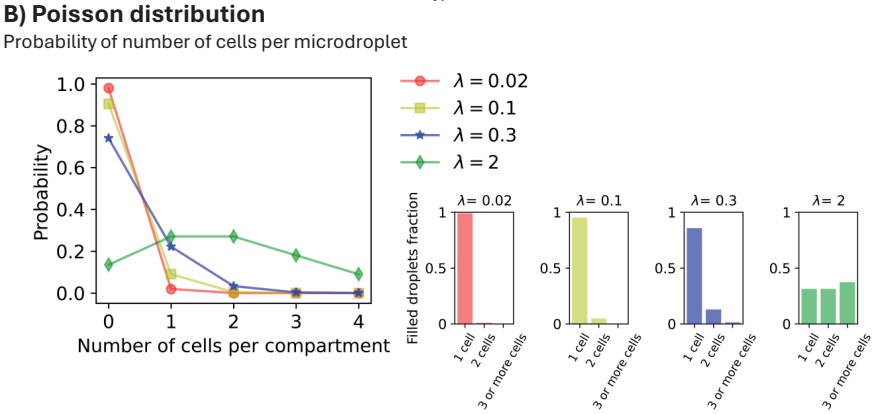

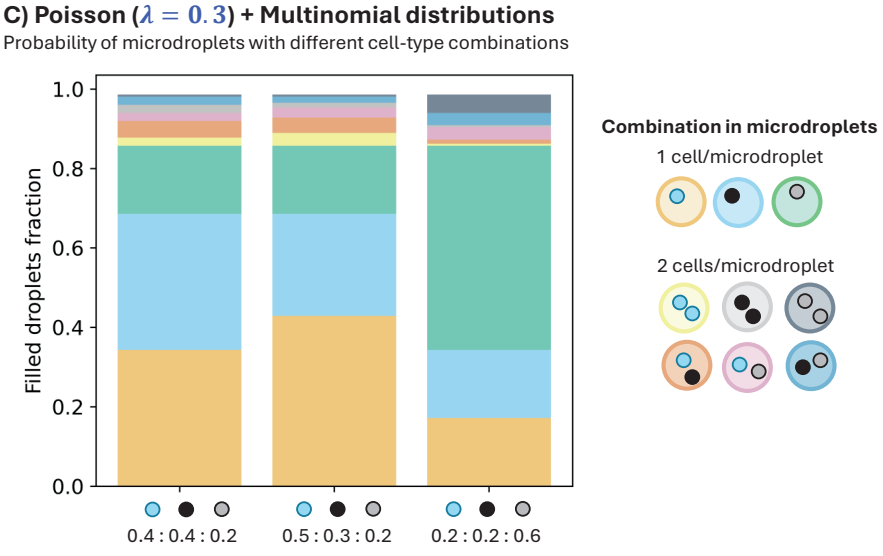

Figure 3: Distribution of cells between microdroplets is governed by two statistical models: Poisson distribution (probability of number of cells per microdroplet) and multinomial distribution (probability of different cell-type combinations in each microdroplet).

The mutant pool is typically encapsulated at a low λ to maintain single-strain occupancy while the biosensor is added at a higher λ to ensure that nearly all droplets that contain a mutant have at least one biosensor cell. Hernandez-Valdes *et al*. (2020) (18) enriched amino-acid overproducing *Lactococcus cremoris* mutants by encapsulating a mutant library at a λ = 1 (resulting in 58% of filled droplets with one cell) and co-encapsulating a green fluorescent protein (GFP)-based amino acid biosensor strain at an average occupancy of λ = 9 (all droplets contain at least 1 biosensor cell).

Microdroplets are also used to study microbial interactions in communities. For studying pairwise interactions, λ-values of 0.15 or 0.3 could be used, which increases the likelihood of droplets containing two cells (Figure 3B) (9). To study higher-order interactions, changes in pairwise interactions due to the presence of a third or more community members, even higher λ values (= 1 or 2) are desirable to increase the frequency of microdroplets with three or more cell types (Figure 3B) (9,19,20). When studying interactions between strains, apart from considering the fraction of microdroplets with cells and the average occupancy, it is also essential to consider the combinatorial probability of co-encapsulation of different cell types (9) (Figure 3A and C). The combinatorial probability of co-encapsulation is multinomially distributed and is determined by the relative proportions of cell types in the inoculum (Figure 3C). The fraction of microdroplets with a particular cell-type combination can therefore be determined by combining Poisson and multinomial distributions. Maximising the likelihood of unique cell-type encounters helps in studying interaction networks and can be achieved by adjusting the relative abundance of cell types in the inoculum or by merging droplets of different cell types in a controlled manner (21).

4.3. Carrying capacity of microdroplets

The carrying capacity of a microdroplet is the maximum number of cells a microdroplet can support. The carrying capacity of a microdroplet depends on two factors: the droplet volume (μm^3) and the maximum carrying capacity of the growth medium (number of cells per μm^3 of medium). The maximum carrying capacity of the growth medium can depend on various factors, including the concentration of relevant nutrients, growth inhibition by organic products of microbial metabolism and medium alkalinization or acidification. Typically, for bacteria and yeasts, the physical space in the microdroplet is not a limiting factor, as the cell volume is orders of magnitude smaller than the microdroplet volume.

For improved screening resolution, it is important to maximise the number of generations of growth within a microdroplet, which directly relates to the carrying capacity. For example, screening for mutants with increased cell number yield in microdroplets that support a maximum carrying capacity of 10 cells per microdroplet (starting from 1 cell per microdroplet) could enable enrichment of mutants with at least a 10% increase in cell number yield, corresponding to an increase of a single additional cell. Therefore, increasing the carrying capacity of microdroplets enhances

the sensitivity of the screen, enabling the detection of smaller differences in cell number yields.

In certain applications, such as FACS sorting, technical constraints, particularly nozzle size, limit the maximum allowable microdroplet sizes (up to 40 µm). In such cases, droplet carrying capacity can also be improved by increasing the growth medium's carrying capacity.

The basic concepts—microdroplet generation, cell distribution, and carrying capacity—provide the groundwork for working with microdroplets. The next paragraphs explore how microdroplet-based cultivation can be applied in ecological and biotechnological studies.

5. Applications of microdroplet-based systems in ecology and biotechnology

This section first discusses the advantages of microdroplets for high-throughput cultivation experiments. This is followed by a discussion of their application in screening and selection. These applications are listed in Tables 1 and 2 with examples of monocultures and microbial communities respectively.

5.1. High-throughput cultivation

High-throughput, microdroplet-based cultivation enables the identification of strains with improved phenotypes from large mutant pools and facilitates the study of interactions within microbial communities (8,22). Using water-in-oil emulsions, 10^5 to 10^8 droplets (100 µm to 10 µm in diameter) per mL medium can be generated. This scalability allows screening of large mutant libraries or diverse co-culture combinations in a small volume.

Compared to conventional methods for the cultivation of microorganisms, microdroplet-based cultivation substantially reduces the use of media and reagents, which can lead to large cost savings. For instance, Wang *et al.* (2014) (23) reported a 2,000-fold reduction in reagent costs for extracellular metabolite screening when comparing microdroplets to conventional 96-well microtiter plates.

Microdroplet-based cultivation has been successfully applied to select individual mutants with industrially relevant phenotypes from large mutant libraries. For example, Chen *et al.* (2017) (24) screened a library of 10^5 *L. cremoris* mutants to isolate a riboflavin secreter that generated four-fold higher product titres after two rounds of screening. Similarly, Zhu *et al.* (2019) (25) used a pH biosensor to identify a *Bacillus coagulans* mutant with a 52% higher lactic acid titre from a library of 10^6 mutants. In another example, Huang *et al.* (2015) (26) subjected 10^5 *Saccharomyces cerevisiae* mutants to several rounds of sorting and identified mutants with a 30% higher yield of α-amylase.

Beyond screening of monocultures, microdroplet-based platforms also enable

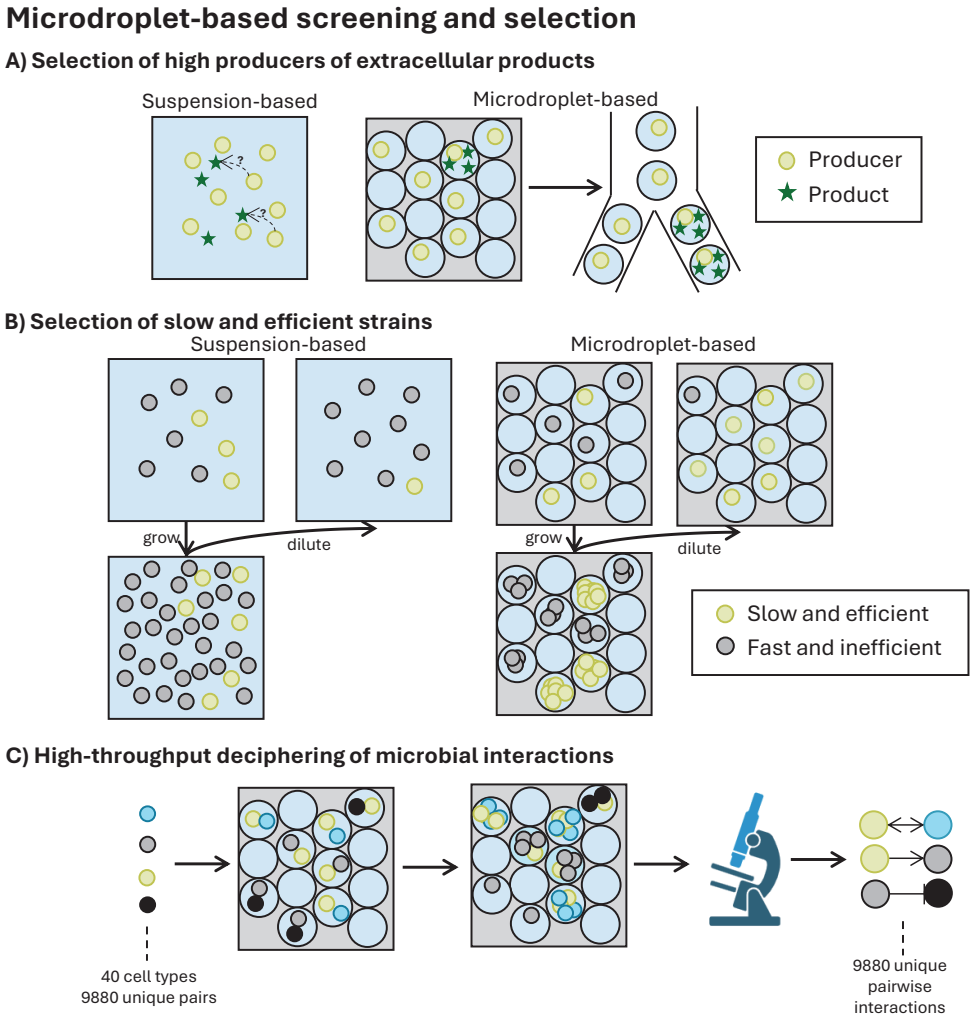

Figure 4: Microdroplet-based screening and selection strategies for monocultures and microbial communities. (A) Selection of high producers of extracellular products: In suspension cultures, mutants share a single compartment, thereby allowing extracellular products to diffuse and making it difficult to identify high-producing mutants. In microdroplet-based cultures, mutants are separated into microcompartments surrounded by an oil phase, retaining the product within the microdroplet and enabling the screening and selection of high producers. (B) Selection of slow and efficient mutants: In suspension-based cultures, fast but inefficient mutants outcompete slower, more efficient mutants during serial propagation. In microdroplet-based cultures, eliminating competition between mutants in different microdroplets allows efficient mutants to grow to higher cell numbers and enables enrichment through serial transfers. (C) High throughput deciphering of microbial interactions: All possible combinations of community members are co-localised in microdroplets and grown. Growth is monitored via microscopy, and interaction networks are deciphered based on co-localised members and their growth patterns. Clip art from Biorender (https://BioRender.com/lf23uka).

fundamental studies on microbial interactions in co-cultures. Kehe *et al*. (2021) (27) developed a high-throughput microdroplet-based system that enables rapid bottom-up construction and screening of microbial communities. Using this platform, they characterised 10^4 interactions among 20 soil bacteria across 40 carbon environments.

5.2. High-throughput screening and selection

Following cultivation in microdroplets, mutants or co-cultures with the desired properties can be obtained by using high-throughput sorting methods. An efficient sorting process links the phenotype of interest (e.g. product formation, biomass concentration or culture pH) to a detectable readout (such as fluorescence). Microdroplets or microbeads with high signal intensity are selectively sorted for enrichment, further analysis, or downstream validation.

Microdroplet sorting is typically performed using on-chip sorting or (fluorescence-activated) cell sorters (FACS). Both offer up to 10^4 times higher sorting throughputs than conventional multi-well plate screening (22). On-chip and FACS-based microdroplet sorting systems can achieve sorting rates ranging from 10^4-10^6 h^{-1} and 10^6-10^8 h^{-1} respectively (8). Despite these high sorting rates, on-chip sorting requires customizable and elaborate setups that may be inaccessible to most academic laboratories. On the other hand, FACS is widely used, making it more adaptable for technology transfer and collaboration. For these practical reasons, the microdroplet sorting experiments described in this thesis are based on FACS.

Beyond high-throughput selection, microdroplets are particularly valuable for identifying and enriching phenotypes that are challenging to detect or isolate in conventional suspension cultures. The following subsections highlight how microdroplets enable selection for improved extracellular product yields or titres, higher biomass yields, and the study of microbial interactions within microbial communities.

5.2.1. Selection for improved production of extracellular products

In industrial biotechnology, the secretion of products into the bulk medium is desirable as this simplifies downstream bioprocessing and reduces costs. In conventional suspension cultures, extracellular products diffuse into the bulk medium, making it difficult to couple product concentrations to any individual producing cell. Such single-cell genotype-phenotype coupling can be achieved by compartmentalising individual producers into microdroplets that retain extracellular hydrophilic products. Microdroplets, when combined with FACS or microfluidic device-based sorting, allow direct selection for high extracellular product concentrations (Figure 4A and Table 1). If the product of interest is inherently fluorescent, fluorescence can serve as a direct read-out, as demonstrated by Wagner *et al*. (2018) (28). They successfully enriched riboflavin-overproducing *Yarrowia lipolytica* strains using FACS sorting of water-in-oil-in-water emulsions. The enriched mutants showed a 54-fold higher total

riboflavin titre, of which 90% was secreted. Alternatively, for non-fluorescent enzymes, enzymatic assays enable coupling of fluorescent read-outs to enzyme activities. Balasubramanian *et al*. (2021) (29) screened 200,000 *Corynebacterium glutamicum* mutants to enrich for six-fold higher *β*-glucosidase activity by using a *β*-glucosidase substrate (fluorescein di-*β*-D-glucopyranoside) that releases a fluorescent product upon hydrolysis.

If the product is not fluorescent, co-culturing with a specially designed biosensor strain provides a strategy to proportionally link product titre to a fluorescence readout. Siedler *et al*. (2017) (30) demonstrated this by co-encapsulating *p*-coumaric-acid-secreting *S. cerevisiae* cells with an *Escherichia coli* transcription factor-based biosensor strain in water-in-oil emulsions. Extracellular *p*-coumaric acid produced by the yeast cells induces YFP expression in the biosensor cells. This strategy enabled microfluidic device-based sorting of high *p*-coumaric overproducing cells. Even for non-fluorescent products, fluorescent staining can sometimes be used to couple product activity to fluorescence read-outs. Scanlon *et al*. (2014) (31) co-cultivated antibiotic-secreting *S. cerevisiae* strains with the human pathogen *Staphylococcus aureus* in agarose microbeads. *S. cerevisiae* strains with over 10000-fold higher product titres were obtained by using a fluorescent live/dead stain for *S. aureus*.

As an alternative to fluorescence-based screening, Hu *et al*. (2024) (32) enriched an *E. coli* strain producing a 52.7% increase in titre of D-phenyllactic acid compared to the parental strain by screening extracellular concentrations via Raman spectroscopy of cells encapsulated in microdroplets. Agnihotri *et al*. (2025) (33) used droplet shrinkage to detect antibiotic-resistant *E. coli* subpopulations from blood infections that occurred at a frequency of 10^{-6}.

Microdroplet screening has also been applied to discover microbial secreters from genotype-phenotype coupling in environmental samples. Partipilo *et al*. (2025) (34) discovered novel electrogenic bacteria, i.e., bacteria capable of extracellular electron transfer, by using a microdroplet-based screening approach designed to enrich for electroactivity. The method detects electrogenic activity in microorganisms from iron-rich lake sediments by monitoring the cell-mediated reduction of Cu(II)-to-Cu(I), which catalyses the conversion of CalFluor488 to a fluorescent product. In another study, Qiao *et al*. (2022) (35) identified extracellular PET-degrading microorganisms (*Kineococcus endophyticus* and *Staphylococcus epidermidis*) by microdroplet-based screening of microorganisms from wastewater samples at a PET textile mill. The screening relied on the hydrolysis of the fluorogenic substrate fluorescein dibenzoate by PETases, yielding the fluorescent product fluorescein.

5.2.2. Selection for slower-growing and efficient strains

Identifying and enriching mutants with high biomass yield on the carbon substrate is valuable for both fundamental research into efficient metabolic strategies and for industrial applications aimed at cost-effective and sustainable biomass production (14,15,36,37).

In conventional suspension batch cultures, competition between cells is predominantly based on specific growth rate (38,39). As a consequence, faster-growing cells will outcompete slower-growing cells, even when the latter have a higher biomass yield on substrate. In other words, batch cultivation in suspension cultures leads to competition for shared resources (such as carbon sources), which act as public goods. In contrast, compartmentalising cells in microdroplets privatises these resources for cells inoculated in an individual droplet and their progeny. Microdroplet-based cultivation thereby enables the selection of strains based on biomass or cell number yield on the privatised carbon source, rather than solely based on specific growth rate (39). Cells with higher biomass or cell number yield will produce more offspring within their respective microdroplets, increasing their proportion in the population with each round of growth. Through serial propagations of microdroplets, these high-yield, efficient cells can be enriched (Figure 4B and Table 1). Using this approach, *L. cremoris* strains with 26% higher biomass yield on glucose (corresponding to 71% more cells) (14) and *S. cerevisiae* strains with increased biomass yields on glucose were enriched (15). Along the same lines, *E. coli* mutants with 23% higher cell number yield on glucose were selected (37).

Micro-compartmented cultivation can also be employed to enrich slow-growing species from environmental samples. McCully *et al.* (2023) (40) used water-in-oil-in-water emulsions to enrich slow-growing *Phascolarctobacterium faecium* from human stool samples. This bacterium is abundant in stool samples and has been classified as 'most wanted' by the Human Microbiome Project due to difficulty in isolating it with conventional cultivation techniques. In a similar study (41), enrichement of bacteria from the mouse gut microbiome using microdroplets preserved higher community diversity compared to enrichment using solid medium plates, where the fastest-growing species outcompeted the slower growers.

To accelerate enrichment of growth-based phenotypes, serial propagation can be replaced by on-chip or FACS-based sorting. Sung *et al.* (2017) (36) used microdroplet weight-based magnetic field sorting on a microfluidic device to separate microdroplets containing different concentrations of microalgal cells. Growth within microdroplets can also be assessed through cell autofluorescence or changes in light scattering measured by flow cytometry (42). Another label-free option is to sort microdroplets to select live cells based on changes in interfacial tension, by linking it to metabolic activity through the use of specific surfactants (43). Additionally, metabolic markers such as resazurin can be used to measure growth in microdroplets by assessing viability and metabolic activity—viable cells reduce resazurin to fluorescent resorufin (27).

5.2.3. Studying microbial interactions

As mentioned above, microorganisms live in communities in diverse environments (e.g., soil, gut, oceans) where interactions shape ecosystem function and stability (46–48). Understanding these microbial interactions provides insights into ecological

Table 1: Overview of applications for screening and selection in biotechnology. w/o: water-in-oil emulsions, w/o/w: water-in-oil-in-water emulsions.

Product	Microorganisms	Type of microdroplets	Encapsulation	Screening Assay (selection approach)	Reference
Amino acids	*L. cremoris*	Microbeads in oil, polydisperse	Co-encapsulation with an *L. cremoris* biosensor	Biosensor Auxotrophic ***L. cremoris*** biosensor based on fluorescence (FACS microdroplet sorting)	(18)
Lactic acid	*E. coli*	w/o, monodisperse	Single-cell encapsulation	Enzyme assay Lactate oxidase coupled to a fluorogenic conversion. (on-chip sorting)	(23)
Riboflavin	*L. cremoris*	w/o, monodisperse	Single-cell encapsulation	Riboflavin autofluorescence (on-chip sorting)	(24)
Lactic acid	*B. coagulans*	w/o/w, monodisperse	Single-cell encapsulation	Fluorescent pH indicator (FACS microdroplet sorting)	(25)
α-Amylase	*S. cerevisiae*	w/o, monodisperse	Single-cell encapsulation	Enzyme assay α-Amylase coupled to a fluorogenic conversion (on-chip sorting)	(26)
Riboflavin	*Y. lipolytica*	w/o/w, monodisperse	Single-cell encapsulation	Riboflavin autofluorescence (FACS microdroplet sorting)	(28)

β- Glucosidase	*C. glutamicum*	w/o, monodisperse	Single-cell encapsulation	Enzyme assay β-Glucosidase coupled to a fluorogenic conversion (on-chip sorting)	(29)
p-Coumaric acid	*S. cerevisiae*	w/o, monodisperse	Co-encapsulation with an *E. coli* biosensor	Biosensor *E. coli,* transcription factor-based fluorescence (on-chip sorting)	(30)
Antimicrobials against S. aureus	*S. cerevisiae*	Microbeads in medium, polydisperse	Co-encapsulation with target *S. aureus*	Fluorescent viability staining of *S. aureus*. (FACS microdroplet sorting)	(31)
D-Phenyllactic acid	*E. coli*	w/o, monodisperse	Single-cell encapsulation	Raman spectroscopy to detect concentrations. (on-chip sorting)	(32)
Biomass	*L. cremoris*	w/o, polydisperse	Single-cell encapsulation	Selection for high cell number yield (serial propagations)	(14)
Biomass	*S. cerevisiae*	w/o, polydisperse	Single-cell encapsulation	Selection for high cell number yield (serial propagations)	(15)

Biomass	*E. coli*	w/o, polydisperse	Single-cell encapsulation	Selection for high cell number yield (serial propagations)	(37)
Biomass	*Algae*	w/o, monodisperse	Single-cell encapsulation	Weight-based microdroplet separation (on-chip sorting)	(36)
Serotonin	*S. cerevisiae*	w/o/w, monodisperse	Single-cell encapsulation	Biosensor Transcription factor-based fluorescence (FACS sorting)	(44)
Murine interleukin 3	*S. cerevisiae*	Microbeads in oil, monodisperse	Co-encapsulation with a murine-dependent mouse cell-line biosensor	Biosensor Murine reporter cells, transcription factor-based fluorescence (FACS sorting)	(45)

principles and opens up possibilities to engineer these communities for key functions (47).

Microdroplet-based techniques enable high-throughput, massively parallel culturing of microbial sub-communities (Figure 4C and Table 2). Kehe *et al*. (2019) (21) developed a nanolitre-scale droplet platform, 'kChip', which merges droplets in microwells to assay pairwise and higher-order communities. Microbial growth and composition are tracked by imaging the kChip, and the resulting data are used to map interactions. The authors applied this platform to identify growth-promoting interactions of *Herbaspirillum frisingense* (a plant symbiont) from 10^5 multispecies communities (constructed from 19 soil isolates) (21). They also extended their platform to decipher 17,600 pairwise interactions between 20 soil bacteria across 40 carbon environments. This effort led to the finding that over 40% of the interactions from the soil microbial communities involved at least one bacterium promoting the growth of another (27). Gopalakrishnappa *et al*. (2024) (49) employed the same platform to study algae-bacteria interactions across 525 environments varying in pH, buffering capacity, and carbon source.

In another study, Hsu *et al*. (2019) (19) developed a microdroplet-based platform, 'MINI-Drop', to determine pairwise and higher-order interactions and tested its potential with studies on synthetic *E. coli* consortia. The approach involves encapsulation of combinations of fluorescently tagged strains in water-in-oil microdroplets for parallel culturing of sub-communities and monitoring growth by fluorescence microscopy. Using computer vision workflows, they identified microdroplets with growth, determined the relative abundances of each fluorescently labelled strain in the microdroplet, and analysed the resulting data to map the interaction network.

A major limitation of current microdroplet-based methods for deciphering microbial interactions is their dependence on isolation of pure culture isolates of community members and the requirement for expressing fluorescent markers via genetic engineering. Therefore, there remains a need for a high-throughput, microdroplet-based approach that is both isolation-independent and does not rely on genetic engineering to decipher microbial interactions.

Microdroplets are not only useful for deciphering interactions in microbial communities but also for studying how spatial structures influence microbial interactions. For example, van Tatenhove-Pel, *et al*. (2021) (9) investigated the evolution of costly cooperation in a synthetic *L. cremoris* consortium using water-in-oil emulsions. By encapsulating cells in microdroplets, they varied the population sizes and the likelihood of co-occurrence, allowing them to study how co-localisation influences cooperative interactions. They serially propagated the consortia in water-in-oil emulsions, starting with different population sizes, to identify conditions that favoured the selection of cooperation.

In a similar study, Park *et al*. (2011) (50) used cultivation in microdroplets on a

microfluidic device combined with fluorescence microscopy to detect rare pairwise cross-feeding (represented 3% of the community) interactions in an *E. coli* mimic community. They showed that such interactions, which are difficult to detect in a 'bulk community', can be uncovered using microdroplets. Extending this strategy to natural communities, Tan *et al.* (2020) (20) co-encapsulated sub-communities from human faecal samples in microdroplets. By sorting microdroplets based on imaging data for cell number yield, they enriched previously uncultivated, low-abundance (< 1% in the sample) commensal bacteria.

In another approach to studying microbial interactions, van Tatenhove-Pel *et al.* (2021) (10) used micro-agarose beads in water-in-oil emulsions to study constraints on interactions driven by concentration gradients of exchanged metabolites. They used micro-agarose beads to vary cell-to-cell distances of *L. cremoris* strains in a three-dimensional aqueous system. They showed that concentration gradients of exchanged metabolites constrain microbial interaction distances to a µm-range.

Although cultivation in water-in-oil droplets has been successfully applied in many experimental contexts, it is important to consider the hydrophobicity of substrates, products and assay reagents used. The oil phase surrounding the microdroplets acts as a barrier for the diffusion of molecules such as sugars between microdroplets, maintaining compartmentalisation. However, hydrophobic molecules such as short-chain alcohols, weak acids and fluorophores transfer into the oil phase, leading to the loss of compartmentalisation (51,52). To circumvent this, several strategies can be employed: rapid enzymatic conversion of a hydrophobic product to a more hydrophilic molecule, modification of molecules to reduce their hydrophobicity, adjusting surfactant concentrations and adding stabilisers like bovine serum albumin (53–55).

6. Growth of *L. cremoris* and *S. cerevisiae* in microdroplets

L. cremoris (previously known as *L. lactis*) is a Gram-positive, coccoid bacterium widely used in food fermentation, and in particular in cheese production (56). *S. cerevisiae* is a yeast traditionally used in baking and alcoholic fermentation, such as beer and wine (57). Both microorganisms have the GRAS (Generally Regarded as Safe) status.

Both species have fully sequenced genomes; *S. cerevisiae* was the first eukaryote to have its genome fully sequenced (58,59) . A wide range of genetic tools and molecular biology techniques is available for both organisms (60–63). *L. cremoris* has been successfully used as a cell factory for the production of lactic acid, which is used in food preservation, and as a precursor for polylactic acid (PLA) (64). *S. cerevisiae* is the organism of choice for industrial production of biofuels, pharmaceutical products and organic acids (65).

Both *L. cremoris* and *S. cerevisiae* have previously been grown in microdroplets for

Table 2: Overview of applications in ecological studies. w/o: water-in-oil emulsions, w/o/w: water-in-oil-in-water emulsions.

Aim	Microorganisms	Type of microdroplets	Encapsulation	Approach	Reference
Identifying previously uncharacterised electrogenic bacteria	Community from iron-rich lake sediments	w/o, monodisperse	Single-cell encapsulation	On-chip sorting based on electroactivity Assay: On electron transfer, reduction of Cu(II) to Cu(I), which catalyses a reaction producing a fluorescent product.	(34)
Identifying PET-degrading microorganisms	Community from PET textile mill wastewater samples	w/o, monodisperse	Single-cell encapsulation	On-chip sorting based on PETase activity. Assay: PETase activity coupled to a fluorogenic conversion.	(35)
Enriching slow-growing, difficult-to-cultivate microorganisms	Community from human stool samples	w/o/w, monodisperse	Single-cell encapsulation	Community composition post-growth in microdroplets was determined. Method: 16sRNA gene amplicon sequencing	(40)
Enriching slow-growing, rare microorganisms	Community from the mouse gut microbiome	w/o, monodisperse	Single-cell encapsulation	On-chip sorting based on microbial growth Method: microscopic imaging of microdroplets	(41)

Identifying growth-promoting interactions of Herbaspirillum frisingense (a plant symbiont)	Community from soil samples	w/o, monodisperse	Co-encapsulation of community members	Monitoring growth of fluorescently labelled sub-communities in microdroplets. Method: fluorescence microscopic imaging of microdroplets	(21)
Deciphering pairwise interactions	Community from soil samples	w/o, monodisperse	Co-encapsulation of community member pairs	Monitoring growth of fluorescently labelled sub-communities in microdroplets. Method: fluorescence microscopic imaging of microdroplets	(27)
Identifying alga-bacteria interactions across different environments	*E. coli-C. reinhardtii*	w/o, monodisperse	Co-encapsulation of the algae and bacterium	Monitoring growth of fluorescently labelled sub-communities in microdroplets. Method: fluorescence microscopic imaging of microdroplets	(49)
Deciphering pairwise and higher-order interactions	Synthetic *E. coli* consortia	w/o, monodisperse	Co-encapsulation of community members	Monitoring growth of fluorescently labelled sub-communities in microdroplets. Method: fluorescence microscopic imaging of microdroplets	(19)
Enriching co-operators in a consortium with a cheater	Synthetic *L. cremoris* consortium	w/o, polydisperse	Co-encapsulation of community members	Serial propagation to select based on high cell number yield	(9)

Detecting rare pairwise cross-feeding	Synthetic *E. coli* consortia	w/o, monodisperse	Co-encapsulation of community member pairs	Monitoring growth of fluorescently labelled sub-communities in microdroplets. Method: fluorescence microscopic imaging of microdroplets	(50)
Characterising difficult-to-cultivate commensals	Community from a human gut sample	w/o, monodisperse	Co-encapsulation of community members	On-chip sorting to enrich potentially cross-feeding commensals	(20)
Determining concentration gradient constraints for cross-feeding	Synthetic *L. cremoris* consortium	Microbeads in oil or medium, polydisperse	Co-encapsulation of community members	Cross-feeding co-cultures were embedded in microbeads or aggregates. Method: growth of fluorescently labelled 'receiver' strain was monitored by flow cytometry.	(10)

various applications. *S. cerevisiae* was grown in water-in-oil-in-water emulsions to enrich for a serotonin-producing strain (44), and in agarose beads to select murine interleukin 3 secreting *S. cerevisiae* cells (45). *L. cremoris* was grown in water-in-oil emulsions to select for high biomass yields (14) and microbeads to study constraints on microbial interactions, such as concentration gradients (10).

Growth in microdroplet environments requires careful medium design to ensure sufficient growth of *L. cremoris*. This bacterium ferments sugars to lactic acid, which decreases the extracellular pH. When the extracellular pH becomes too low, acidification of the cytosol (via weak-acid uncoupling) prevents growth. Alternatively, when the carbon source is supplied in a limiting amount, growth stops at carbon limitation. In this thesis, pH-limited conditions were used to achieve higher cell concentrations (~10^8 cells mL^{-1}).

S. cerevisiae prefers carbon sources such as glucose and fructose. Under anaerobic and oxygen-limited conditions, it ferments these sugars to ethanol and carbon dioxide. Under fully aerobic conditions, *S. cerevisiae* respires sugar substrates when they are provided at a growth-limiting rate (e.g. in aerobic, glucose-limited chemostat and fed-batch cultures) (66). However, when these sugars are in excess, they ferment even under fully aerobic conditions. This phenomenon is known as the Crabtree effect (67,68). The biomass yield (or cell number yield) on sugars from fermentation is lower than from respiration, since part of the sugar is diverted away from biomass formation to ethanol production. In contrast to suspension cultures, S. *cerevisiae* cells in different microdroplets do not compete for glucose, as it is confined within each droplet due to its insolubility in the oil phase. Ethanol, however, partitions into the oil phase and is a commonly available substrate, which all mutants compete for. In microdroplets, when sugars are abundant, it is expected that *S. cerevisiae* predominantly ferments the privatised sugars to ethanol. When sufficient oxygen is available, the yeast subsequently respires and competes for the ethanol. In this thesis, a high cell concentration synthetic medium (HCSM) (69) was used to achieve high cell concentrations on glucose (~10^8 cells mL^{-1}), as it can support growth at high sugar concentrations (80 g L^{-1} glucose).

7. Scope of the thesis

As outlined in the introduction, combining microdroplet cultivation with high-throughput screening offers diverse biotechnological and ecological applications. This thesis applies microbead-based cultivation for *L. cremoris* and *S. cerevisiae*, coupled with microbead sorting to screen industrially relevant phenotypes (**Chapter 2**) and to decipher pairwise microbial interactions (**Chapter 4**). *S. cerevisiae* strains previously enriched for high-yield using microdroplet-based cultivation followed by serial propagations were characterised (**Chapter 3**). Finally, the potential of microbial consortia for industrial applications was reviewed (**Chapter 5**).

Microdroplets enable cost-effective high-throughput screening of strain libraries. Millions of microbeads per millilitre serve as individual cultivation compartments, enabling parallel growth of large mutant libraries in minimal volume. Selection for mutants resistant to antimetabolites—structural analogues that inhibit metabolism and enable fast growth/no-growth screening—has often been used as a strategy to improve production of anabolic products and utilisation of carbon sources without genetic engineering. However, antimetabolites are often expensive and toxic, which contributes to high costs and environmental and safety concerns related to traditional solid-medium and microtiter plate-based screening methods. **Chapter 2** explores the use of a high-throughput, low-volume and label-free microbeads-based screening method to enrich antimetabolite-resistant *S. cerevisiae* strains. The chapter aims to validate the approach by selecting for resistance to a glucose analogue molecule (2-deoxyglucose).

In water-in-oil emulsions, privatisation of resources prevents growth-rate competition between cells encapsulated in different microdroplets. This enables serial propagation of water-in-oil emulsions to select for mutants with higher cell number or biomass yield on the privatised carbon source. Serial propagation of *S. cerevisiae* mutants in water-in-oil emulsions is expected to favour mutants with higher biomass yields through a metabolic shift from (respiro)fermentation toward respiration, i.e., from a less energetically efficient to a more efficient metabolic pathway. Van Tatenhove-Pel *et al.* (2021) (15) applied this approach to serially propagate *S. cerevisiae* mutants in emulsions, and isolated strains with missense mutations in *HXK2* (gene encoding the first enzyme of glycolysis). **Chapter 3** investigates whether selection in water-in-oil emulsions can drive a metabolic shift from less energetically efficient (respiro) fermentation toward more efficient respiration by characterising the previously emulsion-propagated isolates and the enriched *HXK2* mutations.

Beyond high-throughput screening and selection of phenotypes in monocultures, microdroplets can be used to decipher microbial interactions, which shape the function and stability of several ecosystems. Understanding these interactions enables better insight into, and potential engineering of, microbial communities in diverse environments. Existing methods often require laborious isolation of single strains or genetic engineering to express fluorescent markers—tools available only for a limited number of laboratory strains. **Chapter 4** explores the application of a microdroplet-based, isolation-independent, label-free approach to deciphering pairwise interactions in microbial consortia and aims to validate the approach using synthetic *L. cremoris* consortia. This strategy involves the growth of microbial communities in microbeads and sorting microbeads based on growth, while using probabilistic modelling of the experimental workflow to predict pairwise interactions.

Understanding microbial interactions opens up possibilities to derive design principles to develop microbial co-cultures for industrial applications. While microbial co-cultures are widely used in food fermentation processes, industrial biotechnology predominantly relies on monocultures. **Chapter 5** reviews research on defined microbial consortia that offer unique possibilities to mitigate limitations of monocultures as production systems. The review aims to highlight studies providing quantitative data on key industrial process evaluation parameters such as titre, rate, yield and genetic stability and to outline the challenges that currently impede the implementation of microbial consortia in industrial biotechnology.

References

1. Adade EE, Al Lakhen K, Lemus AA, Valm AM. Recent progress in analyzing the spatial structure of the human microbiome: distinguishing biogeography and architecture in the oral and gut communities. Curr Opin Endocr Metab Res. 2021;18:275–83.
2. Abreu NA, Taga ME. Decoding molecular interactions in microbial communities. FEMS Microbiol Rev. 2016;40:648–63.
3. Henderson A, Del Panta A, Schubert OT, Mitri S, van Vliet S. Disentangling the feedback loops driving spatial patterning in microbial communities. NPJ Biofilms Microbiomes. 2025;11.
4. Leewenhoeck A. An abstract of a letter from Mr. Anthony Leewenhoeck at Delft, dated Sep. 17. 1683.
5. Bozan M, Berreth H, Lindberg P, Bühler K. Cyanobacterial biofilms: from natural systems to applications. Trends Biotechnol. 2025;43:318–32.
6. Pronk M, Giesen A, Thompson A, Robertson S, Van Loosdrecht M. Aerobic granular biomass technology: advancements in design, applications and further developments. Water Pract Technol. 2017;12(4):987–96.
7. Blasche S, Kim Y, Mars RAT, Machado D, Maansson M, Kafkia E, *et al*. Metabolic cooperation and spatiotemporal niche partitioning in a kefir microbial community. Nat Microbiol. 2021;6(2):196–208.
8. van Tatenhove-Pel RJ, Hernandez-Valdes JA, Teusink B, Kuipers OP, Fischlechner M, Bachmann H. Microdroplet screening and selection for improved microbial production of extracellular compounds. Curr Opin Biotechnol. 2020;61:72–81.
9. van Tatenhove-Pel RJ, de Groot DH, Bisseswar AS, Teusink B, Bachmann H. Population dynamics of microbial cross-feeding are determined by co-localization probabilities and cooperation-independent cheater growth. ISME J. 2021;15(10):3050–61.
10. van Tatenhove-Pel RJ, Rijavec T, Lapanje A, van Swam I, Zwering E, Hernandez-Valdes JA, *et al*. Microbial competition reduces metabolic interaction distances to the low µm-range. ISME J. 2021;15(3):688–701.
11. Weaver JC, Bliss JG, Powell KT, Harrison GI, Williams GB. Rapid clonal growth measurement at the single-cell level: gel microdroplets and flow cytometry. Nat Biotechnol. 1991;9:873–877.
12. Weaver JC, Williams GB, Klibanov A, Demain AL. Gel microdroplets: Rapid detection and enumeration of individual microorganisms by their metabolic activity. Nat Biotechnol. 1988;6:1084–1089.
13. Devenish SRA, Kaltenbach M, Fischlechner M, Hollfelder F. Droplets as reaction compartments for protein nanotechnology. In Protein Nanotechnology: Protocols, Instrumentation, and Applications. Edited by Gerrard JA. Springer; 2013:269-286.

14. Bachmann H, Fischlechner M, Rabbers I, Barfa N, Dos Santos FB, Molenaar D, *et al*. Availability of public goods shapes the evolution of competing metabolic strategies. Proc Natl Acad Sci U S A. 2013;110(35):14302–7.

15. van Tatenhove-Pel RJ, Zwering E, Boreel DF, Falk M, van Heerden JH, Kes MBMJ, *et al*. Serial propagation in water-in-oil emulsions selects for *Saccharomyces cerevisiae* strains with reduced cell size or increased biomass yield on glucose. Metab Eng. 2021;64:1–14.

16. Link A, McGrath JS, Zaimagaoglu M, Franke T. Active single-cell encapsulation using SAW overcoming the limitations of Poisson distribution. Lab Chip. 2022;22(1):193–200.

17. Liu D, Sun M, Zhang J, Hu R, Fu W, Xuanyuan T, *et al*. Single-cell droplet microfluidics for biomedical applications. Analyst. 2022;147:2294–316.

18. Hernandez-Valdes JA, aan de Stegge M, Hermans J, Teunis J, van Tatenhove-Pel RJ, Teusink B, *et al*. Enhancement of amino acid production and secretion by *Lactococcus lactis* using a droplet-based biosensing and selection system. Metab Eng Commun. 2020;11:e00133.

19. Hsu RH, Clark RL, Tan JW, Ahn JC, Gupta S, Romero PA, *et al*. Microbial interaction network inference in microfluidic droplets. Cell Syst. 2019;9(3):229–42.

20. Tan JY, Wang S, Dick GJ, Young VB, Sherman DH, Burns MA, *et al*. Co-cultivation of microbial sub-communities in microfluidic droplets facilitates high-resolution genomic dissection of microbial 'dark matter'. Integr Biol. 2020;12(11):263–74.

21. Kehe J, Kulesa A, Ortiz A, Ackerman CM, Thakku SG, Sellers D, *et al*. Massively parallel screening of synthetic microbial communities. Proc Natl Acad Sci U S A. 2019;116(26):12804–9.

22. Zeng W, Guo L, Xu S, Chen J, Zhou J. High-throughput screening technology in industrial biotechnology. Trends Biotechnol. 2020;38:888–906.

23. Wang BL, Ghaderi A, Zhou H, Agresti J, Weitz DA, Fink GR, *et al*. Microfluidic high-throughput culturing of single cells for selection based on extracellular metabolite production or consumption. Nat Biotechnol. 2014;32(5):473–8.

24. Chen J, Vestergaard M, Jensen TG, Shen J, Dufva M, Solem C, *et al*. Finding the needle in the haystack: the use of microfluidic droplet technology to identify vitamin-secreting lactic acid bacteria. mBio. 2017;8(3):e00526-17.

25. Zhu XD, Shi X, Wang SW, Chu J, Zhu WH, Ye BC, *et al*. High-throughput screening of lactic acid-producing *Bacillus coagulans* by droplet microfluidic flow cytometry with fluorescence-activated cell sorting. RSC Adv. 2019;9(8):4507–13.

26. Huang M, Bai Y, Sjostrom SL, Hallström BM, Liu Z, Petranovic D, *et al*. Microfluidic screening and whole-genome sequencing identify mutations associated with improved protein secretion by yeast. Proc Natl Acad Sci U S A. 2015;112(34):E4689–96.

27. Kehe J, Ortiz A, Kulesa A, Gore J, Blainey PC, Friedman J. Positive interactions are

common among culturable bacteria. Sci Adv. 2021;7:eabi7159.

28. Wagner JM, Liu L, Yuan SF, Venkataraman MV, Abate AR, Alper HS. A comparative analysis of single-cell and droplet-based FACS for improving production phenotypes: riboflavin overproduction in Yarrowia lipolytica. Metab Eng. 2018;47:346–56.

29. Balasubramanian S, Chen J, Wigneswaran V, Bang-Berthelsen CH, Jensen PR. Droplet-based microfluidic high-throughput screening of *Corynebacterium glutamicum* for efficient heterologous protein production and secretion. Front Bioeng Biotechnol. 2021;9.

30. Siedler S, Khatri NK, Zsohár A, Kjærbølling I, Vogt M, Hammar P, *et al*. Development of a bacterial biosensor for rapid screening of yeast p-coumaric acid production. ACS Synth Biol. 2017;6(10):1860–9.

31. Scanlon TC, Dostal SM, Griswold KE. A high-throughput screen for antibiotic drug discovery. Biotechnol Bioeng. 2014;111:232–43.

32. Hu L, Luo R, Wang D, Lin F, Xiao K, Kang Y. SERS-based microdroplet platform for high-throughput screening of *Escherichia coli* strains for efficient biosynthesis of D-phenyllactic acid. Front Bioeng Biotechnol. 2024;12.

33. Agnihotri SN, Fatsis-Kavalopoulos N, Windhager J, Tenje M, Andersson DI. Droplet microfluidics-based detection of rare antibiotic-resistant subpopulations in *Escherichia coli* from bloodstream infections. Sci Adv. 2025;11:4558.

34. Partipilo G, Bowman EK, Palmer EJ, Gao Y, Ridley RS, Alper HS, *et al*. Single-cell phenotyping of extracellular electron transfer via microdroplet encapsulation. Appl Environ Microbiol. 2025;91(1).

35. Qiao Y, Hu R, Chen D, Wang L, Wang Z, Yu H, *et al*. Fluorescence-activated droplet sorting of PET degrading microorganisms. J Hazard Mater. 2022;424:127417.

36. Sung YJ, Kim JYH, Choi HI, Kwak HS, Sim SJ. Magnetophoretic sorting of microdroplets with different microalgal cell densities for rapid isolation of fast-growing strains. Sci Rep. 2017;7(1):1–11.

37. Rabbers I, Gottstein W, Feist AM, Teusink B, Bruggeman FJ, Bachmann H. Selection for cell yield does not reduce overflow metabolism in *Escherichia coli*. Mol Biol Evol. 2022;39(1):1–10.

38. Mans R, Daran JMG, Pronk JT. Under pressure: evolutionary engineering of yeast strains for improved performance in fuels and chemicals production. Curr Opin Biotechnol. 2018;50:47–56.

39. Bachmann H, Bruggeman FJ, Molenaar D, Branco dos Santos F, Teusink B. Public goods and metabolic strategies. Curr Opin Microbiol. 2016;31:109–15.

40. McCully AL, Loop Yao M, Brower KK, Fordyce PM, Spormann AM. Double emulsions as a high-throughput enrichment and isolation platform for slower-growing microbes. ISME Commun. 2023;3:47.

41. Hengoju S, Abdissa K, Boto ST, Samimi A, Martin K, Jacobsen ID, *et al*. A droplet microfluidic strategy for cultivation, investigation, and high-throughput isolation of mouse gut microbiome bacteria. Appl Environ Microbiol. 2025;91:e00695-25.

42. Zengler K, Toledo G, Rappé M, Elkins J, Mathur EJ, Short JM, *et al*. Cultivating the uncultured. Proc Natl Acad Sci U S A. 2002;99(24):15681-6.

43. Pan CW, Horvath DG, Braza S, Moore T, Lynch A, Feit C, *et al*. Sorting by interfacial tension (SIFT): label-free selection of live cells based on single-cell metabolism. Lab Chip. 2019;19(8):1344–51.

44. Saleski TE, Peng H, Lengger B, Wang J, Jensen MK, Jensen ED. High-throughput GPCR-based autocrine screening for secondary metabolite production in yeast. Biotechnol Bioeng. 2024;121(10):3283–96.

45. Yanakieva D, Elter A, Bratsch J, Friedrich K, Becker S, Kolmar H. FACS-based functional protein screening via microfluidic co-encapsulation of yeast secretor and mammalian reporter cells. Sci Rep. 2020;10(1).

46. Coyte KZ, Schluter J, Foster KR. The ecology of the microbiome: networks, competition, and stability. Science. 2015;350(6261):663-6.

47. Palmer JD, Foster KR. Bacterial species rarely work together. Science. 2022;376(6593):581–2.

48. Ratzke C, Barrere J, Gore J. Strength of species interactions determines biodiversity and stability in microbial communities. Nat Ecol Evol. 2020;4(3):376–83.

49. Gopalakrishnappa C, Li Z, Kuehn S. Environmental modulators of algae-bacteria interactions at scale. Cell Syst. 2024;15(9):838–53.

50. Park J, Kerner A, Burns MA, Lin XN. Microdroplet-enabled highly parallel co-cultivation of microbial communities. PLoS One. 2011;6(2).

51. Fecker T, de KR, van TP. The effect of substrate and product transfer between polydisperse microdroplets on biological high-throughput screens. Sci Rep. 2025.

52. Scheler O, Kaminski TS, Ruszczak A, Garstecki P. Dodecylresorufin (C12R) outperforms resorufin in microdroplet bacterial assays. ACS Appl Mater Interfaces. 2016;8(18):11318–25.

53. Gruner P, Riechers B, Semin B, Lim J, Johnston A, Short K, *et al*. Controlling molecular transport in minimal emulsions. Nat Commun. 2016;7:10392.

54. Abalde-Cela S, Gould A, Liu X, Kazamia E, Smith AG, Abell C. High-throughput detection of ethanol-producing cyanobacteria in a microdroplet platform. J R Soc Interface. 2015;12(106).

55. Skhiri Y, Gruner P, Semin B, Brosseau Q, Pekin D, Mazutis L, *et al*. Dynamics of molecular transport by surfactants in emulsions. Soft Matter. 2012;8(41):10618–27.

56. Vinicius de Melo Pereira G, de Carvalho Neto DP, Junqueira AC, Karp SG, Letti LAJ,

Magalhães Júnior AI, *et al*. Selection criteria for starter culture development in the food fermentation industry. Food Rev Int. 2020;36:135–67.

57. Legras JL, Merdinoglu D, Cornuet JM, Karst F. Bread, beer and wine: *Saccharomyces cerevisiae* diversity reflects human history. Mol Ecol. 2007;16(10):2091–102.

58. Goffeau B, Barrell BG, Bussey H, Davis RW, Dujon B, Feldmann H, *et al*. Life with 6000 genes. Science. 1996;274(5287):546–67.

59. Wegmann U, O'Connell-Motherway M, Zomer A, Buist G, Shearman C, Canchaya C, *et al*. Complete genome sequence of the prototype lactic acid bacterium *Lactococcus lactis* subsp. cremoris MG1363. J Bacteriol. 2007;189(8):3256–70.

60. Börner RA, Kandasamy V, Axelsen AM, Nielsen AT, Bosma EF. Genome editing of lactic acid bacteria: opportunities for food, feed, pharma and biotech. FEMS Microbiol Lett. 2019;366.

61. Mierau I, Kleerebezem M. Ten years of the nisin-controlled gene expression system (NICE) in *Lactococcus lactis*. Appl Microbiol Biotechnol. 2005;68:705–17.

62. DiCarlo JE, Norville JE, Mali P, Rios X, Aach J, Church GM. Genome engineering in *Saccharomyces cerevisiae* using CRISPR-Cas systems. Nucleic Acids Res. 2013;41(7):4336–43.

63. Malcı K, Walls LE, Rios-Solis L. Multiplex genome engineering methods for yeast cell factory development. Front Bioeng Biotechnol. 2020;8.

64. Song AAL, In LLA, Lim SHE, Rahim RA. A review on *Lactococcus lactis*: from food to factory. Microb Cell Fact. 2017;16.

65. Borodina I, Nielsen J. Advances in metabolic engineering of yeast S*accharomyces cerevisiae* for production of chemicals. Biotechnol J. 2014;9:609–20.

66. van Dijken JP, Weusthuis RA, Pronk JT. Kinetics of growth and sugar consumption in yeasts. Antonie Van Leeuwenhoek. 1993;63:343–52.

67. De Deken RH. The Crabtree effect: a regulatory system in yeast. J Gen Microbiol. 1966;44:149–56.

68. Crabtree HG. Observations on the carbohydrate metabolism of tumours. Biochem J. 1929;23(3):536–45.

69. Castrillo JI, Kaliterna J, Weusthuis RA, van Dijken JP, Pronk JT. High-cell-density cultivation of yeasts on disaccharides in oxygen-limited batch cultures. Biotechnol Bioeng. 1996;49(6):621–8.

Chapter 2

Development of a high-throughput label-free method for enrichment of antimetabolite-resistant yeast strains using pico-litre agarose beads.

Sagarika B. Govindaraju, Thibaut J. Wenzel, Jack T. Pronk and Rinke J. van Tatenhove-Pel

Accepted for publication in Applied Microbiology and Biotechnology.

Abstract

Antimetabolites, which are structural analogues of metabolites or carbon sources that exhibit toxicity by disrupting metabolism, can couple phenotypes of interest to growth and thereby facilitate the selection of relevant strains from large mutant pools generated by random mutagenesis. Toxicity and high costs of many antimetabolites provide incentives to minimise liquid volume during cultivation, while still capturing the genetic diversity in large mutant pools. This study aims to explore the use of high-throughput microbead-based cultivation and label-free enrichment of antimetabolite-resistant mutants. The generation of a large number (~10^7 microbeads) of picolitre-sized cultivation compartments using water-in-oil emulsions enables high-throughput, parallel growth of millions of individual mutants in a total medium volume of just 0.3 mL. A reduction in screening medium volume reduces the quantities of expensive antimetabolites required. Employing a fluorescence-activated microbead-sorting-based approach enables label-free screening and selection of mutants based on autofluorescence signals as indicators for growth. The potential of this microbead-based, label-free selection method was demonstrated by enriching a G418 (geneticin) antibiotic-resistant and a glucose analogue (2-deoxyglucose) resistant *Saccharomyces cerevisiae* strains by 16000-fold and 600-fold, respectively, in single-step enrichment experiments.

1. Introduction

The throughput of classical strain improvement has significantly increased due to the implementation of high-throughput screening techniques (1–3). Classical strain improvement involves random mutagenesis followed by mutant selection. This approach is particularly relevant when targeted metabolic engineering strategies are difficult to implement due to limited knowledge of responsible genes, lack of genetic engineering tools, and selection for complex, multigenic phenotypes such as stress tolerance. This approach is also crucial for the food fermentation industry, where regulatory and/or public acceptance issues limit the application of targeted genetic engineering (4–6).

Classical strain improvement typically involves two key steps: (i) generation of genetic diversity, typically by random mutagenesis, and (ii) isolation of improved variants by screening or selection (1,3). Use of random mutagenesis imposes a requirement for high-throughput screening methods that can identify, select, and enrich mutants with desired phenotypes from massive mutant pools (1). When relevant phenotypes can be coupled to growth, higher specific growth rates and/or survival rates enable mutants of interest to dominate cultures upon propagation. For certain phenotypes, such as improved growth-coupled catabolic product formation rates and tolerance to environmental stress factors, adaptive laboratory evolution offers a straightforward way for growth-based selection (1,6,7). It is much more challenging to adopt growth-coupled selection for mutants that generate higher titres, productivities or yields of non-growth-coupled assimilatory products (7). Challenges in implementing growth-coupled strategies also complicate the selection of strains with deregulated catabolite repression, which are highly relevant in industrial biotechnology.

Antimetabolites are compounds whose strong structural similarity to natural metabolites causes interference with metabolic or regulatory mechanisms in wild-type cells (8–10). Resistance to antimetabolites have been widely applied to select for improved synthesis of non-growth-coupled products, and for alleviation of catabolite repression (8–10). In many anabolic product pathways, one or more of the enzymes in the pathway are subject to feedback inhibition by the product or a downstream intermediate (8,9). To overcome such feedback inhibition and thereby enable product accumulation, one effective approach is to render the target enzyme(s) insensitive to feedback inhibition by selecting for tolerance to antimetabolites that mimic the natural inhibitor (8,9,11). Mutants tolerant to inhibition by the antimetabolite are typically also insensitive to feedback inhibition by the native inhibitor and therefore able to accumulate the product whereas, non-tolerant mutants do not survive. Thus, resistance to antimetabolites provides an effective growth/no-growth selection strategy.

Antimetabolites can also be used to alleviate catabolite repression. For example, repression by glucose is a key factor in preventing simultaneous conversion of multiple sugars in feedstocks such as lignocellulosic hydrolysates (12–15). Catabolite

(glucose) repression-negative mutants of *Saccharomyces cerevisiae* can be obtained by selecting for tolerance to the antimetabolite 2-deoxyglucose, a glucose analogue without a hydroxyl group at the second carbon, in the presence of another carbon source (16–18). Similar strategies are applied to deregulate nitrogen-source and phosphate-source repression for improved production of secondary metabolites (8,9).

When selecting for antimetabolite-resistant mutants, spatial separation of mutants ensures that the genetic diversity of mutant pools is maintained. If all mutants are grown in a single compartments, the fastest-growing mutant would outcompete slower growing ones, allowing a single genotype to potentially dominate the population. By spatially separating the individual mutants, growth-based competition is elminated, preserving the diversity of mutants of interest and enabling their selection. Such spatial separation can be achieved by separating colony-forming units on solid medium. However, this approach requires large volumes of culture medium and laboratory consumables, as well as large quantities of antimetabolites. Many antimetabolites are expensive and toxic to humans. Miniaturisation of screening in microtiter plates, combined with the use of liquid-handling robotics, improves screening throughput but is still insufficient to cover the size of mutant pools (1).

Water-in-oil emulsions of agarose microbeads contain a large number of individual picolitre-sized cultivation compartments (~10^7 microbeads) in just 0.3 millilitre of medium (1–3). This study aims to investigate the potential of this multi-parallel cultivation method to select for antimetabolite-resistant mutants from large cell populations while minimising total culture volume. When each microbead, containing medium with an antimetabolite, is inoculated with a single cell, only beads inoculated with an antimetabolite-resistant cell are expected to show growth. Microbeads exhibiting growth can then be selected by (auto)fluorescence-activated microbead-sorting, to enrich for mutants with antimetabolite resistance in a label-free manner—unlike most existing microdroplet-based selection methods, which rely on genetically engineered fluorescent markers (2). The combination of microbead cultivation with microbead-sorting should allow for label-free screening of millions of mutants while using minimal amounts of expensive and toxic antimetabolites. Additionally, since beads are inoculated with single cells, genetic diversity in the mutant population can be fully captured. To test this approach, we developed a microbead-based, label-free method to enrich for antimetabolite-resistant *S. cerevisiae* strains from a population of sensitive *S. cerevisiae* strains. We validated the method by enriching G418 (geneticin) and 2-deoxyglucose (glucose antimetabolite) resistant *S. cerevisiae* strains.

2. Materials and Methods

2.1. Strains, media, and cultivation

Plasmids and *Saccharomyces cerevisiae* strains used in this study are shown in Table

S2 (supplementary section 2) and Table 1, respectively. Plasmids were propagated in *Escherichia coli* XL1-Blue cells (Agilent, Santa Clara, CA, USA). For long-term storage at -80 °C, glycerol was added to late-exponential-phase *S. cerevisiae* cultures and overnight *E. coli* cultures to obtain final concentrations of 30% (v/v) and 25% (v/v), respectively.

The *E. coli* cultures were grown at 37 °C in LB medium supplemented with 100 µg L^{-1} ampicillin for maintenance of plasmids. The *S. cerevisiae* strains were grown at 30 °C in 500 mL or 100 mL round-bottom flasks with 100 mL or 20 mL medium, respectively at 200 rpm in an Innova incubator shaker (New Brunswick Scientific, Edison, NJ) and incubated for 18 h. The *S. cerevisiae* strains were grown either in yeast extract peptone medium (YP, 10 g L^{-1} Bacto yeast extract and 20 g L^{-1} Bacto peptone), two-fold concentrated yeast extract and peptone medium (HCYP, 20 g L^{-1} Bacto yeast extract and 40 g L^{-1} Bacto peptone) or in synthetic medium suitable for cultivation of cultures at high cell concentrations (HCSM). The HCSM was prepared as described by Castrillo *et al*. (1996) (19) but without antifoam and substituting $(NH_4)_2SO_4$ with 9 g L^{-1} urea. Pre-cultures were grown in YP supplemented with 20 g L^{-1} glucose. The HCYP and HCSM were supplemented with 80 g L^{-1} glucose and 80 g L^{-1} sucrose, respectively. When *kanMX* was used for selection, 50 µg mL^{-1} to 600 µg mL^{-1} of sterilised G418 (geneticin) was added to the HCYP medium. Although chemically defined medium (HCSM) is preferred, it was not used for G418-based selection as the growth of the G418 sensitive strains was not effectively inhibited in this medium. This ineffective inhibition was potentially caused by the high concentrations of potassium- and magnesium containing salts in the medium. When 2-deoxyglucose was used for selection, 0.25 mg mL^{-1} to 8 mg mL^{-1} of sterilised 2-deoxyglucose was added to the HCSM medium. Solid medium plates contained 2% (w/v) agar.

2.2. Molecular biology techniques and strain construction

Plasmids were isolated from *E. coli* using the GeneJET Plasmid Miniprep Kit (Thermo Fisher Scientific). Genomic *S. cerevisiae* DNA was isolated as previously described by Lõoke *et al*. (2011) (20). DNA amplifications were performed using Phusion High Fidelity DNA polymerase (Termo Fisher Scientifc, Waltham, MA, USA) for cloning, and DreamTaq PCR Mastermix (Termo Fisher Scientifc) for diagnostic PCRs. For isolation of DNA fragments from the PCR reaction mixture, GeneJET PCR Purifcation Kit (Termo Fisher Scientifc) was used. DNA fragments were separated and visualised on a 1% agarose TAE gel by 30 min electrophoresis at 100 V. The DNA fragments excised from the gel, were purified using the Zymoclean Gel DNA recovery Kit (Baseclear). Gibson assemblies of plasmids were performed using the NEBuilder HiFi DNA Assembly Master Mix (New England Biolabs, Ipswich, MA, USA) and the resulting plasmids were propagated in XL1-Blue chemically competent *E. coli* cells. Transformations of *S. cerevisiae* strains were performed using LiAC/ssDNA/PEG, as previously described by Gietz & Woods (2002) (21). After the transformations, gRNA plasmids were removed as described by Mans *et al*. (2015) (23) and the single colonies were re-streaked at least three consecutive times to ensure isogenic single cell lines. Genomic insertions were

confirmed by performing diagnostic PCRs on the isolated genomic DNA.

Table 1 and Table S2 show the strains and plasmids, respectively, used in this study. In IMX2600, *HXK2* was deleted by introducing pUDR371, along with a double-stranded DNA repair fragment obtained by annealing primers 18833 and 18834 (primers used in the study are listed in supplementary section 1), resulting in strain IMX2748. A *kanMX* integration cassette was amplified from plasmid pUG6 using primers 20226 and 20227. The *kanMX* integration cassette, along with the plasmid pUDR376, was transformed into IMX2600 and IMX2748, resulting in IMI575 and IMI602, respectively. The pGGKd016 was constructed by assembly of part plasmids pYTK002, pYTK047, pYTK072, pYTK074, pYTK083 and pYTK081 using the Golden Gate reaction protocol described by Lee *et al*. (2015) (24). The plasmid pUDE1242 was created by Gibson assembly of three fragments that were PCR amplified from pUDE1111, pUDC329, and pGGKd016 with primer pairs 17634 and 19385, 12382 and 14776, and 14777 and 17008, respectively. A ymNeongreen integration cassette was amplified from pUDE1242 using primers 19247 and 19248. The ymNeongreen integration cassette, along with the plasmid pUDR538, was transformed into IMX2600, resulting in IMX2871. The ymNeongreen marker is codon-optimised for yeast and is characterized as one of the best performing fluorescent protein markers in *S. cerevisiae* (based on *in vivo* brightness, photo-stability) (25).

Table 1: *S. cerevisiae* strains used in this study

S. cerevisiae strain	**Genotype**	**Reference**
CEN.PK113-7D	*MATa URA3 TRP1 LEU2 HIS3*	
IMX2600	*MATa URA3 TRP1 LEU2 HIS3 can1Δ::*cas9-*natNT2*	(26)
IMI575	*MATa URA3 TRP1 LEU2 HIS3 can1Δ::*cas9-*natNT2 X-2::*p*AgTEF-kanMX-*t*AgTEF*	This study
IMX2871	*MATa URA3 TRP1 LEU2 HIS3 can1Δ::*cas9-*natNT2 X-2::* p*TDH3*-ymNeongreen-t*ENO2*	This study
IMX2748	*MATa URA3 TRP1 LEU2 HIS3 can1Δ::*cas9-*natNT2 hxk2Δ::SynPAM*	This study
IMI602	*MATa URA3 TRP1 LEU2 HIS3 can1Δ::*cas9-*natNT2 hxk2Δ::SynPAM X-2::*p*AgTEF-kanMX-*t*AgTEF*	This study

2.3. Analytical methods

Optical density (OD) was measured at 660 nm using a Libra S11 spectrophotometer (Biochrom, Cambridge, United Kingdom). Cell concentration was measured using a BD Accuri™ C6 Plus flow cytometry (BD Biosciences, San Jose, CA, USA). Size and volume distributions of the agarose beads in oil were determined by imaging with a Zeiss Axio Imager Z1 (Carl Zeiss AG, Jena, Germany) and an AxioCam HRm Rev3 detector (60 N-C 1" ×1.0) (Carl Zeiss AG) using the lateral magnification objective ×20. Details on the estimation of the average bead size are described in Section 3 of the supplementary information.

2.4. Preparation of microbeads

Agarose microbeads in oil were prepared as described by van Tatenhove-Pel *et al*. (2021) (27). The emulsions were prepared with a water phase and an oil phase (Novec HFE 7500 fluorinated oil, 3 M, Maplewood, MN, USA) containing 0.2% PicoSurf 1 surfactant (Sphere Fluidics, Cambridge, UK). The water phase contained HCYP medium with 8% (wt/v) glucose or HCSM with 8% (wt/v) sucrose, and 1% (wt/v) agarose with ultra-low gelling temperature (Type IX-A, A2576, Sigma-Aldrich, Saint Louis, MO, USA). Where indicated, G418 or 2-deoxyglucose and yeast cells were also added to the water phase.

Cells from pre-cultures were harvested during exponential growth (at an OD_{660} between 4 and 10). The cells were centrifuged (5 min 3000 x *g*), washed with sterile demineralised water, and after which the cell concentration (cells mL^{-1}) was measured. 2.7×10^6 cells were diluted in 300 µL of HCSM with 8% (wt/v) sucrose or HCYP with 8% (wt/v) glucose for a λ value of 0.2 (supplementary section 4). At this λ value, 90% of inoculated microbeads (excluding empty microbeads)contain one cell (supplementary section 4). Two times the required number of cells to inoculate at a λ value of 0.2 were added to account for loss of cell viability during preparation of the microbeads. To prepare the emulsions, 300 µL of the water phase was mixed with 700 µL of the oil phase with the surfactant using a T10 basic ULTRA TURRAX homogeniser with an S10N-5G dispersing element (IKA, Staufen, Germany) at speed 3 for 5 min. 2 mL round-bottom tubes (Eppendorf, Hamburg, Germany) were used to prepare and incubate the emulsions. Emulsions were prepared at room temperature. Microbeads prepared with HCYP with 8% (wt/v) glucose medium had an average volume of 52.12 pL (supplementary section 3). Microbeads prepared with HCSM with 8% (wt/v) glucose medium had an average volume of 47.40 pL (supplementary section 3). Emulsions were incubated on a HulaMixer® Sample Mixer (Thermo Fisher Scientific, Waltham, MA, USA) at 30°C while rotating at 1 rpm orbital rotation for 40 h. After incubation, microbeads were separated from the oil phase by adding 1.2 mL phosphate-buffered saline (PBS) and 1.5 mL perfluorooctanol (PFO, Alfa Aesar, Ward Hill, MA, USA) to 1 mL of the emulsion and gently mixing. Microbeads partitioned to the water phase (i.e. PBS), which was carefully recovered with a pipette.

2.5. Sorting of microbeads

Before flow cytometry, microbeads larger than 40 µm were removed by filtering over a 40 µm mesh filter (pluriStrainer, PET-mesh). Microbeads smaller than 40 µm were subsequently measured. Forward scatter, side scatter and green fluorescence signal were measured using the 488 nm laser on a BD FACSAria™ II SORP Cell Sorter (BD Biosciences, San Jose, CA, USA), operated with FACSFlow™ software (BD Biosciences) and equipped with a 130 µm nozzle. The green fluorescence signal was detected through a 545/28 nm or a 530/30 nm bandpass filter. Between 96 and 384 events in the gates of interest were sorted with 4-way purity precision on agar plates with YP + 2 wt% glucose. FlowJo™ v10.10 software (BD Life Sciences) was used for data analysis. The

applied gating strategy is described in detail in the supplementary section 5.

2.6. Determining relative abundances of strain types

Relative abundances of strains in the inoculum and after microbead sorting were determined to assess enrichment. Relative abundance of *S. cerevisiae* strains IMX2871 and IMI575 (fluorescent and non-fluorescent strains) in inocula for emulsion cultures was determined by measurement of fluorescence using flow cytometry (10^5 events recorded). To determine the fraction of different cell-types after sorting microbeads in phosphate buffer saline, microbead samples were first vortexed, and then the resulting suspension was plated on YP with 2% glucose (wt/v) solid medium. After incubation of the plates at 30 ^{o}C for at least 18 h, relative abundances of the two strains were determined by counting the fluorescent and non-fluorescent colonies by illuminating plates with Safe Imager 2.0 Blue-light Transilluminator (Invitrogen, MA, USA).

To determine the relative proportions of non-fluorescently labelled resistant and non-resistant strains before inoculating microbeads, we plated the mixtures on YP with 2% (wt/v) glucose solid medium plates with G418 as a selection marker (the 2-deoxyglucose resistant strain is also engineered with resistance to G418). Depending on the target initial fractions (ranging from 1 in 10^2 to 1 in 10^4), between 10^4 to 10^6 cells from each mixture were plated, respectively. Microbeads were inoculated with a mix of the strains, and the beads with growth were sorted on YP with 2% (wt/v) glucose solid medium plates. All colonies from the YP with 2% (wt/v) glucose solid medium plates were scored for growth on YP with 2% (wt/v) glucose solid medium plates with G418 as a selection marker.

3. Results

3.1. Label-free identification of a resistant *S. cerevisiae* strain

To identify microbeads with the growth of an unlabelled resistant strain in the presence of an inhibitor molecule, microbeads were inoculated with G418-sensitive CEN. PK113-7D and G418-resistant IMI575 *Saccharomyces cerevisiae* strains. The G418 is an aminoglycoside antibiotic that inhibits protein synthesis and is commonly used as a selection marker in *S. cerevisiae* (28).

Flow cytometry analysis of empty microbeads showed a distribution of side-scatter and fluorescence signals, which is consistent with their polydispersity. Microbeads were inoculated at a λ-value of 0.2 (supplementary section 4) and incubated for 40 h in the presence of the antibiotic G418. After growth, flow cytometry analysis showed that microbeads inoculated with cells contained an additional population compared to empty microbeads (Figure 1a, c and d). This population was identified as single cells by comparing to a control sample (Figure 1b). The single cells population likely

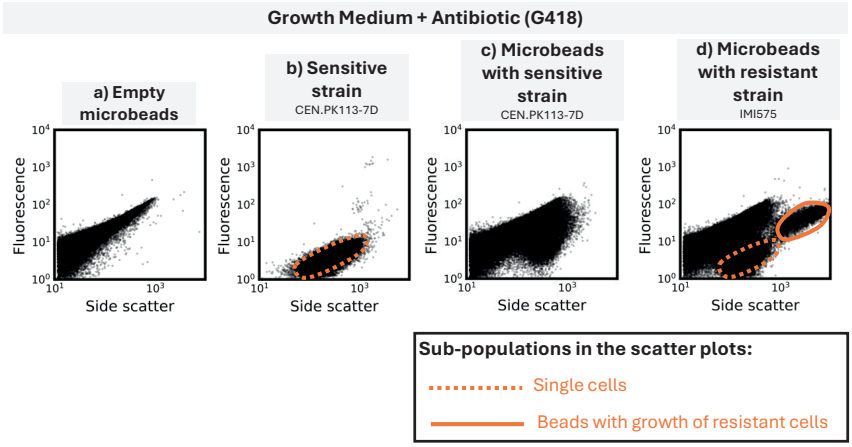

Figure 1: Identification of flow cytometry populations corresponding to (a) empty microbeads, (b) G418-sensitive *S. cerevisiae* strain CEN.PK113-7D single cells, (c) microbeads inoculated with the G418-sensitive strain, and (d) microbeads inoculated with a G418-resistant *S. cerevisiae* strain IMI575. Microbeads were prepared with medium containing G418, inoculated at a λ-value of 0.2, and incubated for 40 h. Additional gating information is provided in supplementary section 5.

arises from damaged microbeads. For microbeads inoculated with the G418-resistant strain IMI575, an additional population with both higher fluorescence and side scatter signal was detected (Figure 1d). This population was identified as microbeads with cell growth, as increased autofluorescence is expected (29-31) with growth and was only observed for the microbeads inoculated with the resistant strain (Figure 1d). Increase in the side scatter signal is consistent with greater internal complexity of the microbeads resulting from cell growth.

These results show that the growth of an unlabelled resistant strain in microbeads can be detected using autofluorescence and/or side scatter as a growth indicator. A detailed overview of the general gating strategy employed is described in the supplementary section 5.

3.2. Enrichment of *S. cerevisiae* cells expressing a fluorescent protein using microbead sorting

The validation of the proposed enrichment method for a specific, low-abundance yeast strain, was tested using mixtures of an ymNeongreen-expressing, fluorescent strain IMX2871 and a *kanMX*-expressing, G418-resistant *S. cerevisiae* strain IMI575.

To minimise the number of microbeads inoculated with more than one cell, while maintaining a sufficient number of inoculated microbeads, microbeads were inoculated at a λ-value of 0.2 (supplementary section 4). As anticipated, after growth, flow cytometry showed a higher fluorescence of microbeads inoculated with the ymNeongreen-expressing *S. cerevisiae* strain IMX2871 than of microbeads inoculated with the *kanMX*-expressing reference strain IMI575 (supplementary section 5). The fluorescence signal from microbeads inoculated with the reference strain

was attributed to the autofluorescence of yeast cells and the agarose matrix used to generate the microbeads (29–31).

Based on the fluorescence of the two strains, a FACS gate was defined to specifically sort the ymNeongreen-expressing strain IMX2871. After sorting, the relative abundances of the two strains were measured using flow cytometry. In three independent single-round sorting experiments, strain IMX2871 was enriched from a starting abundance of 0.096% (1 in 1000) to a final fraction of 78% ± 7%, which represents an 800-fold enrichment.

Even though a fluorescently labelled yeast strain was used for validation of a label-free enrichment method, these results serve as proof of concept that FACS-based microbead sorting can be used to strongly enrich a specific yeast strain from a mixed culture in which it occurs at a low abundance.

3.3. Enrichment of a G418-resistant *S. cerevisiae* strain by using microbead sorting

The next set of experiments aimed to investigate whether the proposed approach in this study can be used to enrich microbeads containing a low-abundance inhibitor-tolerant strain from a mixed population, without using a heterologously expressed fluorescent protein. To this end, experiments were designed to select the *kanMX*-expressing, G418-resistant *S. cerevisiae* strain IMI575 from mixtures with the G418-sensitive strain CEN.PK113-7D.

Concentrations of G418 required to inhibit growth in suspension and microbead cultures were determined (Figure 2). Suspension cultures on HCYP medium with 8% (wt/v) glucose in shake flasks were inoculated at a cell concentration equivalent to one cell per microbead (3×10^7 cells mL^{-1}). The high sugar concentration was used to ensure sufficient growth of the strains within the microbeads to be able to distinguish between microbeads with and without growth. At G418 concentrations between 200 and 600 µg mL^{-1}, cell concentrations in suspension cultures measured after incubation remained unchanged compared to the cell concentration measured immediately after inoculation (Figure 2a).

The same concentration range of G418 that was evaluated in suspension cultures was tested in microbead cultures inoculated at λ-value of 0.2. To quantify inhibition by G418, using flow cytometry, we first identified the percentage of microbeads showing growth (Figure 1 and gated as shown in supplementary section 5). We then normalized the fraction of microbeads showing growth in the presence of G418 to the fraction observed in the absence of the antibiotic (Figure 2b). Using the same 200 to 600 µg mL^{-1} concentration range of G418 used in the suspension cultures, despite variation in the data, clear growth of the resistant strain IMI575 in microbeads was observed (Figure 2b). In contrast to suspension cultures, microbead cultures of the G418-sensitive strain IMX2871 showed growth at G418 concentrations of 200 and 400 µg mL^{-1}. However, also in microbeads, a G418 concentration of 600 µg mL^{-1} sufficed to

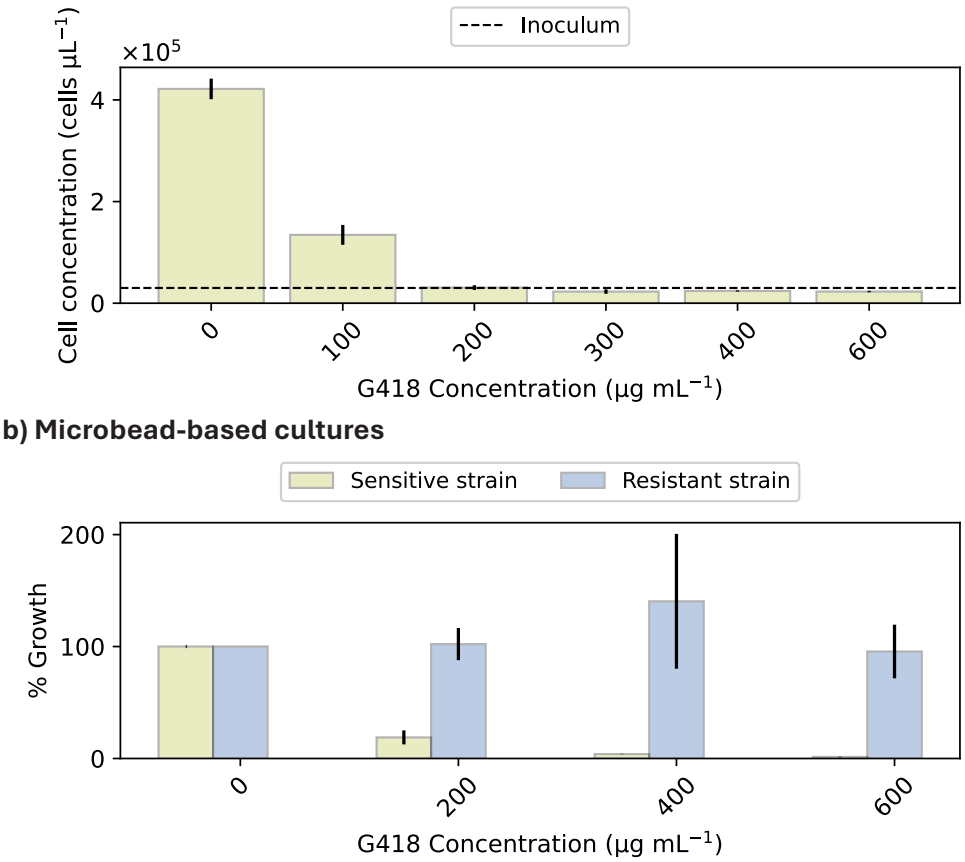

Figure 2: Analysis of growth inhibition of suspension and microbead cultures at different concentrations of G418. (a) Cell concentrations (cells μL^{-1}) at different G418 concentrations (µg mL^{-1}) measured in suspension cultures of the G418-sensitive *S. cerevisiae* strain IMX2871. The dashed line indicates the cell concentration of the inoculum, which corresponds to one cell per microbead. (b) Percentage of microbeads with growth in the presence of G418 normalised to the proportion of microbeads with growth in the absence of G418. Microbeads were inoculated at λ-value of 0.2 with the G418-sensitive strain IMX2871 (yellow bars) or the G418-resistant strain IMI575 (purple bars) and were incubated for 40 h.

prevent growth of the sensitive strain (Figure 2b).

We subsequently assessed whether exposure of microbead cultures of G418-sensitive *S. cerevisiae* to 600 µg mL^{-1} killed or merely inhibited growth. To this end, microbead cultures with and without G418 were inoculated with the sensitive strain CEN.PK113-7D. After 40 h incubation, sorted events corresponding to single cells and microbeads inoculated with cells (gated as shown in supplementary section 5) were placed on non-selective plates to check for growth. Of the sorted events from cultures grown in the absence of G418, 71% ± 4% yielded colony-forming units, while none of the sorted events from G418-supplemented cultures showed any colony-forming units (supplementary section 6). These results indicate that only G418-resistant strains

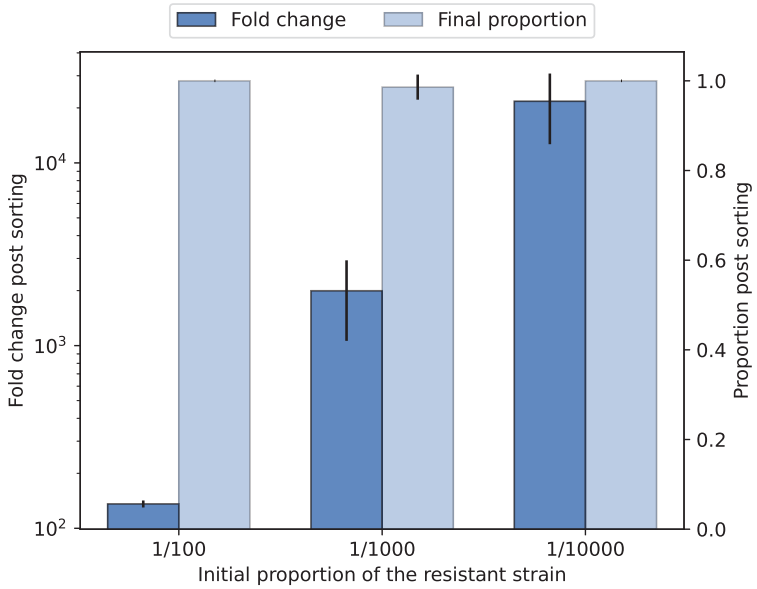

Figure 3: Fold-change and proportion of the G418-resistant *S. cerevisiae* strain IMI575 before and after microbead sorting. The target ratios for the mixtures of the resistant strain IMI575 and the sensitive strain CEN.PK113-7D (1:10^2, 1:10^3 and 1:10^4) correspond to average measured ratios of 1:139 ± 6 (two mixtures), 1:2037 ± 846 (two mixtures) and 1:19135 ± 7879 (two mixtures). Microbeads were inoculated at λ-value of 0.2 with the strain mixtures and incubated in medium containing G418. After incubation for 40 h, microbeads with growth were sorted. Each bar represents the average from four sorting experiments (1:10^2 and 1:10^3) or three experiments (1:10^4). The relative abundances of the resistant and sensitive strains were quantified before and after sorting.

survive G418 exposure in microbeads and subsequent sorting.

To evaluate whether microbeads containing a G418-resistant strain can be selected by FACS microbead sorting when they only represent a small fraction of the total fraction of inoculated beads, mixtures of the resistant strain IMI575 and the sensitive strain CEN.PK113-7D were prepared at ratios of 1:10^2, 1:10^3 and 1:10^4 (Figure 3). Microbeads were then inoculated with these mixtures at a λ-value of 0.2. After incubation for 40 h, microbeads with the highest autofluorescence and side scatter signal were selected. A substantial enrichment of the G418-resistant strain IMI575 was observed for all initial strain ratios (Figure 3). Four separate replicate sort experiments were performed with initial strain mixtures that contained 0.72% ± 0.03% resistant cells. In each replicate sort experiment, microbeads with growth were sorted. All the resulting colonies were resistant cells (100% ± 0%) (Figure 3). Similarly, in four separate sort experiments with mixtures containing 0.059% ± 0.025% resistant cells, 98.60% ± 2.42% of the obtained colonies were resistant cells (Figure 3). In the most extreme case, with an initial proportion of the resistant strain of 0.0063 ± 0.0026%, in three separate sort experiments, all the resulting colonies were resistant cells (100% ± 0%) (Figure 3).

The results demonstrate that microbeads inoculated with a G418-resistant strain can be enriched by 16000-fold in a single round of sorting from a mixture with a sensitive

strain in which it occurs at very low frequencies (1:10^4). The earlier viability assessment shows that G418-sensitive strains do not recover after exposure to G418 under these conditions, which explains the high enrichment observed after sorting, even in the presence of known sorting inefficiencies.

3.4. Enrichment of a 2-deoxyglucose-resistant *S. cerevisiae* strain by using microbead sorting

To assess whether the proposed approach for enriching specific, low-abundance phenotypes from microbead cultures can be applied to select for cells resistant to a non-lethal antimetabolite. 2-deoxyglucose was used as a model antimetabolite. 2-Deoxyglucose is a glucose analogue that lacks a hydroxyl group at the second carbon, mimics glucose, and thereby represses the utilisation of alternative carbon sources (32). 2-Deoxyglucose is commonly used to select for yeast mutants that, due to alleviation of glucose catabolite repression, can convert other carbon sources in the presence of glucose (16-18).

To determine the concentration of 2-deoxyglucose to inhibit the growth of suspension cultures on sucrose (Figure 4A), batch cultures were inoculated with the sensitive *S. cerevisiae* strain CEN.PK113-7D or the *hxk2Δ* resistant strain IMX2748. The resistant strain lacks *Hxk2,* as this deletion has been shown to confer the strain resistance to 2-deoxyglucose in the presence of sucrose. There are several hypotheses for reduced toxicity due to the deletion of Hxk2: reduced phosphorylation to 2-deoxyglucose-6-phosphate (16,18,33), alleviation of repression of sucrose invertase (Suc2) (17,18), and/or possible detoxification of 2-deoxyglucose-6-phosphate via the expression of 2-deoxyglucose-6-phosphatases (32). Microbead cultures were inoculated at a cell concentration of 3×10^7 cells mL^{-1} (corresponding to one cell per microbead). At 2-deoxyglucose concentrations of 0.5 g L^{-1} or higher, for CEN.PK113-7D, no increase in the cell number was observed after inoculation (Figure 4a and b). In similar experiments with the *hxk2Δ* strain IMX2748, clear growth was observed at all tested 2-deoxyglucose concentrations, although final cell concentrations showed a negative correlation with 2-deoxyglucose concentration (Figure 4b). This correlation is likely due to the toxicity of 2-deoxyglucose, which is still taken up by the cell and, due to phosphorylation by hexose kinases, causes accumulation of non-metabolizable intermediates and ATP depletion (32,34).

To test growth inhibition by 2-deoxyglucose in sucrose-grown microbead cultures, they were inoculated at a λ-value of 0.2 with the sensitive *S. cerevisiae* strain CEN.PK113-7D or the *hxk2Δ* resistant strain IMI602. Growth at different 2-deoxyglucose concentrations by flow cytometry was based on autofluorescence and side scatter signal (Figure 1). To quantify inhibition by 2-deoxyglucose, using flow cytometry, we first estimated the percentage of microbeads showing growth (gated as shown in supplementary section 5). We then normalized the proportion of microbeads showing growth in the presence of 2-deoxyglucose to the proportion observed in the absence of the antimetabolite (Figure 4b). Based on these experiments, a 2-deoxyglucose

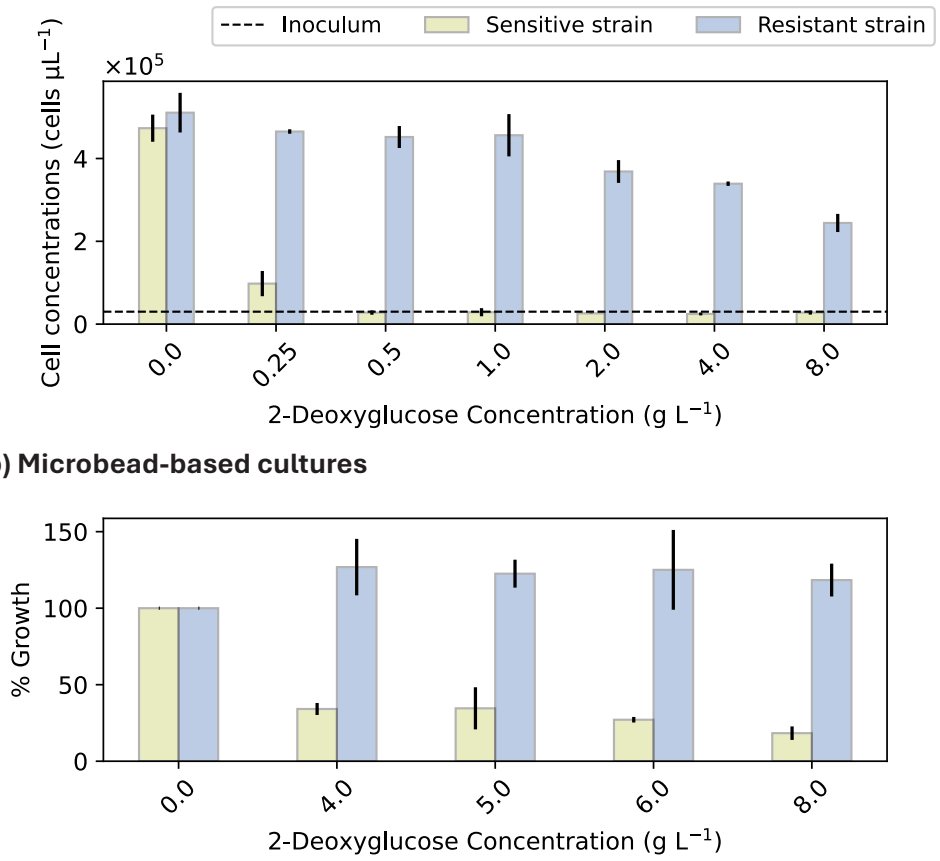

Figure 4: Analysis of growth inhibition of suspension and microbead cultures at different concentrations of 2-deoxyglucose. (a) Cell concentrations (cells µL^{-1}) at different 2-deoxyglucose concentrations (g L^{-1}) measured in suspension cultures of the 2-deoxyglucose-sensitive strain CEN.PK113-7D (yellow bars) and the 2-deoxyglucose-resistant strain IMX2748 (purple bars). The dashed line indicates the cell concentration of the inoculum, which corresponds to one cell per microbead. (b) Percentage of microbeads with growth in the presence of 2-deoxyglucose normalised to the proportion of microbeads with growth in the absence of 2-deoxyglucose. Microbeads were inoculated at λ-value of 0.2 with the 2-deoxyglucose-sensitive strain CEN.PK113-7D (yellow bars) or 2-deoxyglucose-resistant strain IMI602 (purple bars) and incubated for 40 h.

concentration of 8 g L^{-1} was chosen for further studies in microbead cultures. As observed for G418, microbead cultures were less sensitive to 2-deoxyglucose than suspension cultures (Figure 4a and b).

To assess the effect of 2-deoxyglucose on a sensitive strain, microbeads were inoculated with the sensitive strain CEN.PK113-7D in the absence and presence of the inhibitor at 8 g L^{-1}. After 40 h of incubation, FACS events identified as single cells and microbeads inoculated with cells (gated as shown in supplementary section 5) were plated on non-selective medium plates. Of the events sorted from microbead cultures grown in the absence of 2-deoxyglucose, 84 ± 11% showed growth as colony-forming

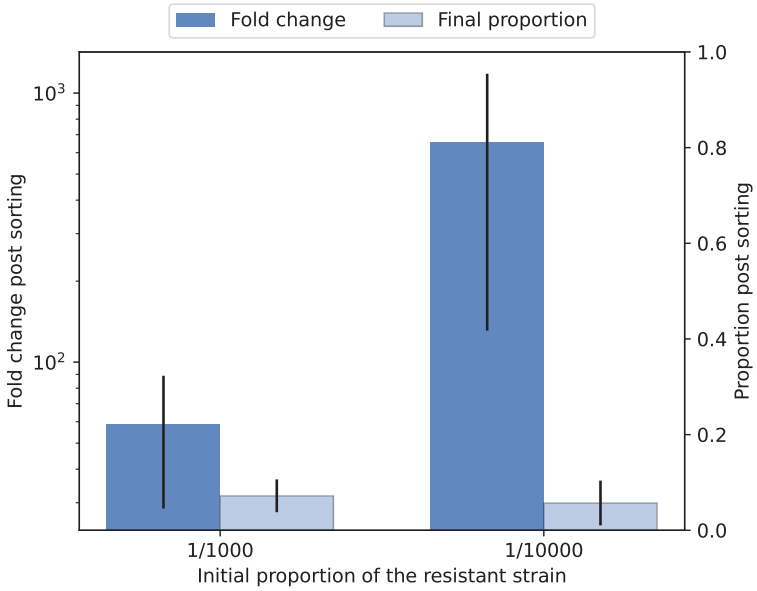

Figure 5: Fold-change and proportion of the 2-deoxyglucose-resistant *S. cerevisiae* strain IMI602 before and after microbead sorting. The target ratios for the mixtures of the resistant strain IMI575 and the sensitive strain CEN.PK113-7D (1:10^3 and 1:10^4) correspond to average measured ratios of 1:806 ± 50 (two mixtures) and 1:11755 ± 409 (two mixtures). Microbeads were inoculated at λ-value of 0.2 with the strain mixtures and incubated in medium containing 2-deoxyglucose. After incubation for 40 h, microbeads with growth were sorted. Each bar represents the average from six sorting experiments (1:10^3) or three experiments (1:10^4). The relative abundances of the resistant and sensitive strains were quantified before and after sorting.

units on plates. A much lower fraction of colony-forming units (9 ± 6%) was observed for events sorted from microbead cultures grown in the presence of 2-deoxyglucose (supplementary section 6). These results show that only a small percentage of 2-deoxyglucose-sensitive strains can form colonies after incubation with 8 g L^{-1} 2-deoxyglucose in microbeads, followed by microbead-sorting.

To test the feasibility of sorting microbead populations for low-abundance microbeads containing 2-deoxyglucose-inhibition-resistant cells, the resistant strain IMI602 and the sensitive strain CEN.PK113-7D were mixed at ratios of 1:10^3 and 1:10^4. Microbeads were inoculated with these mixtures at λ-value of 0.2 and, after incubation for 40 h, beads with high autofluorescence and side scatter signals were selected. For both initial strain ratios, this procedure yielded an enrichment of the 2-deoxyglucose-resistant strain IMI602 (Figure 5). IMI602 was also engineered to be resistant to G418 to enable determination of relative abundances (pre- and post-sorting) by screening for resistance to the antibiotic. In each separate replicate sort experiment, microbeads with growth (gated as shown in the supplementary section 5) were sorted. In mixtures initially containing 0.12% ± 0.0076% of strain IMI602, from six separate replicate sort experiments, the resistant strain was enriched to 7.15% ± 3.12%. Similarly, for mixtures containing 0.0085% ± 0.00029%, from three separate replicate

sort experiments, the resistant strain was enriched to 5.70% ± 3.77% (Figure 5).

The results show that, although the enrichment of the resistant strain did not reach 100%, an approximately 600-fold enrichment of an antimetabolite-resistant strain was achieved in a single round of sorting, starting from a strain mixture in which it represented approximately $1:10^4$ of the population. The earlier viability assessment showed that 2-deoxyglucose-sensitive strains can recover after exposure to 2-deoxyglucose under these conditions. This, together with potential (co-)sorting of populations outside the gated population to be sorted could explain the presence of sensitive strain.

4. Discussion

The results presented in this study demonstrate cultivation in agarose-bead-in-oil emulsions combined with label-free high-throughput sorting, enabling fast and efficient selection of antimetabolite-resistant *S. cerevisiae* strains from large populations of cells. Use of microbeads minimised costs by enabling the reduction of the water phase of the selection cultures to 0.3 mL. A 600 to 16000-fold enrichment of microbeads with resistant cells in the subsequent sorting step minimised the medium requirement for further selection on solid media or in microtiter plates. This approach has the potential to strongly reduce the amounts of antimetabolites and other laboratory consumables needed in screening campaigns. Finding a non-toxic replacement for the fluorinated oil used in the cultivation step is a relevant challenge in attempts to further reduce the environmental impact of this approach. By using autofluorescence and side scatter signals as an indicator for growth, sorting of microbeads with resistant cells could be performed without expressing a heterologous fluorescent protein.

In cases where autofluorescence signals from the microorganism of interest are too weak to use as an indicator for selection of microbeads with growth, the use of fluorescent markers that are activated by cellular metabolism (35,36) may offer an interesting alternative.

Although complete enrichment of the 2-deoxyglucose-resistant strain was not achieved, a 600-fold enrichment was observed. In the most challenging case, with an initial resistant fraction of 0.0085% ± 0.00029%, the resistant strain was enriched to 5.70% ± 3.77%. This pre-enrichment demonstrates that applying the proposed approach to a mutant pool can drastically reduce the screening effort from ~10^5 mutants to only a few hundred. Such a substantial reduction enables feasible identification of mutants of interest, for example, using 96-well plate-based assays. Subsequent rounds of sorting are expected to further increase enrichment. Altogether, the proof of concept using the antimetabolite 2-deoxyglucose showcases significant enrichment of the strain of interest, despite a non-lethal effect of the antimetabolite.

Use of water-in-oil emulsions implies that partitioning of hydrophobic antimetabolites

into the oil phase may complicate the adoption of this method. If this problem cannot be addressed by increasing the amount of antimetabolite added to the assays, without considerably increasing the costs of screening, it may be attempted to increase their concentration in the water phase by measures such as adding bovine serum albumin, adjusting surfactant concentrations, or chemically modifying the antimetabolite (37-39). Growth in emulsions may also be influenced by factors such as oxygen supply and pH. However, these variables would not affect the enrichment outcome, provided the cells undergo sufficient number of doublings within the microbeads to allow reliable distinction between growth and no growth.

Minimum inhibitory concentrations (MICs) of both G418 and 2-deoxyglucose in microbead cultures were higher than in suspension cultures. Context dependency of MIC values does by no means preclude the use of microbead-based selection, but was not anticipated in this study since, based on their partition coefficients, G418 and 2-deoxyglucose (LogP values are -1.37 and -3.07, respectively) should remain in the aqueous phase (40). Instead, the different MICs in microbead and suspension cultures may reflect different physiology of microbead-grown cultures, partial inactivation or degradation of inhibitors during emulsion preparation, and/or binding to agarose.

In cases where an inhibitor fully blocks re-growth of sensitive cells, as observed in this study for selection with the antibiotic G418, using low-volume suspension cultures, selection of mutant mixtures in the presence of such an antimetabolite might suffice. However, selection in suspension cultures could result in loss of genetic diversity, as the fastest-growing surviving mutants will dominate the population. Eliminating this competition by spatial segregation in microbeads allows for more representative sampling of the genetic diversity of mutant pools.

2-Deoxyglucose-resistant yeast cells were selected by growing them on sucrose, a substrate whose utilisation by *S. cerevisiae* is repressed by glucose (41,42). In *S. cerevisiae*, metabolism of sucrose is initiated by hydrolysis to fructose and glucose, a reaction that predominantly occurs extracellularly (43). In the microbead emulsions, the fructose and glucose are retained in the water phase, which implies that they are only accessible for the clonal culture inside the microbead. This privatisation of resources differs from the situation in suspension cultures and solid media, where all cells share extracellular substrates as well as extracellular enzymes. The simple, label-free selection and screening method described in this study may therefore be applicable for the selection of microorganisms that efficiently hydrolyse extracellular substrates. Such an application may, for example, be relevant for the improvement of yeast strains for consolidated bioprocessing (i.e., simultaneous extracellular hydrolysis and fermentation of polymeric or oligomeric saccharides) (15).

In setting up the microbead cultivation and sorting strategy, we used the antibiotic G418 as a model inhibitor. Rapid detection and identification of effective antibiotic regimes of clinical isolates are critical for enabling timely treatment of microbial infections. Conventional assays often require long incubation times to reach

detectable cell concentrations (44, 45). Boedicker *et al*. (2008) (44) and Agnihotri *et al*. (2025) (45) addressed this problem by using small-volume confinements to increase the local cell concentration. However, their strategies required specialised microfluidic devices and imaging. The simpler microbead-emulsion method presented here may offer a simple high-throughput alternative that, as long as a flow cytometer or FACS is available, can easily be implemented in clinical laboratories.

In conclusion, the high-throughput microbead-based selection method offers a label-free, cost-reducing alternative to conventional methods for enriching antimetabolite-resistant *S. cerevisiae* strains. The method was validated by achieving a 600-fold enrichment of a 2-deoxyglucose (glucose analogue) resistant *S. cerevisiae* strain and a 16000-fold enrichment of a G418 (antibiotic) resistant *S. cerevisiae* strain. Beyond this application, the simple, label-free and high-throughput design may also be applicable for selecting mutants with improved extracellular product hydrolysis substrates and rapid identification of effective antibiotic regimes with clinical isolates.

Acknowledgments

We would like to thank Anna Wronska for the construction of the plasmid pGGKd016, Miriam Cammaert for the construction of the plasmid pUDE1242 and the strain IMX2871 and Rose Vossen for the construction of the strain IMX2748.

We would like to thank Ilse de Lange and Noël van Peij from DSM-Firmenich (Delft, the Netherlands) for valuable discussions.

Author contributions

JTP, RJvT, and TW conceptualised the work. JTP, RJvT, and SBG designed experiments. SBG wrote the original draft of the manuscript, which was reviewed and edited by JTP, RJvT, and TW. SBG performed the experiments and conducted data analysis. All authors read and approved the final manuscript.

This work was supported by DSM-Firmenich (Delft, the Netherlands) and Delft University of Technology.

Supplementary material

Supplementary section 1: Primers used in this study

Table S1: Primers used in this study

Primer	Sequence (5'-3')
12382	ATCCTAACTCGAGAGTGCTTTTAAC
13662	TCCTCGGGCAGAGAAACTCG
13663	GTGAGCCTCTTACCTGTTTG
14776	CGCCTTGATCGTTGGGAACC
14777	ATTCAGCTCCGGTTCCCAACG
17008	CGTCTGCAATTATCGGCCAG
17634	CTGGCCGATAATTGCAGACG
18833	TTGTAGGAATATAATTCTCCACACATAATAAGTACGTTAATTAAATAAAAGTAGAATT TCACCTAGACGAGGACTTAATTTGTAAATTAAGTTTGAACAACAAGAAGGTGCCC TTTTTTT
18834	AAAAAAAGGGCACCTTCTTGTTGTTCAAACTTAATTTACAAATTAAGTCCTCGTCTA GGTGAAATTCTACTTTTATTTAATTAACGTACTTATTATGTGTGGAGAATTATATTCCTA CAA
19199	GGATCGCAGTGGTGAGTAACC
19247	GTCATAACTCAATTTGCCTATTTCTTACGGCTTCTCATAAAACGTCCCACACTATTC AGGGGTATTTTTCAAACTGCAAATTCAAGAA
19248	TCACAGAGGGATCCCGTTACCCATCTATGCTGAAGATTTATCATACTATTCCTCCG CTCGAACGCAGTTCGAGTTTATCATTATC
19385	AAGCACTCTCGAGTTAGGATTTAGGATCCCTTGTACAATT
19584	TTGCCATTCTCACCGGATTC
20226	GCTGAAGATTTATCATACTATTCCTCCGCTCGTTTCTTTTTTCAGTGAGGTGTGTCG TGAAGATCTGTTTAGCTTGCCTCG
20227	ATTCTCGCCAAGGCATTACCATCCCATGTAAGAACGGAATAAAACAGCATTCGAA GGTTATTCGACACTGGATGGCG

Supplementary section 2: Plasmids used in this study

Table S2: Plasmids used in this study

Plasmid name	Relevant characteristics	Reference
pUDR371	2µm ampR *kanMX gRNA-HXK2*	(22)
pUG6	ColE1 ampR *loxP-kanMX-loxP*	(46)
pUDR376	2µm ampR *amdSYM gRNA-X2*	(47)
pUDE1111	2µm ampR *hygR ConLS*-p*TDH3*-ymNeongreen-t*ADH1-ConR1*	(48)
pUDC329	*CEN/ARS URA3* p*TEF1-preSU9-ymTq2*-t*ENO2*	(49)
pYTK002	camR *ConLS*	(24)
pYTK047	camR *GFPdropout*	(24)
pYTK072	camR ConRE	(24)
pYTK074	camR *URA3*	(24)
pYTK083	ampR ColE1	(24)
pYTK081	CamR *CEN6/ARS4*	(24)
pGGKd016	*CEN6/ARS4 ampR URA3 ConLS-GFP dropout-ConRE*	This study
pUDE1242	*CEN6/ARS* ampR *URA3* p*TDH3*- ymNeongreen-t*ENO2*	This study
pUDR538	2µm ampR *hphNT1 gRNA-X2*	(50)

Supplementary section 3: Microbead size and volume distributions of agarose microbeads

We prepared agarose microbead emulsions as described in the materials and methods section. We imaged the resulting polydisperse microbeads with a microscope (Figure S1A, 9 images per emulsion). The images were subsequently analysed with ImageJ to identify the microbeads and determine their size (Figure S1B). Microbeads on the edges of the images and small microbeads (up to 2 µm in diameter) were excluded from the analysis. Based on these ImageJ results, average microbead diameter and volume distributions were determined.

The average number of cells in a microbead is defined by the λ-value of the Poisson distribution. The λ-value is dependent on the number of cells added to the water phase and the average size of microbeads. Since we use polydisperse emulsions, we have a distribution of microbead sizes (Figure S1D and F). Although smaller microbeads (< 20 µm) are more abundant (Figure S1D and F), due to a low volume of these microbeads, they occupy a small fraction of the total water phase (Figure S1C and E). When cells are homogenously mixed in the water phase, only a small fraction of the cells is harboured within the small microbeads due to the low volume fraction of the water phase occupied by these microbeads. Most of the cells in the water phase will be distributed over the larger microbeads. We reasoned that the average diameter of microbeads that occupy the highest volume fraction represents the average diameter of the emulsion and can be used to determine the λ-value.

The average diameter (± standard error of the mean) of microbeads that occupy the largest volume fraction was calculated to be 52.12 pL ± 14.19 pL (diameter of 44.10 µm ± 3.75 µm, n=8) for HCYP with 8% (wt/v) glucose medium and 47.40 pL ± 5.10 pL (diameter of 44.53 µm ± 1.55 µm, n=8) for HCSM with 8% (wt/v) glucose medium.

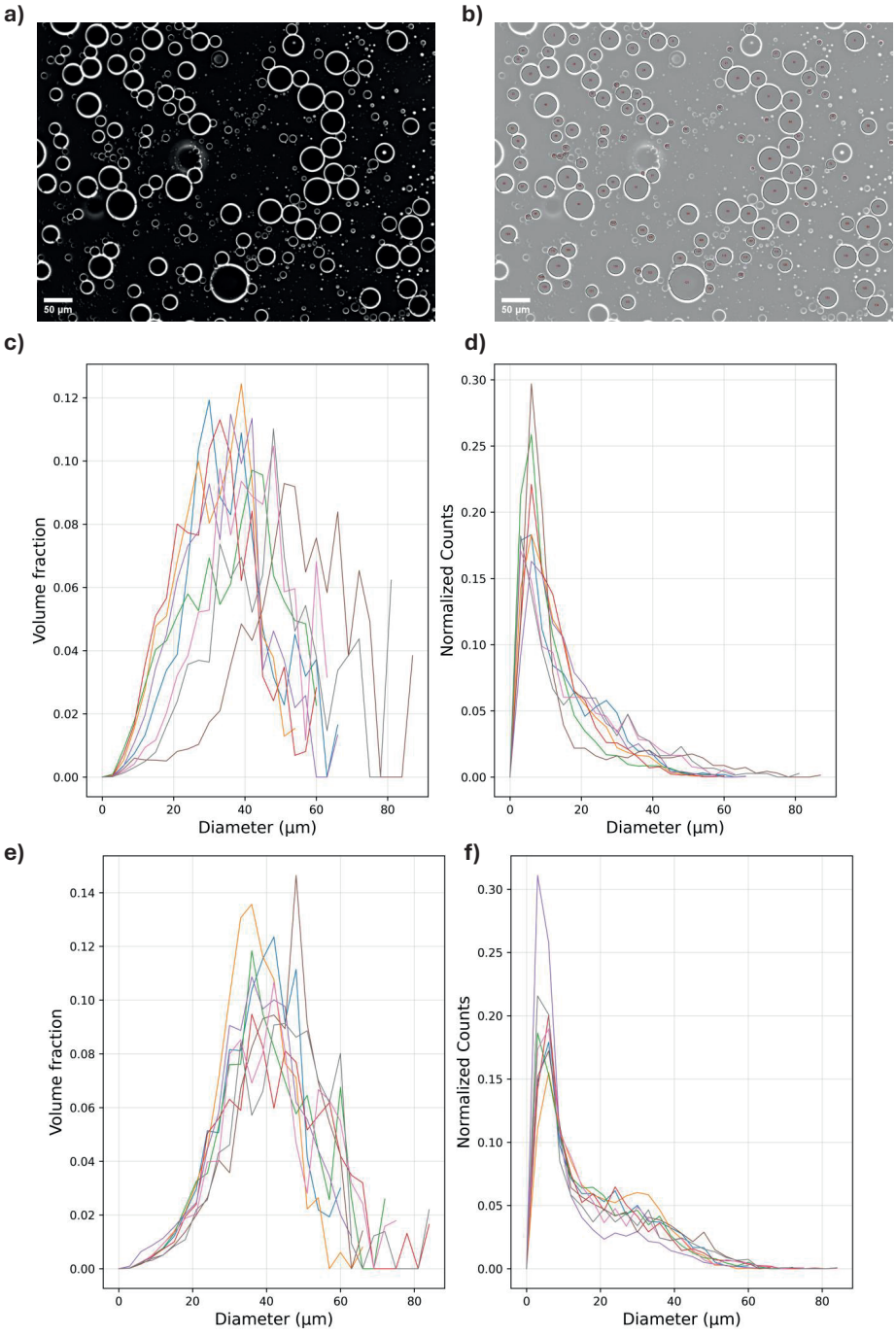

Figure S1: (a) Microscopic image of agarose microbeads. (b) Agarose microbeads identified in (a) by ImageJ analysis. (c and e) Microbead diameter distribution based on volume fraction of the water phase for with 8% (wt/v) glucose and HCSM with 8% (wt/v) glucose medium respectively and (d and f) Microbead diameter distribution based on counts for HCYP with 8% (wt/v) glucose and HCSM with 8% (wt/v) glucose medium respectively, counts were normalized to the total number of microbeads analysed per emulsion.

Supplementary section 4: Poisson distribution

To prevent inoculation of microbeads with multiple cells, we aimed to minimise microbeads with 2 or more cells. At a λ-value of 0.2, 90% of the inoculated microbeads contain 1 cell. Although at a lower λ-value (such as a λ-value of 0.02), there are no microbeads with two or more cells, the proportion of filled microbeads is an order of magnitude lower, which reduces the throughput of the method by the same magnitude. We therefore decided to use a λ-value of 0.2.

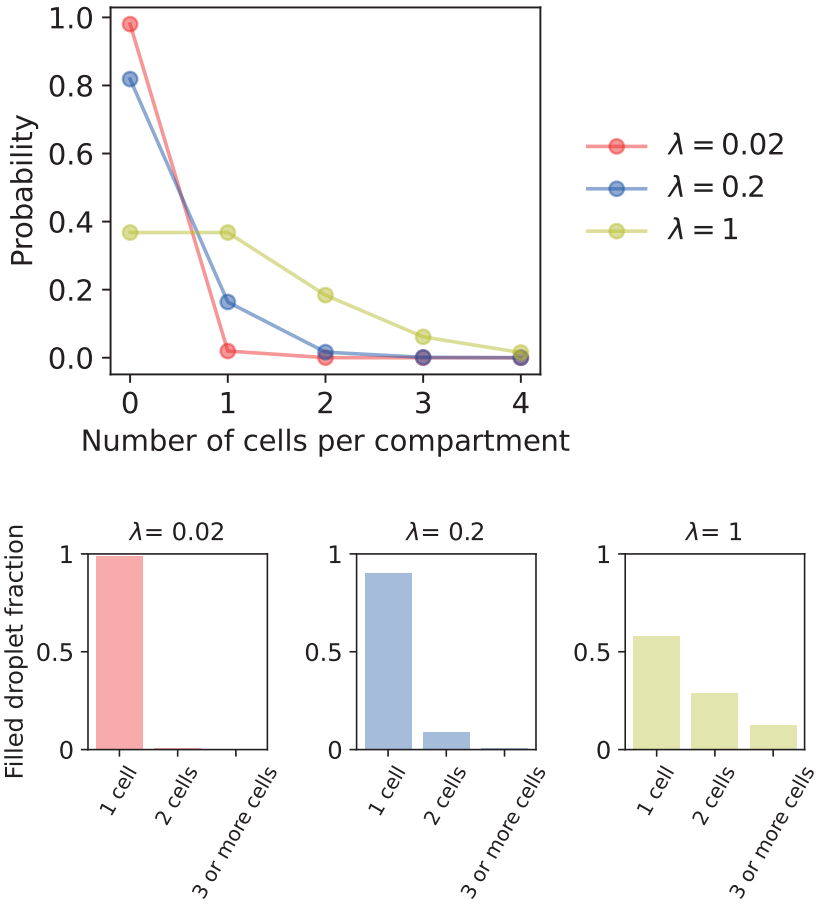

Figure S2: Poisson distribution for λ-values of 0.02, 0.2 and 1. The line plot shows the probability of compartments containing 0 to 4 cells per compartment. The bar plots show the fraction of filled compartments containing 1, 2 and 3 or more cells

Supplementary section 5: Gating strategy

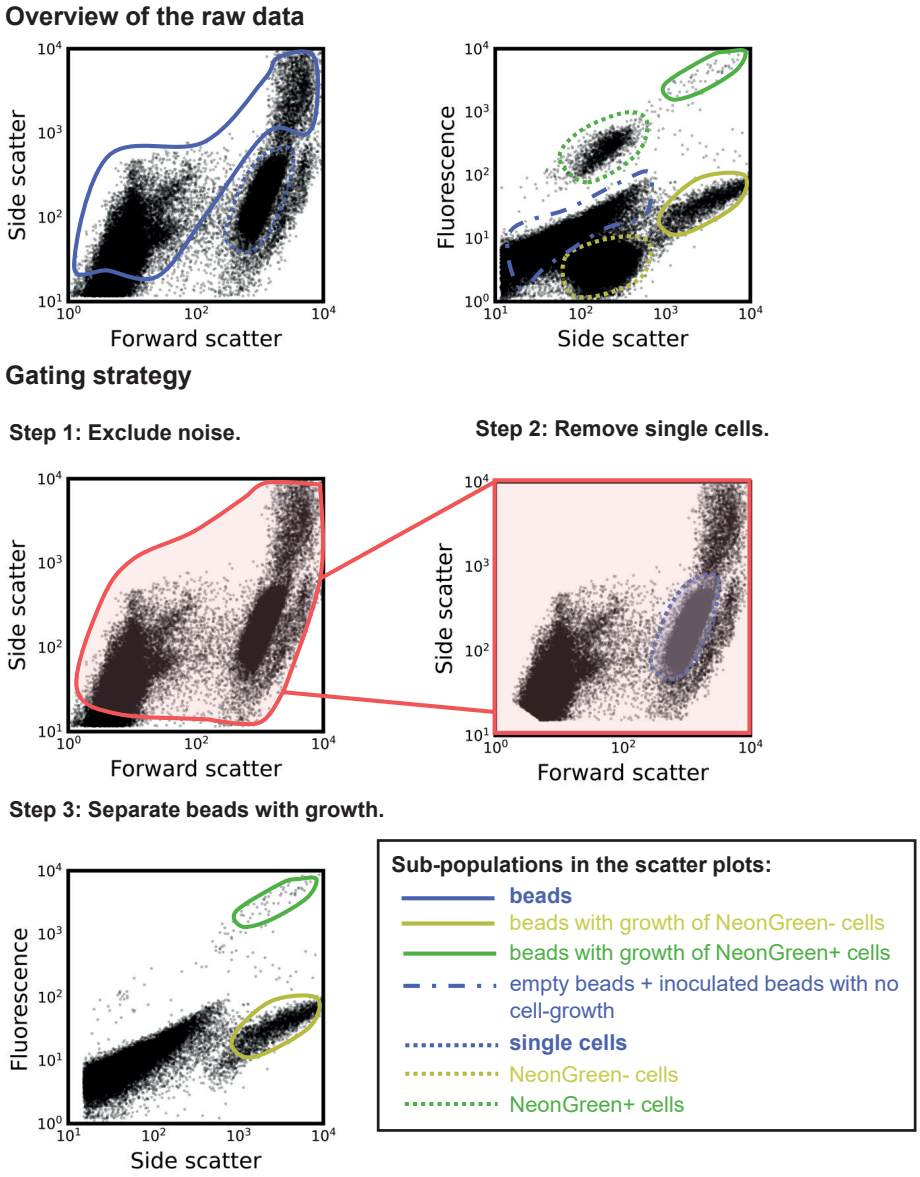

Figure S3: General gating strategy for flow cytometry data. Gating was performed using control samples representing individual sub-populations: single cells, empty microbeads, microbeads with growth of fluorescently labelled cells, and microbeads with growth of non-fluorescently labelled cells.

Supplementary section 6: Post-sorting survival of sensitive strain

We sorted 384 events identified as single cells and microbeads with growth (gated as shown in supplementary section 5) from sensitive strains grown in emulsions containing either G418 or 2-deoxyglucose in HCSM + 8% (wt/v) glucose or sucrose, respectively. The sorted cells were plated on a solid medium of YP + 2% (wt/v) glucose. Survival percentage was calculated by normalising the number of colonies observed after sorting to the total number of events sorted (=384 events) on the solid medium of YP + 2% (wt/v) glucose.

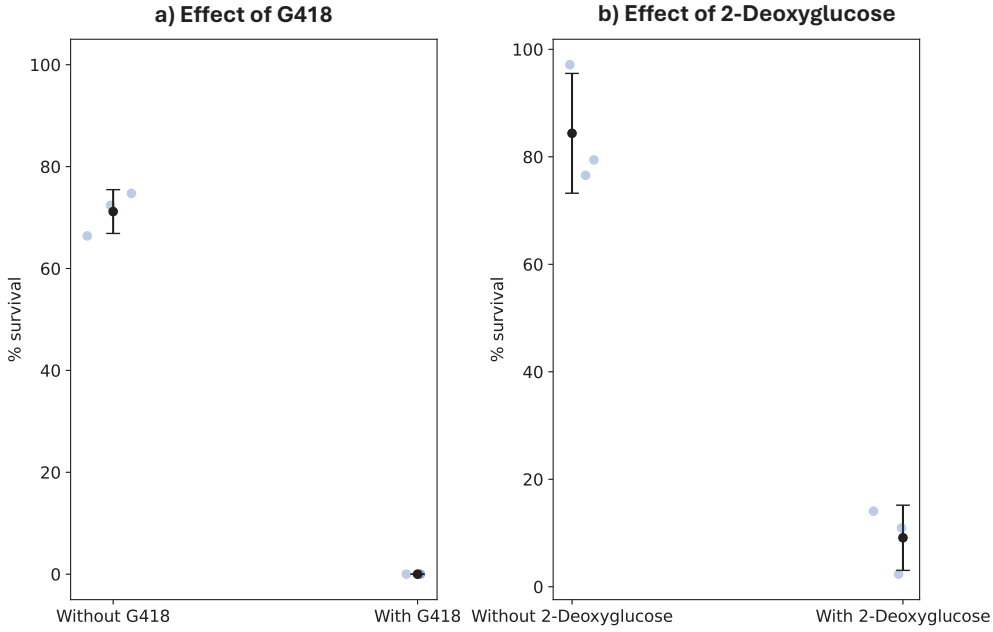

Figure S4: (a) Survival percentage after sorting cells from emulsions inoculated with a sensitive strain grown with or without G418 in HCSM + 8% (wt/v) glucose. (b) Survival percentage after sorting cells from emulsions of a sensitive strain grown with or without 2-deoxyglucose in HCSM + 8% (wt/v) sucrose. All samples were sorted on solid medium of YP + 2% (wt/v) glucose. The survival percentage was calculated by normalising the number of colonies observed after sorting to the total number of events sorted (=384 events) on YP + 2% (wt/v) glucose solid medium. Each coloured point represents the survival percentage of an individual replicate, and the black points represent the means and standard deviations.

References

1. Zeng W, Guo L, Xu S, Chen J, Zhou J. High-Throughput Screening Technology in Industrial Biotechnology. Trends in Biotechnology. 2020;38:888–906.
2. van Tatenhove-Pel RJ, Hernandez-Valdes JA, Teusink B, Kuipers OP, Fischlechner M, Bachmann H. Microdroplet screening and selection for improved microbial production of extracellular compounds. Current Opinion in Biotechnology. 2020;61:72–81.
3. Zhou S, Alper HS. Strategies for directed and adapted evolution as part of microbial strain engineering. Journal of Chemical Technology and Biotechnology. 2019;94:366–376.
4. Marshall RJ. Food Safety: A Practical and Case Study Approach. Springer-Verlag; 2006. ISBN: 978-0-387-33957-3
5. Marsit S, Dequin S. Diversity and adaptive evolution of *Saccharomyces* wine yeast: a review. FEMS Yeast Research. 2015;15.
6. Bachmann H, Pronk JT, Kleerebezem M, Teusink B. Evolutionary engineering to enhance starter culture performance in food fermentations. Current Opinion in Biotechnology. 2015;32:1–7.
7. Mans R, Daran JMG, Pronk JT. Under pressure: evolutionary engineering of yeast strains for improved performance in fuels and chemicals production. Current Opinion in Biotechnology. 2018;50:47–56.
8. Adrio JL, Demain AL. Genetic improvement of processes yielding microbial products. FEMS Microbiology Reviews. 2006;30:187–214.
9. Fiedurek J, Trytek M, Szczodrak J. Strain improvement of industrially important microorganisms based on resistance to toxic metabolites and abiotic stress. Journal of Basic Microbiology. 2017;57:445–459.
10. Cardoso JGR, Zeidan AA, Jensen K, Sonnenschein N, Neves AR, Herrgård MJ. MARSI: Metabolite analogues for rational strain improvement. Bioinformatics. 2018;34(13):2319–2321.
11. Luttik MAH, Vuralhan Z, Suir E, Braus GH, Pronk JT, Daran JM. Alleviation of feedback inhibition in *Saccharomyces cerevisiae* aromatic amino acid biosynthesis. Metabolic Engineering. 2008;10:141–153.
12. Jung MY, Jung HM, Lee J, Oh MK. Alleviation of carbon catabolite repression in *Enterobacter aerogenes*. Biotechnology for Biofuels. 2015;8:106.
13. Shrestha S, Awasthi D, Chen Y, Gin J, Petzold CJ, Adams PD, *et al*. Simultaneous carbon catabolite repression governs sugar and aromatic co-utilization in *Pseudomonas putida* M2. Applied and Environmental Microbiology. 2023;89(10).
14. Fox KJ, Prather KL. Carbon catabolite repression relaxation in *Escherichia coli*. Current Opinion in Chemical Engineering. 2020;30:9–16.

15. Gao M, Ploessl D, Shao Z. Enhancing the co-utilization of biomass-derived mixed sugars by yeasts. Frontiers in Microbiology. 2019;9.

16. McCartney RR, Chandrashekarappa DG, Zhang BB, Schmidt MC. Genetic analysis of resistance and sensitivity to 2-deoxyglucose in *Saccharomyces cerevisiae*. Genetics. 2014;198:635–646.

17. Neigeborn L, Carlson M. Mutations causing constitutive invertase synthesis in yeast. Genetics. 1987;115:247–253.

18. Soncini SR, Chandrashekarappa DG, Augustine DA, Callahan KP, O'Donnell AF, Schmidt MC. Spontaneous mutations that confer resistance to 2-deoxyglucose. PLoS Genetics. 2020;16(7).

19. Castrillo JI, Kaliterna J, Weusthuis RA, Van Dijken JP, Pronk JT. High-cell-density cultivation of yeasts on disaccharides. Biotechnology and Bioengineering. 1996;49:621–628.

20. Lõoke M, Kristjuhan K, Kristjuhan A. Extraction of genomic DNA from yeasts for PCR-based applications. Biotechniques. 2011;50:325–328.

21. Gietz RD, Woods RA. Transformation of yeast by lithium acetate/SS-DNA/PEG method. Methods in Enzymology. 2002;350:87–96.

22. Boonekamp FJ, Knibbe E, Vieira-Lara MA, Wijsman M, Luttik MAH, van Eunen K, *et al*. Full humanization of the glycolytic pathway in *Saccharomyces cerevisiae*. Cell Reports. 2022;39:111010.

23. Mans R, van Rossum HM, Wijsman M, Backx A, Kuijpers NGA, van den Broek M, *et al*. CRISPR/Cas9: A molecular Swiss army knife for yeast genome engineering. FEMS Yeast Research. 2015;15(2).

24. Lee ME, DeLoache WC, Cervantes B, Dueber JE. A highly characterized yeast toolkit for modular, multipart assembly. ACS Synthetic Biology. 2015;4:975–986.

25. Botman D, de Groot DH, Schmidt P, Goedhart J, Teusink B. In vivo characterisation of fluorescent proteins in budding yeast. Scientific Reports. 2019;9.

26. van den Broek M, Ortiz-Merino RA, Bennis NX, Wronska AK, Hassing EJ, Daran-Lapujade P, *et al*. Draft genome sequence of the *Saccharomyces cerevisiae* Spy Cas9 expressing strain IMX2600. Microbiology Resource Announcements. 2024;13(2).

27. van Tatenhove-Pel RJ, Rijavec T, Lapanje A, van Swam I, Zwering E, Hernandez-Valdes JA, *et al*. Microbial competition reduces metabolic interaction distances to the low µm-range. ISME Journal. 2021;15:688–701.

28. Wach A, Brachat A, Pöhlmann R, Philippsen P. New heterologous modules for gene disruptions in *Saccharomyces cerevisiae*. Yeast. 1994;10:1793–1808.

29. Siano SA, Mutharasan R. NADH and flavin fluorescence responses of starved yeast cultures. Biotechnology and Bioengineering. 1989;34:660–670.

30. Podrazký O, Kuncová G, Krasowska A, Sigler K. Monitoring yeast growth and stress responses by two-dimensional fluorescence spectroscopy. Folia Microbiologica. 2003;48.

31. Maslanka R, Kwolek-Mirek M, Zadrag-Tecza R. Autofluorescence of *Saccharomyces cerevisiae* cells caused by glucose metabolism products. Journal of Microbiological Methods. 2018;146:55–60.

32. Laussel C, Léon S. Cellular toxicity of the metabolic inhibitor 2-deoxyglucose and associated resistance mechanisms. Biochemical Pharmacology. 2020;182.

33. Schmidt MC, O'Donnell AF. 'Sugarcoating' 2-deoxyglucose: mechanisms that suppress its toxic effects. Current Genetics. 2021;67:107–114.

34. Luzia L, Battjes J, Zwering VE, Jansen DB, Melkonian C, Teusink B. A fast method to distinguish fermentative and respiratory metabolisms in single yeast cells. bioRxiv. 2023.

35. Kehe J, Kulesa A, Ortiz A, Ackerman CM, Thakku SG, Sellers D, *et al*. Massively parallel screening of synthetic microbial communities. PNAS. 2019;116:12804–12809.

36. Maurice CF, Turnbaugh PJ. Quantifying the metabolic activities of human-associated microbial communities. FEMS Microbiology Reviews. 2013;37:830–848.

37. Skhiri Y, Gruner P, Semin B, Brosseau Q, Pekin D, Mazutis L, *et al*. Dynamics of molecular transport by surfactants in emulsions. Soft Matter. 2012;8:10618–10627.

38. Gruner P, Riechers B, Semin B, Lim J, Johnston A, Short K, *et al*. Controlling molecular transport in minimal emulsions. Nature Communications. 2016;7:10392.

39. Scheler O, Kaminski TS, Ruszczak A, Garstecki P. Dodecylresorufin outperforms resorufin in microdroplet bacterial assays. ACS Applied Materials & Interfaces. 2016;8:11318–11325.

40. Royal Society of Chemistry (2025) ChemSpider. https://www.chemspider.com. Accessed 4 Sept 2025

41. Kayikci Ö, Nielsen J. Glucose repression in *Saccharomyces cerevisiae*. FEMS Yeast Research. 2015;15:fov068.

42. Raamsdonk LM, Diderich JA, Kuiper A, Van Gaalen M, Kruckberg AL, Berden JA, *et al*. Co-consumption of sugars or ethanol and glucose in an *HXK2*-deleted yeast strain. Yeast. 2001;18:1023–1033.

43. Basso TO, de Kok S, Dario M, do Espirito-Santo JCA, Müller G, Schlölg PS, *et al*. Engineering sucrose metabolism in *Saccharomyces cerevisiae*. Metabolic Engineering. 2011;13:694–703.

44. Boedicker JQ, Li L, Kline TR, Ismagilov RF. Detecting bacteria by stochastic confinement in nanoliter droplets. Lab on a Chip. 2008;8:1265–1272.

45. Agnihotri SN, Fatsis-Kavalopoulos N, Windhager J, Tenje M, Andersson DI. Droplet

microfluidics-based detection of rare antibiotic-resistant subpopulations. Science Advances. 2025;11:4558.

46. Güldener U, Heck S, Fiedler T, Beinhauer J, Hegemann JH. A new efficient gene disruption cassette for repeated use in budding yeast. Nucleic Acids Research. 1996;24:2519–2524.

47. Wronska AK, Haak MP, Geraats E, Slot EB, van den Broek M, Pronk JT, *et al*. Engineering biotin-independent growth in *Saccharomyces cerevisiae*. Applied and Environmental Microbiology. 2020;86(12).

48. Bennis NX, Kostanjšek M, van den Broek M, Daran JMG. Improving CRISPR-Cas9 genome integration in interspecific hybrid yeasts. New Biotechnology. 2023;76:49–62.

49. Koster CC, Kleefeldt AA, van den Broek M, Luttik M, Daran JM, Daran-Lapujade P. Long-read direct RNA sequencing of the mitochondrial transcriptome of *Saccharomyces cerevisiae*. Yeast. 2024;41:256–278.

50. Bouwknegt J, Wiersma SJ, Ortiz-Merino RA, Doornenbal ESR, Buitenhuis P, Giera M, *et al*. A squalene-hopene cyclase in *Schizosaccharomyces japonicus*. PNAS. 2021;118:e2105225118.

Chapter 3

Saccharomyces cerevisiae mutants selected by propagation in water-in-oil emulsion cultures exhibit increased biomass and cell number yields on glucose in aerobic batch cultures.

Sagarika B. Govindaraju, Marius Dohmen, Jack T. Pronk and Rinke J. van Tatenhove-Pel

Abstract

Saccharomyces cerevisiae can dissimilate glucose either by respiration or by fermentation. Although respiration yields approximately eight-fold more ATP per mole of glucose, *S. cerevisiae* predominantly ferments glucose even under aerobic conditions when this substrate is present in excess. The lower ATP stoichiometry of (respiro)fermentative metabolism is reflected by lower biomass yields on glucose. Growth in water-in-oil emulsions, in which micro-compartmentalisation leads to the privatisation of glucose, confers a selective advantage to mutants with a higher cell number yield on glucose. In a previous study, a chemically mutagenised *S. cerevisiae* population was serially propagated in water-in-oil emulsions. In this study, we characterise the resulting isolates. As anticipated, most isolates showed higher biomass yields and lower ethanol yields in aerobic, glucose-grown batch suspension cultures. Whole-genome sequencing revealed that all emulsion-propagated isolates contained single-nucleotide mutations in *HXK2*, which encodes the predominant hexokinase enzyme in glucose-grown *S. cerevisiae*. To test the hypothesis that these mutations were responsible for a shift towards a more respiratory metabolism and, consequently, to higher biomass yields, they were reverse engineered into two different, non-evolved *S. cerevisiae* strain backgrounds. All the reverse engineered strains showed higher biomass yields and lower ethanol yields. Comparisons with *hxk2Δ* strains indicated that the mutations in *HXK2* eliminated the catalytic activity of hexokinase. In two different genetic backgrounds, higher biomass yields on glucose of the reverse engineered strains were accompanied by higher cell number yields and reduced cell sizes. These findings demonstrate that emulsion-based selection can enrich *S. cerevisiae* variants with an improved ATP stoichiometry of dissimilatory metabolism.

1. Introduction

A central question in microbiology is how microorganisms reorganise their metabolism in response to changing environmental conditions. Many microorganisms and mammalian cells can dissimilate sugars such as glucose via two or more different pathways with different ATP stoichiometries (1–6). However, even under conditions that in principle allow for the use of the pathway with the highest ATP stoichiometry, many organisms employ a less ATP-efficient pathway. This phenomenon is known as overflow metabolism (the Warburg effect in cancer cells and the Crabtree effect in yeasts) (1,4,7). From an evolutionary perspective, overflow metabolism has been explained as an ability of the less efficient dissimilation pathway to support faster growth, albeit at a lower biomass yield (8–10).

Overflow metabolism is observed in several industrially relevant microorganisms (2,3,5,6), including *Saccharomyces cerevisiae*. This yeast is used for industrial production of a wide range of compounds, including ethanol, pharmaceuticals, hydrocarbons and organic acids (11,12). *S. cerevisiae is* a facultative fermentative yeast that, under anaerobic conditions, ferments glucose to ethanol. This fermentative glucose metabolism yields 2 mol ATP (mol glucose)$^{-1}$ and enables a biomass yield on glucose of 0.1 g biomass (g glucose)$^{-1}$ (6,8,9,13). Under aerobic conditions, a fully respiratory dissimilation of glucose to carbon dioxide and water can, in this yeast, generate up to 16 mol ATP (mol glucose)$^{-1}$, which supports a biomass yield of 0.5 g biomass (g glucose)$^{-1}$ (6,8,9,13). Although respiration of glucose has a higher ATP stoichiometry than glucose fermentation, it supports a lower maximum specific growth rate (6,8,9). In sugar-limited cultures of *S. cerevisiae*, such as chemostat or fed-batch cultures, glucose dissimilation is fully respiratory at low specific growth rates and, above a threshold specific growth rate, becomes respiro-fermentative. This onset of alcoholic fermentation coincides with a decrease in the biomass yield on glucose (6,8,9).

Several hypotheses may explain why *S. cerevisiae* does not exhibit a fully respiratory dissimilation of glucose in aerobic batch cultures. The occurrence of the Crabtree effect in *S. cerevisiae* has been attributed to limitations on the capacity of metabolic pathways involved in respiratory metabolism, constraints on proteome allocation, imbalances in redox-cofactors, or limits to Gibbs free-energy dissipation (6,14–18). However, there is a broad consensus that aerobic fermentation confers a selective advantage in glucose-rich environments: fermentation enables faster growth and, thereby, helps to outcompete other microorganisms (19,20). Ethanol formation may have a further advantage in natural environments, as it inhibits many competing species more strongly than the yeast itself (20,21). Moreover, *S. cerevisiae* can subsequently re-assimilate the ethanol (19,20), although fermentation followed by ethanol assimilation comes at a cost of an additional 4 mol ATP (mol glucose)$^{-1}$, compared to the complete respiration of the sugar (22).

Previous studies investigating the causes and ecological consequences of overflow

metabolism in *S. cerevisiae* mostly relied on theoretical models (14–16,18) and experimental analyses of known metabolic targets (23–26). Laboratory evolution provides an attractive approach to uncover novel genetic mutations that promote higher biomass yields. Typically, such experiments are performed in well-mixed suspension cultures, where selection pressure primarily favours faster growth (27,28). Spatially structured environments, such as water-in-oil emulsions, impose a different selective regime. Within these emulsions, single cells are encapsulated in droplets, surrounded by an oil phase in which glucose is insoluble. This compartmentalisation privatises glucose, eliminates competition for the sugar between cells in different microdroplets, and thereby favours cells that efficiently convert glucose into biomass, even when their growth rate is low. Over successive propagations, which involve breaking up the emulsion after each growth cycle, this setup enriches for cells with higher cell number yields on the substrate (29–31). Bachmann *et al.* (2013) (30) demonstrated this principle in microdroplet cultivation experiments with *Lactococcus cremoris*. In these experiments, selection was shown to lead to a metabolic shift from homolactic (2 mol ATP (mol glucose)$^{-1}$) to mixed-acid fermentation (3 mol ATP (mol glucose)$^{-1}$). Although the selection pressure in micro-compartmented systems is primarily on cell-number yield, Bachmann *et al.* (2013) (30) showed that increased cell-number yield can correlate with an increased biomass yield (as opposed to selecting for smaller cells without a change in biomass yield). In a similar study, van Tatenhove-Pel *et al.* (2021) (29) serially propagated chemically mutagenized *S. cerevisiae* cells in glucose-containing water-in-oil emulsions. When these mutants were characterised in aerobic batch suspension cultures, they exhibited increased cell-number yield but not increased biomass yield. However, the standard deviations reported for biomass yield data were high (29). The present study aims to reinvestigate whether serial propagations in water-in-oil emulsions favour the selection of increased biomass yields in addition to increased cell-number yields.

Interestingly, all isolates enriched by van Tatenhove-Pel *et al.* (2021) (29) contained single-nucleotide mutations in the *HXK2* gene, in addition to harbouring mutations in cell-cycle and glucose repression genes. *HXK2* encodes the major isoenzyme of hexokinase in *S. cerevisiae*. The occurrence of different single-nucleotide *HXK2* mutations in independently evolved cell lines suggested that they were involved in the modulation of glycolytic flux and, thereby, affected the distribution of glucose carbon over respiration and fermentation. In addition to recharacterising the emulsion-propagated isolates, the present study also seeks to determine whether the identified *HXK2* mutations alone can recapitulate the phenotypes observed in the enriched isolates. The mutations in *HXK2* were reverse engineered in two different, non-mutagenized *S. cerevisiae* laboratory strain backgrounds, and their impact on the *in vivo* activity of Hxk2 was assessed in growth studies after their introduction in a *hxk1* and *hxk2* null background.

2. Materials and Methods

2.1. Strains and maintenance

Saccharomyces cerevisiae strains used in this study are shown in Table 1. Plasmids (Table S2) were propagated in *Escherichia coli* XL1-Blue cells (Agilent, Santa Clara, CA, USA). For long-term storage at -80 °C, glycerol was added to late-exponential-phase *S. cerevisiae* cultures and overnight *E. coli* cultures to obtain final concentrations of 30% (v/v) and 25% (v/v), respectively.

2.2. Media and cultivation

E. coli cultures were grown at 37 °C in LB medium supplemented with 100 μg L^{-1} ampicillin for maintenance of plasmids. *S. cerevisiae* strains were grown at 30 °C in synthetic medium (SM) (32). The medium was supplemented with 20 g L^{-1} glucose, 20 g L^{-1} galactose or 20 g L^{-1} fructose. When *kanMX, natNT2* or *hphNT1* markers were used for selection, 200 mg L^{-1} G418, 100 mg L^{-1} nourseothricin or 200 mg L^{-1} hygromycin B, respectively, were added to the media. Solid medium plates were prepared by adding 2% (w/v) agar to the media. Aerobic shake-flask cultures were grown at 200 rpm in an Innova incubator shaker (New Brunswick Scientific, Edison, NJ), in 100-mL or 500-mL round-bottom flasks containing 20 mL or 100 mL medium, respectively. For the preparation of spot plates, strains were pre-grown on SM with 20 g/L galactose, and exponentially growing cells were harvested by centrifugation at 3000 g for 5 min at 4 °C, washed with sterile water, resuspended to a concentration of 10^7 cells mL^{-1} and subsequently diluted to 10^6, 10^5, 10^4 and 10^2 cells mL^{-1}. 10 μL of each dilution was plated on SM solid medium plates supplemented with 20 g L^{-1} glucose or 20 g L^{-1} fructose. Plates were incubated for three days at 30 °C.

2.3. Molecular biology techniques

Plasmids were isolated from *E. coli* using the GeneJET Plasmid Miniprep Kit (Thermo Fisher Scientific). Genomic *S. cerevisiae* DNA was isolated as previously described by Lõoke et al. (2011) (33). DNA amplifications were performed using Phusion High-Fidelity DNA polymerase (Thermo Fisher Scientific, Waltham, MA, USA) for cloning, and DreamTaq PCR Mastermix (Thermo Fisher Scientific) for diagnostic PCRs. For isolation of DNA fragments from the PCR reaction mixture, GeneJET PCR Purification Kit (Thermo Fisher Scientific) was used. DNA fragments were separated and visualised on a 1% (wt/v) agarose TAE gel by 30 min electrophoresis at 100 V. The DNA fragments excised from the gel were purified using a Zymoclean Gel DNA recovery Kit (Baseclear). Gibson assembly of plasmids was performed with the NEBuilder HiFi DNA Assembly Master Mix (New England Biolabs, Ipswich, MA, USA) and the resulting plasmids were propagated in XL1-Blue chemically competent *E. coli* cells. *S. cerevisiae* strains were transformed with the LiAC/ssDNA/PEG method (Gietz & Woods, 2002) (34). After transformation, gRNA plasmids were removed as described by Mans *et al.* (2015) (35) and the single colonies were re-streaked at least three consecutive times to ensure

isogenic single cell lines. Correct genomic insertion was verified by diagnostic PCR on isolated genomic DNA. Oligonucleotide primers used in this study are listed in Table S3.

2.4. Plasmid construction

pUDR869 was constructed by Gibson assembly of two PCR-amplified fragments derived from pROS12 as a template: a linearised backbone obtained with primer 6005 and a 2µm fragment amplified with primer 20063. pUDR870 was generated in the same manner, except that the 2µm fragment was amplified with primers 20063 and 12923.

2.5. Strain construction

A Cas9 expression cassette was integrated at the *CAN1* locus of *S. cerevisiae* S288C by in vivo assembly and integration of two cassettes containing Cas9 and the *natNT2* marker, respectively, resulting in the strain IMX2747. The Cas9 cassette was PCR amplified from p*414-TEF1*p-*cas9-CYC1*t (36) using primers 2873 and 4653. The *natNT2* cassette was PCR amplified from pUG-natNT2 using primers 3093 and 5542. The *HXK2* gene in strain IMX2747 was deleted by introducing pUDR371, along with a double-stranded DNA repair fragment obtained by annealing primers 18833 and 18834, resulting in strain IMX2764.

HXK2 alleles carrying point mutations were PCR amplified from genomic DNA of the emulsion-propagated *S. cerevisiae* isolates EZ11, EZ12, EZ14, EZ27, EZ31, EZ36 and EZ37 with primers 2794 and 5319. The *HXK2* variants of the mentioned EZ strains were integrated into *S. cerevisiae* IMX2748 along with pUDR471, resulting in strains IMX2756 (based on EZ11), IMX2761 (based on EZ12), IMX2757 (based on EZ14), IMX2758 (based on EZ27), IMX2762 (based on EZ31), IMX2763 (based on EZ35) and IMX2760 (based on EZ37). Using the same approach, *HXK2* variants were integrated into IMX2764, resulting in the strains IMX2824 (based on EZ11), IMX2825 (based on EZ12), IMX2828 (based on EZ14), IMX2826 (based on EZ27), IMX2827 (based on EZ31), IMX2829 (based on EZ35) and IMX2830 (based on EZ37). Strains IMX2824, IMX2825, IMX2828, and IMX2829 were found to have lost respiratory competence (Figure S3). The relevant transformations were therefore repeated with the same procedure, except that transformants were selected based on growth on a mixture of ethanol and glycerol. This approach yielded the respiratory competent strains in IMX3186 (based on EZ11), IMX3187 (based on EZ12), IMX3188 (based on EZ14), and IMX3189 (based on EZ36). In strains IMX2600, IMX2748, IMX2756, IMX2761, IMX2757, IMX2758, IMX2762, IMX2763 and IMX2760, *HXK1* was deleted by introducing pUDR869 together with a double-stranded DNA repair fragment obtained by annealing primers 20064 and 20065, resulting in strains IMK1067, IMK1090, IMK1078, IMK1071, IMK1068, IMK1070, IMK1081, IMK1080 and IMK1079. An overview of the strains is provided in Figure S6.

In strains IMX2757 and IMX2600, *HXK1* and *GLK1* were deleted by introducing pUDR870 along with a double-stranded DNA repair fragment obtained by annealing

primers 20064 and 20065 and 12925 and 12926, resulting in strains IMK1069 and IMK1066, respectively. IMK1119 was constructed by transforming IMK1066 with pUDR371 together with a double-stranded DNA repair fragment obtained by annealing primers 18833 and 18834.

2.6. Analytical methods

Optical density (OD) of cultures was measured at 660 nm using a Libra S11 spectrophotometer (Biochrom, Cambridge, United Kingdom). Cell concentration was measured using a BD Accuri™ C6 Plus flow cytometer (BD Biosciences, San Jose, CA, USA). Cell size was measured using a Beckman Multisizer 4e Coulter Counter (Beckman Coulter, Brea, CA, USA). Dry weight was measured by filtering 20 mL culture on a pre-weighed nitrocellulose filter with a pore size of 0.45 µm; the filters were washed with demineralised water and dried for 20 min in a microwave oven at 360 W and weighed again. Concentrations of sugars, organic acids, and ethanol were measured via HPLC analysis on an Agilent 1260 HPLC (Agilent Technologies, CA, USA), equipped with a Bio-Rad HPX 87H column (Bio-Rad, CA, USA). Detection was performed by an Agilent refractive index detector and an Agilent 1260 VWD detector.

2.7. Calculations

Specific growth rate was calculated by linear regression of plots of $\log_{10}OD_{660}$ versus time during the exponential growth phase on glucose. Biomass yield on glucose was calculated by measuring dry weight at two time points during exponential growth (after the culture reached an OD_{660} of 5), along with the corresponding amount of glucose consumed. Biomass directly after inoculation was assumed to be negligible. Ethanol yield on glucose was determined by linear regression of ethanol produced versus glucose consumed. Cell number yield on glucose was calculated from the linear regression of the number of cells produced versus glucose consumed. Cell volume was calculated from cell diameter, assuming a spherical shape, measured at two time points during exponential growth (OD_{660} between 1.5 and 4).

Statistical analyses were performed using one-tailed t-tests, with p-values < 0.05 considered statistically significant.

2.8. Structural modelling of Hxk2 proteins

Homology modelling of wild type and mutant variants of Hxk2 was performed using ColabFold (37). The top-ranked predicted structures (rank 1, unrelaxed, i.e., highest-confidence models without energy-based refinement) were aligned and visualised in PyMol.

Table 1: *S. cerevisiae* strains used in this study. Strains marked with * showed no growth on non-fermentable carbon sources, ethanol and glycerol and were subsequently reconstructed to strains indicated by **.

Strain name	Relevant genotype	Parental Strain	Source
S288C	*MATα SUC2 URA3 HIS3 LEU2 TRP1 gal2 mal2 mel flo1 flo8-1 hap1 ho bio1 bio6*	-	-
CEN.PK113-7D	*MATa SUC2 URA3 HIS3 LEU2 TRP1 MAL2-8c*	-	-
EZ11	Enriched S288C with *HXK2* (T212I)	S288C	(29)
EZ12	Enriched S288C with *HXK2* (G235D)	S288C	(29)
EZ14	Enriched S288C with *HXK2* (G311D)	S288C	(29)
EZ27	Enriched S288C with *HXK2* (G461D)	S288C	(29)
EZ31	Enriched S288C with *HXK2* (P74S+T212I)	S288C	(29)
EZ36	Enriched S288C with *HXK2* (G418D)	S288C	(29)
EZ37	Enriched S288C with *HXK2* (S158F)	S288C	(29)
IMX2747	*MATα SUC2 URA3 HIS3 LEU2 TRP1 gal2 mal2 mel flo1 flo8-1 hap1 ho bio1 bio6 can1Δ::cas9-natNT2*	S288C	This study
IMX2600	*MATa SUC2 URA3 HIS3 LEU2 TRP1 MAL2-8c can1Δ::cas9-natNT2*	CEN.PK113-7D	(38)
IMX2764	*MATα SUC2 URA3 HIS3 LEU2 TRP1 gal2 mal2 mel flo1 flo8-1 hap1 ho bio1 bio6 can1Δ::cas9-natNT2 hxk2Δ::SynPAM*	IMX2747	This study
IMX2824*	*MATα SUC2 URA3 HIS3 LEU2 TRP1 gal2 mal2 mel flo1 flo8-1 hap1 ho bio1 bio6 can1Δ::cas9-natNT2 hxk2Δ::HXK2(T212I)*	IMX2764	This study
IMX2825*	*MATα SUC2 URA3 HIS3 LEU2 TRP1 gal2 mal2 mel flo1 flo8-1 hap1 ho bio1 bio6 can1Δ::cas9-natNT2 hxk2Δ::HXK2(G235D)*	IMX2764	This study
IMX2826	*MATα SUC2 URA3 HIS3 LEU2 TRP1 gal2 mal2 mel flo1 flo8-1 hap1 ho bio1 bio6 can1Δ::cas9-natNT2 hxk2Δ::HXK2*(G461D)	IMX2764	This study
IMX2827	*MATα SUC2 URA3 HIS3 LEU2 TRP1 gal2 mal2 mel flo1 flo8-1 hap1 ho bio1 bio6 can1Δ::cas9-natNT2 hxk2Δ::HXK2*(P74S+T212I)	IMX2764	This study
IMX2828*	*MATα SUC2 URA3 HIS3 LEU2 TRP1 gal2 mal2 mel flo1 flo8-1 hap1 ho bio1 bio6 can1Δ::cas9-natNT2 hxk2Δ::HXK2*(G311D)	IMX2764	This study

IMX2829*	*MATα SUC2 URA3 HIS3 LEU2 TRP1 gal2 mal2 mel flo1 flo8-1 hap1 ho bio1 bio6 can1Δ::cas9-natNT2 hxk2Δ::HXK2*(G418D)	IMX2764	This study
IMX2830	*MATα SUC2 URA3 HIS3 LEU2 TRP1 gal2 mal2 mel flo1 flo8-1 hap1 ho bio1 bio6 can1Δ::cas9-natNT2 hxk2Δ::HXK2*(S158F)	IMX2764	This study
IMX3186**	*MATα SUC2 URA3 HIS3 LEU2 TRP1 gal2 mal2 mel flo1 flo8-1 hap1 ho bio1 bio6 can1Δ::cas9-natNT2 hxk2Δ::HXK2(T212I)*	IMX2764	This study
IMX3187**	*MATα SUC2 URA3 HIS3 LEU2 TRP1 gal2 mal2 mel flo1 flo8-1 hap1 ho bio1 bio6 can1Δ::cas9-natNT2 hxk2Δ::HXK2(G235D)*	IMX2764	This study
IMX3188**	*MATα SUC2 URA3 HIS3 LEU2 TRP1 gal2 mal2 mel flo1 flo8-1 hap1 ho bio1 bio6 can1Δ::cas9-natNT2 hxk2Δ::HXK2*(G311D)	IMX2764	This study
IMX3189**	*MATα SUC2 URA3 HIS3 LEU2 TRP1 gal2 mal2 mel flo1 flo8-1 hap1 ho bio1 bio6 can1Δ::cas9-natNT2 hxk2Δ::HXK2*(G418D)	IMX2764	This study
IMX2748	*MATa SUC2 URA3 HIS3 LEU2 TRP1 MAL2-8c can1Δ::cas9-natNT2 hxk2Δ:: SynPAM*	IMX2600	Chapter 2
IMX2756	*MATa SUC2 URA3 HIS3 LEU2 TRP1 MAL2-8c can1Δ::cas9-natNT2 hxk2Δ::HXK2(T212I)*	IMX2748	This study
IMX2757	*MATa SUC2 URA3 HIS3 LEU2 TRP1 MAL2-8c can1Δ::cas9-natNT2 hxk2Δ::HXK2*(G311D)	IMX2748	This study
IMX2758	*MATa SUC2 URA3 HIS3 LEU2 TRP1 MAL2-8c can1Δ::cas9-natNT2 hxk2Δ::HXK2*(G461D)	IMX2748	This study
IMX2760	*MATa SUC2 URA3 HIS3 LEU2 TRP1 MAL2-8c can1Δ::cas9-natNT2 hxk2Δ::HXK2*(S158F)	IMX2748	This study
IMX2761	*MATa SUC2 URA3 HIS3 LEU2 TRP1 MAL2-8c can1Δ::cas9-natNT2 hxk2Δ::HXK2(G235D)*	IMX2748	This study
IMX2762	*MATa SUC2 URA3 HIS3 LEU2 TRP1 MAL2-8c can1Δ::cas9-natNT2 hxk2Δ::HXK2*(P74S+T212I)	IMX2748	This study
IMX2763	*MATa SUC2 URA3 HIS3 LEU2 TRP1 MAL2-8c can1Δ::cas9-natNT2 hxk2Δ::HXK2*(G418D)	IMX2748	This study
IMK1066	*MATa SUC2 URA3 HIS3 LEU2 TRP1 MAL2-8c can1Δ::cas9-natNT2 hxk1Δ glk1Δ*	IMX2600	This study
IMK1067	*MATa SUC2 URA3 HIS3 LEU2 TRP1 MAL2-8c can1Δ::cas9-natNT2 hxk1Δ*	IMX2600	This study

IMK1068	*MATa SUC2 URA3 HIS3 LEU2 TRP1 MAL2-8c can1Δ::cas9-natNT2 hxkΔ::HXK2*(G311D) *hxk1Δ*	IMX2757	This study
IMK1069	*MATa SUC2 URA3 HIS3 LEU2 TRP1 MAL2-8c can1Δ::cas9-natNT2 hxk2Δ::HXK2*(G311D) *hxk1Δ glk1Δ*	IMX2757	This study
IMK1070	*MATa SUC2 URA3 HIS3 LEU2 TRP1 MAL2-8c can1Δ::cas9-natNT2 hxk2Δ::HXK2*(G461D) *hxk1Δ*	IMX2758	This study
IMK1071	*MATa SUC2 URA3 HIS3 LEU2 TRP1 MAL2-8c can1Δ::cas9-natNT2 hxk2Δ::HXK2(G235D) hxk1Δ*	IMX2761	This study
IMK1078	*MATa SUC2 URA3 HIS3 LEU2 TRP1 MAL2-8c can1Δ::cas9-natNT2 hxk2Δ::HXK2(T212I) hxk1Δ*	IMX2756	This study
IMK1079	*MATa SUC2 URA3 HIS3 LEU2 TRP1 MAL2-8c can1Δ::cas9-natNT2 hxk2Δ::HXK2*(S158F) *hxk1Δ*	IMX2760	This study
IMK1080	*MATa SUC2 URA3 HIS3 LEU2 TRP1 MAL2-8c can1Δ::cas9-natNT2 hxk2Δ::HXK2*(G418D) *hxk1Δ*	IMX2763	This study
IMK1081	*MATa SUC2 URA3 HIS3 LEU2 TRP1 MAL2-8c can1Δ::cas9-natNT2 hxk2Δ::HXK2*(P74S+T212I) *hxk1Δ*	IMX2762	This study
IMK1090	*MATa SUC2 URA3 HIS3 LEU2 TRP1 MAL2-8c can1Δ::cas9-natNT2 hxk2Δ hxk1Δ*	IMX2748	This study
IMK1119	*MATa SUC2 URA3 HIS3 LEU2 TRP1 MAL2-8c can1Δ::cas9-natNT2 hxk2Δ hxk1Δ glk1Δ*	IMK1066	This study

3. Results

3.1. Emulsion-propagated isolates show increased biomass and cell number yields on glucose

In a previous study (29), a chemically mutagenized population of *Saccharomyces cerevisiae* S288C was subjected to 21 propagations in water-in-oil emulsions, in which selection favours variants with higher cell number yields on the limiting substrate. The previous study reported that the growth of the isolates exhibited higher cell number yields, while the biomass yields were not significantly changed. However, the standard deviations of the biomass dry weight measurement were high. In the present study, the seven emulsion-propagated isolates were recharacterised in a synthetic medium routinely used for laboratory cultivations (32). Characterisations were performed in aerobic, glucose-grown shake-flask cultures.

Increased cell-number yield on the limiting substrate can be caused by a higher biomass yield (g dry weight (g glucose)$^{-1}$) at a constant cell size, a smaller cell size at the same biomass yield, or by a combination of changes in cell size and biomass yield. Compared to the parental strain S288C, all isolates showed a significant 73% ± 27% increase in cell number yield on glucose (cells (pmole glucose)$^{-1}$) and a significant 15% ± 4% decrease in cell volume (μm^3), except for EZ11 (Figure 1). Along with the smaller cell size, the isolates, except EZ11, exhibited a significant 27% ± 5% increase in biomass yield on glucose (Figure 1). The increase in the biomass yield on glucose was accompanied by a small (4% ± 1%) but significant decrease in ethanol yield (mol ethanol (mol glucose)$^{-1}$), while specific growth rates (h^{-1}) remained unchanged or decreased (by 11% ± 2%) (Figure 1).

3.2. Reverse engineered *S. cerevisiae* strains with *HXK2* alleles show higher biomass yields on glucose

All seven emulsion-propagated isolates contained single-nucleotide missense mutations in *HXK2* (Table S1 and Figure S1) (29). Hxk2 catalyses the first step of glycolysis by phosphorylating glucose to glucose-6-phosphate. To examine whether the different missense mutations affected the activity of Hxk2 and thereby caused the observed metabolic shift in the emulsion-propagated isolates, we reverse engineered the *HXK2* mutations into the pre-mutagenesis parental strain S288C and into another commonly used laboratory strain of *S. cerevisiae*, CEN.PK113-7D (38). The resulting engineered strains were characterised during exponential growth in aerobic shake-flask cultures on SM with 20 g L^{-1} glucose.

In the S288C background, four of the seven reverse engineered strains exhibited decreased specific growth rates (Figure S2). Specific growth rates of these strains were at or below the critical growth rate at which the S288C-related strain X2180 started to respire in aerobic, glucose-limited chemostat cultures (39). However, these strains continued to produce ethanol in shake-flask cultures on 20 g L^{-1} glucose (Figure S2).

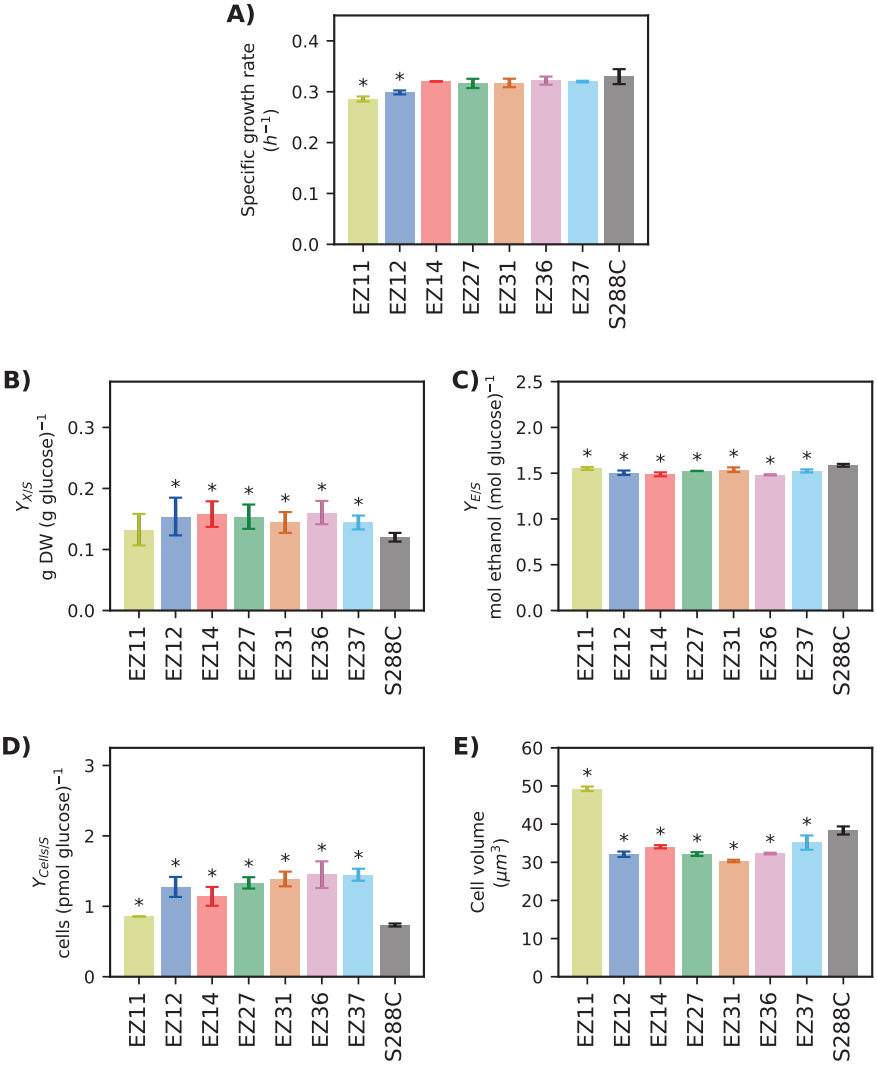

Figure 1: Physiological characteristics of emulsion-propagated *S. cerevisiae* isolates and their parental strain S288C strain when grown in aerobic shake-flask cultures on SM supplemented with 20 g $(L)^{-1}$ glucose. **(A) Specific growth rate (h^{-1})** as calculated from OD_{660} measurements during exponential growth on glucose. **(B) Biomass yield (g dry weight (g glucose)$^{-1}$)** as calculated from culture dry weights measured at two time points during exponential growth, along with the corresponding glucose concentrations. Culture dry weights immediately after inoculation were assumed to be negligible. **(C) Ethanol yield (mol ethanol (mol glucose)$^{-1}$)** as calculated from ethanol and glucose concentrations at three or more time points during exponential growth on glucose. **(D) Cell number yield (cells (pmole glucose)$^{-1}$)** as calculated from cell and glucose concentrations at three or more time points during the exponential growth on glucose. **(E) Cell volume (µm³)** as measured at two time points during exponential growth on glucose. Error bars represent standard deviations of independent replicates (n ≥ 2). Asterisks indicate significant differences ($p < 0.05$) between emulsion-propagated isolates and the S288C strain, as determined by one-tailed t-tests.

Deletion of *HXK2* has been associated with a re-localisation of Ras proteins from the plasma membrane to the mitochondria, where they are involved in activating adenylate cyclase (Cyr1) in the Ras/cAMP/PKA signalling pathway. This mitochondrial localisation of Ras proteins has been linked to mitochondrial dysfunction (40,41). The inability of four of the reverse engineered strains to grow on non-fermentable carbon sources such as ethanol and glycerol (Figure S3) indicated a loss of respiratory capacity. To obtain respiratory competent strains, the strains were reconstructed by selecting transformants on media containing the non-fermentable carbon sources, ethanol and glycerol.

The reverse engineered S288C strains showed both significantly higher biomass (22% ± 4%) and lower ethanol yields (5% ± 1%, except IMX2827) on glucose than the reference strain IMX2747 ('wild type'), while their specific growth rates did not show a significant difference (Figure 2). This phenotype is similar to that of the emulsion-propagated isolates and was consistent with a major role of the mutations in *HXK2* in causing the observed shift in glucose metabolism towards respiration.

Similar to most of the emulsion-propagated isolates (Figure 1), all seven reverse engineered S288C strains exhibited a significantly higher cell number yield on glucose by 50% ± 26% than the reference strain IMX2747 (Figure 2). This increase coincided with a significant reduction of their cell size by 19% ± 5% relative to the reference strain IMX2747.

Reverse engineered strains that were constructed in the CEN.PK113-7D strain background showed significantly higher biomass yields on glucose by 93% ± 18%, along with significantly lower ethanol yields (24% ± 4%) and cell volumes (27% ± 2%) than those of the reference strain IMX2600 ('wild type') (Figure 3). The CEN.PK-based strains exhibited significantly lower specific growth rates (18% ± 4%) and higher cell number yields (148% ± 57%) than their reference strain IMX2600 (Figures 2 and 3). Despite some strain-background-dependent differences, *HXK2* mutations in both strain backgrounds showed an increased biomass yield and lower ethanol yield on glucose upon introducing the mutated *HXK2* alleles (Figures 2 and 3), consistent with a shift in glucose metabolism towards respiration.

3.3. Complementation experiments with *HXK2* alleles selected in microdroplet cultures indicate loss of *in vivo* catalytic activity

In view of the important role of the different mutated *HXK2* alleles in the observed physiological changes in the mutagenized strains selected from microdroplet cultures, we examined their effect on the *in vivo* activity of Hxk2 function. To this end, we first compared the physiology of the reverse engineered strains to their corresponding *hxk2Δ* strains.

Based on biomass and ethanol yields on glucose, most of the CEN.PK113-7D and S288C reverse engineered strains resembled their *hxk2Δ* controls (IMX2748 and IMX2764). All reverse engineered strains in both backgrounds had biomass yields on

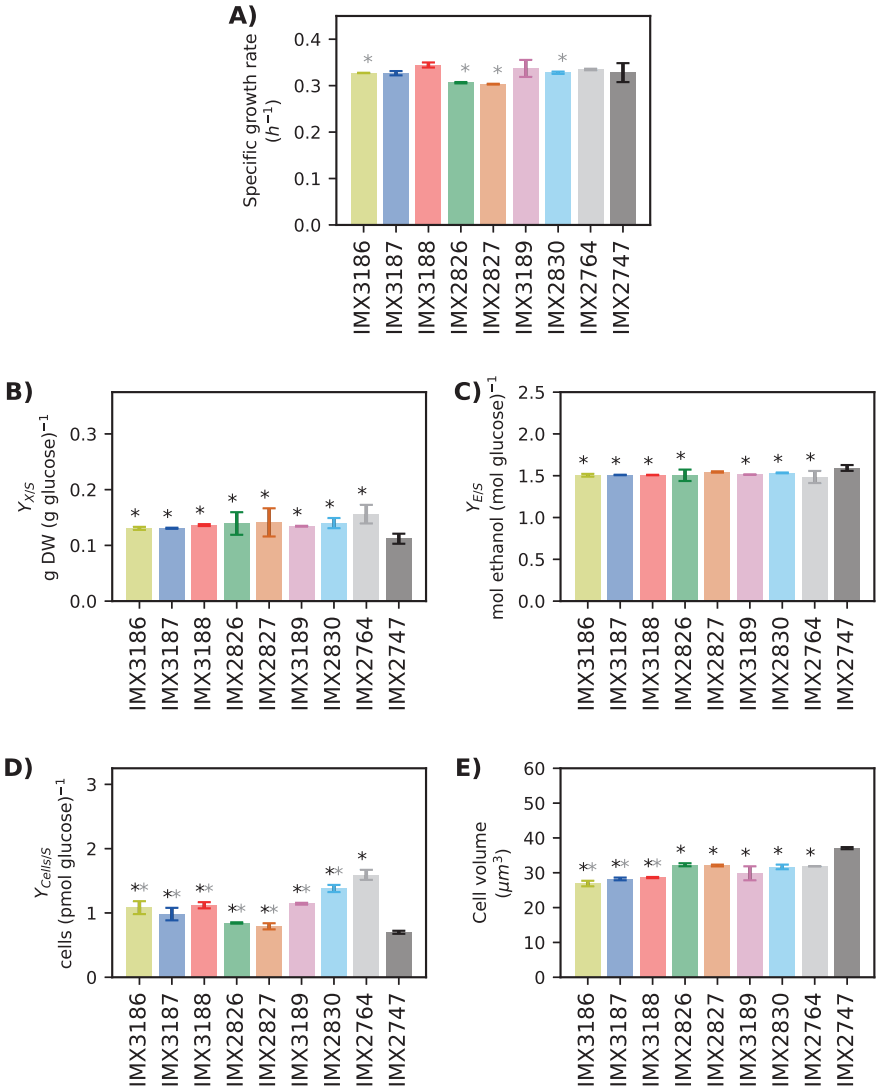

Figure 2: Physiological characteristics of reverse engineered *S. cerevisiae* strains with mutations in *HXK2* in the S288C strain background, the *hxk2Δ* strain IMX2764 and the 'wild type' strain IMX2747 when grown in aerobic shake-flask cultures on SM supplemented with 20 g (L)$^{-1}$ glucose. **(A) Specific growth rate (h^{-1})** as calculated from OD_{660} measurements during exponential growth on glucose. **(B) Biomass yield (g dry weight (g glucose)$^{-1}$)** as calculated from culture dry weights measured at two time points during exponential growth, along with the corresponding glucose concentrations. Culture dry weights immediately after inoculation were assumed to be negligible. **(C) Ethanol yield (mol ethanol (mol glucose)$^{-1}$)** as calculated from ethanol and glucose concentrations at three or more time points during exponential growth on glucose. **(D) Cell number yield (cells (pmole glucose)$^{-1}$)** as calculated from cell and glucose concentrations at three or more time points during the exponential growth on glucose. **(E) Cell volume (µm^3)** as measured at two time points during exponential growth on glucose**.** Error bars represent standard deviations of independent replicates (n ≥ 2). Black asterisks indicate significant differences ($p < 0.05$) between the reverse engineered S288C strains and IMX2747('wild type'), and grey asterisks indicate significant differences ($p < 0.05$) between the reverse engineered strains and IMX2764 (*hxk2Δ*), as determined by one-tailed t-tests.

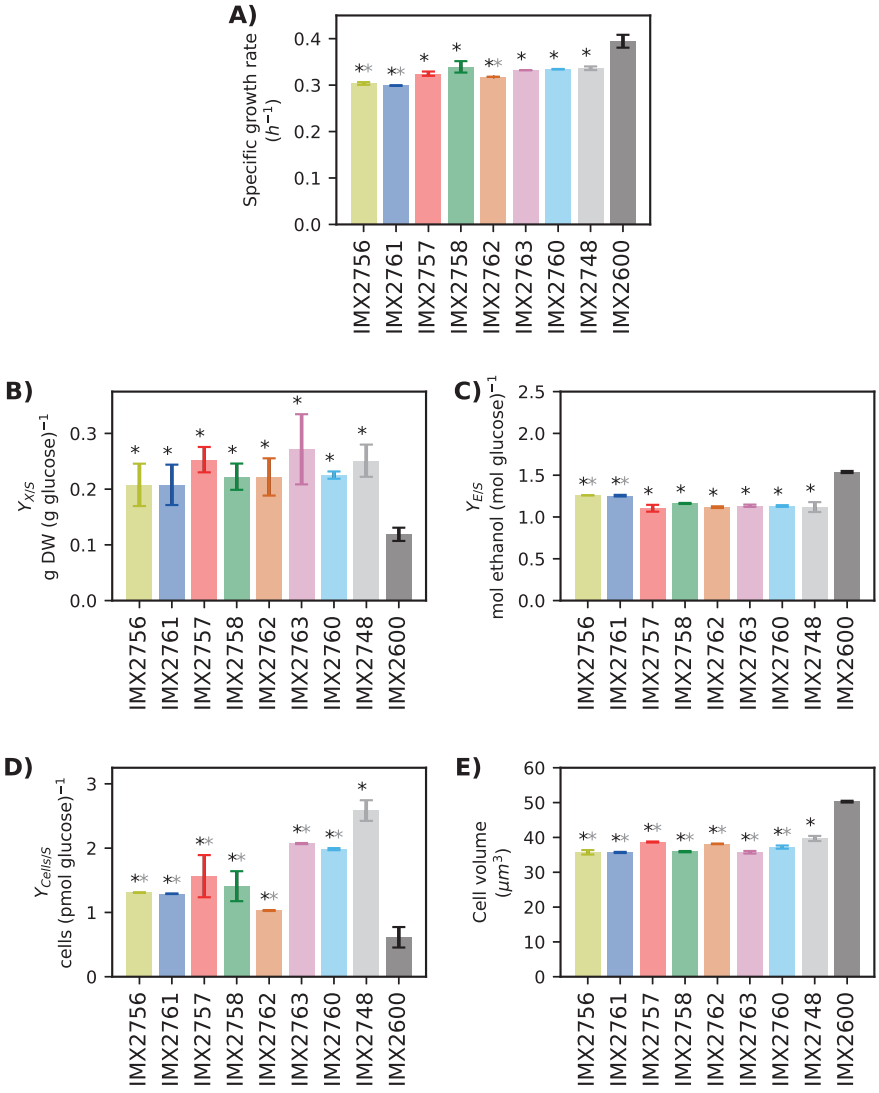

Figure 3: Physiological characteristics of reverse engineered *S. cerevisiae* strains with mutations in *HXK2* in the CEN.PK113-7D strain background, the *hxk2Δ* strain IMX2748 and the 'wild type' strain IMX2600 when grown in aerobic shake-flask cultures on SM supplemented with 20 g $(L)^{-1}$ glucose. **(A) Specific growth rate (h^{-1})** as calculated from OD_{660} measurements during exponential growth on glucose. **(B) Biomass yield (g dry weight (g glucose)$^{-1}$)** as calculated from culture dry weights measured at two time points during exponential growth, along with the corresponding glucose concentrations. Culture dry weights immediately after inoculation were assumed to be negligible**. (C) Ethanol yield (mol ethanol (mol glucose)$^{-1}$)** as calculated from ethanol and glucose concentrations at three or more time points during exponential growth on glucose. **(D) Cell number yield (cells (pmole glucose)$^{-1}$)** as calculated from cell and glucose concentrations at three or more time points during the exponential growth on glucose. **(E) Cell volume (μm^3)** as measured at two time points during exponential growth on glucose**.** Error bars represent standard deviations of independent replicates ($n \geq 2$). Black asterisks indicate significant differences ($p < 0.05$) between the reverse engineered CEN.PK113-7D strains and IMX2600 ('wild type'), and grey asterisks indicate significant differences ($p < 0.05$) between the reverse engineered strains and IMX2748 (*hxk2Δ*), as determined by one-tailed t-tests.

glucose similar to those of their *hxk2Δ* controls (Figures 2 and 3). In the CEN.PK113-7D background, five out of seven reverse engineered strains showed ethanol yields similar to that of strain IMX2748 (Figure 3), while in the S288C background, six out of seven strains displayed ethanol yields similar to that of strain IMX2764 (Figure 2).

These similarities between the CEN.PK113-7D reverse engineered strains and their respective *hxk2Δ* strains suggested that the different single-nucleotide mutations caused a (near-)complete loss of Hxk2 catalytic activity under the tested conditions. To further investigate this, we compared the growth on fructose of the reverse engineered CEN.PK113-7D strains with that of the congenic strain IMK1090 (*hxk1Δ hxk2Δ*). While strain IMK1090 retains an active glucokinase (Glk1), this enzyme is reported to be unable to phosphorylate fructose. Therefore, no growth was expected in the absence of functional Hxk2 or Hxk1. Contrary to this expectation, IMK1090 (*hxk1Δ hxk2Δ)* showed slight growth on synthetic medium with fructose (Figure 4). However, this growth was much less than that of strains IMX2600 ('wild type') and IMK1067 (*hxk1Δ*). In contrast, the growth of the reverse engineered strains on fructose resembled that of IMK1090 (*hxk1Δ hxk2Δ)*, which further indicated that the *HXK2* mutations resulted in a (near-)complete loss of catalytic activity (Figure 4).

To examine whether the point mutations caused structural alterations in Hxk2, we generated homology models of the protein (37) and aligned the structures of the mutant variants with that of the wild type. These structural comparisons revealed minor or no conformational changes, suggesting that the loss of catalytic activity was not caused by major structural disruptions (Figure S5).

4. Discussion

Selection using water-in-oil emulsions has been suggested to promote metabolic reorganisation toward dissimilatory pathways with higher ATP yields per mole of substrate (29,30). In this study, we re-examined the physiology of *Saccharomyces cerevisiae* mutants that had been previously selected by van Tatenhove-Pel *et al*. (2020) (29) through 21 serial propagations in water-in-oil emulsions. This re-examination was motivated by the high standard deviations observed in the biomass dry weight measurements reported in the previous study. Furthermore, we explored the basis of the observed physiological changes by reverse-engineering specific missense mutations in *HXK2,* identified in the emulsion-propagated isolates (29), into both the ancestral strain and a commonly used laboratory strain.

Our results show that microcompartment growth of *S. cerevisiae* selects for maximising progeny production by increasing both cell number and biomass yields on the privatised substrate glucose, by 73 ± 27% and 27% ± 5%, respectively. The increase in biomass yield is accompanied by a 4% ± 1% reduction in ethanol yield, indicating a metabolic shift towards a more respiratory metabolism. Although serial propagations in emulsions were performed in a synthetic medium optimised for high cell concentrations with 80 g L^{-1} glucose (42), the isolates were characterised in a

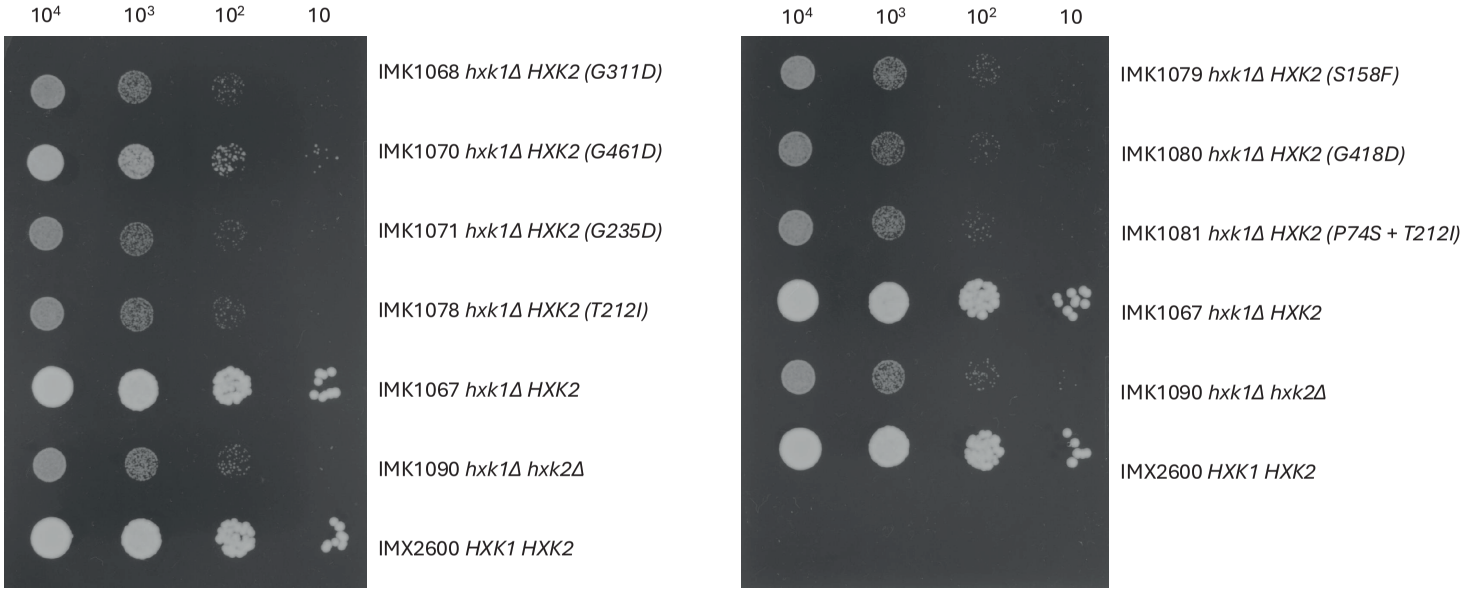

Figure 4: Growth of *HXK2* mutant strains in the CEN.PK113-7D background (*HXK2* Δhxk1*) along with IMK1067 (*Δhxk1*), IMK1090 (*Δhxk1 Δhxk2*) and their ancestor IMX2600 on SM with 20 g $(L)^{-1}$ fructose**.** Pictures were taken after three days of incubation.

synthetic medium that is routinely used with 20 g L^{-1} glucose (32). Despite differences in medium composition and sugar concentration, the emulsion-propagated isolates showed higher cell number yields, consistent with selection in water-in-oil emulsions.

Another aim of this study was to investigate the molecular basis underlying the phenotypes of isolates selected through serial propagation in water-in-oil emulsions. All emulsion-propagated isolates carried distinct missense mutations in *HXK2* (29), in addition to mutations in genes involved in cell-cycle regulation and glucose repression. Our results demonstrate that the phenotypes of these isolates can be recapitulated by reverse-engineering only the *HXK2* alleles into the ancestral strain (S288C). The resulting S288C strains exhibited a 22± 4% increase in biomass yield, a 50 ± 26% increase in cell number yield, and a 5 ± 1% reduction in ethanol yield.

It was initially anticipated that, due to the predominance of missense mutations in *HXK2* in all the independently evolved isolates, these mutations would shift metabolism from fermentation toward respiration by altering the regulatory role of Hxk2 and help elucidate Hxk2's moonlighting role as a transcriptional regulator. This expectation was based on previous studies proposing that *S. cerevisiae* Hxk2, under glucose-excess conditions, translocates to the nucleus where it acts as a transcriptional repressor (43,44). However, a recent study (45) challenged these findings, showing that Hxk2 is excluded from the nucleus under glucose-excess conditions and has a negligible role in transcriptional regulation.

The identified *HXK2* mutations resulted in loss of catalytic activity, as inferred by the physiology of the reverse engineered strains compared to a *hxk2Δ* strain during growth on glucose. In addition, the reverse engineered strains in a *hxk1Δ* strain background showed similar growth to a *hxk1Δ hxk2Δ* strain on fructose. Structural modelling predicted minor or no conformational changes in the protein structure, although substrate binding affinity remains to be tested. The proximity of the mutations to ATP- and substrate-binding sites, particularly with Ser158 involved in glucose binding and Gly235, Gly461, Gly418, and Thr212 involved in ATP binding (46,47), and the high conservation of Gly235 and Gly418 among hexokinases from yeast, humans and other organisms (46), suggests that these mutations disrupt catalytic activity despite not causing major conformational alterations.

The prevalence of the missense rather than truncations, frameshifts, or nonsense mutations was unexpected given that these mutations appear to cause loss of catalytic activity of Hxk2. This could stem from the mutagenic bias of the chemical mutagen EMS used by van Tatenhove-Pel *et al*. (2021) (29), which favours G/C to A/T transitions (48), which is consistent with the *HXK2* mutations identified in the emulsion-propagated isolates (Table S1).

The mutations possibly render Hxk2 inactive, which is the major isoform in *S. cerevisiae* (45,49), thereby reducing carbon flux into glycolysis. This flux reduction allows a large fraction of glucose to be metabolised through the higher ATP-yielding dissimilation pathway, whose capacity is otherwise constrained by several factors,

including the catalytic capacity of specific enzymes (8,50,51), proteome allocation constraints (14,50), Gibbs free energy dissipation limits (16), redox balancing capacity (23,52) or a combination of these factors (15).

Our results indicate that the missense mutations in *HXK2*, which were consistently identified in all emulsion-propagated isolates, contribute to improved ATP yield by redirecting carbon from fermentation toward respiration. However, the physiological outcomes of this shift differed between strain backgrounds, highlighting strain-dependent effects of the mutations in *HXK2*. In the reverse engineered CEN.PK113-7D strains, increased biomass and reduced ethanol yields were accompanied by lower specific growth rates. This aligns with observations from van Hoek *et al.* (1998) (9), who reported that, in aerobic continuous cultures of CEN.PK113-7D, biomass yield decreases with increasing growth rate due to a shift from respiratory to (respiro) fermentative metabolism. The biomass yields of the reverse engineered strains correspond closely to those reported by van Hoek *et al.* (1998) (9) (0.23 g biomass dry weight (g glucose)$^{-1}$) at a dilution rate of 0.35 h^{-1}, similar to growth rates observed here. This suggests that reduced specific glucose consumption rates of the reverse engineered strains increased their biomass yields.

In contrast, although the reverse engineered S288C strains also showed increased biomass yields and reduced ethanol yields, their growth rates were unchanged, consistent with previous findings for *hxk2Δ* mutants of the closely related FY4 strain (53,54). The differing phenotypes of *hxk2* mutants in S288C and CEN.PK113-7D strain backgrounds may reflect strain-specific mechanisms compensating for the loss of Hxk2. Although Hxk1, Hxk2 and Glk1 amino acid sequences are identical in both strains (55–57), differences in their regulation could account for the observed variation in phenotypes. A potentially relevant genetic difference between the strains is a point mutation in *CYR1* in CEN.PK113-7D (58). *CYR1* encodes adenylate cyclase, the enzyme responsible for synthesising cAMP, a key component of the Ras/cAMP/PKA signalling pathway that regulates cell growth in response to glucose and other nutrients in *S. cerevisiae* (59). Kümmel *et al.* (2010) (53) proposed that this pathway could compensate for glucose repression in S288C *hxk2Δ* but not in CEN.PK113-7D *hxk2Δ*, resulting in a more pronounced increase in biomass yield and reduction in specific growth rate in CEN.PK-based strains.

Overall, our results show that compartmentalised growth of *S. cerevisiae* on glucose in water-in-oil emulsions (29) selects for increased cell number and biomass yields, along with reduced cell size and a metabolic shift toward respiration. The physiological changes appear to be driven by loss-of-function mutations in *HXK2*. These findings highlight the potential of emulsion-based selection as a powerful approach to evolve metabolic strategies in *S. cerevisiae,* favouring dissimilation pathways with higher ATP yield per mole glucose and to elucidate their underlying molecular mechanisms.

Acknowledgments

We would like to thank Michelle Rossouw for her assistance with a growth study. We would like to thank Rose Vossen for the construction of strains IMX2747, IMX2764, IMX2824, IMX2825, IMX2826, IMX2827, IMX2828, IMX2829, and IMX2830, and Linda Li for the construction of strains IMX2756, IMX2760, IMX2757, IMX2758, IMX2761, IMX2762, and IMX2759.

Author contributions

JTP, SBG and RJvT conceptualised the work. JTP, RJvT, and SBG designed experiments. SBG wrote the original draft of the manuscript, which was reviewed and edited by JTP and RJvT. SBG and MD performed the experiments and conducted data analysis. All authors read and approved the final manuscript.

SBG, JTP and RJvT are funded by Delft University of Technology.

Supplementary information

Table S1: *HXK2* mutations identified in emulsion-propagated S288C isolates and reverse engineered in CEN.PK113-7D and S288C. The positions of the mutations in the protein structure are shown in Figure S1.

Amino acid change	Nucleotide change	Strains	Mutation description	Reference
T212I	ACT →ATT	EZ11, EZ31, IMX2824, IMX3186, IMX2827, IMX2756, IMX2762	ATP-binding site	(46)
G235D	GGT →GAT	EZ12, IMX2825, IMX3187, IMX2761	ATP-binding site	(46)
G311D	GGT→GAT	EZ14, IMX2828, IMX3188, IMX2757		
G461D	GGT →GAT	EZ27, IMX2826, IMX2758	ATP-binding site	(46)
P74S	CCA →TCA	EZ31, IMX2827, IMX2762		
G418D	GGT →GAT	EZ36, IMX2829, IMX3189, IMX2763	ATP-binding sites	(46,47)
S158F	TCT →TTT	EZ37, IMX2830, IMX2760	Glucose-binding site	(46,47)

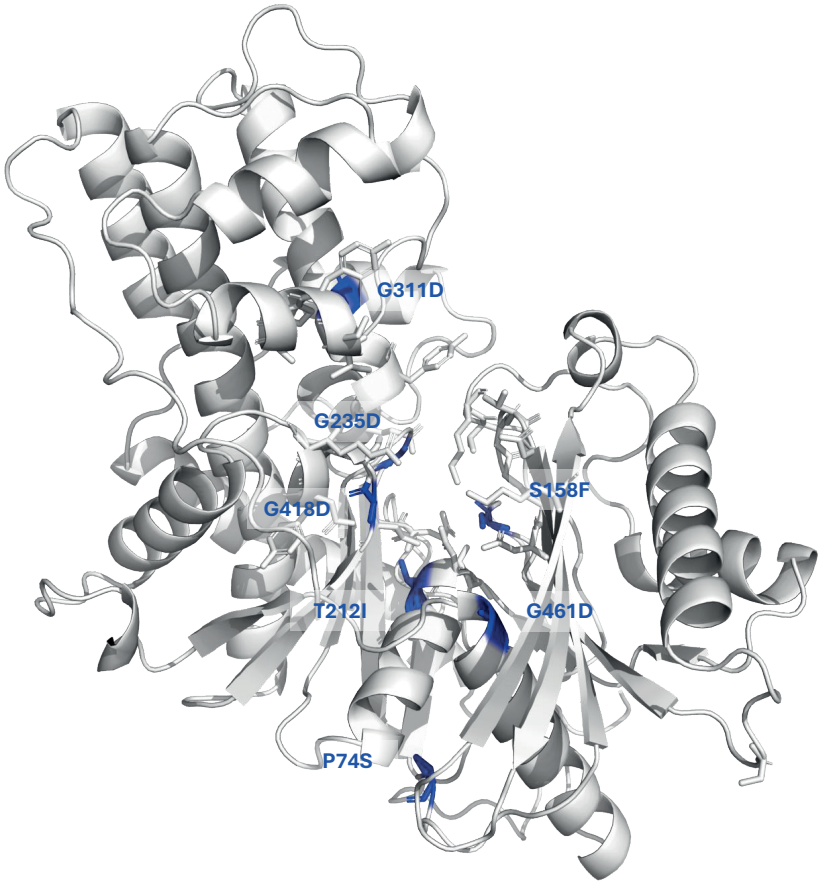

Figure S1: Positions of mutated Hxk2 residues (shown in blue) in the homology model of Hxk2 generated using ColabFold (37).

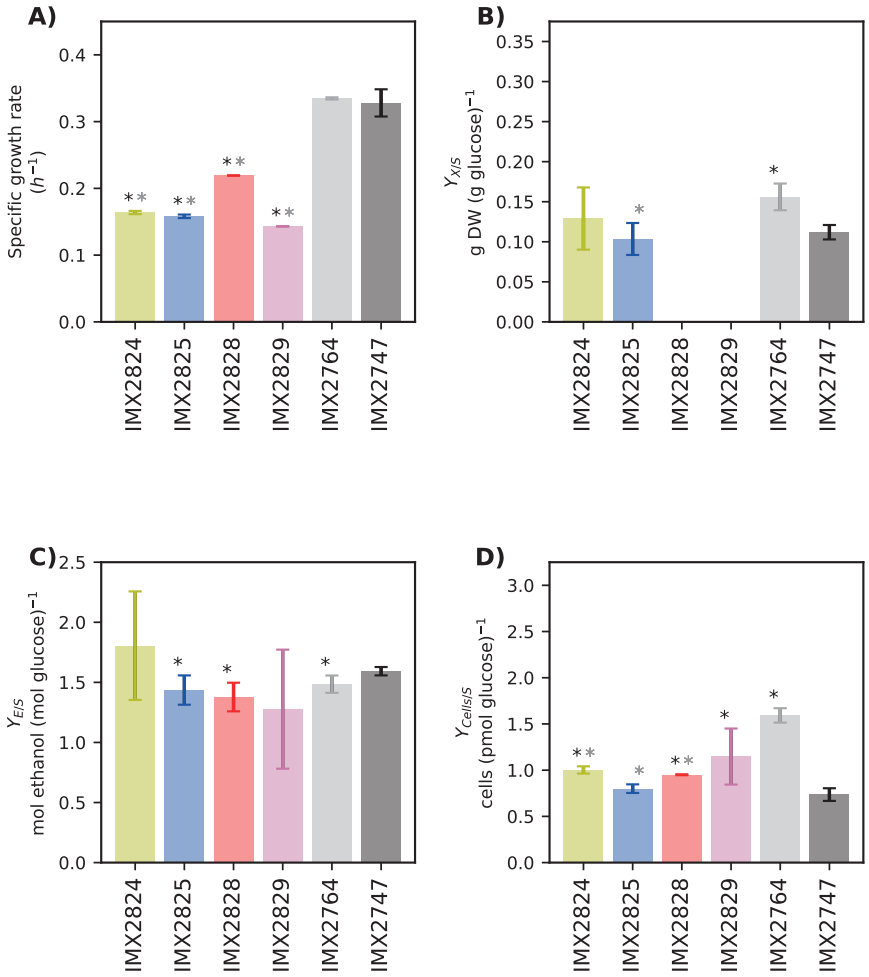

Figure S2: Physiological characteristics of reverse engineered *S. cerevisiae* strains (IMX2824, IMX2825, IMX2828 and IMX2829) with mutations in *HXK2 in* the S288C strain background, the *hxk2Δ* strain IMX2764 and the 'wild type' strain IMX2747 when grown in aerobic shake-flask cultures on SM supplemented with 20 g $(L)^{-1}$ glucose. **(A) Specific growth rate (h^{-1})** as calculated from OD_{660} measurements during exponential growth on glucose. (**B) Biomass yield (g dry weight (g glucose)$^{-1}$)** as calculated from culture dry weights measured at two time points during exponential growth, along with the corresponding glucose concentrations. Culture dry weights immediately after inoculation were assumed to be negligible. **(C) Ethanol yield (mol ethanol (mol glucose)$^{-1}$)** as calculated from ethanol and glucose concentrations at three or more time points during exponential growth on glucose. **(D) Cell number yield (cells (pmole glucose)$^{-1}$)** as calculated from cell and glucose concentrations at three or more time points during the exponential growth on glucose. **(E) Cell volume (μm^3)** as measured at two time points during exponential growth on glucose**.** Error bars represent standard deviations of independent replicates (n ≥ 2). Black asterisks indicate significant differences ($p < 0.05$) between the reverse engineered S288C strains and IMX2747('wild type'), and grey asterisks indicate significant differences ($p < 0.05$) between the reverse engineered strains and IMX2764 (*hxk2Δ*), as determined by one-tailed t-tests.

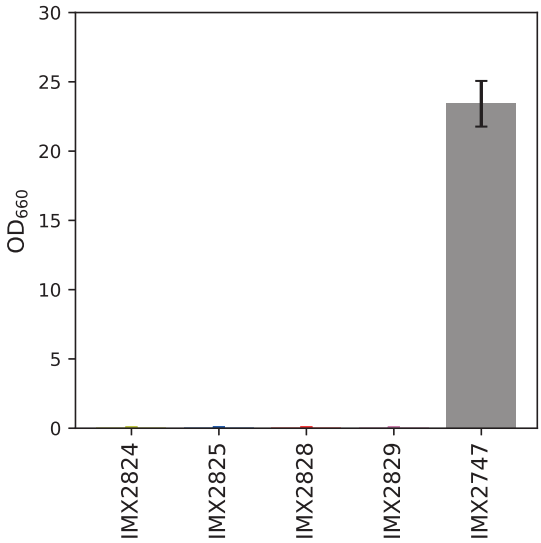

Figure S3: Final OD_{660} values of *HXK2* mutants in the S288C strain background (IMX2824, IMX2825, IMX2828 and IMX2829) and the 'wild type' strain IMX2747 after incubation for 5 days in SM medium with 20 g L^{-1} ethanol, 20 g L^{-1} glycerol, inoculated at an OD_{660} of 0.1. Indicated values are averages ± standard deviations of three independent replicates.

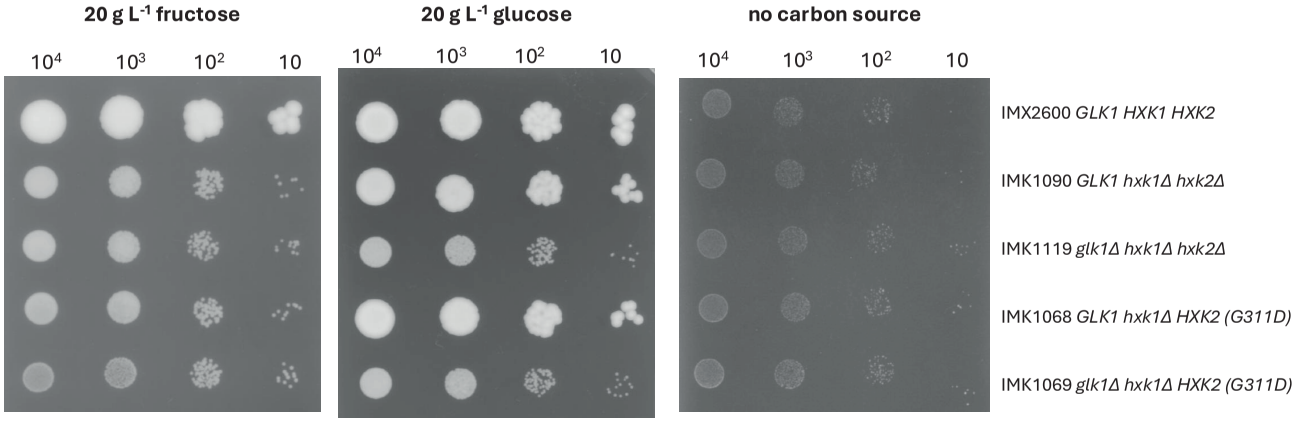

Figure S4: Growth of *HXK2* mutant strains in the CEN.PK113-7D background (*HXK2* hxk1Δ* and *HXK2* hxk1Δ glk1Δ*) along with IMK1090 (*hxk1Δ hxk2Δ)*, IMK1119 (*hxk1Δ hxk2Δ glk1Δ*) and the 'wild type' strain IMX2600 on SM with 20 g L^{-1} fructose, 20 g L^{-1} glucose or no carbon source. Pictures were taken after four days of incubation.

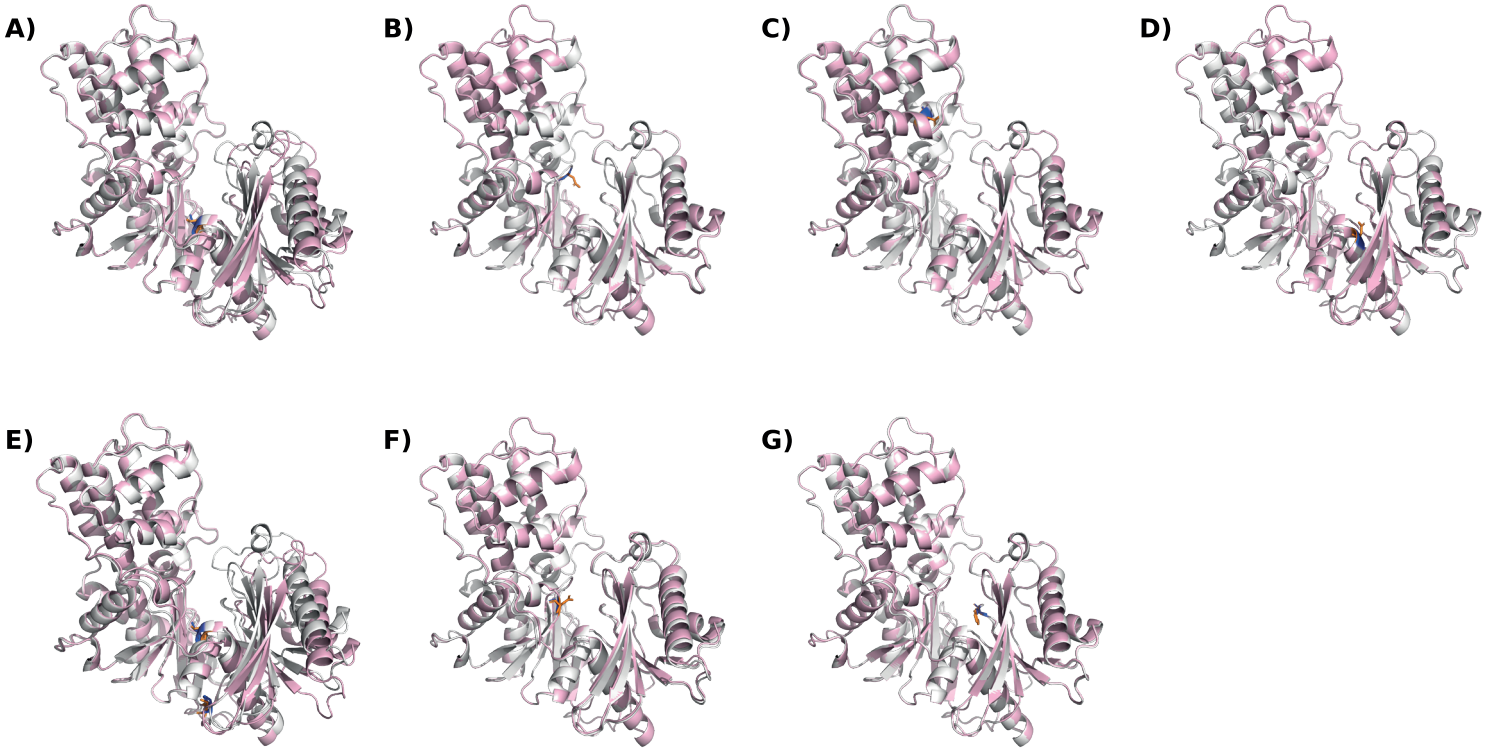

Figure S5: Superimposed homology models of *S. cerevisiae* Hxk2 wild type (white) and mutant variants (pink), generated using the ColabFold pipeline (37). The position of the wild type residue is shown in blue, and the corresponding mutated residue in orange. (A) T212I; (B) G235D; (C) G311D; (D) G461D; (E) P74S + T212I; (F) G418D; (G) S158F.

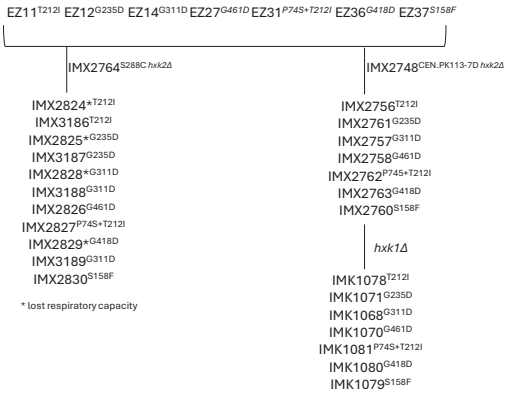

Figure S6: Overview of *HXK2* mutations identified in emulsion-propagated isolates (EZ) and the corresponding reverse-engineered *S. cerevisiae* strains (S288C and CEN.PK113-7D).

Table S2: Plasmids used in this study.

Plasmid name	Relevant characteristics	Reference
p414-TEF1p-Cas9-CYC1t	*CEN6/ARS4* ampR *TRP1* p*TEF1-cas9*-t*CYC1*	(36)
pUG-natNT2	PCR template for *natNT2*	(60)
pUDR371	2µm ampR *kanMX* gRNA-*HXK2*	(61)
pUDR471	2µm ampR *kanMX* gRNA-SynPAM	(62)
pROS12	2µm ampR *hphNT1* gRNA-*CAN1.Y* gRNA-*ADE2.Y*	(35)
pUDR869	2µm ampR *hphNT1* gRNA-*HXK1*	This study
pUDR870	2µm ampR *hphNT1*gRNA-*HXK1* gRNA-*GLK1*	This study

Table S3: Primers used in this study.

Primer name	Sequence (5'-3')
6005	GATCATTTATCTTTCACTGCGGAGAAG
20063	TGCGCATGTTTCGGCGTTCGAAACTTCTCCGCAGTGAAAGATAAATGATCA GAAGACTTTGTGAATTGATGTTTTAGAGCTAGAAATAGCAAGTTAAAATAAGG CTAGTCCGTTATCAAC
12923	TGCGCATGTTTCGGCGTTCGAAACTTCTCCGCAGTGAAAGATAAATGATCT GCTTACTTCATCGAACAAAGTTTTAGAGCTAGAAATAGCAAGTTAAAATAAG GCTAGTCCGTTATCAAC
2873	TCAGACTTCTTAACTCCTGTAAAAACAAAAAAAAAAAAAGGCATAGCAATA AGCTGGAGCTCATAGCTTC
4653	GTGCCTATTGATGATCTGGCGGAATGTCTGCCGTGCCATAGCCATGCCTT CACATATAGTCCGCAAATTAAAGCCTTCGAG
3093	ACTATATGTGAAGGCATGGCTATGGCACGGCAGACATTCCGCCAGATCAT CAATAGGCACCTTCGTACGCTGCAGGTCGAC
5542	CTATGCTACAACATTCCAAAATTTGTCCCAAAAAGTCTTTGGTTCATGATCTT CCCATACGCATAGGCCACTAGTGGATCTG
18833	TTGTAGGAATATAATTCTCCACACATAATAAGTACGTTAATTAAATAAAAGTAG AATTTCACCTAGACGAGGACTTAATTTGTAAATTAAGTTTGAACAACAAGAA GGTGCCCTTTTTTT
18834	AAAAAAAGGGCACCTTCTTGTTGTTCAAACTTAATTTACAAATTAAGTCCTC GTCTAGGTGAAATTCTACTTTTATTTAATTAACGTACTTATTATGTGTGGAGA ATTATATTCCTACAA
2794	CACCTTCGCCACTGTCTTATCTAC
5319	GCAAGAGAAAAAAAACGAGCAATTGTTAAAAG
20064	AATTCTTTTCTTTTAATCAAACTCACCCAAACAACTCAATTAGAATACTGAAA AAATAAGTGAAAAAAATGTAATGAAATATAAATGTGTTTTTCCCTCCCTTAATA TTATTATTCTTAT
20065	ATAAGAATAATAATATTAAGGGAGGGAAAAACACATTTATATTTCATTACATTT TTTTCACTTATTTTTTCAGTATTCTAATTGAGTTGTTTGGGTGAGTTTGATTAAA AGAAAAGAATT
12925	GCCCAACTCAGCTTCCGTAAACCACAACACCACCACTAATACAACTCTAT CATACACAAGTCTTTTTACATTTTTTTGGTTTGTGTACGTATCCCACCGTACTT ACCATCTTCTCTCCTT
12926	AAGGAGAGAAGATGGTAAGTACGGTGGGATACGTACACAAACCAAAAAAA TGTAAAAAGACTTGTGTATGATAGAGTTGTATTAGTGGTGGTGTTGTGGTTTA CGGAAGCTGAGTTGGGC

References

1. De Deken RH. The Crabtree effect: a regulatory system in yeast. J Gen Microbiol. 1966;44:149–56.
2. Sonenshein AL. Control of key metabolic intersections in *Bacillus subtilis*. Nat Rev Microbiol. 2007;5:917–27.
3. Thomas TD, Ellwood DC, Michael V, Longyear C. Change from homo- to heterolactic fermentation by *Streptococcus lactis* resulting from glucose limitation in anaerobic chemostat cultures. J Bacteriol. 1979;139:345–51.
4. Warburg O. Injuring of respiration on the origin of cancer cells. Science. 1956;123:309–14.
5. Wolfe AJ. The acetate switch. Microbiol Mol Biol Rev. 2005;69(1):12–50.
6. van Dijken JP, Weusthuis RA, Pronk JT. Kinetics of growth and sugar consumption in yeasts. Antonie Van Leeuwenhoek. 1993;63(3-4):343–52.
7. Crabtree H G. Observations on the carbohydrate metabolism of tumours. Biochem J. 1929;23(3):536–47.
8. Postma E, Verduyn C, Scheffers WA, van Dijken JP. Enzymic analysis of the Crabtree effect in glucose-limited chemostat cultures of *Saccharomyces cerevisiae*. Appl Environ Microbiol. 1989;55(2):468–77.
9. van Hoek P, van Dijken JP, Pronk JT. Effect of specific growth rate on fermentative capacity of baker's yeast. Appl Environ Microbiol. 1998;64(11):4226–33.
10. Basan M, Hui S, Okano H, Zhang Z, Shen Y, Williamson JR, *et al*. Overflow metabolism in *Escherichia coli* results from efficient proteome allocation. Nature. 2015;528(7580):99–104.
11. Borodina I, Nielsen J. Advances in metabolic engineering of yeast *Saccharomyces cerevisiae* for production of chemicals. Biotechnol J. 2014;9(5):609–20.
12. Hong KK, Nielsen J. Metabolic engineering of *Saccharomyces cerevisiae*: a key cell factory platform for future biorefineries. Cell Mol Life Sci. 2012;69(14):2671–90.
13. Bakker BM, Overkamp KM, van Maris AJA, Ko P, Luttik MAH, van Dijken JP, *et al*. Stoichiometry and compartmentation of NADH metabolism in *Saccharomyces cerevisiae*. FEMS Microbiol Rev. 2001;25(1):15–37.
14. Elsemman IE, Rodriguez Prado A, Grigaitis P, Garcia Albornoz M, Harman V, Holman SW, *et al*. Whole-cell modeling in yeast predicts compartment-specific proteome constraints that drive metabolic strategies. Nat Commun. 2022;13(1):1–12.
15. de Groot DH, Lischke J, Muolo R, Planqué R, Bruggeman FJ, Teusink B. The common message of constraint-based optimization approaches: overflow metabolism is caused by two growth-limiting constraints. Cell Mol Life Sci. 2020;77(3):441–53.

16. Niebel B, Leupold S, Heinemann M. An upper limit on Gibbs energy dissipation governs cellular metabolism. Nat Metab. 2019;1(1):125–32.

17. van Dijken JP, Scheffers WA. Redox balances in the metabolism of sugars by yeasts. FEMS Microbiol Lett. 1986;32(3-4):199–224.

18. Xia J, Sánchez BJ, Chen Y, Campbell K, Kasvandik S, Nielsen J. Proteome allocations change linearly with the specific growth rate of Saccharomyces cerevisiae under glucose limitation. Nat Commun. 2022;13(1):1–10.

19. Pfeiffer T, Morley A. An evolutionary perspective on the Crabtree effect. Front Mol Biosci. 2014;1:1–6.

20. Dashko S, Zhou N, Compagno C, Piškur J. Why, when, and how did yeast evolve alcoholic fermentation? FEMS Yeast Res. 2014;14(7):826–32.

21. Sahana GR, Balasubramanian B, Joseph KS, Pappuswamy M, Liu WC, Meyyazhagan A, *et al*. A review on ethanol tolerance mechanisms in yeast: current knowledge in biotechnological applications and future directions. Process Biochem. 2024;138:1–13.

22. Kozak BU, van Rossum HM, Niemeijer MS, van Dijk M, Benjamin K, Wu L, *et al*. Replacement of the initial steps of ethanol metabolism in *Saccharomyces cerevisiae* by ATP-independent acetylating acetaldehyde dehydrogenase. FEMS Yeast Res. 2016;16(2):1–9.

23. Vemuri GN, Eiteman MA, McEwen JE, Olsson L, Nielsen J. Increasing NADH oxidation reduces overflow metabolism in *Saccharomyces cerevisiae*. Proc Natl Acad Sci U S A. 2007;104(7)

24. Dai Z, Huang M, Chen Y, Siewers V, Nielsen J. Global rewiring of cellular metabolism renders *Saccharomyces cerevisiae* Crabtree negative. Nat Commun. 2018;9(1):1–8.

25. Otterstedt K, Larsson C, Bill RM, Ståhlberg A, Boles E, Hohmann S, *et al*. Switching the mode of metabolism in the yeast *Saccharomyces cerevisiae*. EMBO Rep. 2004;5(5):532–7.

26. Elbing K, Larsson C, Bill RM, Albers E, Snoep JL, Boles E, *et al*. Role of hexose transport in control of glycolytic flux in *Saccharomyces cerevisiae*. Yeast. 2004;21(9):5323–30.

27. Bachmann H, Bruggeman FJ, Molenaar D, Branco dos Santos F, Teusink B. Public goods and metabolic strategies. Curr Opin Microbiol. 2016;31:109–15.

28. Mans R, Daran JMG, Pronk JT. Under pressure: evolutionary engineering of yeast strains for improved performance in fuels and chemicals production. Curr Opin Biotechnol. 2018;50:47–56.

29. van Tatenhove-Pel RJ, Zwering E, Boreel DF, Falk M, van Heerden JH, Kes MBMJ, *et al*. Serial propagation in water-in-oil emulsions selects for *Saccharomyces cerevisiae* strains with a reduced cell size or an increased biomass yield on glucose. Metab Eng. 2021;64:1–14.

30. Bachmann H, Fischlechner M, Rabbers I, Barfa N, Dos Santos FB, Molenaar D, *et al*. Availability of public goods shapes the evolution of competing metabolic strategies. Proc Natl Acad Sci U S A. 2013;110(35):14302–7.

31. Rabbers I, Gottstein W, Feist AM, Teusink B, Bruggeman FJ, Bachmann H. Selection for cell yield does not reduce overflow metabolism in *Escherichia coli*. Mol Biol Evol. 2022;39(1):1–10.

32. Verduyn C, Postma E, Scheffers WA, van Dijken JP. Effect of benzoic acid on metabolic fluxes in yeasts: a continuous-culture study on the regulation of respiration and alcoholic fermentation. Yeast. 1992;8(7):501–17.

33. Lõoke M, Kristjuhan K, Kristjuhan A. Extraction of genomic DNA from yeasts for PCR-based applications. Biotechniques. 2011;50(5):325–8.

34. Gietz RD, Woods RA. Transformation of yeast by lithium acetate/single-stranded carrier DNA/polyethylene glycol method. Methods Enzymol. 2002;350:87–96.

35. Mans R, van Rossum HM, Wijsman M, Backx A, Kuijpers NGA, van den Broek M, *et al*. CRISPR/Cas9: a molecular Swiss army knife for simultaneous introduction of multiple genetic modifications in *Saccharomyces cerevisiae*. FEMS Yeast Res. 2015;15(2):1–15.

36. DiCarlo JE, Norville JE, Mali P, Rios X, Aach J, Church GM. Genome engineering in *Saccharomyces cerevisiae* using CRISPR-Cas systems. Nucleic Acids Res. 2013;41(7):4336–43.

37. Mirdita M, Schütze K, Moriwaki Y, Heo L, Ovchinnikov S, Steinegger M. ColabFold: making protein folding accessible to all. Nat Methods. 2022;19(6):679–82.

38. van den Broek M, Ortiz-Merino RA, Bennis NX, Wronska AK, Hassing EJ, Daran-Lapujade P, *et al*. Draft genome sequence of the *Saccharomyces cerevisiae* Spy Cas9 expressing strain IMX2600, a laboratory and platform strain from the CEN.PK lineage for cell-factory research. Microbiol Resour Announc. 2024;13(2):e00000-24.

39. van Dijken JP, Bauer J, Brambilla L, Duboc P, François JM, Gancedo C, *et al*. An interlaboratory comparison of physiological and genetic properties of four *Saccharomyces cerevisiae* strains. Enz Microb Technol. 2000;27

40. Broggi S, Martegani E, Colombo S. Live-cell imaging of endogenous Ras-GTP shows predominant Ras activation at the plasma membrane and in the nucleus in *Saccharomyces cerevisiae*. Int J Biochem Cell Biol. 2013;45(2):384–94.

41. Amigoni L, Martegani E, Colombo S. Lack of *HXK2* induces localization of active Ras in mitochondria and triggers apoptosis in the yeast *Saccharomyces cerevisiae*. Oxid Med Cell Longev. 2013;2013.

42. Castrillo JI, Kaliterna J, Weusthuis RA, van Dijken JP, Pronk JT. High-cell-density cultivation of yeasts on disaccharides in oxygen-limited batch cultures. Biotechnol Bioeng. 1996;49(6):621–8.

43. Vega M, Riera A, Fernández-Cid A, Herrero P, Moreno F. Hexokinase 2 is an intracellular

glucose sensor of yeast cells that maintains the structure and activity of Mig1 protein repressor complex. J Biol Chem. 2016;291(14):7267–85.

44. Moreno F, Ahuatzi D, Riera A, Palomino CA, Herrero P. Nutrient sensing through the plasma membrane of eukaryotic cells: glucose sensing through the Hxk2-dependent signalling pathway. Biochem Soc Trans. 2005;33(1):265–8.

45. Lesko MA, Chandrashekarappa DG, Jordahl EM, Oppenheimer KG, Bowman RW, Shang C, *et al*. Changing course: glucose starvation drives nuclear accumulation of hexokinase 2 in Saccharomyces cerevisiae. PLoS Genet. 2023;19(5):e1010245.

46. Kuser PR, Krauchenco S, Antunes OAC, Polikarpov I. The high-resolution crystal structure of yeast hexokinase PII with the correct primary sequence provides new insights into its mechanism of action. J Biol Chem. 2000;275(27):20814–21.

47. UniProt Consortium. *HXK2* – Hexokinase-2. UniProtKB. 2025. Available from: https://www.uniprot.org/uniprotkb/P04807

48. Greene EA, Codomo CA, Taylor NE, Henikoff JG, Till BJ, Reynolds SH, *et al*. Spectrum of chemically induced mutations from a large-scale reverse-genetic screen in *Arabidopsis*.

49. Herrero P, Galíndez J, Ruiz N, Martínez-Campa C, Moreno F. Transcriptional regulation of the *Saccharomyces cerevisiae HXK1*, *HXK2* and GLK1 genes. Yeast. 1995;11(2):137–44.

50. Nilsson A, Nielsen J. Metabolic trade-offs in yeast are caused by F1F0-ATP synthase. Sci Rep. 2016;6:1–10.

51. Pronk JT, Steensma HY, van Dijken JP. Pyruvate metabolism in *Saccharomyces cerevisiae*. Yeast. 1996;12(16):1607–33.

52. Verhagen KJ, van Gulik WM, Wahl SA. Dynamics in redox metabolism, from stoichiometry towards kinetics. Curr Opin Biotechnol. 2020;64:116–23.

53. Kümmel A, Ewald JC, Fendt SM, Jol SJ, Picotti P, Aebersold R, *et al*. Differential glucose repression in common yeast strains in response to HXK2 deletion. FEMS Yeast Res. 2010;10(3):322–32.

54. Winston F, Dollard C, Ricupero-Hovasse SL. Construction of a set of convenient *Saccharomyces cerevisiae* strains that are isogenic to S288C. Yeast. 1995;11(1):53–5.

55. Saccharomyces Genome Database. YCL040W (*GLK1*) — strain alignment. Stanford (CA): SGD; 2025. Available from: https://www.yeastgenome.org/strainAlignment?locus=YCL040W

56. Saccharomyces Genome Database. YFR053C (*HXK1*) — strain alignment. Stanford (CA): SGD; 2025. Available from: https://www.yeastgenome.org/strainAlignment?locus=YFR053C

57. Saccharomyces Genome Database. YGL253W (*HXK2*) — strain alignment.

Stanford (CA): SGD; 2025. Available from: https://www.yeastgenome.org/strainAlignment?locus=YGL253W

58. Vanhalewyn M, Dumortier F, Debast G, Colombo S, Ma P, Winderickx J, *et al*. A mutation in *Saccharomyces cerevisiae* adenylate cyclase, Cyr1(K1876M), specifically affects glucose- and acidification-induced cAMP signalling and not the basal cAMP level. Mol Microbiol. 1999;33(2):363–76.

59. Santangelo GM. Glucose signalling in *Saccharomyces cerevisiae*. Microbiol Mol Biol Rev. 2006;70(1):253–82.

60. de Kok S, Nijkamp JF, Oud B, Roque FC, de Ridder D, Daran JM, *et al*. Laboratory evolution of new lactate transporter genes in a *jen1Δ* mutant of *Saccharomyces cerevisiae* and their identification as *ADY2* alleles by whole-genome resequencing and transcriptome analysis. FEMS Yeast Res. 2012;12(3):359–74.

61. Boonekamp FJ. Modular engineering of synthetic glycolytic pathways in *Saccharomyces cerevisiae*. 2020.

62. Perli T, Moonen DPI, van den Broek M, Pronk JT, Daran JM. Adaptive laboratory evolution and reverse engineering of single-vitamin prototrophies in *Saccharomyces cerevisiae*. Appl Environ Microbiol. 2020;86(12):e01234-20.

Chapter 4

Deciphering microbial interactions using a label-free microbead sorting approach.

Sagarika B. Govindaraju, Daan H. de Groot and Rinke J. van Tatenhove-Pel

Manuscript under review at ISME communications.

Abstract

Microorganisms form communities, and their interactions shape the function and stability of these communities. Understanding these interactions can aid in revealing ecosystem dynamics, enhancing community function, and informing the design of synthetic consortia for industrial applications. Deciphering microbial interactions is challenging due to the difficulty of culturing natural microorganisms and the exponential increase in experiments with expanding consortium size. One approach to improving culturing throughput is the use of microcompartments such as agarose microbeads. Microbead-based techniques enable the generation of large numbers of picolitre-sized compartments, facilitating high-throughput, parallel studies of microbial sub-communities. However, the existing microbead-based techniques for deciphering microbial interactions are dependent on single-culture isolates of consortium members and/or labelling of consortium members with fluorescent markers via genetic engineering. In this study, we propose a microbead-based, label-free method that eliminates the requirement of single-cell isolates to predict microbial interactions. This approach involves an isolation-independent manner of microbead inoculation with different sub-communities and microbead sorting to separate sub-communities based on growth. Using a probabilistic model, we predict interactions based on cell concentrations and relative abundances in the inoculum and after microbead sorting. We successfully predicted pairwise interactions in two three-member consortia. Additionally, we computationally showcased the validity of this approach for predicting pairwise interactions in larger consortia.

1. Introduction

Microorganisms exist in communities in diverse environments such as soil, oceans, and human bodies. Interactions between the microorganisms shape the function and stability of these communities and thereby also the ecosystems (1–3). By deciphering microbial interactions, we can gain deeper insight into ecosystem dynamics, identify ways to improve community function, and even derive design principles to develop synthetic consortia for industrial applications.

To decipher microbial interactions, one can use isolation-independent and isolation-dependent approaches. Isolation-independent approaches determine interactions without needing single-cell isolates of community members. They predict interactions, to the level of metabolites exchanged, by using inter- and intra-species metabolic fluxes. They leverage advanced imaging and/or omics technologies to analyse community composition (1,4,5). However, these approaches postulate possible interactions, and it is challenging to experimentally verify the deduced interactions. Alternatively, isolation-dependent approaches predict types of interactions (1,4,5) (e.g., cooperation, inhibition, competition) in natural microbial communities by constructing and studying synthetic mimic communities from culturable microorganisms (1,4,5). Isolation-dependent approaches directly use growth and species abundance-based data to decipher interactions. However, given the challenge of obtaining single culture isolates of microorganisms from environmental samples, typically, synthetic communities that mimic the natural communities are constructed, but these synthetic communities often fail to fully capture the complex interactions in natural communities (1,4–7). In addition, as the size of a microbial consortium increases, the scale of experiments grows exponentially, as these approaches necessitate culturing of all possible combinations of strains and species.

One way to enhance culturing throughput is to utilise microcompartments. Microdroplet-based techniques enable the generation of large numbers of water-in-oil emulsions in a small volume (about 10^7 microbeads with a diameter of 40 µm in 1 mL), allowing high-throughput parallel studies of sub-communities. The applicability of microcompartments to predict microbial interactions has been previously demonstrated (7–9). Growth and relative abundances in microdroplets were determined by labelling the different cell types with fluorescent markers and monitoring the growth of each sub-community. Therefore, these methods still require single culture isolates of the community members and genetic accessibility of the isolates to label them with fluorescent markers (7,9).

In this study, we investigated an agarose microbead-based, isolation-independent, and label-free approach to predict microbial interactions. This approach involves inoculating microbeads with different sub-communities, sorting them based on growth. Subsequent prediction of microbial interactions is based only on cell concentrations and relative abundances in the inoculum and after microbead-sorting, using a Bayesian inference model. Measurement errors in the cell-type

abundance data was explicitly modelled to achieve accurate estimation of interaction parameters. Our results show that we can predict pairwise interactions in two different three-member consortia. Furthermore, we computationally validated this approach to predict pairwise interactions in larger consortia with diverse interactions.

2. Materials and Methods

2.1. Strains, media, and culture conditions

Table 1 describes the strains that were used in this study. *Lactococcus cremoris* strains were grown in chemically defined medium for prolonged cultivations (CDMpc) (10). For growth on casein as a nitrogen source, 2 g L^{-1} of casein sodium salt (from bovine milk, C8654, Sigma-Aldrich, Saint Louis, MO, USA) was added to the medium instead of the amino acids (CDMpc_cas). For growth in CDMpc with limiting amounts of amino acids and glucose, 1% of the amino acid concentration in CDMpc and 0.02% (wt/v) glucose were added to CDMpc_cas (CDMpc_cas,aa,glu). For preparation of agar plates, 2% (wt/v) sterilised agar was added to CDMpc + 0.5% (wt/v) trehalose or M17 (CM0817, Oxoid, Ireland) + 0.5% (wt/v) glucose. For long-term storage at -80 °C, glycerol was added to overnight cultures of *L. cremoris* to obtain a final concentration of 25% (v/v).

We grew the pre-cultures of *L. cremoris* NZ9000 Glu^- Lac^+ and *L. cremoris* NZ5500 in CDMpc + 0.09% (wt/v) lactose, and the pre-cultures of *L. cremoris* MG610, *L. cremoris* MG1363-GFP, and *L. cremoris* MG1363 in CDMpc + 0.09% (wt/v) glucose. Pre-cultures were incubated at 30 °C statically for at least 16 h. Co-cultures or monocultures of the strains when grown in CDMpc_cas,aa,glu + 0.5% (wt/v) lactose, were incubated for at least 40 h at 30 °C statically. The cultures were de-coagulated after growth by adding sodium hydroxide to increase the pH to no more than 7.

We determined the relative proportions of *L. cremoris* MG1363 and *L. cremoris* MG1363-GFP in the inoculum for emulsions using flow cytometry. We determined the proportions of these two strains after microbead sorting in phosphate-buffered saline (PBS) by vortexing the solution with microbeads and plating on M17 + 0.5% (wt/v) glucose agar plates. After incubation at 30 °C for at least 40 h, we counted the resulting fluorescent and non-fluorescent colonies by illuminating the plate with Safe Imager 2.0 Blue-light Transilluminator (Invitrogen, MA, USA).

To determine the fraction of different cell types after microbead sorting, we vortexed the sort-tubes containing microbeads and PBS. We then plated the resulting suspension on agar plates with CDMpc + 0.5% (wt/v) trehalose, which supports the growth of all strains. The plates were incubated at 30 °C for at least 40 h. From each trehalose plate, 48-95 randomly picked colonies were individually inoculated in four different media: 1) CDMpc + 0.5% (wt/v) lactose, 2) CDMpc + 0.5% (wt/v) lactose + 10 µg/mL erythromycin, 3) CDMpc_cas + 0.5% (wt/v) glucose and, 4) CDMpc + 0.5%

Table 1: Strains used in this study.

Strain	Relevant genotype	Description	Reference
NZ9000 Glu$^-$ Lac$^+$	*L. cremoris* NZ9000*ΔglkΔptnABCD* carrying pMG8020 (derivative of pLP712, carrying *lacFEGABCD*) and contains a 657-bp deletion in *ptcBA*.	Uses the galactose moiety of lactose as a carbon source and secretes the glucose moiety. Cannot use casein as a nitrogen source.	(11)
MG610	*L. cremoris* MG1363 with two copies of *prtMP* integrated into the genome, erythromycin resistant.	Uses glucose as a carbon source and casein or amino acids as a nitrogen source.	(12)
NZ5500	*L. cremoris* MG5267 with a loxP-ery-usp45p-melA-loxP fragment integrated into the genome, erythromycin resistant.	Uses lactose and glucose as carbon sources. Cannot use casein as a nitrogen source.	(13)
MG1363	Wildtype.	Uses glucose as a carbon source. Cannot use casein as a nitrogen source.	(14)
MG1363-GFP	*L. cremoris* MG1363 carrying pSEUDO::P_{usp45}-*gfp*.	Expresses GFP. Uses glucose as a carbon source. Cannot use casein as a nitrogen source.	(15)

(wt/v) glucose. Each colony was assigned a number, and the same numbered colony was inoculated in all four media to allow direct comparison. The ability of each colony to grow on these media was used to distinguish the strains as follows:

- Colonies that grow in media 1, 2 and 4 are *L. cremoris* NZ5500.
- Colonies that grow only in medium 1 are *L. cremoris* NZ9000 Glu$^-$ Lac$^+$.
- Colonies that grow in media 3 and 4 are *L. cremoris* MG610.
- Colonies that grow only in medium 4 are *L. cremoris* MG1363.

Colonies that deviated from these described growth profiles were excluded from the analysis, which were no more than 4% of the screened colonies.

2.2. Analytical methods

Optical density (OD) was measured at 660 nm using a Libra S11 spectrophotometer (Biochrom, Cambridge, United Kingdom). Cell concentration and microbeads were measured using a BD Accuri™ C6 Plus flow cytometry (BD Biosciences, San Jose, CA, USA). Concentrations of sugars, organic acids, and ethanol were measured via HPLC analysis on an Agilent 1260 HPLC (Agilent Technologies, CA, USA), equipped with a

Bio-Rad HPX 87H column (Bio-Rad, CA, USA). Detection was performed by an Agilent refractive index detector and an Agilent 1260 VWD detector. The size and volume distributions of the microbeads in oil were determined by imaging the emulsions using a Zeiss Axio Imager Z1 (Carl Zeiss AG, Jena, Germany) and an Axio Cam HRm Rev3 detector (60 N-C 1" ×1.0; Carl Zeiss AG) using the lateral magnification objective ×20. Details on the estimation of the average microbead size are described in Supplementary section 1.

2.3. Preparation of microbeads

Agarose microbeads in oil were prepared with a water phase and an oil phase (Novec HFE 7500 fluorinated oil, 3 M, Maplewood, MN, USA) containing 0.2% PicoSurf 1 surfactant (Sphere Fluidics, Cambridge, UK). The water phase contained CDMpc_cas or CDMpc_cas,aa,glu with 1% (wt/v) agarose with ultra-low gelling temperature (Type IX-A, A2576, Sigma-Aldrich, Saint Louis, MO, USA) and, when required, cells. At this low agarose concentration, we do not expect significant limitations in diffusion of nutrients.

Cells from pre-cultures were harvested when the OD_{660} was between 0.15-0.40. The cells were centrifuged (5 min 3000 x *g*), washed with PBS, and the cell concentration was measured. The cells were diluted based on inoculation Poisson λ-values (0.02 or 0.3) in CDMpc_cas or CDMpc_cas,aa,glu + 0.5% (wt/v) lactose. To prepare the emulsions, 300 µL of the water phase was mixed with 700 µL of the oil phase with the surfactant using a T10 basic ULTRA TURRAX homogeniser with an S10N-5G dispersing element (IKA, Staufen, Germany) at speed 2.5 for 5 minutes. The microbeads had an average volume of 49.65 pL ± 8.02 pL (diameter of 44.15 µm ± 2.37 µm, n=8, Supplementary section 1). The agarose was solidified by placing the emulsions on ice for at least 20 minutes. The emulsions were incubated statically at 30 °C for at least 40 h. After incubation, the microbeads were separated from the oil phase by adding 1.2 mL PBS and 1.5 mL perfluorooctanol (PFO, Alfa Aesar, Ward Hill, MA, USA) to 1 mL of the emulsion and gently mixing. The microbeads partitioned to the water phase, i.e., PBS, which was gently pipetted out.

2.4. Sorting of microbeads

Before measuring on the flow cytometer or the FACS, the microbeads were filtered with a 40 µm mesh (pluriStrainer, PET-mesh). Microbeads smaller than 40 µm were further analysed. The forward scatter, side scatter, and the green fluorescence signal were measured using the 488 nm laser. We analysed the microbeads with a flow cytometer and sorted them with the BD FACSAria™ II SORP Cell Sorter (BD Biosciences, San Jose, CA, USA) operated with the FACSFlow™ software (BD Biosciences) using a 130 µm nozzle. The green fluorescence signal was detected through a 545/28 nm or a 530/30 nm bandpass filter. Microbeads were sorted based on the sorting thresholds depicted in Figure S5 step 4, in tubes with 800 µL PBS or on agar plates with CDMpc + 0.5% (wt/v) trehalose. FlowJo™ v10.10 software (BD Life Sciences) was used for data

analysis. Details about the gating strategy are shown in Supplementary section 5.

2.5. Interaction model and Bayesian inference procedure

To predict pairwise interactions within a microbial consortium, we developed a simple interaction model with a Bayesian inference procedure. The model, implemented in Python, consists of 4 steps which are described in detail in Supplementary section 6. In short, the model calculates two interaction parameters: the relative growth of a pair of cell types in a microbead (denoted as G_{ij}) and the proportion of each cell type after growth (denoted as $f_{i|ij}$). The growth term G_{ij} is relative to a reference cell type pair that grows until medium depletion. First, we explicitly model the multinomial measurement noise to estimate the initial cell-type fractions in the inoculum, based on the observed initial counts and using the experimentally targeted fractions as prior information. Second, based on these initial fractions, an interaction model calculates the fraction of microbeads filled with each combination of cell types. Third, for a given set of interaction parameters, the model calculates the proportions of the cell types in the final population, *i.e.*, after growth in the microbeads and microbead-sorting. Given these predicted final cell-type proportions, the model calculates the likelihood of the observed final counts by accounting for multinomial measurement noise again. Finally, taking into account prior information on the interaction parameters, the model numerically finds the parameter values that have a maximum posterior probability (with a 68% posterior probability interval) given the observed final counts.

2.6. Computational validation using simulated data

To validate the inference model for larger consortia, we created simulated experimental datasets using the interaction model for consortia with up to six members. Each dataset was generated with a randomized set of initial cell-counts. These cell counts were generated by assuming a total sampled number of cells to be 96 or 1000 cells and by applying random multinomial sampling. For each condition tested, five replicate datasets were simulated. Two types of consortia were designed: consortia where none of the cell types could grow independently, *i.e.*, no isolated growth, and consortia where one or two cell types were capable of isolated growth. In scenarios where there is a negative interaction, we assume that both the cell types exhibit isolated growth, and depending on the direction of the interaction, we expect at least one of the cell types to grow. We defined growth until medium depletion relative to the reference cell type pair, which should always grow until medium depletion. Detailed implementation of the computational validation is described in supplementary section 7.

One-sided t-tests were performed to test for significant increases in one condition compared to another, whereas two-sided t-tests were used to test for significant differences in either direction.

All computational results were obtained using Python code, which is freely available on GitHub at https://github.com/Sagarikabg/Deciphering_Microbial_Interactions.git.

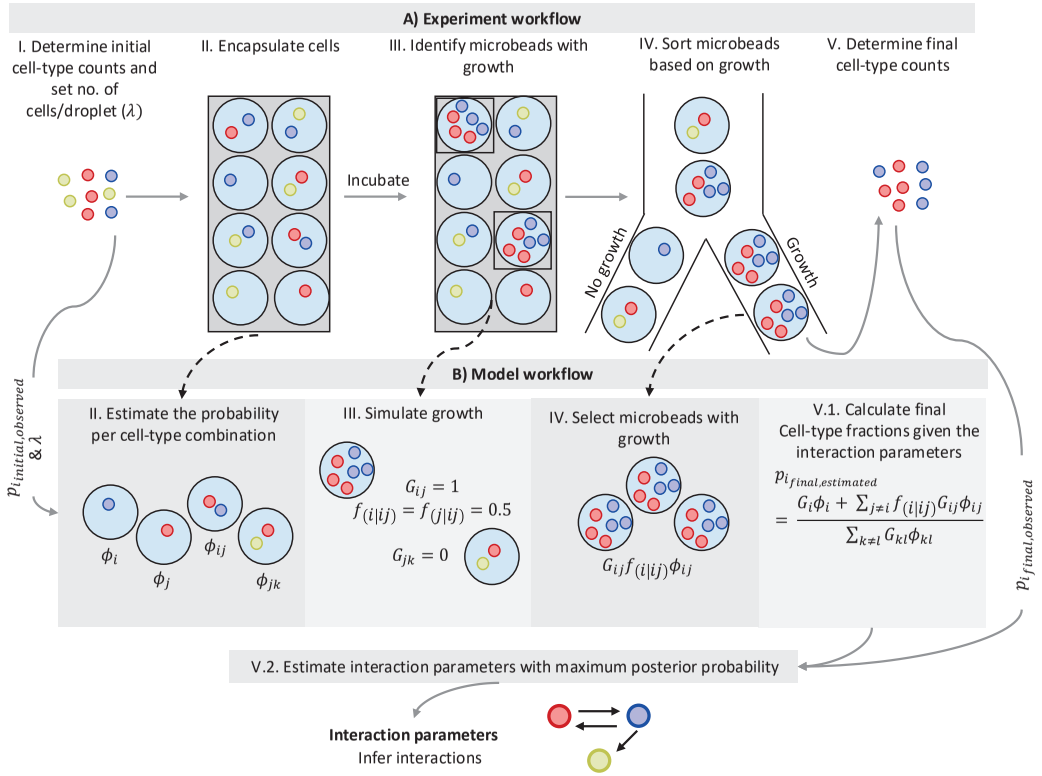

Figure 1: Schematic overview of the experimental workflow (A) and the corresponding modelling steps (B) to decipher pairwise interactions in a microbial consortium. We first determine the abundances of individual cell types in a microbial consortium (I.A) and then encapsulate cells in microbeads at a pre-determined λ-value, *i.e.*, at an expected number of cells per microbead. Using the initial abundances of cell types and the λ-value, we can estimate the probability of each cell-type combinations (Φ_{ij}) in the microbeads (II.B). After incubating until the stationary phase, we identify microbeads with growth using flow cytometry (III.A). In the model, growth in microbeads can be simulated using interaction terms; growth terms (G_{ij}) and strain-fraction term ($f_{i|ij}$) (III.B). Microbeads with growth are sorted (IV.A, IV.B), and the final abundances of cell types are determined (V.A). Using the λ-value, interaction parameters and initial and final cell-type fractions, we can calculate the final cell-type fractions (V.B.1). We estimate interaction parameters with the maximum posterior probability by incorporating potential prior information on the interaction parameters and the final cell-type counts (V.B.2). Using these interaction parameters, we can then infer interactions between the consortium members.

3. Results

3.1. Method to decipher microbial interactions

This study presents a label-free, isolate-independent method to infer microbial interactions in consortia (Figure 1), enabling analysis without the need for genetic engineering or prior isolation of individual consortium members. The approach also does not require prior knowledge of the nutritional requirements of the consortium members. It only relies on cell concentration and relative abundance data under the experimental conditions. The approach consists of three key steps:

1. High-throughput cultivation of sub-consortia: Consortium members are randomly encapsulated in oil-separated microbeads, each acting as an independent growth compartment. This allows cultivation in ~10^7 microbeads (40 µm diameter) per mL. The distribution of cells between compartments follows a Poisson and multinomial distribution which are determined by the total inoculum cell concentration and composition. Because cells are partitioned over a large number of compartments (~10^7 per sample), stochastic deviations from the expected fractions are averaged out.
2. Growth-based separation and composition analysis: We use an autofluorescence signal threshold to distinguish and sort sub-consortia that show growth. This is based on a shift in the autofluorescence signal of microbeads with growth of cells compared to microbeads that were only inoculated (Figure S5). The relative abundances of cell types are then determined in the sorted population (Figure 1A).
3. Inference of interaction parameters: We use a simple interaction model together with a Bayesian inference procedure to estimate interaction parameters for all cell-type pairs present in the consortium (Figure 1B). We explicitly model the multinomial sampling that leads to the observed cell-type counts, incorporate prior knowledge where applicable, and report uncertainty estimates on all inferred values.

3.2. Synthetic consortia design for method validation

To test the approach, we used two synthetic consortia of *L. cremoris* strains with known interactions. *L. cremoris* can grow both in the presence and in the absence of oxygen, and it can reach and can grow to high cell concentrations in microbeads (19). Both consortia contain the same bi-directional cross-feeding strains, A and B (Figure 2). Strain A (*L. cremoris* NZ9000Glu-Lac+) hydrolyses lactose intracellularly, uses galactose, and secretes glucose; it relies on peptides for nitrogen (11). Strain B (*L. cremoris* MG610) uses glucose and casein as carbon and nitrogen sources, respectively (12). It expresses an extracellular protease that hydrolyses casein into peptides. The two consortia differ in the third strain: C or C*. Strain C (*L. cremoris* NZ5500) uses both lactose and glucose and peptides (13). Strain C* (*L. cremoris*

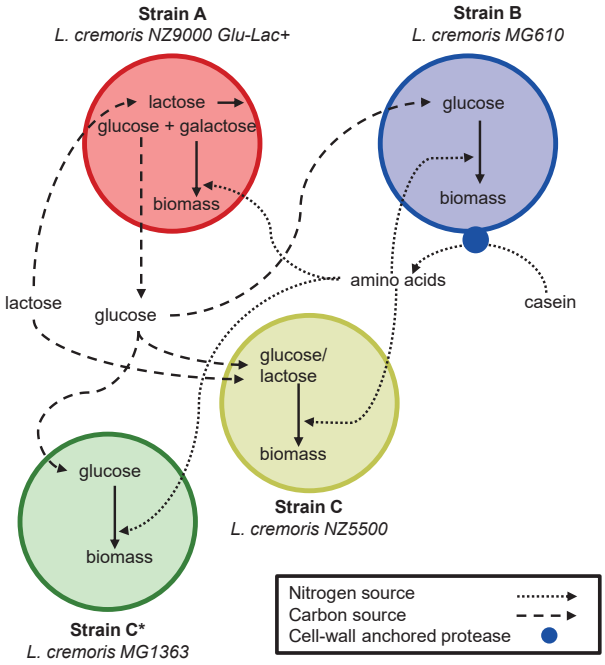

Figure 2: Synthetic consortia of *L. cremoris* strains used in this study. Strain A uses the galactose moiety of lactose as a carbon source and secretes glucose. It uses peptides (amino acids) as a nitrogen source. Strain B uses glucose as a carbon source. It can use casein as a nitrogen source by degrading it extracellularly into peptides. Strain C uses lactose and glucose as carbon sources and peptides as a nitrogen source. Strain C* uses only glucose as a carbon source and peptides as a nitrogen source.

MG1363) uses only glucose and peptides (14).

In a medium with lactose and casein as the sole carbon and nitrogen sources, respectively, all strains require at least a partner strain to grow (Supplementary section 3). Growth is ultimately limited by acidification due to lactate production, from now on referred to as growth until medium depletion. Natural systems often consist of many nutrients, which allows low-level background growth of individual species (16–18). To mimic this, we added low concentrations of glucose and amino acids to the lactose-casein medium (CDMpc_cas,aa,glu + lactose). The data on the growth of the mono- and co-cultures in suspension under conditions that mimic microbead growth, including inoculum cell concentration, medium composition and incubation conditions are provided in supplementary section 3. This data is used later in the study to validate the inferred pairwise interactions.

3.3. Determining the growth of individual consortium members

To test whether cells grow individually until medium depletion, we inoculated microbeads such that most filled microbeads contain one cell (at $\lambda = 0.02$, 99% of the filled microbeads contain one cell) (Supplementary section 2).

As a positive control for growth, we inoculated the consortia (Figure 2) in CDMpc + glucose + lactose medium, in which all cells can fully grow. After incubation, we analysed the emulsions by flow-cytometry and, as expected, we observed a shift in the fluorescence signal for microbeads with growth compared to a sample of empty microbeads (Figure S6). In contrast, when the consortia were inoculated in microbeads of CDMpc_cas,aa,glu + lactose medium, as expected, we did not observe a shift in the fluorescence signal for microbeads with growth compared to a sample of empty microbeads (Figure S6).

Altogether, these results indicate that the consortium members (Figure 2) individually do not grow in CDMpc_cas,aa,glu + lactose medium, which is consistent with the results we observed in suspension cultures (Supplementary section 3).

3.4. Deciphering pairwise interactions

To test whether the proposed approach can resolve pairwise interactions, we applied it to a consortium of strains A, B, and C (Figure 2) and evaluated whether we could predict the three pairwise interactions. We prepared three sets of emulsions; each inoculated with a different set of randomly chosen initial abundances of strains (Figure 3B). The random selection of initial strain abundances was based on the rationale that inference of interaction parameters be independent of the starting composition, provided that all strains are represented. The microbeads prepared with the medium CDMpc_cas,aa,glu + lactose were inoculated such that most of the filled microbeads contain no more than 2 cells per microbead (Supplementary section 2) (λ = 0.3, 90.25% of microbeads with two or more cells contain two cells). By using this λ-value, we maximise microbeads with two cells and minimise microbeads with three or more cells. After estimating initial abundances of strains, we inoculated, incubated, and sorted microbeads with growth. Finally, we determined the final abundances of strains.

Using the data on the growth of monocultures, initial abundances of strains (Figure 3B), the λ-value, and the final abundances of strains (Figure 3B), we employed our Bayesian inference model to estimate the interaction parameters for the three pairwise interactions (Figure 3C & Supplementary section 6).

Since we can only predict relative growth between strain combinations, we fix the growth of the strain pair A and B to 1. The proportions of strains A (0.40, posterior probability interval or ppi 0.37 – 0.42) and B (0.60, ppi 0.63-0.58) after growth and the absence of monoculture growth of the strains until medium depletion, suggest a bi-directional cross-feeding interaction between the strains (Figure 3C and D). This conclusion is supported by suspension culture data, which shows growth of the strain pair until medium depletion and similar strain proportions after growth (Supplementary section 3). This interaction is attributed to cross-feeding, where strain A provides glucose and strain B supplies amino acids (Figure 2).

The growth terms of the strain pair B and C (1.14, ppi 1.01 - 1.29), the proportions

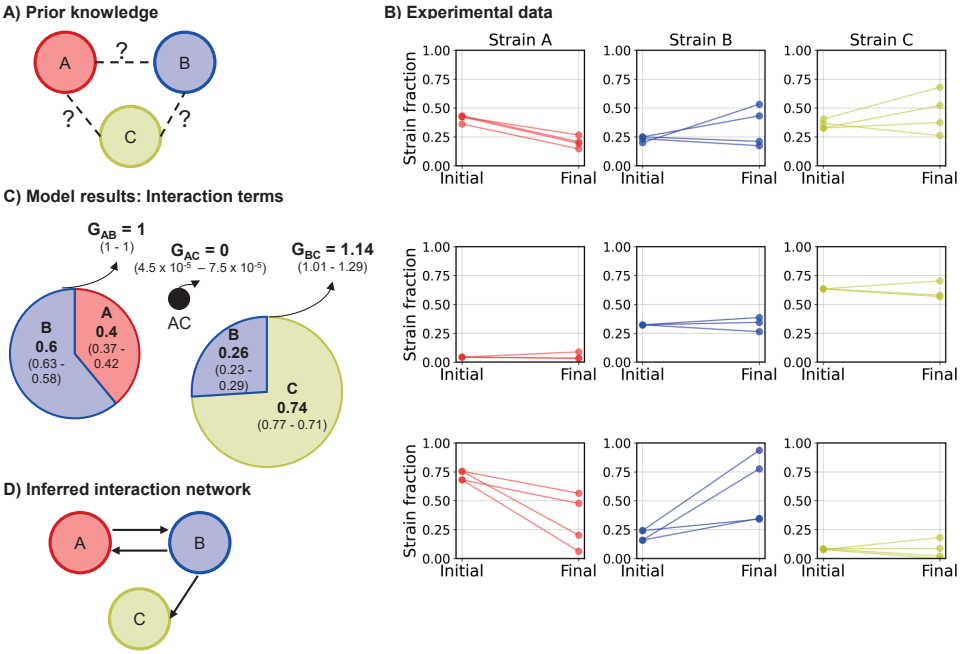

Figure 3: Inference of all pairwise interactions in a three-member consortium. (A) Prior knowledge where we provide no prior information on the interaction parameters. (B) Experimental data depicting the fractions of strains before and after microbead sorting. Microbeads with CDMpc_cas,aa,glu + 0.5 wt% lactose medium were inoculated at a λ of 0.3. Each panel represents data from experiment sets with different randomly chosen initial strain fractions. Individual lines represent individual experimental replicates (n = 3 or 4). Strains A, B, and C are represented by red, blue, and yellow colours, respectively. (C) Interaction parameters predicted by the probabilistic model. Each circle represents a pairwise interaction, and the radius of the circle is proportional to the growth of strain pairs relative to the growth of strain pair A and B. The slices of the circles represent the proportions of the individual strains in a pair after growth. The posterior probability interval of the inferred parameters is within brackets. (D) Inferred pairwise interactions from the interaction parameters.

of strains B (0.26, ppi 0.23-0.29) and C (0.74, ppi 0.77-0.71) and the absence of monoculture growth of the strains until medium depletion, suggests that strain B facilitates the growth of strain C (Figure 3C and D). This interaction is further supported by data from suspension cultures (Supplementary section 3). The growth of strain B is limited by the small amount of glucose in the medium, and strain C also competes for the glucose. Assuming both strains exhibit equal growth rates and cell yields on glucose, the initial 'background' growth of each strain can be estimated to 2 cells per microbead, and we expect the final total cell concentration of 9 cells per microbead. Based on this, we expect the final proportion of B to be approximately 0.22, which aligns with the model predictions. This interaction could be attributed to strain B's ability to grow on the limited glucose, producing sufficient amino acids to support strain C's growth on lactose until medium limitation (Supplementary section 3).

The growth term for strain pair A and C (4.5×10^{-5}, ppi 4.5×10^{-5}– 7.5×10^{-5}) suggests that they do not grow when co-localised (Figure 3C and D). These results correspond to what we observed in suspension cultures (Supplementary section 3).

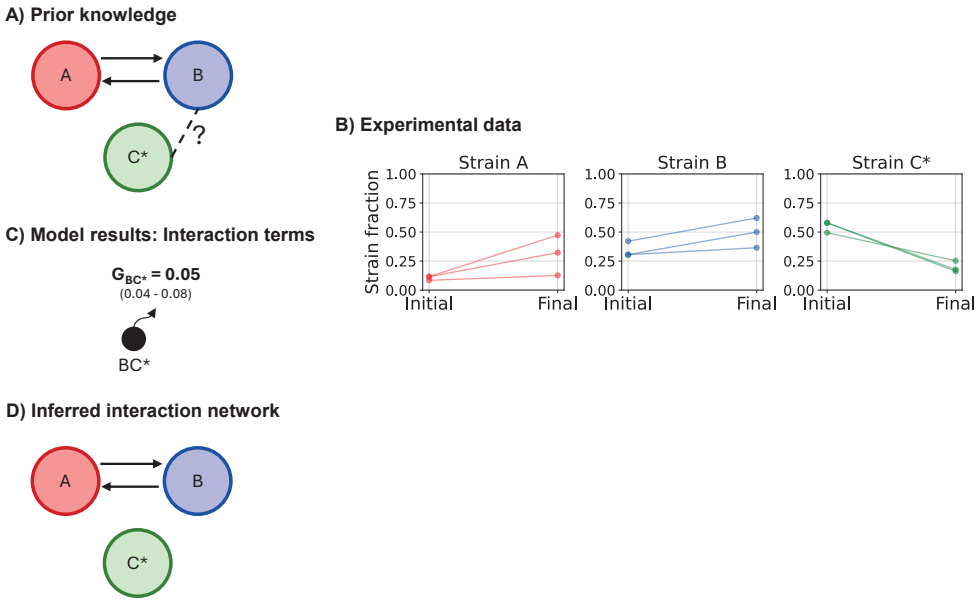

Figure 4: Inference of an unknown pairwise interaction in a three-member consortium using prior information. (A) Prior knowledge where prior information for interactions between strain pairs A-B and A-C* is provided, and no prior information is provided on the interaction parameters for strain pairs B-C*. (B) Experimental data depicting the change in fractions of strains before and after microbead sorting. Microbeads with CDMpc_cas,aa,glu + 0.5 wt% lactose medium were inoculated at a λ of 0.3. Each panel represents data from experiment sets with different consortia. Individual lines represent individual experimental replicates (n=3). Strains A, B, and C* are represented by red, blue, and green colours, respectively. (C) Interaction parameters for the interactions between strains B and C* predicted by the probabilistic model. Interactions between strains A and B and strains A and C* are fixed. Each circle represents a pairwise interaction; the radius of the circles is proportional to the growth of the strain pairs and B and C*. The slices of the circles represent the proportions of the individual strains after growth. The posterior probability interval of the inferred parameters is within brackets. (D) Inferred pairwise interactions between strains B and C* from the interaction parameters.

Altogether, we demonstrate that using microbead sorting, we can decipher all the pairwise interactions within a three-member consortium. Despite not providing any prior information to the inference model, it accurately predicts interaction parameters. Moreover, the accuracy of the inferred parameters indicates that our assumed microbeads occupancy in the model closely matched the true occupancy, similar to what was observed in previous studies (7,19).

3.5. Extending method validation to a different consortium using prior information

To further validate the approach, we tested whether we could decipher a pairwise interaction in another consortium using prior information. The consortia in Figure 2 have the same strains A and B but differ in strain C*. We tested whether we could decipher the interaction between strains B and C*. We therefore repeated the same experiment with the consortium A, B, and C* with the goal to infer the interaction parameters between the strain pair B-C*. We incorporated in the inference model prior information on the known interaction parameters; we thus set the interaction

parameters to the parameters previously predicted (Figure 3C) between all the strain pairs except for B and C*.

The growth term for the strain pair B and C* (0.05, ppi 0.04 - 0.08) indicates that these strains, when co-localised, do not grow (Figure 4C). This result corresponds to what we observed in suspension cultures and to our knowledge of the synthetic consortium (Supplementary section 3). Although strain B's growth on the limiting amount of glucose might be sufficient to support the growth of strain C until medium depletion by using lactose as the carbon source, strain C* cannot use lactose and grow until medium depletion despite the presence of sufficient amounts of amino acids. Altogether, these results support that we can reliably decipher pairwise interactions in two different consortia.

3.6. Computationally deciphering pairwise interactions in larger consortia

We aimed to computationally evaluate whether we can decipher pairwise interactions within larger consortia. We designed consortia ranging from 4 to 6 members and simulated the growth of these consortia at a, like in the experiments, Poisson λ of 0.3. We chose this λ to maximise microbeads with two cells and minimise microbeads with three or more cells (90.2% of microbeads with two or more cells contain two cells).

We simulated data for different numbers of experiments, where each experiment is initiated with a random set of initial cell-type proportions in the consortium. Each experiment provides us with measurements of the initial and final cell-type proportions; in a consortium with N cell types, we get $(N\text{-}1)$ independent measurements. However, we need to fit $\frac{(N-1)N}{2}$ set of growth factors (G_{ij}) and relative proportions ($f_{i|ij}$). We therefore expect better prediction of interaction parameters for larger consortia by the inference model as the number of experiments and thereby the number of independent measurements increases. Particularly when the number of independent measurements exceeds the number of unknown interaction parameters.

Based on five sets of random initial fractions of consortium members (i.e. five replicate simulated datasets) and the consortia design, the final fractions were calculated with the simulation model (supplementary section 7). After generating the simulation data, we used this data to decipher interactions with our inference model. We ignore all higher-order interactions (between three or more cell types) in the simulations as well as in the inference model, since we set the λ to 0.3, where only 1% of microbeads with cells contain three or more cells. We estimated inference errors per interaction parameter— absolute differences between the interaction parameters predicted by the inference model and the corresponding interaction parameters used in the simulation. We estimated two sets of inference errors: one for the growth term (G_{ij}) and one for the cell-type fractions ($f_{i|ij}$) (only considered when the corresponding $G_{ij} > 0.1$). We represented these inference errors with the distribution from five sets of random initial fractions of consortium members (independent replicates) (Figure 5).

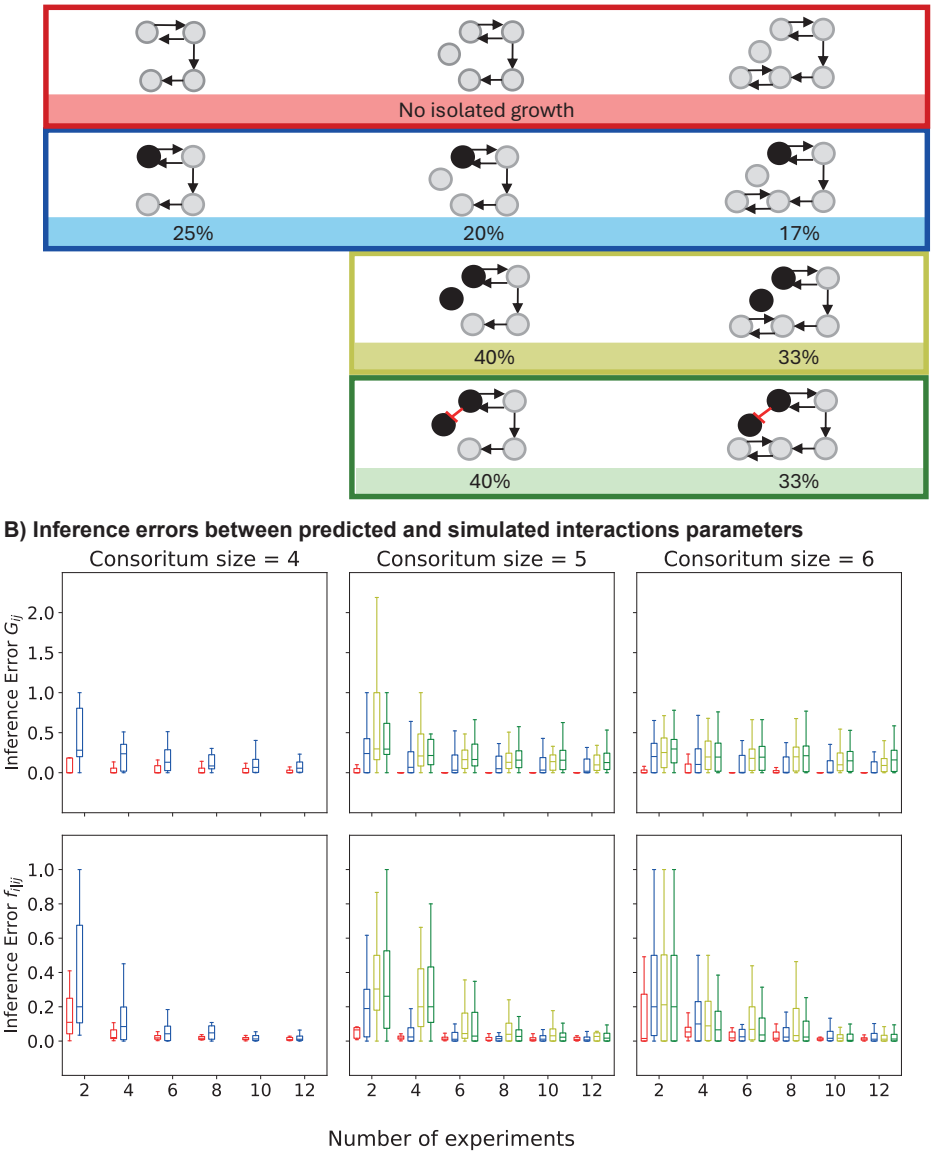

Figure 5: Computational validation to infer interactions in larger consortia. Inference errors between predicted and simulated interaction parameters. (A) Consortia were designed for simulation; the cell types that do not grow by themselves, i.e. with no isolated growth, are represented in grey and cell types that grow by themselves are represented in black. The percentage of consortium members capable of isolated growth is indicated below each consortium. (B) The distribution of inference errors of the growth (G_{ij}) and cell-type fraction terms ($f_{i|ij}$) for different numbers of experiments, where the inference error is the absolute difference between the interaction parameters predicted by the inference model and the corresponding interaction parameters used in the simulation For these simulations, the λ was set to 0.3 and number of colonies to determine cell type abundances was set to 1000. The number of experiments corresponds to the number of unique sets of initial cell-type counts. The individual box plots represent the distribution of the inference errors for five random replicates for the same number of experiments. The colours of the box plots correspond to the consortia configurations in panel (A).

We simulated sampling either 96 colonies or 1000 colonies to estimate the abundances of the different cell-types for the inference model. In our Bayesian inference model, we only explicitly model the noise from multinomial sampling when estimating cell-type counts, assuming the other experimental sources of noise are negligible. Sampling 96 colonies (Figure S8) represent a 'high noise' scenario, and 1000 colonies corresponds to a 'low noise scenario' (Figure 5). The decrease in the average inference error with an increased number of sampled colonies could be attributed to decreased sampling noise. Therefore, in the analyses below, we focus on the 1000 colonies sampling condition, where lower noise levels allow clearer visualisation of the observed trends.

In our simulations, we constructed consortia in which none of the cell types could grow independently (Figure 5A). In this case, we observed that the inference errors are low regardless of the consortium size (Figure 5B). We then incorporated one or two independently growing cell types into the simulated consortia (Figure 5A); we define this as isolated growth. In the presence of isolated growth, for a given consortium size, we observed that the inference errors in most cases increases with the proportion of cell types capable of isolated growth (Figure 5B). For example, irrespective of consortium size and the number of experiments, inference errors for both interaction parameters are significantly higher ($p<0.05$) for consortia with one cell type capable of isolated growth compared to consortia with no isolated growth. In addition, for consortia of sizes 5 and 6 across different number of experiments, inference errors for both interaction parameters are significantly higher ($p<0.05$) in consortia with two cell-types capable of isolated growth compared to those with only one such cell type.

While the inference errors generally decrease with an increasing number of experiments, they do not reach the lower errors observed in conditions without isolated growth (Figure 5B). This is expected since, given that the expected number of cells per microbead is 0.3 in these simulations, many of the microbeads with cells (=86%) will have only 1 cell. As a consequence, when cell types can grow in isolation, they will heavily contribute to the final population of cells. Although larger errors are expected, the model can still recover the interaction parameters to a reasonable accuracy. We attribute this to the large number of colonies sampled to determine cell-type fractions (=1000). In addition to incorporating isolated growth, we introduced a negative interaction between two cell types capable of isolated growth (Figure 5). The resulting inference errors followed the same trend as that observed in the corresponding consortia with isolated growth alone (Figure 5). The errors were not significantly different ($p>0.05$).

In summary, the inference errors are lowest under conditions without isolated growth and generally increase with the rise in the proportion of consortium members capable of isolated growth for a given consortium size. Introducing a negative interaction between cell types capable of isolated growth does not alter this trend.

We validated the method for a range of interactions, including commensalism (+/0), mutualism (+/+), and amensalism (0/-). The same approach can be extended to

decipher other negative interactions, such as competition (-/-) and antagonism (+/-), as well as neutral interactions (0/0). Using this framework, we can infer these interactions based on whether a cell-type's growth decreases (negative) or remains unchanged (neutral) when co-localized with another cell-type.

4. Discussion

We proposed and validated a novel microbead-based approach to decipher microbial interactions in a label-free, isolation-independent manner, unlike existing microdroplet-based methods that require single culture isolates and the expression of fluorescent markers via genetic engineering (7–9). This approach enables inoculation of microbeads with all possible sub-consortia combinations and enrichment of sub-consortia based on growth, using autofluorescence as an indicator. We validated this approach by deciphering pairwise interactions in two synthetic three-member consortia.

Natural microbial communities are often found in nutrient-rich environments, such as the gut. In such environments, we expect background growth of consortium members, i.e., individual growth to a low cell concentration (16–18). However, in the presence of another consortium member with a positive interaction (such as commensalism and mutualism), a higher cell concentration could be reached. Background growth adds noise to the relative abundance data, making it challenging to derive interaction parameters. This was shown in a study where sub-consortia in microdroplets were intermittently mixed between each propagation (19). In the early rounds, background growth of monocultures introduced noise into the relative abundance data, complicating accurate identification of interactions. As a result, multiple rounds of serial propagations were required to obtain reliable interaction data. To reduce the effect of background growth, we incorporated microbead sorting. Using microbead sorting, we can select monocultures and sub-consortia that grow until medium depletion and eliminate the microbeads with only background growth. Our results show that we can decipher pairwise interactions among the consortium members despite the presence of background growth.

We demonstrated computationally that interactions can also be deciphered in larger consortia. The prediction accuracy was highest without isolated growth. For a given consortium size, the accuracy decreased as the proportion of cell types capable of isolated growth increased. More experiments, i.e. providing more data, improved the prediction accuracy, but errors remained higher than in cases without isolated growth. The pattern persisted even in the presence of a negative interaction, such as amensalism. This is because, at a λ of 0.3, 86% of microbeads inoculated with cells contain only one cell. This results in a high relative contribution of cell types capable of isolated growth to changes in the final cell-type fractions, reducing data resolution for accurate interaction parameter inference. Increasing λ may improve the inference accuracy by reducing the proportion of microbeads inoculated with a single

cell. However, this would increase microbeads with three or more cells, introducing higher-order interactions (where the presence of a third community member modifies a pairwise interaction) that require additional model parameters. Alternatively, controlled inoculation of all microbeads with two cell types per microbead using surface acoustic waves or inertial focusing (20,21), could improve inference.

Although we only validated the approach using synthetic microbial consortia, it has the potential to be adapted to natural microbial communities. This additionally requires (i) stabilising consortia isolated from environmental samples, (ii) determining relative abundances of cell types in both the inoculum and post-sorting, and (iii) generating inocula with varied relative abundance profiles. Stabilisation can be achieved by serial passaging in the target medium to filter out non-growing cell types (22,23). Relative abundances can be assessed via amplicon sequencing of species-specific rRNA genes (1). To introduce variations in relative abundances, without isolating individual species, we can use stochastic methods such as serial dilution with random aliquoting of different dilutions (though this may favour dominant species) or use perturbations like nutrient pulses, temperature shifts, or pH changes.

The application of the proposed approach in this study to enable inference of microbial interactions directly from natural communities still faces several limitations. First, the method relies on autofluorescence to detect growth in sub-communities, but autofluorescence could vary across species due to physiological differences. We can overcome this by using alternatives, such as staining for viability (24) or metabolic activity (9), or tracking droplet-level changes in size (25) or weight due to growth (26). Second, species-specific traits can also introduce bias. For instance, agarose-degrading microbes may break down microbeads, causing loss of microbeads harbouring these cell types and skewing the estimation of interaction parameters. We can mitigate this by switching to alginate microbeads or adopting water-in-oil-in-water emulsions, which are compatible with microbead sorting. A key limitation, however, is that the method currently is restricted to soluble carbon sources and nutrients that do not readily partition into the oil phase.

Commonly used ecological models like the Generalised Lotka-Volterra model and Generalised Consumer-Resource model define interactions by employing growth rates and abundance data over time (4,6,27). Our approach does not consider growth rates but defines interactions based on abundance data from a single time point, usually after medium depletion. This limits our approach in capturing dynamic changes such as growth-dependent interactions and cell-concentration-dependent co-operation (28). However, after microbead sorting, each enriched sub-consortia can be characterised further in suspension cultures to track dynamic changes. Thus, our approach acts as an initial high-throughput screen, after which sub-communities of interest can be investigated further with more specific methods.

In addition to determining pairwise interactions, the approach presented in this study has the potential to decipher higher-order interactions. The challenge with determining higher-order interactions is the additional interaction parameters to

estimate. To solve this problem, we envision an iterative scheme. We first inoculate at a low λ-value to determine monoculture growth parameters. By inoculating with a low number of cells per microbead, we ensure that cells are growing by themselves, such that these growth parameters can be inferred reliably. Subsequently, we can increase the λ-value to infer pairwise interactions. In this iteration, we can then use the previous results on the monoculture growth parameters to constrain the prior expectation for these parameters. Knowing the pairwise interactions, we can proceed to determine triplet interactions. To have sufficient resolution to predict triplet interactions, it is crucial to balance the proportion of microbeads inoculated with three or more cells relative to those that show growth when inoculated with one to two cells. Determining higher-order interactions using microbead-based methods is also constrained by the carrying capacity of microbeads. If the carrying capacity of microbeads is 10 cells, then we are limited to deciphering pairwise interactions to ensure sufficient cell doublings within a microbead. We can mitigate the carrying capacity limitation by alleviating medium limitation (sugar, pH, nutrients, etc.) and/or by increasing the bead size. However, for droplets or beads larger than about 50 pL, conventional FACS is no longer suitable; instead, we require large particle sorters (29).

In light of future experimental developments, it is important to note that the Bayesian inference model developed in this study explicitly only models the multinomial sampling noise arising from our plating-based determination of the initial and final cell-type frequencies. However, we ignore other potential noise sources (such as errors introduced during microbead-sorting, or biological variation in growth between cells from the same strain in different microbeads). Under the current experimental conditions, these noise sources were negligible compared to the multinomial sampling noise. This assumption may not hold in slightly altered experiments, for example when working with larger consortium sizes or less well-characterized strains. Therefore, it is essential to identify the dominant sources of measurement noise, and adapt the model accordingly.

Although alternative microdroplet-based methods enable high-throughput inference of higher-order interactions and control over co-occupancy, they typically rely on genetically engineering fluorescent labels into each cell type to monitor sub-consortium growth (7–9), which is often not feasible for natural consortia. Species-specific fluorescent labelled rRNA probes (FISH) offer a non-genetic-engineering alternative (1), but traditional FISH compromises cell viability. Promising advances in LIVE-FISH (30, 31) combined with microbead-based cultivation (7–9) could enhance the throughput of deciphering interactions in natural microbial consortia.

Apart from deciphering interactions, the proposed method can be applied to elucidate rare growth-promoting interactions which are expected to evolve under restrictive conditions, such as mutualistic cooperation (3,8,19,28). Existing approaches are limited by the reliance on culturable isolates, which constrains them to a few phylogenetic groups. Since, for example, cooperation often results in higher cell

concentrations, the proposed method could be adapted for high-throughput screening of consortia of such interactions. This could enable the elucidation of interactions yielding higher cell concentrations across diverse environments that reveal different interactions, helping to derive principles driving their evolution and selection.

The approach presented in this study can also be extended for developing synthetic consortia for industrial biotechnology applications. Recent research on valorising complex mixed substrates from waste streams shows that consortia of specialists — where each member is specialised to convert one of the substrates to the product — outperform generalist microorganism that converts all of the substrates to a product (32-34). However, the key challenge is the stability of these specialist consortia. Since efficient substrate consumption by stable consortia would result in higher biomass yields, the proposed method provides a high-throughput approach to screen for high biomass yields of sub-consortia on substrate mixtures. Thereby, enabling enrichment of stable specialist sub-consortia from a large mutant pool. Beyond growth, the method can be adapted to screen for diverse phenotypes by incorporating stains or assays targeting metabolic activity, respiration, nucleic acid content, and other biochemical traits.

The label-free and isolation-independent approach proposed in this study has the potential to decipher interactions in diverse and unexplored natural microbial consortia. It paves the way for research to understand interactions driving the stability and function of microbial consortia and offers opportunities to define design principles for industrial applications of microbial consortia.

Acknowledgements

We would like to thank Jack T. Pronk for conceptual project discussions, Nienke Alkemade for testing the defined medium used for cultivations and Marijke A. H. Luttik for technical support.

Author contributions

RJvT conceptualised the work. DHdG built the theoretical models. RJvT and SBG designed experiments. SBG performed experiments and conducted data analysis. All authors read and approved of the final manuscript. SBG wrote the original draft of the manuscript, which was reviewed and edited by RJvT and DHdG.

RJvT and SBG are funded by Delft University of Technology.

Supplementary information

Supplementary section 1: Microbead size and volume distributions

We prepared agarose microbead emulsions as described in the materials and methods section. We imaged the resulting polydisperse microbeads with a microscope (Figure S1A, 9 images per emulsion). The images were subsequently analysed with ImageJ to identify the microbeads and determine their size (Figure S1B). Microbeads on the edges of the images and small microbeads (up to 2 µm in diameter) were excluded from the analysis. Based on these ImageJ results, average microbead diameter and volume distributions were determined.

The average number of cells in a microbead is defined by the λ-value of the Poisson distribution. The λ-value is dependent on the number of cells added to the water phase and the average size of microbeads. Since we use polydisperse emulsions, we have a distribution of microbead sizes. Although smaller microbeads (< 20 µm) are more abundant (Figure S1D), due to a low volume of these microbeads, they occupy a small fraction of the total water phase (Figure S1C). When cells are homogenously mixed in the water phase, only a small fraction of the cells is harboured within the small microbeads due to the low volume fraction of the water phase occupied by these microbeads. Most of the cells in the water phase will be distributed over the larger microbeads. We reasoned that the average diameter of microbeads that occupy the highest volume fraction represents the average diameter of the emulsion and can be used to determine the λ-value.

The average diameter (± standard error of the mean) of microbeads that occupy the largest volume fraction was calculated to be 49.65 pL ± 8.02 pL (44.15 µm ± 2.37 µm, n=8).

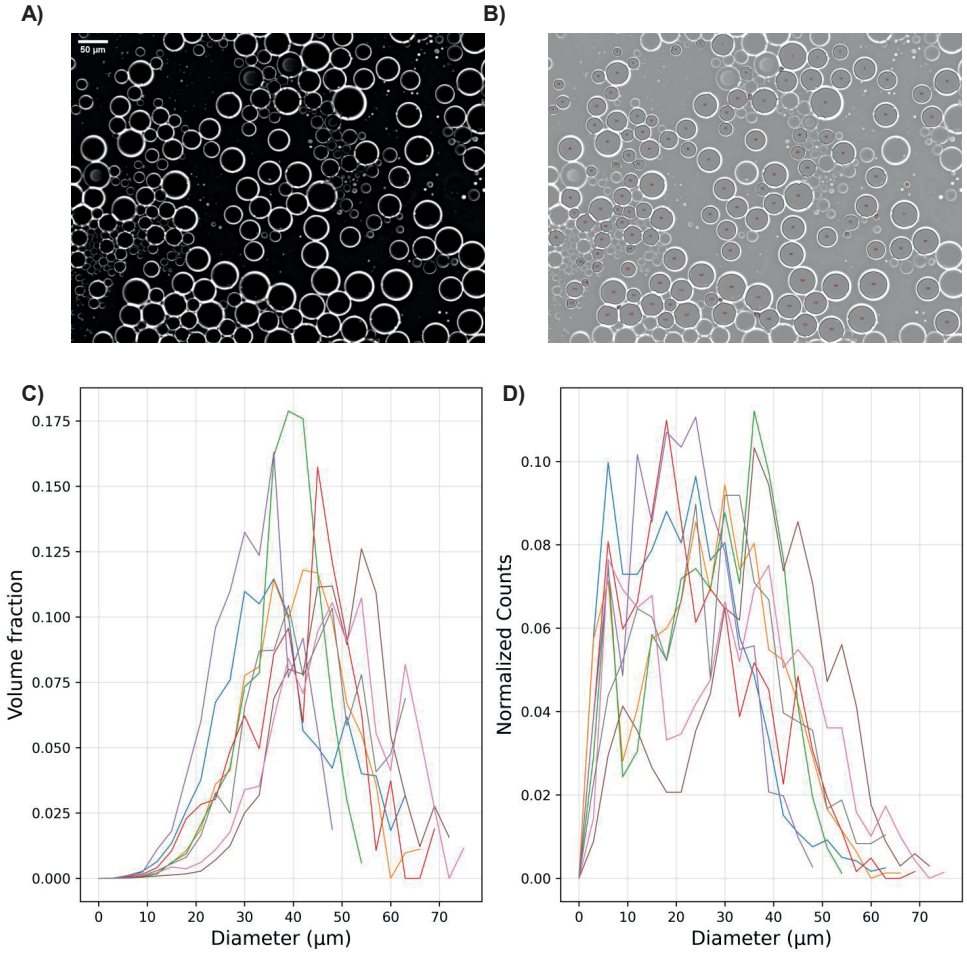

Figure S1: (A) Microscopic image of agarose microbeads. (B) Agarose microbeads identified in (A) by ImageJ analysis. (C) Microbead diameter distribution based on volume fraction of the water phase and (D) Microbead diameter distribution based on counts, where counts were normalised to the total number of microbeads analysed per emulsion.

Supplementary section 2: Poisson distribution

To determine the growth of individual consortium members we used a λ-value of 0.02, at which 99% of filled microbeads contain one cell. However, at this λ, 98% of microbeads are empty. Since we can generate many microbeads (10^7), this still allows us to analyse 10^5 microbeads per sample. (Figure S2)

To determine pairwise interactions, we used a λ-value of 0.3. At this λ-value, we expect 74% empty microbeads. However, 90% of microbeads with two or more cells contain two cells. This allows us to maximize the number of microbeads with two cells and minimise the number of microbeads with three or more cells.

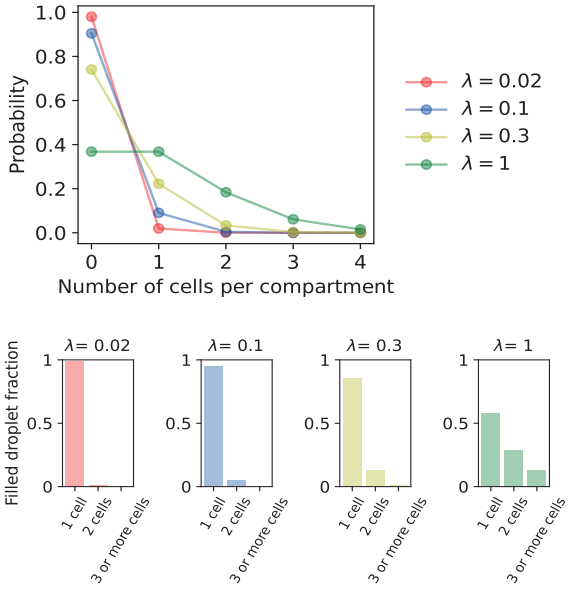

Figure S2: Poisson distribution for λ-values of 0.02, 0.1, 0.3 and 1. The line plot shows the probability of compartments containing 0 to 4 cells per compartment. The bar plot shows the fraction of filled compartments containing 1, 2 and 3 or more cells.

Poisson distribution formula to estimate the amount of cell culture required to prepare emulsions:

V = volume of the water phase (µL, usually 300 µL)

D = mean microbead diameter (µm)

C_{cells} = cell-culture concentration (cells μL^{-1})

λ = average microbead occupancy

A = amount of cell culture to use (µL)

$$A = \frac{\lambda \cdot V \cdot 10^9}{\frac{4}{3} \cdot \pi \cdot (0.5 \cdot D)^3 \cdot C_{\text{cells}}}$$

Supplementary section 3: Mono- and co-culture analysis

To test if the consortia grow as expected, we determined the growth of monocultures and co-cultures of the consortia in suspension cultures. These cultures were inoculated in CDMpc_cas,aa,glu + lactose medium at cell concentrations mimicking 2 cells per microbead. Monocultures of strains A and C, limited by amino acids in the medium, exhibited a 1.63 ± 0.047 and 1.86 ± 0.047 fold increase in cell concentrations, respectively (Figure S3). Monocultures of B and C*, limited by glucose in the medium, showed a 2.33 ± 0.26 and 1.73 ± 0.094 fold increase in cell concentrations (Figure S3 & S4). In co-cultures, cross-feeding between strains A and B allowed growth until medium depletion, with a 5.03 ± 0.54 fold change in cell concentration (Figure S3). After growth, the proportions of strains A and B were 0.49 ± 0.085 and 0.51 ± 0.085, respectively (Figure S3). The strain pair B and C also grew until medium depletion, with a 5.00 ± 0.24 fold increase in cell concentration (Figure S3). However, only strain C is detected after growth (Figure S3). This suggests that the glucose-limited growth of strain B was sufficient to break down enough casein to supply amino acids for strain C to grow until medium depletion, which uses lactose as the carbon source. Growth of the strain pair A and C was amino acid limited, with a 1.80 ± 0.082 fold increase in cell concentration (Figure S3). Growth of the strain pair A and C*, limited by amino acids, showed a 2.00 ± 0.082 fold increase in cell concentration (Figure S3). Growth of the strain pair B and C* was limited by glucose, with a 2.06 ± 0.094 fold increase in cell concentration (Figure S3).

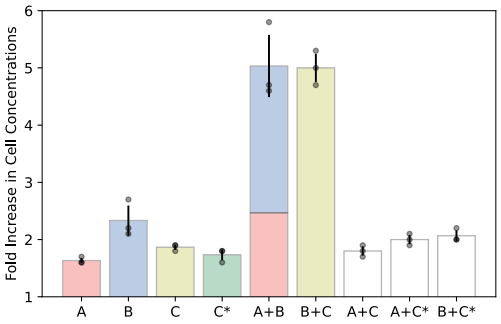

Figure S3: Average fold increase in stationary phase cell concentrations (n=3) of suspension cultures incubated in medium CDMpc_cas,aa,glu + 0.5 wt% lactose for monocultures and co-cultures. Monocultures and co-cultures were inoculated at initial cell concentrations of $6{\cdot}10^7$ cells mL^{-1}. These inoculation cell concentrations correspond to an average of 2 cells per 40 µm microbead. Co-cultures were inoculated with 32.4% A and 67.6% B, 53.6% B and 46.4% C, 54.4% A and 45.6% C, 56.5% A and 43.5% C* and 48.3% B and 51.7% C*. The proportions of strains A, B, C and C* after growth are indicated by the colours red, blue, yellow and green, respectively. Strain pairs A and C, A and C*, and B and C* did not grow until medium depletion; hence, their proportions were not measured after growth.

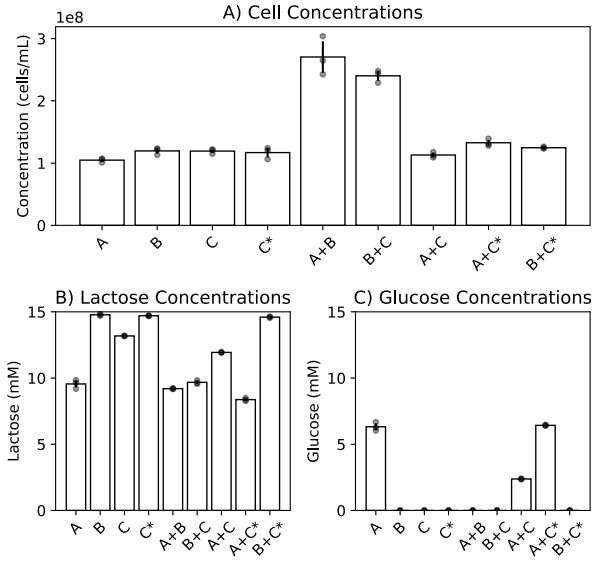

Figure S4: Average cell (A), lactose (B) and glucose (C) concentrations of stationary phase cells (n=3) of suspension cultures incubated in medium CDMpc_cas,aa + 14.6 mM lactose + 1.1 mM glucose for mono-cultures, and co-cultures. Cultures were inoculated at initial cell concentrations of $6{\cdot}10^7$ cells mL^{-1}. These inoculation concentrations correspond to 2 cells per 40 µm microbead. Co-cultures were inoculated at the following ratios: A + B (0.32,0.68), B + C (0.54,0.46), A + C (0.49,0.51), A + C* (0.57,0.43), and B + C* (0.48,0.52).

Supplementary section 4: Assessment of the experimental workflow

To test whether we achieve growth in microbeads, identify microbeads with growth using flow cytometry, and selectively enrich for sub-populations, we designed an experiment with a mixture of wild-type and GFP-expressing *Lactococcus cremoris* strains. We grew the mixture in microbeads, sorted using a FACS for the high-fluorescence microbead population, and tested if we selectively enriched the GFP-expressing strains from the mixture.

To ensure that each inoculated microbead has only one cell, we inoculated microbeads at a λ-value of 0.1. At this λ-value, 95% of the filled microbeads contain 1 cell per microbead (Figure S2). We identified microbeads with growth based on a fluorescence threshold on the FACS (Figure S5). We observed a shift in fluorescence for microbeads with the growth of *L. cremoris* MG1363-GFP and for *L. cremoris* MG1363 (Figure S5). Although *L. cremoris* MG1363 is not fluorescently labelled, we still observed a shift in fluorescence for microbeads with growth of the strain, due to the autofluorescence of the cells. To selectively enrich for *L. cremoris* MG1363-GFP, we sorted microbeads with the highest fluorescence signal, and we subsequently measured the relative abundances of the strains.

The results show that *L. cremoris* MG1363-GFP was enriched from a starting proportion of 7.1 ± 0.4 % to a final proportion of 57.5 ± 13.2 % (n=4). The presence of non-fluorescent *L. cremoris* MG1363 is possibly due to inaccuracies in sorting and possible adhesion of *L. cremoris* MG1363 to the surface of microbeads inoculated with *L. cremoris* MG1363-GFP. Despite these factors, *L. cremoris* MG1363-GFP was enriched by a factor of eight in a single enrichment round.

Altogether, these results show that we can achieve growth of *L. cremoris* strains in microbeads and, using flow cytometry, we can identify microbeads with growth for both fluorescently labelled and unlabelled strains. We also show that we can selectively enrich for a sub-population of cells from a mixture by sorting microbeads using a FACS.

Supplementary section 5: Gating Strategy

Gating was performed using control samples representing individual sub-populations: single cells, empty microbeads, microbeads with growth of fluorescently labelled cells, and microbeads with growth of non-fluorescently labelled cells. (Figure S5).

Note: The presence of single cells populations suggests occasional microbead damage, which we expect to be unbiased i.e., we expect damage to microbeads to be random, not specific to microbeads inoculated with certain strains or combinations. Therefore, this does not affect the inference of interaction parameters. In our experiments, only a small fraction of microbeads (≈1000 beads) out of 10^7 microbeads generated are sorted for parameter inference, so defects in a small fraction of microbeads have negligible impact due to the large number of microbeads available for analysis.

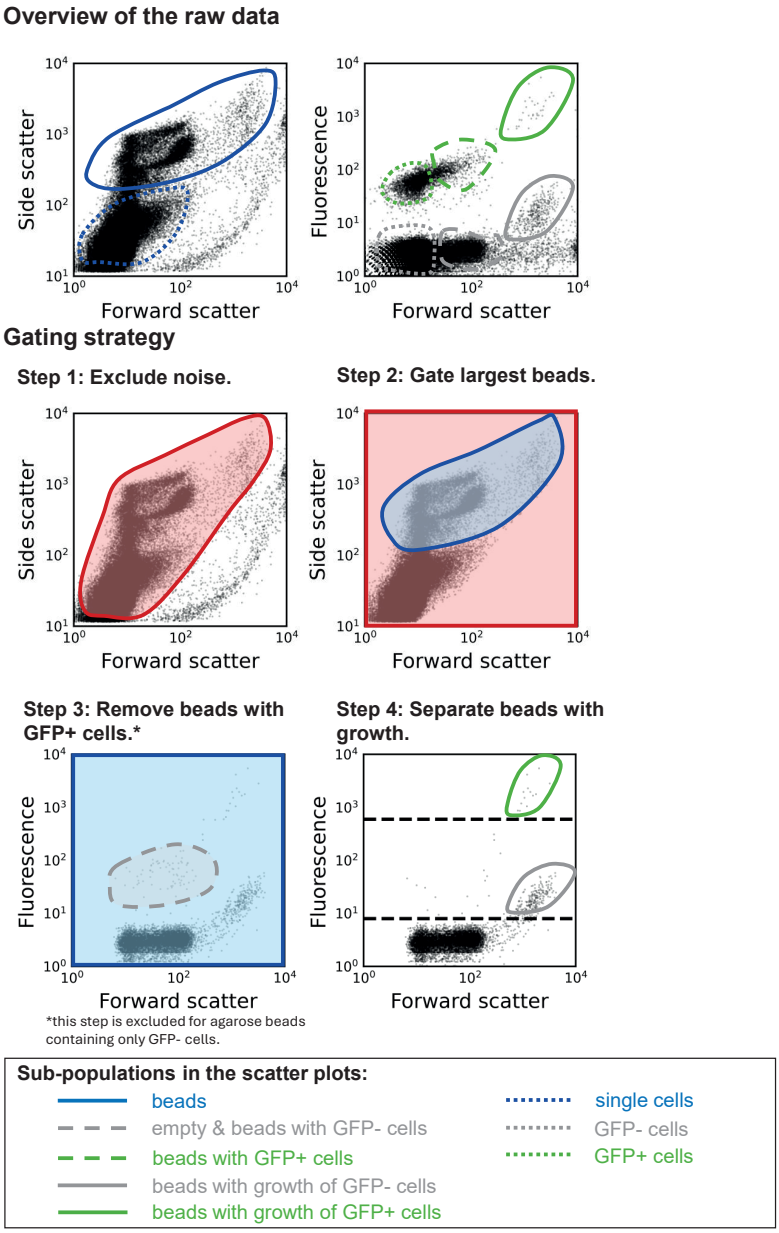

Figure S5: General gating strategy for flow cytometry data.

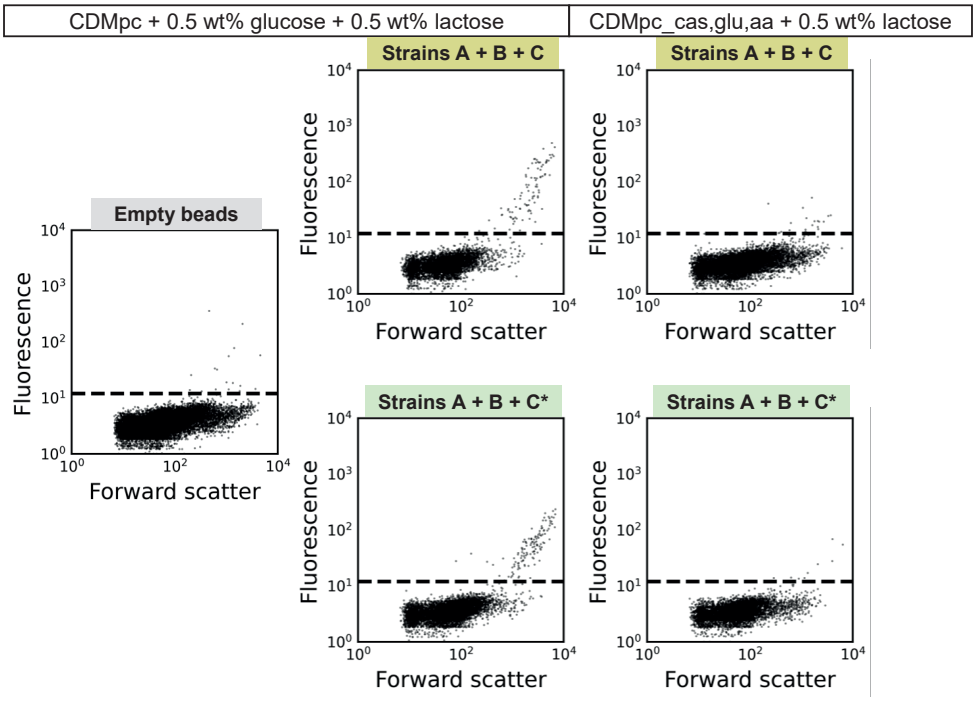

Figure S6: Flow cytometry gating strategy and data analysis. Empty microbeads and microbeads inoculated with a consortium of strains A, B and C (top) and strains A, B and C* (bottom) at a λ-value of 0.02 were measured after incubation. The inoculum consisted of 47% strain A, 29% strain B and 24% strain C (top) or 41% strain A, 21% strain B and 38% strain C*. Microbeads were prepared with medium CDMpc + 0.5 wt% lactose + 0.5 wt% glucose (left) and CDMpc_cas, glu, aa + 0.5 wt% lactose (right). Flow cytometry data were gated based on the strategy in Figure S8. The scatter plots are representative plots from three independent replicate samples.

Supplementary section 6: Bayesian inference of the interaction parameters

In this section, we describe how we infer the pairwise interaction parameters from the measured cell type abundances. The available data are measurements of the cell-type proportions before and after the growth phase. These proportions are measured by selecting a random number of cells and determining their cell type. For each experiment, we thus get a vector, $\vec{d}(0)$, with cell-type counts before the growth phase, and a similar vector, $\vec{d}(T)$, of cell-type counts after the growth phase. Here, we will, given a set of parameters $G_{ij}, f_{(i|ij)}$, write down an expression of the likelihood. By introducing prior distributions on the parameters, we subsequently write down the posterior probability for the parameters. Given this posterior probability function, we can numerically find the parameters with maximum posterior probability and a corresponding posterior probability interval.

The likelihood will reflect the different steps in the experiment, which we will describe in order.

Step 1: Determining initial cell-type fractions

Before inoculating the microbeads, the cells are mixed to obtain targeted proportions (captured by a vector $\vec{t}$). However, we can not be certain that the true proportions $\vec{p}(0)$ exactly match the targeted fractions. Therefore, we take a sample of cells and determine their cell type, leading to counts $\vec{d}(0)$. The probability of these counts is multinomially distributed with probabilities given by the true proportions, $\vec{p}(0)$:

$$P(\vec{d}(0) \mid \vec{p}(0)) = \frac{(\sum_i d_i(0))!}{d_1(0)!d_2(0)\cdots} \prod_i p_i(0)^{d_i(0)}$$

The targeted proportions give us prior information on the true fractions, which we capture by using a Dirichlet prior centred around the fractions t and with a precision controlled by a hyperparameter ν :

$$P(\vec{p}(0)) = \Gamma(\nu) \prod_i \frac{p_i(0)^{\nu t_i - 1}}{\Gamma(\nu t_i)}.$$

By multiplying the probability of the data and the prior, we get an expression proportional to the posterior for $\vec{p}(0)$, which is again taking the shape of a Dirichlet distribution:

$$P(\vec{p}(0) \mid \vec{d}(0), \vec{t}, \nu) \propto C\,(\nu, t_i, d_i(0)) \times \prod_i \frac{p_i(0)^{\nu t_i + d_i(0) - 1}}{\Gamma(\nu t_i + d_i(0))},$$

where $C\,(\nu, t_i, d_i(0))$ is a term that does not depend on $\vec{p}(0)$. We will now assume that we can ignore the uncertainty on $\vec{p}(0)$, such that we will set these proportions to their maximum posterior estimate. This is given by:

$$p_i(0) = \frac{\nu t_i + d_i(0)}{\nu + \sum_i d_i(0)}$$

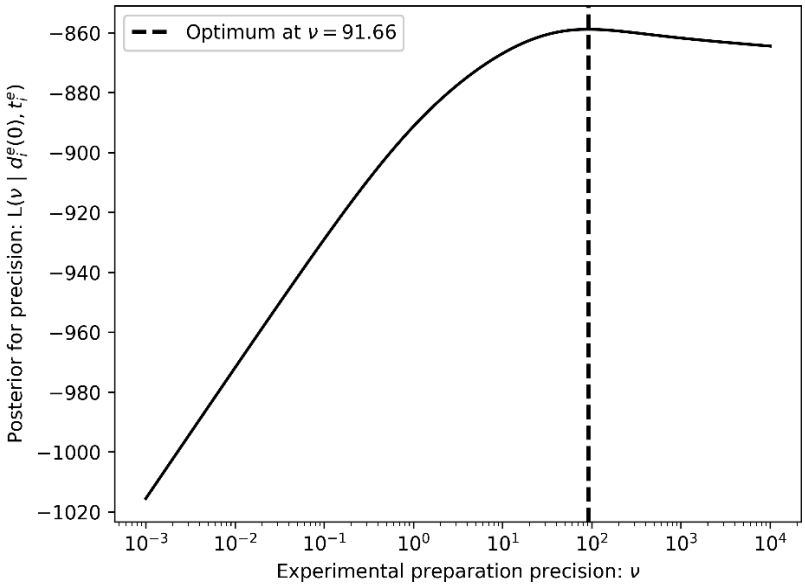

Figure S7: Probability of the initial count data as a function of experimental preparation precision ν. The dashed vertical line indicates the optimum at ν= 91.66.

Optimisation of the precision parameter, ν

The parameter ν captures the precision with which the cell-type fractions are prepared. This precision is independent of the experiment, which is why we use several experiments to determine this parameter. We thus maximise the probability of the data of several experiments with respect to ν. For this, let $P\left(\vec{d}^e(0), \vec{p}^e(0) | \vec{t}^e, \nu\right)$ be the joint probability of counts and true proportions for the experiment e. The total probability of the data given the parameter ν is given by:

$$P\left(\vec{d}^1(0), \ldots \vec{d}^E(0) \mid \nu\right) = \prod_e \left(\int d\vec{p}^e(0) P\left(\vec{d}^e(0), \vec{p}^e(0) \mid \vec{t}^e, \nu\right)\right)$$

This integral is easy to solve by using that the joint probability is directly proportional to a Dirichlet distribution. We numerically maximised this probability to obtain an optimal value of ν = 91.66 (Figure S7).

Step 2: Distribution of cells over microbeads

Now that we have estimated the cell-type proportions in the inoculum, we can describe the random distribution over the microbeads. The number of cells per microbead is Poisson-distributed with a mean λ. The number of cells in a microbead is thus described by:

$$P(n) = \frac{\lambda^n e^{-\lambda}}{n!}$$

In this work, we set the λ to 0.3, which ensures that, although most of the microbeads (=96%) contain 0 or 1 cell, most of the microbeads with 2 or more cells contain 2 cells (=90%). Therefore, in the model, we ignore the small percentage of microbeads with 3 or more cells.

We can now compute the frequencies at which the different cells occur in microbeads. The fraction of microbeads with a pair *i* and *j* is given by

$$\phi_{ij} = \lambda^2 e^{-\lambda}\, p_i\,(0)\, p_j\,(0)$$

while the fraction of microbeads with only one cell type *i* is given by:

$$\phi_i = \lambda e^{-\lambda}\, p_i\,(0) + \lambda^2 e^{-\lambda}\, p_i\,(0)^2$$

We assume that the fraction of microbeads for a given cell type pair is given exactly by these probabilities since the number of microbeads in a sample is large (~10^7 microbeads).

Step 3: Growth of cells in the microbeads

Cells that are co-localised in a microbead will interact with each other and grow based on the interactions until resources in the medium are depleted. We characterise the growth by two interaction parameters: $G_{ij}, f_{(i|ij)}$. G_{ij} denotes the average number of cells which will eventually exist in a microbead that was inoculated with an *i,j*-pair, while $f_{(i|ij)}$ denotes the fraction of the cells in the droplet that will be of type *i* (Note that we thus have $f_{(i|ij)} = 1 - f_{(j|ij)}$. For a microbead inoculated with an *i,j*-pair, the eventual number of cells of type *i* will thus be $G_{ij} \times f_{(i|ij)}$. Therefore, the final number of cells of type *i* can be expressed in terms of these parameters and the probabilities of finding a certain pair of cell-types in a microbead ϕ_{ij}:

$$N_i(T) = G_i\phi_i + \sum_{j\neq i} G_{ij} f_{(i|ij)} \phi_{ij}$$

The final cell-type fractions are given by:

$$p_i(T) = \frac{N_i(T)}{\sum_j N_j(T)}$$

Step 4: Determining final cell-type fractions and the likelihood of the final counts

Given these predicted final fractions $\vec{p}(T)$, the probability of the experimentally measured final counts is again multinomially distributed:

$$P(\vec{d}(T) \mid \vec{p}(T)) = \frac{\sum_i d_i(T))!}{d_1(T)!d_2(T)\cdots} \prod_i p_i(T)^{d_i(T)},$$

where we should note that the final fractions are directly dependent on the interaction parameters G_{ij} and $f_{(i|ij)}$. To estimate these interaction parameters, we need to obtain a posterior for the parameters by multiplying the probability of the data by prior distributions $P(G_{ij})$ and $P(f_{(i|ij)})$. Subsequently, we maximise this posterior distribution by jointly optimising all interaction parameters.

Since G_{ij} is a relative growth factor, we will define its prior in log-space, and we want to capture our prior information by setting a mean and a standard deviation. The natural choice is therefore a log-normal distribution:

$$P\left(C_{ij}\right) = \frac{1}{C_{ij}\sqrt{2\pi}} \exp\left(-\frac{\left(\log\left(C_{ij}\right)-\mu\right)^2}{2\sigma^2}\right)$$

When we do not have any prior information, we can capture this by making the standard deviation go to infinity (which we will capture by denoting σ = -1 in the following). In that case, the prior is uniform in log-space.

Since the parameters $f_{(i|ij)}$ are fractions, we will use one-dimensional Dirichlet-priors defined by a mean μ^f and a precision v^f. To gain some intuition for this precision, we can also set it by defining a mean and a variance σ^2, where $v^f = \frac{\mu^f(1-\mu^f)}{\sigma^2} - 1$

The Dirichlet distribution for $f_{(i|ij)}$ is given by:

$$P(f) = \frac{\Gamma(v^f)}{\Gamma(v^f\mu^f)\Gamma(v^f(1-\mu^f))} f^{v^f(\mu^f-1)}(1-f)^{v^f(1-\mu^f)-1}$$

Determination of the posterior probability interval for the estimated interaction parameters

After computing the maximum posterior value for the parameters, we want to quantify the uncertainty on the estimated parameter values by calculating posterior probability intervals. To determine this interval for a specific parameter, we vary the parameter and re-optimise the other parameters. In particular, let's say we want to determine the uncertainty for the parameter x which has the maximum posterior value x^*, and let's denote by $L(x)$ the log-posterior as a function of this parameter, where all other parameters are set to their optimal values. If the posterior were a perfect Gaussian distribution, the standard deviation of the parameter x would coincide with the distance from the optimum where the log-posterior drops by 0.5. Therefore, we approximate such an error bar by determining the lower and upper bounds for x at which the log-posterior has dropped by 0.5, i.e., we define the lower bound of the posterior probability interval by demanding:

$$L\left(x^*\right) - L\left(x_{lb}\right) = 0.5,$$

and similar for the upper bound. If the posterior were Gaussian distributed, this interval would thus correspond to a 68% probability interval.

Prior information for the inference model to predict interactions using experimental data

Table S1: Prior information i.e. means and standard deviations for priors of G_{ij} and $f_{i|ij}$ parameters provided to the inference model to decipher pairwise interactions for the consortium with strains A, B and C. When prior information is available, it is captured in the means and standard deviations of the priors. When no prior information is available, G_{ij} is taken to be uniform in the log-scale and $f_{i|ij}$ to be uniform in the unit interval. This is captured as 'uniform' in the standard deviations for the priors.

Priors for means of G_{ij} parameters			
	Strain A	**Strain B**	**Strain C**
Strain A	0.0001	1	1
Strain B	1	0.0001	1
Strain C	1	1	0.0001
Priors for standard deviations of G_{ij} parameters			
	Strain A	**Strain B**	**Strain C**
Strain A	0.01	uniform	uniform
Strain B	uniform	0.01	uniform
Strain C	uniform	uniform	0.01
Priors for means of $f_{i|ij}$ parameters			
	Strain A	**Strain B**	**Strain C**
Strain A	1	0.5	0.5
Strain B	0.5	1	0.5
Strain C	0.5	0.5	1
Priors for standard deviations of $f_{i|ij}$ parameters			
	Strain A	**Strain B**	**Strain C**
Strain A	0.01	uniform	uniform
Strain B	uniform	0.01	uniform
Strain C	uniform	uniform	0.01

Table S2: : Prior information i.e. means and standard deviations for priors of G_{ij} and $f_{i|ij}$ parameters provided to the inference model to decipher pairwise interactions between strains B and C* in the consortium with strains A, B and C*. When prior information is available, it is captured in the means and standard deviations of the priors. When no prior information is available, G_{ij} is taken to be uniform in the log-scale and $f_{i|ij}$ to be uniform in the unit interval. This is captured as 'uniform' in the standard deviations for the priors.

Priors for means of G_{ij} parameters			
	Strain A	**Strain B**	**Strain C***
Strain A	0.0001	1	0.0001
Strain B	1	0.0001	1
Strain C*	0.0001	1	0.0001
Priors for standard deviations of G_{ij} parameters			
	Strain A	**Strain B**	**Strain C***
Strain A	0.01	uniform	0.01
Strain B	uniform	0.01	uniform
Strain C*	0.01	uniform	0.01
Priors for means of $f_{i|ij}$ parameters			
	Strain A	**Strain B**	**Strain C***
Strain A	1	0.4	0.5
Strain B	0.6	1	0.5
Strain C*	0.5	0.5	1
Priors for standard deviations of $f_{i|ij}$ parameters			
	Strain A	**Strain B**	**Strain C***
Strain A	0.01	0.03	uniform
Strain B	0.03	0.01	uniform
Strain C*	uniform	uniform	0.01

Prior information for the inference model to predict interactions using simulated data is available on GitHub at https://github.com/Sagarikabg/Deciphering_Microbial_Interactions.git.

Supplementary section 7: Computationally deciphering interactions in larger consortia

In this section we describe the steps for the computational validation of the proposed approach to decipher interactions in larger consortia.

Step 1: Consortia design

Consortia consisting of four to six members were designed. Two types of consortia were designed: (1) consortia where none of the cell-types could grow independently, *i.e.*, no isolated growth, and (2) consortia where one or two cell types were capable of isolated growth. In scenarios where there is a negative interaction, we assume that both the cell types exhibit isolated growth, and depending on the direction of the interaction, we expect at least one of the cell types to grow.

Based on these consortia design, $G_{ij}, f_{(i|ij)}$ were defined accordingly. These values are available on GitHub at https://github.com/Sagarikabg/Deciphering_Microbial_Interactions.git.

Step 2: Simulation data

Experimental data was simulated by first generating random target cell-type counts. These cell counts were generated by assuming a total sampled number of cells to be 96 or 1000 cells and by applying random multinomial sampling. This data is collected in count vector $\vec{d}(0)$. To account for experimental sampling noise, the initial counts were modelled as a multinomial sample of the cell-type proportions $\vec{p}(0)$ by using the experiment precision parameter as described in supplementary section 6.

Using the initial strain proportions, the fraction of microbeads with different cell-type compositions was modelled as described in supplementary section 6. The number of offspring cells that a cell-combination in a microbead will give rise to is modelled using the parameters $G_{ij}, f_{(i|ij)}$. Based on the fraction of microbeads with a certain cell-type composition and the model for interactions, the eventual final cell-type frequencies were determined. These frequencies were subsequently converted into final cell-type counts by multinomial sampling to account for sampling noise by assuming the total number of sampled cells to be 96 or 1000.

Step 3: Inference model

To estimate these interaction parameters, we need to obtain a posterior for the parameters by multiplying the probability of the simulated data (simulated final cell-type fractions $\vec{p}(T)$) by prior distributions Subsequently, we maximise this posterior distribution by jointly optimising all interaction parameters. Mathematical details are described in supplementary section 6.

Step 4: Assessing the prediction

Inference error was computed as the absolute difference between the interaction parameters predicted by the inference model and the corresponding interaction parameters

used in the simulation. The inference error for $f_{(i|ij)}$ parameters was only computed for all cell-type combinations where the corresponding G_{ij} simulation value was lager than 0.1.

For the data represented in the main text, we simulated the number of colonies sampled to determine the cell-type fractions to 1000 (Figure 5). To test the effect of the number of colonies to be sampled on inference errors, we reduced this number to 96 (Figure S8). This resulted in overall higher inference errors compared to when the 1000 colonies were sampled.

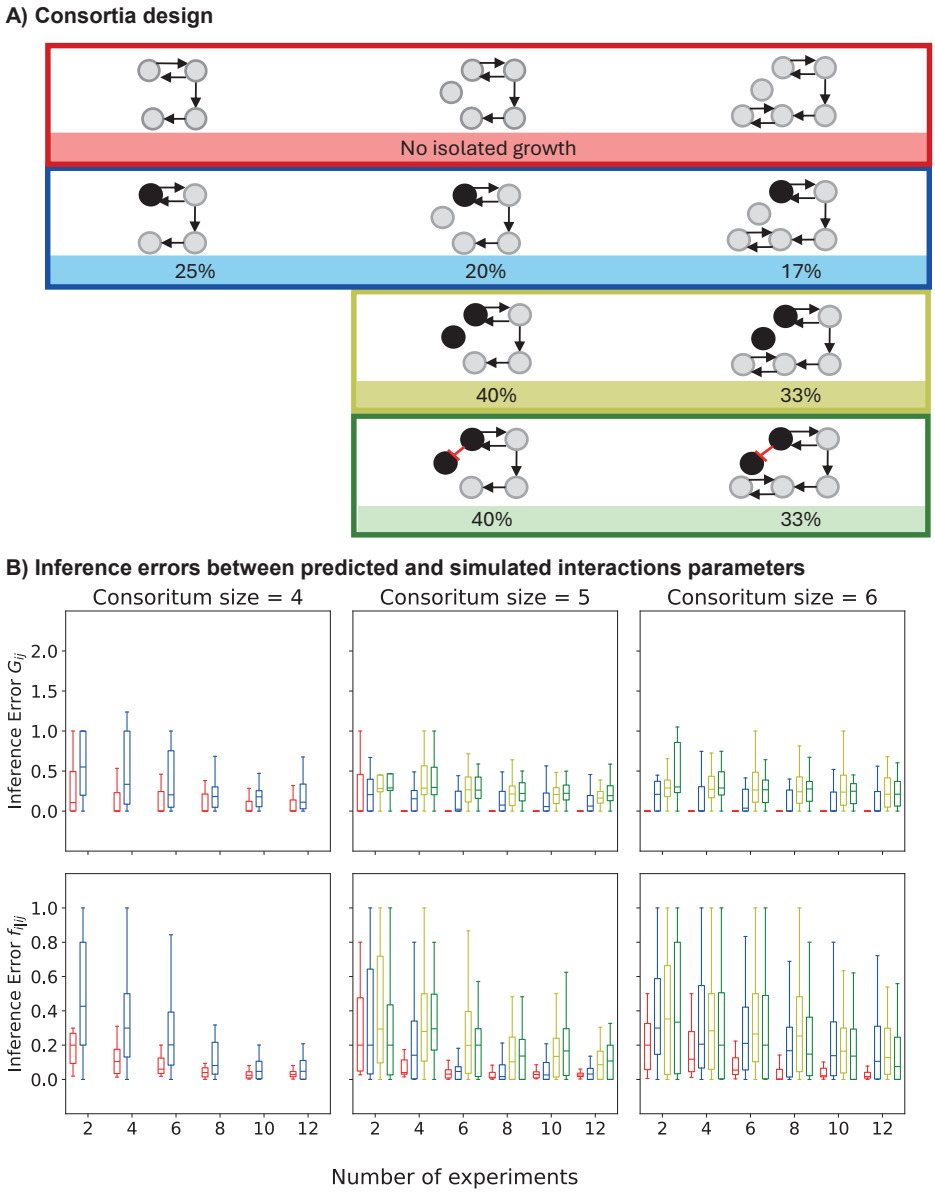

Figure S8: Computational validation to infer interactions in larger consortia. Inference errors between predicted and simulated interaction parameters. (A) Consortia were designed for simulation; the cell types that do not grow by themselves, i.e. with no isolated growth, are represented in grey and cell types that grow by themselves are represented in black. The percentage of consortium members capable of isolated growth is indicated below each consortium. (B) The distribution of inference errors of the growth (G_{ij}) and cell-type fraction terms ($f_{i,ij}$) for different numbers of experiments, where the inference error is the absolute difference between the interaction parameters predicted by the inference model and the corresponding interaction parameters used in the simulation For these simulations the λ was set to 0.3 and number of colonies to determine cell type abundances was set to 96. The number of experiments corresponds to the number of unique sets of initial cell-type counts. The individual box plots represent the distribution of the inference errors for five random replicates for the same number of experiments. The colours of the box plots correspond to the consortia configurations in panel (A).

References

1. Abreu NA, Taga ME. Decoding molecular interactions in microbial communities. FEMS Microbiol Rev 2016;40:648–663.
2. Coyte KZ, Schluter J, Foster KR. The ecology of the microbiome: networks, competition, and stability. Science 2015;350:663–666.
3. Palmer JD, Foster KR. Bacterial species rarely work together. Science 2022;376:581–582.
4. Antoniewicz MR. A guide to deciphering microbial interactions and metabolic fluxes in microbiome communities. Curr Opin Biotechnol 2020;64:230–237
5. Tang L. Micorbial interactions. Nat Methods 2019;16:19.
6. Venturelli OS, et al. Deciphering microbial interactions in synthetic human gut microbiome communities. Mol Syst Biol 2018;14:e8157.
7. Hsu RH, et al. Microbial interaction network inference in microfluidic droplets. Cell Syst 2019;9:229–242.e4.
8. Kehe J, et al. Positive interactions are common among culturable bacteria. Sci Adv 2021;7:eabe1598.
9. Kehe J, et al. Massively parallel screening of synthetic microbial communities. Proc Natl Acad Sci USA 2019;116:12804–12809.
10. Price CE, et al. Adaptation to glucose limitation is modulated by the pleiotropic regulator CcpA, independent of selection pressure strength. BMC Evol Biol 2019;19:19.
11. Pool WA, et al. Natural sweetening of food products by engineering *Lactococcus lactis* for glucose production. Metab Eng 2006;8:456–464.
12. Leenhouts KJ, et al. Chromosomal stabilization of the proteinase genes in *Lactococcus lactis*. Appl Environ Microbiol 1991;57:2568–2575.
13. Bachmann H, Kleerebezem M, van Hylckama Vlieg JET. High-throughput identification and validation of in situ-expressed genes of *Lactococcus lactis*. Appl Environ Microbiol 2008;74:4727–4736.
14. Wegmann U, et al. Complete genome sequence of *Lactococcus lactis* subsp. cremoris MG1363. J Bacteriol 2007;189:3256–3270.
15. van Tatenhove-Pel RJ, et al. Ampicillin-treated *Lactococcus lactis* MG1363 populations contain persisters and viable but non-culturable cells. Sci Rep 2019;9:388.
16. Blasche S, et al. Emergence of stable coexistence in a complex microbial community through metabolic cooperation and spatio-temporal niche partitioning. bioRxiv 2019:541870.
17. Gobbetti M, Corsetti A, Rossi J. The sourdough microflora: interactions between lactic

acid bacteria and yeasts in carbohydrate metabolism. Appl Microbiol Biotechnol 1994;41:456–460.

18. Sieuwerts S, et al. Mixed-culture transcriptome analysis reveals the molecular basis of growth in *Streptococcus thermophilus* and *Lactobacillus delbrueckii* subsp. bulgaricus. Appl Environ Microbiol 2010;76:7775–7784.
19. van Tatenhove-Pel RJ, et al. Population dynamics of microbial cross-feeding determined by co-localization probabilities. ISME J 2021;15:3050–3061.
20. Link A, et al. Active single-cell encapsulation using SAW overcoming Poisson distribution limitations. Lab Chip 2022;22:193–200.
21. Liu D, et al. Single-cell droplet microfluidics for biomedical applications. Analyst 2022;147:2294–2316.
22. Diaz-Colunga J, et al. Top-down and bottom-up cohesiveness in microbial community coalescence. Proc Natl Acad Sci USA 2022;119:e2111261119.
23. Goldford JE, et al. Emergent simplicity in microbial community assembly. Science 2018;361:469–474.
24. Scanlon TC, Dostal SM, Griswold KE. A high-throughput screen for antibiotic drug discovery. Biotechnol Bioeng 2014;111:232–243.
25. Agnihotri SN, et al. Droplet microfluidics-based detection of rare antibiotic-resistant subpopulations in E. coli. Sci Adv 2025;11:eadv4558.
26. Sung YJ, et al. Magnetophoretic sorting of microdroplets by microalgal density for rapid strain isolation. Sci Rep 2017;7:1–11.
27. van den Berg NI, et al. Ecological modelling approaches for predicting emergent properties in microbial communities. Nat Ecol Evol 2022;6:855–865.
28. Bull JJ, Harcombe WR. Population dynamics constrain evolution of cooperative cross-feeding. PLoS One 2009;4:e4115.
29. van Tatenhove-Pel RJ, et al. Microdroplet screening and selection for improved microbial production of extracellular compounds. Curr Opin Biotechnol 2020;61
30. Batani G, et al. FISH and cell sorting of living bacteria. Sci Rep 2019;9:1868.
31. Lewis WH, et al. Innovations to culturing the uncultured microbial majority. Nat Rev Microbiol 2021;19:225–240.
32. Flores AD, et al. Catabolic division of labor enhances D-lactate and succinate production in engineered *E. coli* co-cultures. Front Bioeng Biotechnol 2020;8:329.
33. Saini M, et al. Synthetic consortium of *E. coli* for n-butanol production from glucose–xylose mixtures. J Agric Food Chem 2017;65:10040–10047.
34. Verhoeven MD, et al. Fermentation of glucose–xylose–arabinose mixtures by a synthetic consortium of *S. cerevisiae* strains. FEMS Yeast Res 2018;18:foy075.

Chapter 5

Unlocking the potential of defined co-cultures for industrial biotechnology: opportunities and challenges.

Sagarika B. Govindaraju*, Tobias Fecker*, Michelle Rossouw, Jack T. Pronk and Rinke J. van Tatenhove-Pel
*These authors contributed equally to this work.

Essentially as published in New Biotechnology (2025) 91: 89-99.
doi: 10.1016/j.nbt.2025.11.009

Abstract

Large-scale microbial-biotechnology processes for production of chemicals almost exclusively rely on pure cultures of microbial strains. Especially for extensively engineered pure cultures, process performance can be negatively affected, which can be caused by issues such as pathway imbalance, deterioration of productivity caused by genetic instability and enzyme promiscuity. An increasing number of studies demonstrate that, under 'academic' laboratory conditions, the use of defined co-cultures (i.e. deliberate mixtures of known microbial strains) offers unique possibilities for mitigating such drawbacks. These advantages differ for dissimilatory products, whose synthesis from one or more carbon substrates provides cells with free energy, and assimilatory products, whose synthesis requires a net input of free energy. Based on advances in experimental and theoretical research, this paper highlights how defined co-cultures can address several limitations of monocultures for production of low-molecular-weight compounds. From this largely academic perspective, we outline the key challenges for scaling these systems to industry, which underscore the need for innovative solutions and continued research in this area.

1. Introduction

In industrial biotechnology, production processes traditionally use single microbial strains (monocultures). While in many cases effective, such monocultures can suffer from problems such as genetic instability resulting in loss of productivity, pathway imbalance and incompatibility of envisioned production strains with the functional expression of key enzymes. Defined co-cultures, i.e. mixtures of known microbial strains, have been proposed as a means to address these challenges.

A large body of knowledge generated in microbial ecology underscores the importance of microbial interactions for the functionality and stability of natural microbial communities (1–3). Microbial co-cultures are widely applied in food fermentation processes, to enhance product quality parameters such as nutritional value and flavor (4–6). Underlying metabolic interactions in these processes include commensalism (one species benefits and the other is neither harmed nor helped), mutualism (both species benefit) and parasitism (one species benefits and the other is harmed) (7). In contrast to food fermentation processes, industrial biotechnology, which uses microorganisms for production of chemicals, only rarely makes use of co-cultures of different strains or species (8,9). Instead, it predominantly relies on monocultures of microbial strains, whose performance in industrial processes is often extended or improved by classical strain improvement and/or genetic engineering.

Products of industrial biotechnology range from fragrances and pharmaceuticals to transport fuels and chemical building blocks. Based on their connection to microbial energy metabolism, products of industrial biotechnology can be divided into two distinct categories: dissimilatory and assimilatory products. Figure 1 depicts both categories schematically. Since the advantages of co-cultures differ for these products, this review is split into two main parts: one around dissimilatory and one around assimilatory products. Dissimilatory products are compounds whose synthesis from a carbon substrate provides the cell with ATP. Examples include fermentation products such as ethanol and lactate, whose large-scale production typically occurs in anaerobic or oxygen-limited batch cultures. Assimilatory products are compounds whose synthesis from a carbon substrate requires a net investment of ATP and biosynthetic precursors. Therefore, in contrast to dissimilatory product formation, assimilatory product formation competes for ATP with cellular growth and maintenance. Assimilatory products produced by microorganisms include a wide and growing range of molecules, for which the biosynthetic pathways have often been introduced and/or improved by extensive genetic engineering. Examples of assimilatory products include structurally diverse molecules such as alkaloids, terpenoids, fatty acids, flavonoids, phenylpropanoids, and polyketides. To efficiently generate the ATP required for product formation, they are typically manufactured in aerobic fed-batch or continuous fermentation processes.

The TRY acronym (titer, rate, yield) captures three key performance indicators of industrial biotechnology processes (10). Titer refers to the final concentration of

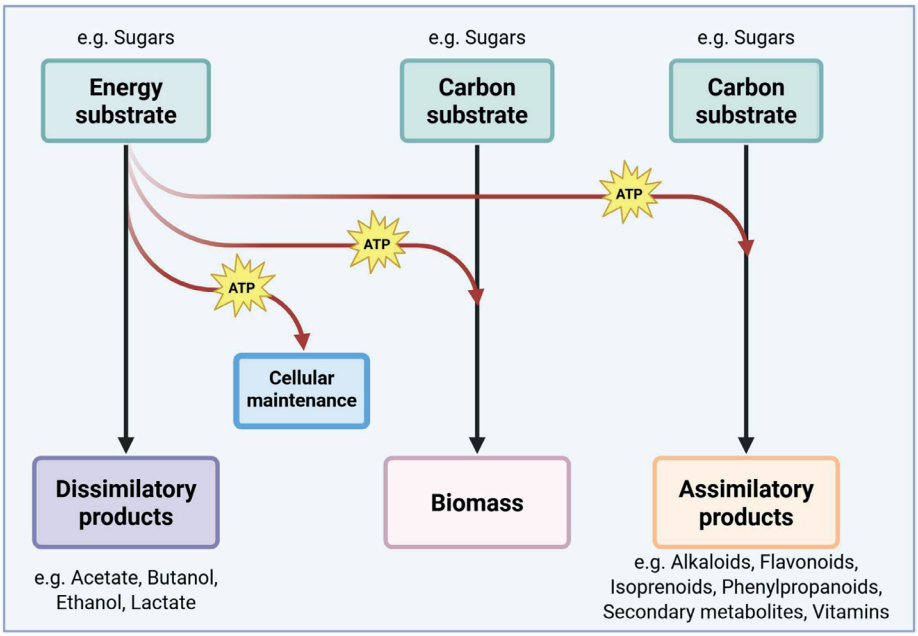

Figure 1: Dissimilatory and assimilatory products. Dissimilatory products are compounds whose synthesis from (a) substrate(s) provides the cell factory with ATP, which can be used for growth and cellular maintenance. Synthesis of assimilatory products from (a) substrate(s) requires a net ATP input and is therefore dependent on dissimilatory pathways to generate ATP. Created in BioRender. https://BioRender.com/lf23uka

the product (c_p, kg product per m^3), which is highly relevant for efficient product purification by processes such as distillation or chromatography. Moreover, titer impacts the required bioreactor volume and, thereby, required capital investments. Rate can be expressed as productivity of the entire reactor (R_p, kg product per hour). Volumetric productivity (r_p, kg product per m^3 per hour) links productivity to installed reactor volume and is the product of the biomass concentration (c_x) and the biomass specific-production rate (q_p, kg product per kg biomass per hour). Processes with a higher volumetric productivity r_p require lower capital investments in installed bioreactor volume. The third key performance indicator is the product yield on substrate ($Y_{p/s}$, kg of product formed per kg of consumed substrate), which is equal to the ratio of the product-formation and substrate-consumption rates ($Y_{p/s} = R_p/R_s = r_p/r_s = q_p/q_s$). The $Y_{p/s}$ has a particularly strong impact on process economy for commodity products, for which feedstock costs can make up a large fraction of the overall production costs. For example, costs of the carbohydrate feedstock can account for up to 70% of the costs of yeast-based ethanol production (11).

Genetic stability of high-performance cell factories can be an additional key performance indicator in large-scale applications. Industrial fermentation processes for assimilatory processes are operated at reactor volumes of up to several hundred m^3, while bioreactor volumes for ethanol fermentation can even run into several thousand m^3. This implies that the 'seed train' needed to scale up from milliliter-scale

frozen culture samples encompasses many generations during which a strain's full production capacity needs to be maintained. Genetic stability is even more important when fermentation processes are operated continuously or as serial batch cultures with the aim to improve process economics and/or sustainability.

The aim of this paper is to review results from fundamental, application-inspired studies aimed at investigating if and how the use of defined microbial co-cultures can circumvent or mitigate limitations of monocultures as production systems. It primarily discusses results from studies that generated quantitative information on parameters such as titer, rate, yield and genetic stability. In addition, it focuses on production of low molecular weight compounds. Discussion of high molecular weight compounds (e.g. proteins and biopolymers), and their production processes including consolidated bioprocessing, which combines enzyme production and fermentation in one step (12–16), is therefore outside the scope of this review. The different relationships of assimilatory and dissimilatory product formation with cellular energy metabolism (Figure 1) generate different challenges in monocultures and, consequently, provide different opportunities for the use of defined co-cultures. We therefore separately discuss co-culture strategies for dissimilatory and assimilatory product formation. These examples are summarized in Table 1. Based on this information, we subsequently outline key challenges that need to be addressed to enable broader use of defined co-cultures in industrial biotechnology. Together, these insights underline the potential of defined co-cultures to further develop and improve industrial biotechnology.

2. Dissimilatory products

The large product volumes and narrow profit margins of dissimilatory products (10) imply that small improvements of titer, rate and/or yield can already confer significant economic benefits. Improving product yield on substrate ($Y_{p/s}$), for example by reducing by-product formation, is especially important because substrate costs strongly influence process economics (10,11). Recycling of biomass from one fermentation process to the next can help to improve volumetric productivity (r_p) (29). When contamination by undesirable competing microorganisms is kept at bay, such biomass recycling strategies can work very well because dissimilatory product formation from a single substrate is linked to growth and survival and therefore confers a selective advantage to fast-producing mutants (30,31). To improve process sustainability and reduce land use for production of fermentation feedstocks, conversion of sugar mixtures generated by hydrolysis of lignocellulosic agricultural residues is intensively explored (32,33). Below, we will discuss examples of how the use of defined co-cultures has been explored as a means to (i) improve $Y_{p/s}$ by minimizing by-product formation (section 2.1), (ii) improve volumetric productivity (r_p) during conversion of sugar mixtures (section 2.2) and (iii) improve genetic stability in repeated batch cultures grown on sugar mixtures (section 2.3). These scenarios are illustrated in Figure 2A-C.

Table 1: Selection of references on defined microbial co-cultures for industrial biotechnology, for which titer, rate, yield and/or stability of strain performance are quantitatively described.

Product	Substrate(s)	Target	Strategy	Titer/Rate/Yield of co-culture (monoculture between brackets)	Ref.
Ethanol	Glucose	Increase **product yield** on substrate through conversion of by-products to product.	Co-culture of PRK-RuBisCo based and A-ALD-based *S. cerevisiae* strains, where the A-ALD strain converts by-products from the PRK-RuBisCo strain (acetate and acetaldehyde).	1.67 (1.64, PRK-RuBisCo-based strain) g ethanol · (g glucose)$^{-1}$	(17)
1,3-propanediol	Glycerol	Increase **product yield** on substrate through conversion of by-products to product.	Co-culture of *Klebsiella spp* and *Shewanella oneidensis*, where S. oneidensis oxidizes the by-product lactate from *Klebsiella spp* supplying electrons for its product formation.	0.44 (0.41) g 1,3-PD · (g glycerol)$^{-1}$	(18)
Lactate	Glucose and xylose	Increase **volumetric productivity** through improved sugar utilization kinetics.	Co-culture of two *E. coli* strains, each specialized in glucose and xylose consumption.	5.8 (2.6) g lactate · L^{-1} · h^{-1}	(19)
n-Butanol	Glucose and xylose	Increase **volumetric productivity** through improved sugar utilization.	Co-culture of two *E. coli* strains, each specialized in glucose and xylose consumption.	0.12* (0.072*) g n-butanol · L^{-1} · h^{-1}	(20)

Ethanol	Arabinose, glucose and xylose	Improved **genetic stability** during long term cultivation on sugar mixture.	Co-culture of three *S. cerevisiae* strains, each specialized in arabinose, glucose and xylose consumption.	Cycle length: stable at 35 h for 1000 h cultivation (increase from 25 h to 51h)	(21)
Rosmarinic acid	Glucose	Increase **product titer** by pathway modularization.	Employ engineered three-strain *E. coli* co-culture to balance complex diverging-converging biosynthetic pathway by improved metabolic flux.	74 (4.5) $mg \cdot L^{-1}$	(22)
Caffeyl alcohol	Glucose	Increase **product titer** by spatial separation to avoid negative impact of enzyme promiscuity.	Co-culture of p-CA-producing and HpaBC-expressing *E. coli* strains to prevent L-dopa by-product formation due to HpaBC promiscuity.	0.4 (0.03) $g \cdot L^{-1}$	(23)
Eugenol	Glycerol and glucose	Increase **product titer** by preventing intermediate toxicity and enzyme promiscuity through pathway modularization.	Tripartite *E. coli* co-culture separating coumarate, ferulic acid, and eugenol modules to avoid substrate competition and toxic build-up.	0.07 (0) $g \cdot L^{-1}$	(24)
Anthocyanidin-3-O-glucosides	Glucose	Increase **product titer** of anthocyanin through pathway modularization.	Four-strain polyculture distributing 15 pathway enzymes across modules to reduce metabolic burden and enable de novo anthocyanin biosynthesis.	~ 9.5* (0*) mg pelargonidin-3-O-glucoside $\cdot L^{-1}$	(25)

Oxygenated taxanes	Xylose and acetate	Extend **product range** and improve **product titer** by addressing host-specific enzyme functional expression challenge.	Modular co-culture of *E. coli* producing taxadiene and *S. cerevisiae* expressing plant P450 fusion protein to support oxygenation steps in taxane biosynthesis.	0.03 (0) $g \cdot L^{-1}$	(26)
Various strigolactones	Glucose	Extend **product range** and improve **product titer** by addressing host-specific enzyme functional expression challenge.	Bipartite *E. coli* and *S. cerevisiae* co-culture: *E. coli* produces carlactone (3 enzyme-types), while yeast expresses downstream P450 enzymes for conversion to specific strigolactones.	Up to 47 (0) $\mu g \cdot L^{-1}$	(27)
(S)-Norcoclaurine	Glucose and xylose	Improve **product titer** by binary modularization of two-species co-culture and module optimization.	*S. stipitis* produces shikimate from mixed sugars; *S. cerevisiae*, engineered with Aspergillus shikimate transporters, imports shikimate and converts it to (S)-norcoclaurine.	11.5 (0.1) $mg \cdot L^{-1}$	(28)

*Values calculated based on information in figures or in text.

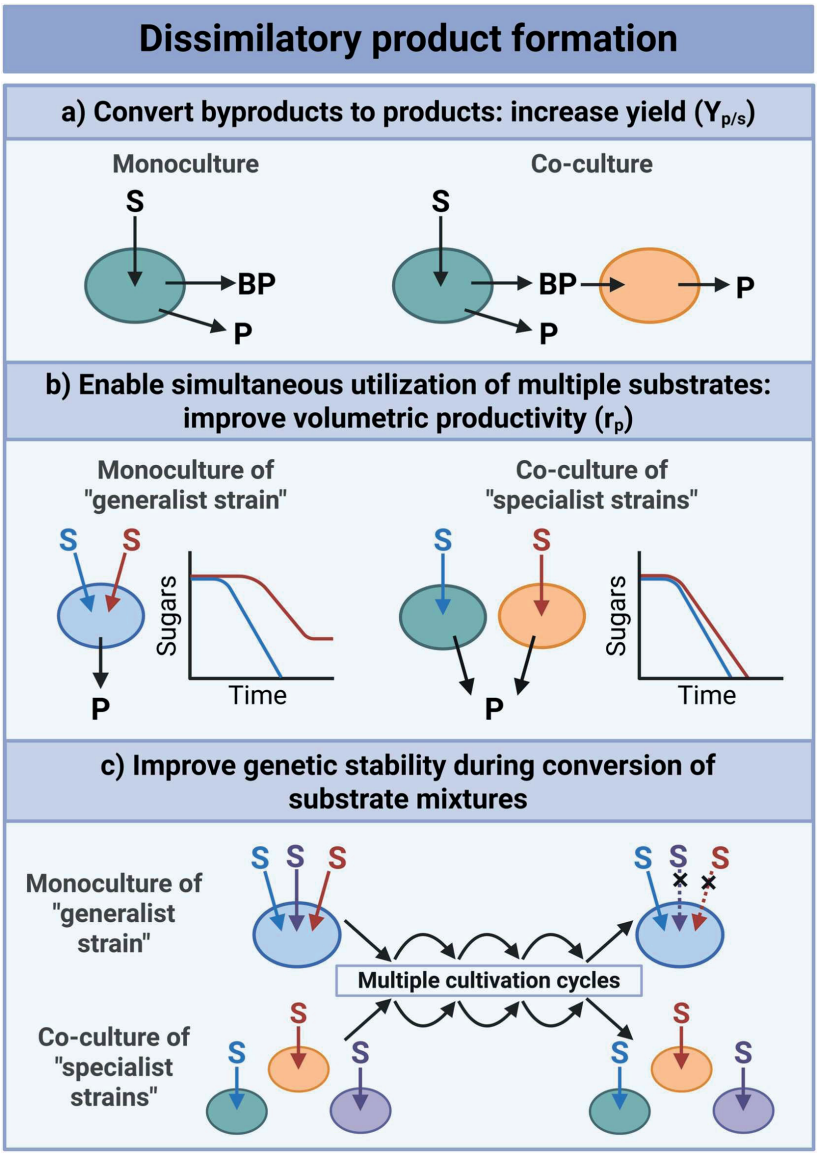

Figure 2: Potential benefits of using defined co-cultures to improve titer, rate, yield and stability during production of low molecular weight dissimilatory products. (A) In defined co-cultures, microorganisms can utilize or sequester by-products formed by other microorganisms to increase overall product yield from substrate. (B) Defined co-cultures of specialist strains (utilizing a single substrate) could allow for a higher consumption rate of each substrate due to preferential substrate utilization by the generalist strain. (C) Generalist strains are more likely to become genetically unstable after multiple cultivation rounds on substrate mixtures than specialist strains, resulting in diminished substrate utilization capabilities. S = substrate; P = product; BP = By-product. Created in BioRender. https://BioRender.com/zsu15iq

2.1. Minimizing by-product formation to improve yield

Ethanol production with the yeast *Saccharomyces cerevisiae* is the largest-volume process (ca. 100 Mton per year (31)) in industrial biotechnology. In anaerobic cultures of this yeast, including the large-scale batch cultures used for industrial ethanol production, glycerol formation serves as essential 'redox sink' for re-oxidation of a surplus of NADH generated in biosynthetic reactions. Without mitigating measures, glycerol formation would account for a loss of 4% of the carbohydrate feedstock used for yeast-based ethanol production (34).

A metabolic engineering strategy to eliminate glycerol formation was based on functional expression of heterologous genes encoding the two signature enzymes of the Calvin cycle for CO_2 fixation, phosphoribulokinase (PRK) and ribulose-1,5-bisphosphate carboxylase/oxygenase (RuBisCo). Introduction of functional PRK and RuBisCo in *S. cerevisiae* enabled a redox-cofactor-neutral conversion of glucose to 3-phosphoglycerate, whose subsequent NADH-dependent conversion to ethanol and CO_2 could replace the role of glycerol as redox sink. In fast-growing, glucose-grown anaerobic batch cultures, this strategy enabled an over 10% higher $Y_{p/s}$ (35). However, at suboptimal growth rates, which occur in the later stages of industrial processes due to ethanol accumulation and depletion of non-sugar nutrients, an overcapacity of the engineered PRK-RuBisCo bypass led to formation of the by-products acetaldehyde and acetate (36). An alternative metabolic engineering strategy for coupling reoxidation of 'excess' NADH to ethanol formation was based on introduction of a heterologous acetylating acetaldehyde dehydrogenase (A-ALD) (37). Together with native yeast enzymes, A-ALD enables the NADH-dependent reduction of acetate to ethanol. However, the concentration of acetate in 'first-generation' feedstocks for ethanol production such as corn starch hydrolysates is too low to completely replace glycerol production in acetate-reducing yeast strains. Co-cultivation of an engineered PRK/RuBisCo-based and an A-ALD-based strain was shown to combine the advantages of the two strains: low concentrations of acetate present in the medium, as well as acetaldehyde and acetate generated by the PRK/RuBisCo strain, were efficiently converted to ethanol by the A-ALD strain, while the PRK/RuBisCo strain supported acetate- and acetaldehyde-independent, high-yield ethanol production. Optimization of the inoculation ratio of this commensalistic co-culture enabled overall fermentation times equal to those of monocultures of the PRK/RuBisCo strain (17).

Wang *et al.* (2023) (18) explored a strategy for channelling by-products into product formation that involves two bacterial species. Anaerobic cultures of the *Klebsiella* strain used in this study produced 1,3-propanediol (1,3-PD) from glycerol, a conversion that requires a net input of electrons in the form of NADH. In the *Klebsiella* strain, this NADH is made available by converting part of the glycerol to more oxidized by-products such as acetate and lactate (38), which limits the maximum yield of 1,3-PD on glycerol. To mitigate by-product formation, the *Klebsiella* strain was co-cultivated with an exo-electrogenic *Shewanella oneidensis* strain. The rationale of this co-cultivation strategy was that *S. oneidensis* can oxidize lactate, generated by the *Klebsiella* strain,

to acetate and CO_2 and transfer the electrons that are released during this oxidation to the *Klebsiella* strain. This interspecies electron transfer may occur either via exported $FMNH_2$ and reduced riboflavin or via direct interspecies electron transfer through pili (18,39). The *Klebsiella* strain then uses the electrons for reducing glycerol to 1,3-PD. Consistent with this mutualistic mechanism, co-cultivation of the two bacteria led to a 7.3% higher yield of 1,3-PD on glycerol than observed in monocultures of the *Klebsiella* strain.

Overall, these examples show that co-cultures can be used to convert by-product into product, thereby improving product yield on substrate.

2.2. Improving mixed-substrate utilization

Combined chemical and enzymatic hydrolysis can release fermentable sugars from agricultural residues such as corn stover and sugar cane bagasse, as well as from 'energy crops' such as switchgrass (32,33). Use of such 'second-generation' feedstocks offers a large potential for improving the carbon footprint of industrial biotechnology. However, in contrast to feedstocks such as cane sugar or hydrolysed corn starch, these feedstocks contain mixtures of multiple sugars, with glucose and two pentose sugars, xylose and arabinose as main contributors. Industrial microorganisms such as *S. cerevisiae* and *Escherichia coli* have been extensively engineered to construct 'generalist' strains that convert mixtures of these three sugars. While these strains achieve high product yields on the sugar mixture under anaerobic conditions, their fermentation kinetics are often suboptimal. Engineered strains typically first consume the glucose at a high rate, while pentoses are consumed in a second, much slower sugar fermentation phase, thereby reducing the volumetric productivity r_p (21,40).

Generalist strains need to simultaneously synthesize enzymes for multiple substrate-conversion pathways. Monod pioneered research on diauxic growth, which is the sequential use of preferred and less-preferred substrates when these are provided together in batch cultures (41). The resulting bi-phasic growth illustrates how natural evolution yielded regulation mechanisms that, in the presence of non-limiting concentrations of multiple substrates, prevent simultaneous allocation of cellular resources to multiple substrate-utilization pathways. Instead, microorganisms have evolved to maximize growth rate by allocating cellular resources to fast conversion of a single substrate at a time (42). This principle led to multiple application-inspired studies, in which fermentation kinetics of defined co-cultures of 'substrate specialist strains' in cultures grown on sugar mixtures were compared with those of monocultures of a generalist strain.

Flores *et al.* (2020) (19) compared fermentation kinetics in aerobic cultures on a glucose-xylose mixture of an *E. coli* generalist strain capable of converting glucose and xylose, with those of a bipartite co-culture of glucose- and xylose-specialist *E. coli* strains grown on the same medium. An over 2-fold higher volumetric productivity of lactate was observed in the co-cultures than in cultures of the generalist strain (5.8 g lactate L^{-1} h^{-1} versus 2.6 g L^{-1} h^{-1}). In a conceptually similar study, Saini *et al.* (2017)

(20) compared product formation in anaerobic cultures, grown on a glucose-xylose mixture, of a generalist *E. coli* strain and a co-culture of two sugar-specialist strains, all engineered for *n*-butanol production. In a 36-h growth experiment, the generalist strain produced 2.6 g L^{-1} *n*-butanol and converted only about 60% of the available sugars. Over the same period, the co-culture produced 4.4 g L^{-1} n-butanol and achieved near-complete sugar conversion (20). The improved productivities observed in these studies are consistent with an improved protein allocation in the co-culture and/or elimination of a pathway interference in generalist strains.

The above examples, as well as additional studies (43,44), show that the use of co-cultures of specialist strains can improve production rates during conversion of mixed substrates.

2.3. Enhancing genetic stability during sequential batch cultivation on mixed substrates

Dissimilatory product formation can, via generation of ATP (Figure 1), be directly coupled to growth rate. This principle has been extensively used to increase product formation rates by adaptive laboratory evolution in serial-batch monocultures (30). Selection for improved fermentation kinetics has also been documented for the Brazilian bioethanol industry, in which ethanol production from cane sugar involves recycling of yeast biomass from one culture to the next over multi-month campaigns (31). In contrast to these observations on single-substrate cultures, studies in which serial-batch monocultures of 'generalist' strains were grown on mixtures of carbon substrates, reported a deterioration of overall fermentation kinetics (Figure 2B and 2C, (21,45,46)). An *S. cerevisiae* strain engineered for efficient conversion of glucose, xylose and arabinose showed a progressive increase of overall fermentation times when subjected to sequential batch cultivation cycles on mixtures of xylose and arabinose (45) or glucose, xylose and arabinose (21,46).

In a batch culture grown on equivalent concentrations of multiple substrates, the largest number of generations occurs during growth on the most preferred substrate. In serial batch cultures, selective pressure for faster utilization of a substrate is proportional to the number of generations of growth on that substrate. In cultures grown on substrate mixtures, competition for cellular resources or other interference of pathways will therefore preferentially select for faster utilization of the already favoured substrate, at the expense of growth rates on the less preferred substrates. The resulting evolution towards substrate specialization rather than towards co-utilization presents a challenge in developing biomass-recycling strategies for the industrial fermentation of sugar mixtures with monocultures of generalist strains.

A co-culture of specialist strains that can each ferment only a single substrate in a mixture is not expected to show deterioration of fermentation kinetics during serial batch cultivation on substrate mixtures. Instead, in such cultures, each strain is anticipated to experience selective pressure to improve growth rate on its 'assigned' sugar. This concept was experimentally tested by Verhoeven *et al.* (2018) (21), who

used metabolic engineering and adaptive laboratory evolution to obtain specialist *S. cerevisiae* strains that were able to anaerobically ferment xylose or arabinose when grown on a mixture of glucose, xylose and arabinose. A non-engineered strain of *S. cerevisiae* that cannot ferment pentose sugars was used as glucose specialist. A consortium of the three specialist strains was grown in anaerobic sequential batch cultures on glucose, xylose and arabinose, whose relative concentrations were chosen to mimic those in lignocellulosic hydrolysates. In a control experiment with a generalist strain, overall fermentation time increased from approximately 25 h in the first cycle of sequential batch fermentation to over 50 h in the 24th cycle (Figure 2B). In contrast, over a similar number of cycles, fermentation kinetics of co-cultures of the three specialist strains improved rather than deteriorated (21).

While confirming that the use of specialist strains circumvents the degeneration of fermentation kinetics that was observed in monocultures of a generalist strain, the study of Verhoeven *et al.* (2018) (21) also identified a potential trade-off. The strong preference of the specialist strain for glucose led to a rapid build-up of biomass. Despite the lower biomass-specific conversion rates of xylose and arabinose, this biomass build-up still enabled a high volumetric conversion rate of these pentoses after glucose had been consumed. Instead, in the consortium of specialist strains, the lower conversion rate of the pentoses led to a longer overall conversion time than observed for the generalist strain. While fermentation kinetics of the consortium improved during serial batch cultivation, the overall fermentation time after the 24th cycle was still ca. 20% slower than observed in the first cycles of serial batch cultivation of the generalist strain. This trade-off is influenced by the relative concentrations of the individual substrates, which determine the initial biomass concentration of each specialist strain upon initiation of the next growth cycle.

The above example shows that, in co-cultures, strains can be engineered to convert only one of the substrates in a substrate mixture. When producing a dissimilatory and therefore growth-coupled product, each specialist strains is under selective pressure to optimize its biomass specific productivity (q_p). This selective pressure prevents the deterioration of fermentation kinetics that is seen during prolonged batch cultivation of generalist strains on sugar mixtures.

In summary, for dissimilatory processes, defined co-cultures can improve yield, substrate range, and long-term genetic stability by distributing metabolic tasks over specialized strains.

3. Assimilatory products

In comparison with dissimilatory products, assimilatory processes (whose synthesis requires a net energy input) face different challenges. These include competition of growth and product formation for cellular resources, long product pathways, and a need to synthesize complex, non-native enzymes. In these cases, co-cultures offer alternative options to improve process performance.

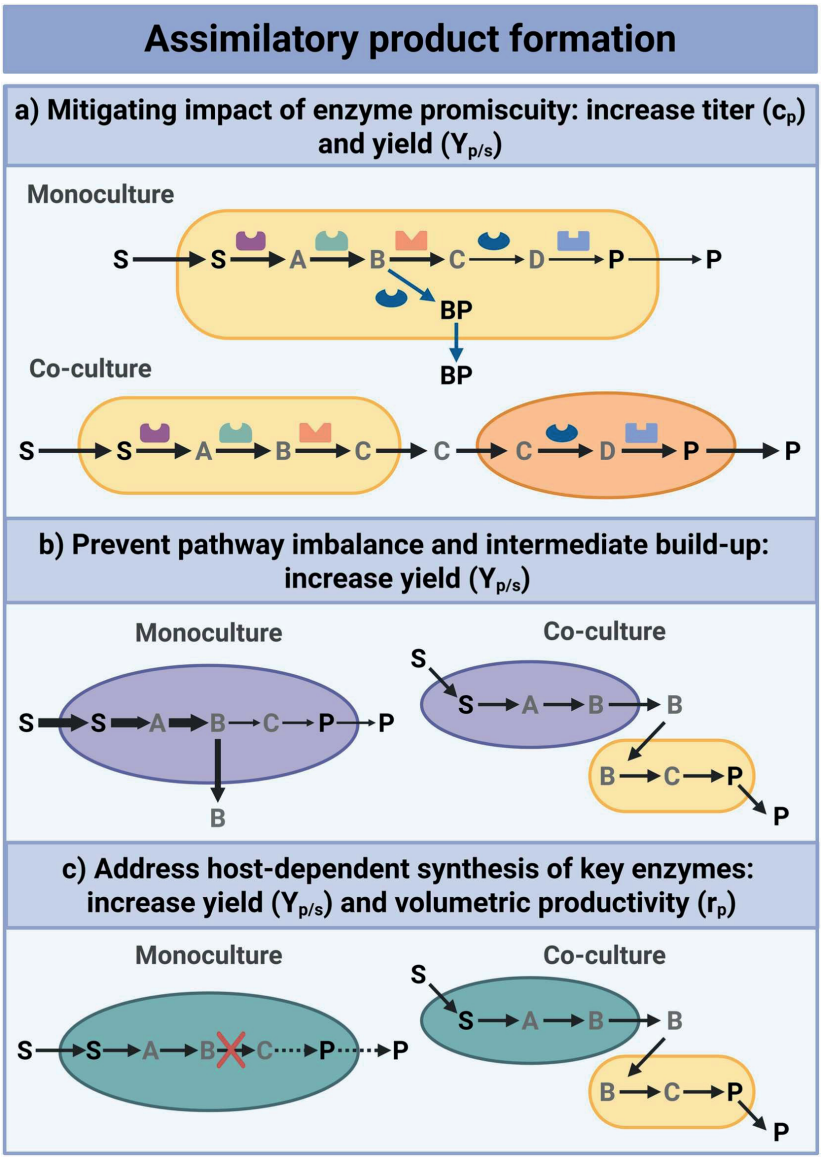

Figure 3: Potential benefits of using co-cultures to improve titer, rate, yield and stability during production of low molecular weight assimilatory products. (A) Enzyme promiscuity can cause by-product formation in long heterologously expressed product pathways. Co-cultures could mitigate this reduction in product yield by splitting pathways over separate modules, thereby spatially segregating the promiscuous enzyme from its substrate. (B) Co-cultures can be used to reduce the accumulation of (toxic) intermediates that would otherwise inhibit growth and lower product yield. (C) Co-cultures of different species can be used to overcome host-specific limitations of enzyme expression. S = substrate; P = product; BP = By-product. Created in BioRender. https://BioRender.com/nw7b4y7

Introduction of metabolic pathways for synthesis of complex, non-native assimilatory products by microbial cell factories can require expression of dozens of genes, sourced from multiple donor organisms (47,48). Producing all the encoded enzymes in a single engineered microorganism can be challenging. The umbrella term 'metabolic burden' is often used to capture negative effects of such intensive metabolic engineering on performance and genetic stability of the resulting strains (49,50). Most studies on the use of co-cultures for assimilatory product formation aim to mitigate metabolic burden by spatial segregation of product-pathway modules in different microbial strains (51).

Native protein synthesis is already the most ATP-intensive process in growing, wild-type microbial cells (52). Since, moreover, cell-volume and membrane-surface limitations impose constraints on cellular protein content (53,54), expression of heterologous pathways will compete with native cell functions for amino acids, ATP and proteome space. The impact of this competition is especially large when product pathways involve enzymes that have a low catalytic turnover rate (k_{cat}) and therefore need to be expressed at high levels to sustain relevant *in vivo* fluxes. The resulting negative impact on growth rate can confer a substantial selective advantage to less- or non-producing mutants (55). It is often assumed that even distribution of pathway enzymes over different strains can alleviate this protein burden and, thereby, enable improved productivity of co-cultures (51,56). However, based on theoretical considerations (57), equal distribution of pathway-related protein mass over multiple strains does not in itself enable a higher biomass-specific conversion rate than is obtained in a monoculture. Instead, unless equal distribution affects intracellular concentrations of pathway intermediates and/or effectors and thus enables a higher *in-vivo* substrate saturation (V/V_{max}) of rate-controlling enzymes, it will not influence the overall protein requirement. Achieving a given rate of product formation will then, per g of biomass, require the same amount of protein in mono- and co-cultures (58). Transport of pathway intermediates between co-culture partners can decrease efficiency due to dilution of intermediates in the extracellular space and/or costs associated with the expression of transporters (51,57). To have a net positive impact, co-cultivation strategies should therefore address metabolic burden issues that substantially constrain monoculture performance and cannot be addressed by straightforward metabolic engineering. Below, we will discuss examples of how the use of defined co-cultures can address challenges associated with catalytic promiscuity of pathway enzymes, by-product formation caused by pathway imbalance, and sub-optimal expression of key enzymes. Figure 3A, B and C schematically show the advantage of co-cultures for each of these challenges. In addition, we will discuss engineering of transport reactions, definition of metabolic modules and the relevance and control of the relative abundance of co-culture partners.

3.1. Addressing enzyme-related constraints in complex pathways

Enzyme promiscuity, i.e., the ability of an enzyme to perform different reactions (59), is a common challenge in the implementation of complex product pathways in

industrial microorganisms (60,61). The same holds for by-product formation caused by imbalances in engineered product pathways. Research on engineering of microbial cell factories for production of phenylpropanoids stimulated multiple studies on how these challenges can be mitigated by co-cultivation strategies.

Enzyme promiscuity can lead to by-product formation, which lowers the product yield on the substrate. This is particularly problematic for long heterologous pathways, as it creates side reactions that compete with the main product path. Co-cultures can offer a solution by separating the enzyme and the metabolite for which it has promiscuous activity.

This enzyme promiscuity, for example, played a key role in a study on metabolic engineering of *E. coli* to produce monolignols (23). Engineering of the native shikimate pathway for aromatic amino-acid synthesis, combined with introduction of a 5-step pathway for conversion of tyrosine to *p*-coumaryl alcohol (*p*-CA), enabled *p*-CA titers in shake-flask cultures of up to 0.5 g L^{-1}. However, extension of the *p*-CA pathway by overexpression of a 4-hydroxyphenylacetate-3-hydroxylase (HpaBC) that converts *p*-CA to caffeyl alcohol (CfA), yielded a CfA titer of only 0.03 g L^{-1}. This low titer was attributed to promiscuity of HpaBC which, in addition to the desired reaction, also converted tyrosine into the undesirable by-product L-dopa. Based on the observation that *p*-CA, but not tyrosine, easily crosses the *E. coli* cell membrane, the *p*-CA-producing strain was co-cultivated with a strain that overexpressed HpaBC in an otherwise wild-type background. After optimization of the inoculum ratio of the two strains, a CfA titer of 0.4 g L^{-1} was achieved in shake-flask-grown commensalistic co-cultures, indicating that expression of the promiscuous HpaBC enzyme in a separate strain successfully prevented by-product formation (23).

Brooks *et al.* (2023) (24) implemented a pathway in *E. coli* for production of the plant metabolite eugenol, in which tyrosine is first converted to coumarate, whose hydroxylation then yields caffeate. In the following two reactions, caffeate is first methylated to yield ferulic acid, which is then converted into feruloyl-CoA by the enzyme 4-hydroxycinnamoyl-CoA ligase (4-CL). However, in addition to ferulic acid, 4-CL can also use coumarate as a substrate (24,62), thereby diverting this key precursor from product formation. To address promiscuity of 4-CL and other enzymes in the eugenol pathway and to prevent build-up of the toxic intermediate coumarate, a tripartite co-culture was designed and constructed. The first *E. coli* strain was engineered for efficient *de novo* production of coumarate (Module 1), a second strain for the two-step conversion of coumarate to ferulic acid (Module 2), and a third strain for the 5-step conversion of ferulic acid to eugenol (Module 3). This modular design effectively separated 4-CL, which was highly expressed in Module 3, from upstream metabolites. In addition, increasing the inoculum size of the strain carrying Module 2 relative to that of the other two strains prevented accumulation of toxic levels of coumarate. A eugenol titer of 0.07 g L^{-1} was achieved in shake-flask cultures of the tripartite commensalistic co-culture, while no eugenol production was detected in a monoculture of an *E. coli* strain carrying all three modules. An additional advantage of

the modular co-culture approach was demonstrated by further experiments, in which genetic modification or omission of Module 2 enabled production of chavicol and hydroxychavicol, respectively (24).

The above examples illustrate that by dividing the pathway between multiple strains, the promiscuous enzyme's side reaction was effectively bypassed, improving the yield of the desired product. Moreover, as also demonstrated by a study on the production of anthocyanins by tetrapartite *E. coli* co-cultures (25), the combination of strains optimized for precursor generation with 'terminal product formation' strains enables flexible 'mix and match' strategies for extending product range.

Pathway imbalances in a single strain can reduce product yields on substrate, for example by accumulation of intermediates. Balancing the activities of individual pathway enzymes is particularly challenging in the case of non-linear pathways, where optimal distribution of intermediates requires careful tuning of the *in vivo* activities of enzymes active at metabolic branchpoints. By separating pathways in different strains in a co-culture, these pathway imbalances can be relieved. Li *et al.* (2019) (22) investigated this strategy using rosmarinic acid (RA) production by engineered *E. coli* strains as the experimental model. RA is formed by condensation of two molecules derived from the phenylpropanoid pathway: caffeoyl-CoA (Caf-CoA) and salvianic acid A (SalvA). Pathways towards Caf-CoA and SalvA diverge at 4-hydroxyphenylpyruvate (4-HPP). Conversion of 4-HPP to Caf-CoA starts with a two-step conversion of HPP into coumarate, after which two enzymes, including the abovementioned HpaBC hydroxylase, convert coumarate to Caf-CoA. Conversion of 4-HPP to SalvA is catalyzed by HpaBC and a D-lactate dehydrogenase. In this two-enzyme conversion, the order of the hydroxylase and reduction reactions is interchangeable. The ability of HpaBC to catalyze three reactions involved in the synthesis of two pathway intermediates presents a major challenge for pathway balancing in monocultures. This challenge was addressed by splitting RA biosynthesis into three pathway modules allocated to three different *E. coli* strains. Module 1 was engineered for *de novo* production of coumarate, Module 2 for *de novo* SalvA production and Module 3 for conversion of coumarate (generated by Module 1) to Caf-CoA and its condensation with SalvA (generated by Module 2) to yield RA. This tripartite co-culture strategy spatially segregated the roles of HpaBC in SalvA and Caf-CoA production and, by tuning the relative inoculum ratios of the three strains, presented a means to prevent build-up of coumarate to toxic levels. After empirically optimizing the inoculum ratios, a tripartite co-culture yielded an RA titer of 0.10 g L^{-1} in glucose-grown shake-flask cultures, which was approximately 20-fold higher than the titer obtained with a monoculture carrying the entire RA pathway (22). Overall, this example shows that using a commensalistic co-culture to separate different enzymes can prevent the accumulation of (toxic) intermediates, thereby enabling increased product yields on substrate.

Another challenge in monoculture designs relates to host-dependent (dis)abilities to functionally express specific enzymes or enzyme classes. This problem can even rule out popular industrial microorganisms as production platforms. In such

cases, using co-cultures with specialist strains of species that express the missing enzyme(s) can result in improved product yields and rates of product formation. The potential of defined co-cultures for circumventing challenges related to expression of specific types of enzymes is illustrated by research on microbial production of oxyfunctionalized taxanes. Already in 2010 (26), *E. coli* was successfully engineered to produce taxadiene, a key precursor for biosynthesis of oxygenated taxanes, including the anticancer drug paclitaxel. However, synthesis of oxygenated taxanes from taxadiene depends on hydroxylases whose *in vivo* activity requires a cytochrome P450 reductase. *Escherichia coli* does not naturally contain P450 enzymes (63), and heterologous expression of these proteins can be challenging. Mostly due to its ability to anchor P450 proteins to intracellular membranes, *S. cerevisiae* is a preferred host for expressing this class of enzymes (64). This inspired Zhou *et al.* (2015) (65) to study the co-cultivation of a taxadiene-producing *E. coli* strain with an *S. cerevisiae* strain that highly expressed a fusion protein of the plant taxadiene 5α-hydroxylase and P450 reductase that together catalyse the first oxygenation step in paclitaxel biosynthesis. Co-cultures of the two species were grown on xylose. Since xylose cannot be used by wild-type *S. cerevisiae,* growth of the yeast depended on consumption of acetate generated by the *E. coli* strain. After optimization of the expression of the hydroxylase-P450 reductase fusion protein in *S. cerevisiae* and of acetate production by *E. coli*, the titer of the targeted oxygenated taxane in fed-batch co-cultures reached 0.03 g L^{-1}. Introduction of expression cassettes encoding a second hydroxylase-P450 reductase protein and an acetylase into the *S. cerevisiae* strain enabled production of a next intermediate in the paclitaxel synthesis pathway. The versatility of this modular approach was further demonstrated by its application to the production of other compounds whose synthesis involves P450-dependent oxyfunctionalization reactions (65).

Wu *et al.* (2021) (27) demonstrated how, in bipartite co-cultures, engineered *E. coli* and *S. cerevisiae* strains could mutually complement species-specific limitations related to functional expression of key product-pathway enzymes. Their study focused on microbial production of strigolactones, an important class of plant signalling molecules. Strigolactone synthesis starts from β-carotene, whose production has been demonstrated in engineered strains of *E. coli* and *S. cerevisiae* (66). Three plant enzymes are required for conversion of β-carotene to carlactone, the central precursor for all strigolactones: a [2Fe-2S]-containing isomerase and two enzymes that catalyse oxidative cleavage reactions, one of which is a non-heme-iron-dependent enzyme. These three enzymes could be functionally expressed in *E. coli*, which enabled construction of a carlactone-producing strain. However, in line with previously reported challenges in cytosolic expression of heterologous iron-sulfur proteins in the yeast cytosol (67), attempts to produce carlactone in *S. cerevisiae* were unsuccessful. Conversely, the subsequent conversion of carlactone to specific strigolactones, which involves P450-dependent oxidation reactions, could be established in *S. cerevisiae* but not in *E. coli*. This inspired the authors to develop a flexible, bipartite co-cultivation strategy. Co-cultivating the carlactone-producing *E. coli* strain with a range of *S.*

cerevisiae strains engineered for conversion of carlactone to specific strigolactones enabled production of the targeted compounds, thereby opening the way for studies on their biological functions (27).

The above examples illustrate that, when a specific pathway enzyme cannot be functionally expressed in a preferred industrial microorganism, co-cultivation with another microorganism that does functionally express the enzyme can expand the product range.

3.2. Definition of pathway modules and transport reactions

In implementing division-of-labour strategies for assimilatory product formation, as discussed in the previous paragraph, optimal design of metabolic modules is essential. Here, 'metabolic modules' refer to segments of a production pathway that are assigned to a single co-cultivation partner. By assigning different modules to different strains, each strain handles a part of the pathway. Design of functional modules should address primary objectives, such as mitigating effects of enzyme promiscuity, circumventing host-specific protein expression challenges and preventing pathway imbalance. A second criterium, is the availability of mechanisms for transport of relevant intermediates between co-cultivation partners. This, for instance, ensures that an intermediate produced by Strain A can be exported and taken up efficiently by Strain B, either by free diffusions or via membrane transporters. To increase flexibility in the design of metabolic modules, several studies explored (over)expression of native or heterologous transporter genes, which in several cases had to be newly identified.

In a study aimed at metabolic engineering of *E. coli* for production of *cis*,*cis*-muconate, Zhang *et al.* (2015) (68) observed accumulation of the shikimate pathway intermediate 3-dehydroshikimate (DHS) by engineered strains. Based on this observation, a co-culture strategy was devised, in which a first *E. coli* strain converted xylose to DHS via the shikimate pathway, while a second strain, grown on glucose as carbon source, converted DHS to *cis,cis*-muconate via three heterologous enzymes. The inability of *E. coli* to import DHS under the experimental conditions was addressed by identification and overexpression, in the latter strain, of a native gene that encoded a functional DHS transporter. After optimization of strains and process conditions, this co-cultivation strategy enabled a *cis,cis*-muconate yield on sugar that corresponded to 51% of the theoretical maximum.

Transporter engineering with the aim to improve co-culture performance can also involve export of key intermediates, as exemplified by a study on co-cultures of two *E. coli* strains (69), of which the first overexpressed and exported tyrosine, which was then converted to 4-hydroxystyrene by a second strain expressing two heterologous enzymes. Expression of a *Petunia* gene encoding a plastid amino-acid transporter improved export of tyrosine by the former strain, thereby enabling a two-fold higher 4-hydroxystyrene titer in co-cultures than observed in a co-culture with a strain lacking the heterologous transporter.

A division-of-labour strategy for producing the benzylisoquinoline alkaloid precursor (*S*)-norcoclaurine was based on the availability of a *Scheffersomyces stipitis* strain that produced high levels of the pathway intermediate shikimate (28). Since genetic engineering tools for this non-conventional yeast were less well developed than for *S. cerevisiae*, a co-cultivation strategy was based on conversion of shikimate, produced by *Sch. stipitis*, to (*S*)-norcoclaurine by an extensively engineered *S. cerevisiae* strain. The inability of *S. cerevisiae* to efficiently import shikimate was addressed by identification of two *Aspergillus niger* shikimate transporter genes and their functional expression in the (*S*)-norcoclaurine-producing *S. cerevisiae* strain. This strategy enabled (*S*)-norcoclaurine titers in co-cultures that were two orders of magnitude higher than observed in a monoculture of the *S. cerevisiae* strain. Flexibility in modularization of the long biosynthetic pathways towards benzylisoquinoline alkaloids was further extended by a study on identification, expression in *S. cerevisiae* and functional analysis of six *Papaver somniferum* benzylisoquinoline alkaloid transporter genes (70). Using these transporters, the opiate pathway was split into three modules assigned to three *S. cerevisiae* strains. Engineering of the strain carrying the ultimate reactions enabled formation of different alkaloid products via a mix and match strategy.

Identification and functional expression of relevant transporters increase options to further refine optimization of modular co-cultivation strategies, for example to prevent uneven distribution of pathway proteins over co-cultivated strains, based on algorithms for calculating protein allocation such as Gecko (71,72). In addition, it may be possible to use energy-coupled transport mechanisms to optimize substrate saturation of low-k_{cat} enzymes and/or thermodynamic driving force for *in vivo* activity of spatially segregated metabolic models. The latter concept was theoretically explored by Bekiaris *et al.* (2021) (58), who developed the ASTHERISC algorithm. This algorithm integrates genome-scale models with thermodynamic reaction parameters to predict optimal pathway module definition. Although such options to integrate systems biology into the design of co-cultivation strategies are highly interesting, we are not aware of studies in which they have been experimentally tested.

3.3. Optimizing and controlling relative abundance of co-cultivation partners

Achieving and maintaining an optimal relative abundance of co-culture partners is a key challenge in division-of-labour strategies that are based on spatial segregation of product-pathway modules. This is important, because imbalance between the co-culture partners can lead to one outperforming the other, resulting in suboptimal production. Not surprisingly, modifying inoculum ratios is a common and often successful approach for optimizing the performance of such co-cultures in laboratory studies (see e.g. (22,25,73,74)). However, specific growth rates of individual strains, and impacts of changing conditions during growth, can lead to population dynamics that negatively affect co-culture performance. In the absence of measures to stabilize relative abundance, impacts of population dynamics are likely to be even

more pronounced under the intensive, dynamic cultivation conditions in large-scale industrial processes. Co-culture systems might therefore require monitoring of cell concentrations and the use of feedback control to maintain the balance. This can, for example, be done by process analytical techniques, as discussed in a recent review (75).

The use of mixtures of carbon substrates, of which only one can be used by each strain, has been successfully applied to stabilize relative abundance of strains in co-cultures (e.g. (68,76,77)). Alternatively, using consortium partners with different auxotrophic requirements enables the control of their relative abundance by supplying the required growth factors. This concept was used by Treloar *et al*. (2020) (78) to develop a deep-reinforcement-learning strategy to control relative abundance of two *E. coli* strains of which one was auxotrophic for arginine and the other for tryptophan. Simulations demonstrated the potential of this approach to control population composition and optimize productivity when supply of strain-specific substrates or growth factors can be coupled to online analysis of product concentration, for example by Raman spectroscopy or reporter proteins (79,80).

Inspired by studies in microbial ecology (81), self-stabilization of population composition can be based on mutual complementation of auxotrophies by cross-feeding of growth factors (74,82,83). Li *et al*. (2022) (84) explored how introducing such mutual dependencies can be applied to stabilize co-cultures of an *E. coli* strain that produces caffeate with a second strain that converts caffeate to salidroside. Strains expressing one of the two pathway modules were engineered to depend on production of either glutamate-derived amino acids or TCA-cycle intermediates by the other strain. In batch co-cultures of the mutually dependent strains, salidroside titers measured at the end of fermentation were independent of the inoculation ratio and over 2-fold higher than in cultures grown without engineered auxotrophies. The same study also demonstrated how, in the same context, a synthetic regulatory circuit based on a caffeate-responsive biosensor was used to enable ‘on-demand’ modulation of culture composition. To this end, the biosensor was coupled to expression of a degradation-prone version of a key enzyme in glutamate metabolism, thereby tuning the abundance of the caffeate-producing strain to its consumption by the salidroside-producing strain (84).

While the approaches discussed above demonstrate how relative abundance of strains in laboratory co-cultures can be stabilized and even be subjected to ‘on-demand tuning’, we have not found studies in which genetic stability of such advanced co-cultures has been tested during long-term cultivation.

4. Outlook

There are few documented examples of the large-scale application of defined microbial co-cultures for production of low-molecular-weight compounds (9,85). However, these reports either contain limited information (9), or are a bioconversion type of process (85). This is not surprising as, from an industrial perspective, development and implementation of co-culture-based processes introduces additional levels of complexity compared to monoculture-based processes. Inspired by rapid developments in synthetic biology and protein engineering (86,87), industrial research may therefore, especially for issues such as pathway imbalance, preferentially explore options for advanced engineering of monocultures. In this outlook, we provide suggestions on how future academic research may help to more precisely define situations in which defined co-cultures can, in an industrial context, outperform monocultures.

4.1. Start with the end in mind

When design, construction and analysis of co-cultures are performed with the aim to contribute to development of industrial processes, they should, just like other research in bioprocess engineering (88), start with the intended industrial application firmly in mind. The design of co-culture strategies should be based on a clear definition of which industrially relevant challenges in monocultures are addressed. Carefully designed experiments will be needed to evaluate co-culture performance under industrial conditions - for example, controlling starting strain ratios, feeding strategies, and using new bioreactor setups that can accommodate multiple organisms. This problem-based approach is illustrated by studies on the use of co-cultures for circumventing enzyme promiscuity (23,24), non-compatibility of the expression of specific enzymes with production strains (27,65) and genetic instability in generalist strains growing on sugar mixtures (21). In contrast, problem definition is often less explicit when use of co-cultures is motivated from redistribution of metabolic burden, sometimes based on the incorrect assumption that equal distribution of product-pathway protein over co-culture partners will by definition lead to improved biomass-specific or volumetric productivity (57). Moving beyond such intuitive design will benefit from rigorous quantitative comparison of mono- and co-cultures by integration of theoretical and experimental research on proteome allocation, bioenergetics and thermodynamics in mono- and co-cultures. Such systems biology approaches are also relevant for further optimizing the performance of co-cultures of substrate-specialists for production of dissimilatory products. In most of the academic studies cited in this review, co-culture performance was assessed based on product titer in small-scale laboratory batch cultures. We see a large potential for studies that, based on the existing and highly valuable body of knowledge, aim to quantitatively evaluate co-culture performance in terms of titer, productivity and yield (10) under simulated industrial conditions.

4.2. Compare deterioration of product formation in mono- and co-cultures

In processes aimed at dissimilatory product formation from mixed carbon substrates, co-cultures of 'carbon substrate specialists' have a clear potential to prevent the deterioration of fermentation kinetics observed in monocultures of generalist strains (21). The industrial relevance of this co-cultivation strategy will, in practice, depend on whether strain robustness and feedstock composition allow for biomass recycling through multiple subsequent fermentation cycles. In contrast to dissimilatory product formation, synthesis of assimilatory products competes with growth for cellular energy, proteome space and biosynthetic precursors. This competition provides a selective advantage to mutants with reduced productivity. The impact of such 'protein burden' effects on the genetic stability of co-cultures for assimilatory product formation has not yet been studied in detail. Addressing this knowledge gap is of paramount importance for assessing and improving applicability in industrial processes that, from frozen stock culture to full scale, involve many generations of growth (89).

4.3. Control the relative abundance of the strains

Controlling the relative abundance of co-culture partners under dynamic industrial process conditions can be challenging and requires robust strategies for population control. Techniques such as metabolic engineering of auxotrophic dependencies (74) and model-driven feedback control of key process parameters (78,90) are emerging solutions, but their performance requires validation under industrially relevant conditions. Further development of modelling tools (like in (91,92)) and improving techniques for monitoring and controlling population composition (75) will be crucial to unlocking the potential for industrial application.

We hope that, by inspiring readers to engage with the challenges involved in defined microbial co-cultures, this paper will contribute to the development of these scientifically fascinating systems into mature production platforms for microbial biotechnology. With ongoing advances in synthetic biology and bioprocess engineering, ever more tools become available to fine-tune interactions between co-culture partners and, thereby, optimize stable performance. In addition, quantitative analysis and optimization of co-cultures under simulated industrial conditions is essential for understanding and improving performance of co-cultures in large-scale processes. We are convinced that such research will contribute to a paradigm shift in industrial technology that will lead to much wider use of co-cultures.

5. Conclusion

Defined co-cultures offer unique opportunities to address several problems associated with the use of monoculture processes for production of assimilatory and dissimilatory products. Examples discussed in this review demonstrate, in laboratory-

scale experiments, the use of well-designed co-cultivation strategies can improve yields, expand substrate ranges, prevent genetic instability, and mitigate pathway imbalances.

The next challenge is to gear research towards transitioning from laboratory-scale experiments, often with product titer as main read-out, to full-scale industrial processes. Integration of quantitative studies on co-culture performance under simulated, dynamic industrial process conditions with synthetic biology approaches for optimizing co-culture performance offers an excellent perspective to achieve this goal.

Author contributions

JTP and RJvT conceptualised the work. SBG, TF and JTP wrote the original draft. MR developed the figures. MR, JTP and RJvT reviewed and edited the manuscript. All author read and approved the manuscript.

The work of SBG is funded from the start-up package that RJvT received from Delft University of Technology; the work of TF is funded from the Zero Emission Biotechnology program funded by Delft University of Technology; and the work of MR is funded from the NWO Stevin Prize awarded to JTP by the Dutch Research Foundation.

References

1. Abreu C, Ortiz Lopez A, Gore J. Pairing off: a bottom-up approach to the human gut microbiome. Mol Syst Biol. 2018;14(6).
2. Kehe J, Ortiz A, Kulesa A, Gore J, Blainey PC, Friedman J. Positive interactions are common among culturable bacteria. Sci Adv. 2021;7.
3. Palmer JD, Foster KR. Bacterial species rarely work together. Science. 2022;376(6593):581–2.
4. Melkonian C, Zorrilla F, Kjærbølling I, Blasche S, Machado D, Junge M, *et al*. Microbial interactions shape cheese flavour formation. Nat Commun. 2023;14(1).
5. Michielsen S, Vercelli GT, Cordero OX, Bachmann H. Spatially structured microbial consortia and their role in food fermentations. Curr Opin Biotechnol. 2024;87.
6. Sieuwerts S, Molenaar D, Van Hijum SAFT, Beerthuyzen M, Stevens MJA, Janssen PWM, *et al*. Mixed-culture transcriptome analysis reveals the molecular basis of mixed-culture growth in *Streptococcus thermophilus* and *Lactobacillus bulgaricus*. Appl Environ Microbiol. 2010;76(23):7775–84.
7. Martin BD, Schwab E. Current usage of symbiosis and associated terminology. Int J Biol. 2012;5(1).
8. Zhang Q, Lyu S. Microbial interactions in a vitamin C industrial fermentation system: novel insights and perspectives. Appl Environ Microbiol. 2022;88.
9. IFF. Your Needs Change, Your Yeast Can't. 2021;
10. Konzock O, Nielsen J. TRYing to evaluate production costs in microbial biotechnology. Trends Biotechnol. 2024;
11. Pfromm PH, Amanor-Boadu V, Nelson R, Vadlani P, Madl R. Bio-butanol vs. bio-ethanol: a technical and economic assessment for corn and switchgrass fermented by yeast or *Clostridium acetobutylicum*. Biomass Bioenergy. 2010;34(4):515–24.
12. Mittermeier F, Hafner N, XypoliaVasila K, Weuster-Botz D. Co-cultivation of Aspergillus niger and Trichoderma reesei enables efficient production of enzymes for the hydrolysis of wheat bran. Chem Ing Tech. 2023;95(4):565–75.
13. Zuroff TR, Xiques SB, Curtis WR. Consortia-mediated bioprocessing of cellulose to ethanol with a symbiotic *Clostridium phytofermentans*/yeast co-culture. 2013;
14. Fang H, Deng Y, Pan Y, Li C, Yu L. Distributive and collaborative push-and-pull in an artificial microbial consortium for improved consolidated bioprocessing. AIChE J. 2022;68(11).
15. Park EY, Naruse K, Kato T. One-pot bioethanol production from cellulose by co-culture of *Acremonium cellulolyticus* and *Saccharomyces cerevisiae*. Biotechnol Biofuels. 2012;5.

16. Lu J, Lv Y, Jiang Y, Wu M, Xu B, Zhang W, *et al*. Consolidated bioprocessing of hemicellulose-enriched lignocellulose to succinic acid through a microbial cocultivation system. ACS Sustain Chem Eng. 2020;8(24):9035–45.

17. van Aalst ACA, van der Meulen IS, Jansen MLA, Mans R, Pronk JT. Co-cultivation of *Saccharomyces cerevisiae* strains combines advantages of different metabolic engineering strategies for improved ethanol yield. Metab Eng. 2023;80:151–62.

18. Wang Y, Wan Z, Zhu Y, Hu H, Jiang Y, Jiang W, *et al*. Enhanced 1,3-propanediol production with high yield from glycerol through a novel *Klebsiella–Shewanella* co-culture. Biotechnol Biofuels Bioproducts. 2023;16(1).

19. Flores AD, Choi HG, Martinez R, Onyeabor M, Ayla EZ, Godar A, *et al*. Catabolic division of labor enhances production of D-lactate and succinate from glucose-xylose mixtures in engineered *Escherichia coli* co-culture systems. Front Bioeng Biotechnol. 2020;8.

20. Saini M, Lin LJ, Chiang CJ, Chao YP. Synthetic consortium of *Escherichia coli* for n-butanol production by fermentation of the glucose-xylose mixture. J Agric Food Chem. 2017;65(46):10040–7.

21. Verhoeven MD, De Valk SC, Daran JMG, Van Maris AJA, Pronk JT. Fermentation of glucose-xylose-arabinose mixtures by a synthetic consortium of single-sugar-fermenting *Saccharomyces cerevisiae* strains. FEMS Yeast Res. 2018;18(8):1–12.

22. Li Z, Wang X, Zhang H. Balancing the non-linear rosmarinic acid biosynthetic pathway by modular co-culture engineering. Metab Eng. 2019;54:1–11.

23. Chen Z, Sun X, Li Y, Yan Y, Yuan Q. Metabolic engineering of *Escherichia coli* for microbial synthesis of monolignols. Metab Eng. 2017;39:102–9.

24. Brooks SM, Marsan C, Reed KB, Yuan SF, Nguyen DD, Trivedi A, *et al*. A tripartite microbial co-culture system for de novo biosynthesis of diverse plant phenylpropanoids. Nat Commun. 2023;14(1).

25. Jones JA, Vernacchio VR, Collins SM, Shirke AN, Xiu Y, Englaender JA, *et al*. Complete biosynthesis of anthocyanins using *E. coli* polycultures. mBio. 2017;8(3):1–9.

26. Ajikumar PK, Xiao WH, Tyo KEJ, Wang Y, Simeon F, Leonard E, *et al*. Isoprenoid pathway optimization for Taxol precursor overproduction in *Escherichia coli*. Science. 2010;330(6000):70–4.

27. Wu S, Ma X, Zhou A, Valenzuela A, Zhou K, Li Y. Establishment of strigolactone-producing bacterium-yeast consortium. Sci Adv. 2021;7:4048–65.

28. Gao M, Zhao Y, Yao Z, Su Q, Van Beek P, Shao Z. Xylose and shikimate transporters facilitate microbial consortium as a chassis for benzylisoquinoline alkaloid production. Nat Commun. 2023;14(7797).

29. Kalayu G. Serial re-pitching: its effect on yeast physiology, fermentation performance, and product quality. Ann Microbiol. 2019;69:787–96.

30. Mans R, Daran JMG, Pronk JT. Under pressure: evolutionary engineering of yeast strains for improved performance in fuels and chemicals production. Curr Opin Biotechnol. 2018;50:47–56.

31. Basso LC, De Amorim HV, De Oliveira AJ, Lopes ML. Yeast selection for fuel ethanol production in Brazil. FEMS Yeast Res. 2008;8:1155–63.

32. Zaldivar J, Nielsen J, Olsson L. Fuel ethanol production from lignocellulose: a challenge for metabolic engineering and process integration. Appl Microbiol Biotechnol. 2001;56:17–34.

33. van Maris AJA, Abbott DA, Bellissimi E, van den Brink J, Kuyper M, Luttik MAH, *et al*. Alcoholic fermentation of carbon sources in biomass hydrolysates by *Saccharomyces cerevisiae*: current status. Antonie Van Leeuwenhoek. 2006;90:391–418.

34. van Aalst ACA, de Valk SC, van Gulik WM, Jansen MLA, Pronk JT, Mans R. Pathway engineering strategies for improved product yield in yeast-based industrial ethanol production. Synth Syst Biotechnol. 2022;7(1):554–66.

35. Papapetridis I, Goudriaan M, Vázquez Vitali M, De Keijzer NA, Van Den Broek M, Van Maris AJA, *et al*. Optimizing anaerobic growth rate and fermentation kinetics in *Saccharomyces cerevisiae* strains expressing Calvin-cycle enzymes for improved ethanol yield. Biotechnol Biofuels. 2018;11(1).

36. van Aalst ACA, Jansen MLA, Mans R, Pronk JT. Quantification and mitigation of byproduct formation by low-glycerol-producing *Saccharomyces cerevisiae* strains containing Calvin-cycle enzymes. Biotechnol Biofuels Bioproducts. 2023;16(1).

37. Medina VG, Almering MJH, Van Maris AJA, Pronk JT. Elimination of glycerol production in anaerobic cultures of a *Saccharomyces cerevisiae* strain engineered to use acetic acid as an electron acceptor. Appl Environ Microbiol. 2010;76(1):190–5.

38. Hunt KA, Flynn JM, Naranjo B, Shikhare ID, Gralnick JA. Substrate-level phosphorylation is the primary source of energy conservation during anaerobic respiration of *Shewanella oneidensis* strain MR-1. J Bacteriol. 2010;192(13):3345–51.

39. Lin T, Ding W, Sun L, Wang L, Liu CG, Song H. Engineered *Shewanella oneidensis*–reduced graphene oxide biohybrid with enhanced biosynthesis and transport of flavins enabled a highest bioelectricity output in microbial fuel cells. Nano Energy. 2018;50:639–48.

40. Deutscher J, Francke C, Postma PW. How phosphotransferase system-related protein phosphorylation regulates carbohydrate metabolism in bacteria. Microbiol Mol Biol Rev. 2006;70(4):939–1031.

41. Blaiseau PL, Holmes AM. Diauxic inhibition: Jacques Monod's ignored work. J Hist Biol. 2021;54(2):175–96.

42. Douwenga S, van Olst B, Boeren S, Luo Y, Lai X, Teusink B, *et al*. The hierarchy of sugar catabolization in *Lactococcus cremoris*. Microbiol Spectr. 2023;11(6).

43. Shin J, Liao S, Kuanyshev N, Xin Y, Kim C, Lu T, *et al*. Compositional and temporal division of labor modulates mixed sugar fermentation by an engineered yeast consortium. Nat Commun. 2024;15(1):1–12.

44. Johnston TG, Yuan SF, Wagner JM, Yi X, Saha A, Smith P, *et al*. Compartmentalized microbes and co-cultures in hydrogels for on-demand bioproduction and preservation. Nat Commun. 2020;11(1):1–11.

45. Duperray M, Delvenne M, François JM, Delvigne F, Capp JP. Genomic and metabolic instability during long-term fermentation of an industrial *Saccharomyces cerevisiae* strain engineered for C5 sugar utilization. Front Bioeng Biotechnol. 2024;12.

46. Wisselink HW, Toirkens MJ, Wu Q, Pronk JT, Van Maris AJA. Novel evolutionary engineering approach for accelerated utilization of glucose, xylose, and arabinose mixtures by engineered *Saccharomyces cerevisiae* strains. Appl Environ Microbiol. 2009;75(4):907–14.

47. Galanie S, Thodey K, Trenchard IJ, Interrante MF, Smolke CD. Complete biosynthesis of opioids in yeast. Science. 2015;349(6252):1095–100.

48. Liu X, Ding W, Jiang H. Engineering microbial cell factories for the production of plant natural products: from design principles to industrial-scale production. Microb Cell Fact. 2017;16.

49. Snoeck S, Guidi C, De Mey M. "Metabolic burden" explained: stress symptoms and its related responses induced by (over)expression of (heterologous) proteins in *Escherichia col*i. Microb Cell Fact. 2024;23(1):1–19.

50. Mao J, Zhang H, Chen Y, Wei L, Liu J, Nielsen J, *et al*. Relieving metabolic burden to improve robustness and bioproduction by industrial microorganisms. Biotechnol Adv. 2024;74:108401.

51. Roell GW, Zha J, Carr RR, Koffas MA, Fong SS, Tang YJ. Engineering microbial consortia by division of labor. Microb Cell Fact. 2019;18(1):1–11.

52. Stouthamer AH. A theoretical study on the amount of ATP required for synthesis of microbial cell material. Antonie Van Leeuwenhoek. 1973;39:545–65.

53. Beg QK, Vazquez A, Ernst J, De Menezes MA, Bar-Joseph Z, Barabási AL, *et al*. Intracellular crowding defines the mode and sequence of substrate uptake by *Escherichia coli* and constrains its metabolic activity. Proc Natl Acad Sci U S A. 2007;104(31):12663–8.

54. Berkhout J, Bosdriesz E, Nikerel E, Molenaar D, de Ridder D, Teusink B, *et al*. How biochemical constraints of cellular growth shape evolutionary adaptations in metabolism. Genetics. 2013;194(2):505–12.

55. Rugbjerg P, Myling-Petersen N, Porse A, Sarup-Lytzen K, Sommer MOA. Diverse genetic error modes constrain large-scale bio-based production. Nat Commun. 2018;9(1).

56. Zhang H, Wang X. Modular co-culture engineering, a new approach for metabolic

engineering. Metab Eng. 2016;37:114–21.

57. Tsoi R, Wu F, Zhang C, Bewick S, Karig D, You L. Metabolic division of labor in microbial systems. Proc Natl Acad Sci U S A. 2018;115(10):2526–31.

58. Bekiaris PS, Klamt S. Designing microbial communities to maximize the thermodynamic driving force for the production of chemicals. PLoS Comput Biol. 2021;17(6):1–25.

59. Glasner ME, Truong DP, Morse BC. How enzyme promiscuity and horizontal gene transfer contribute to metabolic innovation. FEBS J. 2020;287:1323–42.

60. Bornscheuer UT, Kazlauskas RJ. Catalytic promiscuity in biocatalysis: using old enzymes to form new bonds and follow new pathways. Angew Chem Int Ed. 2004;43:6032–40.

61. Porokhin V, Amin SA, Nicks TB, Gopinarayanan VE, Nair NU, Hassoun S. Analysis of metabolic network disruption in engineered microbial hosts due to enzyme promiscuity. Metab Eng Commun. 2021;12.

62. Ferrer JL, Austin MB, Stewart C, Noel JP. Structure and function of enzymes involved in the biosynthesis of phenylpropanoids. Plant Physiol Biochem. 2008;46(3):356–70.

63. Leonard E, Koffas MAG. Engineering of artificial plant cytochrome P450 enzymes for synthesis of isoflavones by *Escherichia coli*. Appl Environ Microbiol. 2007;73(22):7246–51.

64. Jiang L, Dong C, Liu T, Shi Y, Wang H, Tao Z, *et al*. Improved functional expression of cytochrome P450s in *Saccharomyces cerevisiae* through screening a cDNA library from Arabidopsis thaliana. Front Bioeng Biotechnol. 2021;9.

65. Zhou K, Qiao K, Edgar S, Stephanopoulos G. Distributing a metabolic pathway among a microbial consortium enhances production of natural products. Nat Biotechnol. 2015;33(4):377–83.

66. Misawa N, Shimada H. Metabolic engineering for the production of carotenoids in non-carotenogenic bacteria and yeasts. J Biotechnol. 1998;59(3):169–81.

67. Biz A, Mahadevan R. Overcoming challenges in expressing iron–sulfur enzymes in yeast. Trends Biotechnol. 2021;39:665–77.

68. Zhang H, Pereira B, Li Z, Stephanopoulos G, Demain AL. Engineering *Escherichia coli* coculture systems for the production of biochemical products. Proc Natl Acad Sci U S A. 2015;112(27):8266–71.

69. Gargatte S, Li Z, Zhou Y, Wang X, Zhuang L, Zhang H. Utilizing a tyrosine exporter to facilitate 4-hydroxystyrene biosynthesis in an *E. coli–E. coli* co-culture. Biochem Eng J. 2021;176.

70. Dastmalchi M, Chang L, Chen R, Yu L, Chen X, Hagel JM, *et al*. Purine permease-type benzylisoquinoline alkaloid transporters in opium poppy. Plant Physiol. 2019;181(3):916–33.

71. Domenzain I, Sánchez B, Anton M, Kerkhoven EJ, Millán-Oropeza A, Henry C, *et al*. Reconstruction of a catalogue of genome-scale metabolic models with enzymatic constraints using GECKO 2.0. Nat Commun. 2022;13(1).

72. Sánchez BJ, Zhang C, Nilsson A, Lahtvee P, Kerkhoven EJ, Nielsen J. Improving the phenotype predictions of a yeast genome-scale metabolic model by incorporating enzymatic constraints. Mol Syst Biol. 2017;13(8).

73. Wang X, Li Z, Policarpio L, Koffas MAG, Zhang H. De novo biosynthesis of complex natural product sakuranetin using modular co-culture engineering. Appl Microbiol Biotechnol. 2020;104(11):4849–61.

74. Peng H, Darlington APS, South EJ, Chen HH, Jiang W, Ledesma-Amaro R. A molecular toolkit of cross-feeding strains for engineering synthetic yeast communities. Nat Microbiol. 2023;8:1–13.

75. Dambruin NA, Pronk JT, Klijn ME. Application of process analytical technology for real-time monitoring of synthetic co-culture bioprocesses. Anal Bioanal Chem. 2025;417:1–12.

76. Liu X, Li L, Liu J, Qiao J, Zhao GR. Metabolic engineering *Escherichia coli* for efficient production of icariside D2. Biotechnol Biofuels. 2019;12(1):1–12.

77. Shahab RL, Brethauer S, Luterbacher JS, Studer MH. Engineering of ecological niches to create stable artificial consortia for complex biotransformations. Curr Opin Biotechnol. 2020;62:129–36.

78. Treloar NJ, Fedorec AJH, Ingalls B, Barnes CP. Deep reinforcement learning for the control of microbial co-cultures in bioreactors. PLoS Comput Biol. 2020;16(4):1–18.

79. Schlembach I, Grünberger A, Rosenbaum MA, Regestein L. Measurement techniques to resolve and control population dynamics of mixed-culture processes. Trends Biotechnol. 2021;39(10):1093–109.

80. Kusuda M, Shimizu H, Toya Y. Reactor control system in bacterial co-culture based on fluorescent proteins using an Arduino-based home-made device. Biotechnol J. 2021;16(12):1–9.

81. Pande S, Merker H, Bohl K, Reichelt M, Schuster S, De Figueiredo LF, *et al*. Fitness and stability of obligate cross-feeding interactions that emerge upon gene loss in bacteria. ISME J. 2014;8(5):953–62.

82. Park YK, Peng H, Hapeta P, Sellés Vidal L, Ledesma-Amaro R. Engineered cross-feeding creates inter- and intra-species synthetic yeast communities with enhanced bioproduction. Nat Commun. 2024;15(1):1–10.

83. Kelly EE, Fischer AM, Collins CH. Drawing up a collaborative contract: Amino acid cross-feeding between interspecies bacterial pairs. Biotechnol Bioeng. 2021;118(8):3138–49.

84. Li X, Zhou Z, Li W, Yan Y, Shen X, Wang J, *et al*. Design of stable and self-regulated

microbial consortia for chemical synthesis. Nat Commun. 2022;13(1).

85. Wang Y, Li H, Liu Y, Zhou M, Ding M, Yuan Y. Construction of synthetic microbial consortia for 2-keto-L-gulonic acid biosynthesis. Synth Syst Biotechnol. 2022;7(1):481–9.

86. McNerney MP, Watstein DM, Styczynski MP. Precision metabolic engineering: The design of responsive, selective, and controllable metabolic systems. Metab Eng. 2015;31:123–31.

87. Listov D, Goverde CA, Correia BE, Fleishman SJ. Opportunities and challenges in design and optimization of protein function. Curr Opin Struct Biol. 2022;72:102–10.

88. Noorman HJ, Heijnen JJ. Biochemical engineering's grand adventure. Chem Eng Sci. 2017;170:677–93.

89. Takors R. Scale-up of microbial processes: impacts, tools and open questions. J Biotechnol. 2012;160(1–2):3–9.

90. Lee TA, Morlock J, Allan J, Lee TA, Morlock J, Allan J, *et al*. Directing microbial co-culture composition using cybernetic control. Cell Rep Methods. 2025;5(3):101009.

91. Dukovski I, Bajić D, Chacón JM, Quintin M, Vila JCC, Sulheim S, *et al*. Computation of microbial ecosystems in time and space (COMETS): an open source collaborative platform for modelling ecosystems metabolism. Nat Protoc. 2021;16(11):5030–82.

92. Garcı B, Garcı L, Nogales J. FLYCOP: metabolic modelling-based analysis and engineering microbial communities. Biotechnol Bioeng. 2018;115:954–63.

Outlook and valorisation

Small-volume and high-throughput enrichment of antimetabolite-resistant strains

Antimetabolites play a key role in microbial strain improvement programmes to select for mutant strains that overproduce anabolic products from tightly regulated pathways or bypass metabolite repression (1–3). Since these compounds are often toxic and expensive, reducing the quantities used during screening is desirable. Chapter 2 demonstrates that microdroplet cultivation enables the screening of 10^6 cells in just 0.3 mL, resulting in an approximately 160000-fold volume reduction compared to conventional plate-based assays (assuming the use of 50 µL assay reagent per mutant). In chapter 2, resistance to the glucose antimetabolite 2-deoxyglucose, which is a relatively inexpensive molecule (4), was used as a model for proof-of-principle experiments. Importantly, the same approach can be readily extended to other, more costly inhibitory molecules, such as roseoflavin (€20,400 g^{-1}) for riboflavin production or amino-acid antimetabolites (approximately €300 g^{-1}) (5–7). These cost savings are accompanied by proportional decreases in the use of toxic antimetabolites and toxic waste disposal. Research on this screening approach was developed with industrial application in mind and was supported by the Taste, Texture and Health business of dsm-firmenich.

Beyond the selection of antimetabolite-resistant strains, low-volume enrichment in microdroplets can also reduce costs for enzyme-based screening assays. For example, Wang *et al.* (2014) (8) reported a 2000-fold reduction in reagent cost relative to conventional 96-well plate assays when using microdroplet-based oxidase enzyme/horseradish peroxidase/Amplex UltraRed assay in a screen for improved xylose consumption.

Biomass-yield selection

In conventional, well-mixed suspension cultures, nutrients provided in the culture medium or released by cells are shared by all cells in the culture. By using microdroplets surrounded by an oil phase, access to nutrients such as sugars is privatised within each microdroplet, thereby eliminating competition between the clonal cell lines in different microdroplets. As described in Chapter 1, the principle of nutrient privatisation has previously been used to select for more efficient

Lactococcus cremoris, Escherichia coli and *Saccharomyces cerevisiae* mutants (9–11). These studies provided valuable insights into metabolic constraints and cellular regulation strategies.

In terms of substrate use, the efficiency of microbial growth can be defined as either the amount of biomass or the number of cells generated per amount of substrate. When defined specifically as biomass yield on substrate, this measure is particularly relevant in industrial biotechnology. Relative to biomass yields of glucose-respiring microbial cultures, glucose-fermenting microorganisms such as *L. lactis, E. coli,* and *S. cerevisiae* generate less ATP per molecule of dissimilated glucose (12–14). This lower ATP yield from dissimilation leads to a lower biomass yield on glucose in fermenting cultures (12–14). However, in the facultatively fermentative yeast *S. cerevisiae*, aerobic (respiro)fermentative growth enables higher specific growth rates than fully respiratory growth (13). Consequently, conventional aerobic batch cultures will select for a low efficiency of glucose-to-biomass conversion (15,16). Single-cell encapsulation in microdroplets eliminates competition between cells in different microdroplets, enabling the selection of efficient (and potentially slower-growing) cells. More efficient *L. lactis* and *S. cerevisiae* (Chapter 3) mutants, with higher cell-number yield as well as higher biomass yield on glucose, were selected through serial propagations of water-in-oil emulsions (9,11, Chapter 3). In contrast, similar experiments with *E. coli* led to the selection of small-cell-size mutants that showed a higher cell-number yield, but not a higher biomass yield (10). This observation underlines that selection pressure in microdroplet systems primarily acts on cell number yield, which may be achieved by a decrease of cell size without an increase of biomass yield. Inadvertent selection for a smaller cell size can therefore complicate the use of micro-compartmented cultivation systems for selecting cell lines with a higher biomass yield. A possible strategy to circumvent this problem may be to first, in a series of subsequent microdroplet cultures, select for a minimum cell size and subsequent selection runs might then select for improved biomass yield.

Previous efforts to enrich for high biomass yield strains have relied on multiple rounds of serial propagation (9,11). Based on an expected positive correlation of autofluorescence and cell number, FACS sorting of microdroplets was explored by us as a method to accelerate enrichment. In competition experiments between the Crabtree-negative (efficient) *S. cerevisiae* TM6* strain (17) and a Crabtree-positive (less efficient) strain, enrichment was unsuccessful; droplets with the efficient strain showed lower autofluorescence, likely due to oxygen limitation. Although the oxygen solubility in the applied oil phase is higher than in water (18), the limited headspace in small-volume cultures may constrain oxygen availability. Careful investigation of how cell concentration affects autofluorescence and scatter signals, oxygen availability, and the structural stability of microbeads at high cell concentrations is required to further explore this method.

Looking ahead, biomass yield selection might take on relevance in the context of a growing interest in producing microbial food and feed from sustainable C1 and/or

C2 carbon sources (methanol, formate, acetate and ethanol), which requires their efficient conversion into biomass (19,20). Single-cell microdroplet encapsulation offers a potentially interesting approach for biomass-yield selection in this context.

However, care should be taken that the small molecules used as carbon sources might partition into the oil phase or transfer between droplets, which would compromise the intended privatisation of resources in individual droplets (21).

Deciphering interactions

Deciphering microbial interactions remains a core challenge in microbial ecology. Existing methods face challenges associated with probing large combinatorial spaces (22–24). These limitations provide a strong incentive to explore high-throughput approaches for studying microbial interactions.

Microdroplet cultivation enables high-throughput experiments in which large numbers of sub-communities are grown in parallel. Chapter 4 demonstrates the deciphering of pairwise interactions through a label-free, isolation-independent, microdroplet-based approach. This approach only requires total cell counts and relative abundances (which can be determined by colony-forming unit counts, 16S-rRNA gene amplicon analysis or metagenome sequence data). However, a key limitation is the rapid increase of parameter space with higher-order interactions, especially in large communities. One way to reduce complexity, as shown by Gibson *et al.* (2025) (25), is to group taxa into modules based on shared interaction structures, resource use or perturbation responses. A further limitation of current microdroplet-based approaches is that they ignore resource dynamics: they capture *what* happens (e.g., microbe B grows better with microbe A) but not *why* (e.g., metabolite exchange, detoxification, or reduced competition). More mechanistic resolution can be obtained by integrating resource labelling to track metabolite consumption/secretion, or by complementing microdroplet-based approaches with ecological modelling. For example, genome scale models can predict cross-fed metabolites and flux distributions and modelling frameworks such as COMETS can also predict the spatial and temporal dynamics of communities (24). Looking ahead, microdroplet-based approaches offer high-throughput coarse-grained tools to survey interactions. Promising sub-communities identified by this strategy can subsequently be examined in greater depth by specific approaches.

Developing co-cultures for industrial biotechnology

A challenge that emerged from Chapter 5, which reviews the potential of defined co-cultures for industrial biotechnology, is controlling relative abundances within co-cultures. Given our limited knowledge of engineering microbial co-cultures, high-throughput screening offers a promising direction to identify stabilised co-cultures from mutant pools. Microdroplet-based screening approaches, as applied in Chapters

2 and 4, can enable label-free discovery of self-stabilising co-cultures. This approach can, for example, be used to develop defined co-cultures for valorising complex, waste-derived substrates. As discussed in Chapter 5, co-cultures of specialist strains, each optimised to convert a single substrate, frequently outperform generalist strains (which convert multiple substrates). However, their implementation in industry is limited by differences in rates of substrate conversion. Stable co-cultures that efficiently and simultaneously consume all substrates can result in higher overall productivity and prevent degeneration of culture performance upon prolonged cultivation. The microdroplet-based approach applied in this thesis provides a high-throughput strategy to screen millions of sub-consortia based on cell numbers and enrich for stable, specialist co-cultures. Once identified, these consortia serve to uncover stabilisation mechanisms, providing design principles for future engineering of industrial co-cultures. Beyond stability, growth-based microdroplet screening platforms enable label-free discovery of novel enzymes and metabolic activities from diverse microbial communities (as outlined in Chapter 1).

Influence of spatial structure on community assembly

Microdroplet cultivation provides a platform to study the influence of spatial structure on community assembly. van Tatenhove-Pel *et al.* (2021) (26), using microdroplets to mimic spatial structure, identified conditions that favour cooperation in the presence of cheaters. They showed that cooperators only benefit when localised with other cooperators; otherwise, cheaters exploit them, reducing overall community benefit. The authors identified a small “window of benefit” where cooperators gain an advantage through co-localisation. Such approaches can also probe conditions favouring costly but community-beneficial behaviours, such as *L. lactis* extracellular protease activity in milk, *S. cerevisiae* extracellular sucrose invertase hydrolysis activity into hexoses, and siderophore secretion to capture poorly soluble iron (16,27,28). In suspension cultures, these public metabolizers are often outcompeted by cheaters or private metabolizers (27), but spatially structured growth enables a systematic study of diffusion constraints and cell-concentration effects to elucidate conditions favouring the selection (29) of this costly behaviour. Le Bec *et al.* (2024) (30) used optogenetic-based spatial structuring to map concentration gradients that favour costly cooperator growth on solid medium plates, which allows two-dimensional analysis. Future studies using microdroplets could extend this to three-dimensional compartmentalised growth, which additionally offers easier manipulation of co-localisation.

Spatial structuring also influences non-hierarchical competitive (rock-paper-scissors) dynamics, where strains dominate in a circular fashion (A outcompetes B, B outcompetes C, and C outcompetes A) (26,31,32). Kerr *et al.* (2002) (32) recreated such a cycle with an antibiotic-producing strain (outcompetes sensitive strain), a resistant strain (outcompetes producer strain), and a sensitive strain (outcompetes resistant strain). In well-mixed suspension cultures, where interactions and dispersal

occur at larger spatial scales, resistant strains were shown to dominate, resulting in loss of diversity. In contrast, local interactions and dispersal were shown to promote coexistence and maintain diversity (32). Microdroplet systems provide a way to mimic such localised dispersal and interaction distances, offering a platform to explore how small-scale structure drives coexistence in communities.

Serial propagation of microdroplets in emulsions can mimic the Haystack model, where growth in isolated patches is followed by dispersal and mixing (26). This resembles biofilm ecology, where communities grow in spatial niches with periodic dispersal (26,33). Replacing serial propagation with FACS-based sorting of microdroplets by growth or other markers can help in mimicking ecological processes such as dominant-species dispersal in biofilms, which prevents competitive exclusion and supports coexistence (33).

In this thesis, a microdroplet-based platform was applied for monoculture screening and studying microbial interactions, leveraging small-volume cultivation and label-free selection. Although microdroplet environments do not fully replicate real-world contexts such as industrial bioreactors or natural spatial structures, they do enable initial screening, identification and characterisation of promising strains and consortia. Overall, this work underscores the potential of microdroplet-based approaches in ecology and biotechnology while aiming to inspire further methodological development.

References

1. Adrio JL, Demain AL. Genetic improvement of processes yielding microbial products. FEMS Microbiology Reviews. 2006;30:187–214.
2. Fiedurek J, Trytek M, Szczodrak J. Strain improvement of industrially important microorganisms based on resistance to toxic metabolites and abiotic stress. Journal of Basic Microbiology. Wiley-VCH Verlag; 2017;57:445–59.
3. Cardoso JGR, Zeidan AA, Jensen K, Sonnenschein N, Neves AR, Herrgård MJ. MARSI: Metabolite analogues for rational strain improvement. Bioinformatics. 2018;34(13):2319–21.
4. Sigma-Aldrich.2-Deoxy-D-glucose.https://www.sigmaaldrich.com/NL/en/product/sigma/d6134. Accessed 11 Sep 2025.
5. Sigma-Aldrich. L-(+)-Canavanine sulfate salt monohydrate (98%). https://www.sigmaaldrich.com/NL/en/product/aldrich/861839. Accessed 11 Sep 2025.
6. Sigma-Aldrich.L-Azetidine-2-carboxylic acid (≥99%). https://www.sigmaaldrich.com/NL/en/product/sigma/a0760. Accessed 11 Sep 2025.
7. Sigma-Aldrich. Roseoflavin. https://www.sigmaaldrich.com/NL/en/product/sigma/sml1583. Accessed 11 Sep 2025.
8. Wang BL, Ghaderi A, Zhou H, Agresti J, Weitz DA, Fink GR, *et al*. Microfluidic high-throughput culturing of single cells for selection based on extracellular metabolite production or consumption. Nat Biotechnol. 2014;32(5):473–8.
9. Bachmann H, Fischlechner M, Rabbers I, Barfa N, Dos Santos FB, Molenaar D, *et al*. Availability of public goods shapes the evolution of competing metabolic strategies. Proc Natl Acad Sci U S A. 2013;110(35):14302–7.
10. Rabbers I, Gottstein W, Feist AM, Teusink B, Bruggeman FJ, Bachmann H. Selection for Cell Yield Does Not Reduce Overflow Metabolism in *Escherichia coli*. Mol Biol Evol. 2022;39(1):1–10.
11. van Tatenhove-Pel RJ, Zwering E, Boreel DF, Falk M, van Heerden JH, Kes MBMJ, *et al*. Serial propagation in water-in-oil emulsions selects for *Saccharomyces cerevisiae* strains with a reduced cell size or an increased biomass yield on glucose. Metab Eng. 2021;64:1–14.
12. Thomas TD, Ellwood DC, Longyear VMC. Change from homo- to heterolactic fermentation by *Streptococcus lactis* resulting from glucose limitation in anaerobic chemostat cultures. J Bacteriol. 1979;138(1):109–17.
13. Van Dijken JP, Weusthuis RA, Pronk JT. Kinetics of growth and sugar consumption in yeasts. Antonie Van Leeuwenhoek. 1993;63:343–52.
14. Wolfe AJ. The acetate switch. Microbiol Mol Biol Rev. 2005;69(1):12–50.

15. Mans R, Daran JMG, Pronk JT. Under pressure: evolutionary engineering of yeast strains for improved performance in fuels and chemicals production. Curr Opin Biotechnol. 2018;50:47–56.

16. Bachmann H, Bruggeman FJ, Molenaar D, Santos FBS, Teusink B. Public goods and metabolic strategies. Curr Opin Microbiol. 2016;31:109–15.

17. Elbing K, Larsson C, Bill RM, Albers E, Snoep JL, Boles E, *et al*. Role of hexose transport in control of glycolytic flux in *Saccharomyces cerevisiae*. Appl Environ Microbiol. 2004;70(9):5322–30.

18. Sklodowska K, Jakiela S. Enhancement of bacterial growth with the help of immiscible oxygenated oils. RSC Adv. 2017;7(65):40990–5.

19. Claassens NJ, Cotton CAR, Kopljar D, Bar-Even A. Making quantitative sense of electromicrobial production. Nat Catal. 2019;2(5):437–47.

20. Lovat SJ, Ben-Nissan R, Milshtein E, Tzachor A, Flamholz A, Leger D, *et al*. Electro-microbial production techno-economic viability and environmental implications. Nature Biotechnology. Nature Research. 2025;43:848–53.

21. T Fecker T de KR van TP. The effect of substrate and product transfer between polydisperse microdroplets on biological high-throughput screens. Sci Rep. 2025;

22. Abreu NA, Taga ME. Decoding molecular interactions in microbial communities. FEMS Microbiology Reviews. 2016;40:648–63.

23. Faust K, Raes J. Microbial interactions: from networks to models. Nat Rev Microbiol. 2012;10(8):538–50.

24. van den Berg NI, Machado D, Santos S, Rocha I, Chacón J, Harcombe W, *et al*. Ecological modelling approaches for predicting emergent properties in microbial communities. Nature Ecology and Evolution. Nature Research. 2022;6:855–65.

25. Gibson TE, Kim Y, Acharya S, Kaplan DE, DiBenedetto N, Lavin R, *et al*. Learning ecosystem-scale dynamics from microbiome data with MDSINE2. Nat Microbiol. 2025;10, pages2550–2564

26. van Tatenhove-Pel RJ, de Groot DH, Bisseswar AS, Teusink B, Bachmann H. Population dynamics of microbial cross-feeding are determined by co-localisation probabilities and cooperation-independent cheater growth. ISME Journal. 2021;15(10):3050–61.

27. Lindsay RJ, Pawlowska BJ, Gudelj I. Privatisation of public goods can cause population decline. Nat Ecol Evol. 2019;3(8):1206–16.

28. Bachmann H, Molenaar D, Kleerebezem M, Van Hylckama Vlieg JE. High local substrate availability stabilises a cooperative trait. ISME Journal. 2011;5(5):929–32.

29. van Tatenhove-Pel RJ, Rijavec T, Lapanje A, van Swam I, Zwering E, Hernandez-Valdes JA, *et al*. Microbial competition reduces metabolic interaction distances to the low µm-range. ISME Journal. 2021;15(3):688–701.

30. Le Bec M, Pouzet S, Cordier C, Barral S, Scolari V, Sorre B, *et al*. Optogenetic spatial patterning of cooperation in yeast populations. Nat Commun. 2024;15:75.

31. Durrett R, Simon L. Allelopathy in Spatially Distributed Populations. J. theor. Biol. 1997;185:165-171.

32. Kerr B, Riley MA, Feldman MW, Bohannan BJM. Local dispersal promotes biodiversity in a real-life game of rock-paper-scissors. Nature. 2002;418(6894):171–4.

33. Holt JD, Schultz D, Nadell CD. Dispersal of a dominant competitor can drive multispecies coexistence in biofilms. Current Biology. 2024;34(18):4129-4142.e4.

Acknowledgements

A PhD is generally viewed as a solitary journey, but it has taken a village to get me here. I am grateful to everyone who has supported me throughout this amazing, rollercoaster 4.5-year adventure.

I have been incredibly lucky to have a great supervisory team whose expertise, experience, and perspectives perfectly complement each other. **Rinke**, thank you for being not only my supervisor but also a mentor and friend. One of your most remarkable qualities as a supervisor is that you always prioritise your PhD students. It has been a wonderful journey with you! Thank you for providing me with a good balance between support and independence and for always being ready to help, whether it was the day before labour or attending video calls with me from the FACS while attending to your children. It goes without saying that you have made an immense contribution to my scientific growth, but what has especially inspired me most is your practical and grounded approach to facing challenges. I will always fondly remember, especially at the start of my PhD, our time together in the lab and our candid conversations about life, choices and most importantly, mental health. I never worried about being your first PhD student; in fact, this adventure has been extra special because of it. **Jack**, thank you for being such a thoughtful and proactive promoter! Your enthusiasm and passion for science are infectious. I am thankful for your invaluable scientific advice and for our walks around the faculty, which often turned into insightful conversations about professional growth. I especially appreciate how you stepped in to support me whenever Rinke was away. I greatly admire your ability to be both an empathic supervisor and an effective leader of the department, even during challenging times. I am inspired by how, despite being so busy, you still manage to be so dependable for your students.

Thank you, **Pascale**, for inviting me to be part of the Metabolic Reprogramming teaching team. It has been one of the most fun experiences of my PhD! I am grateful not only for the opportunity to teach this amazing course but also for the chance to pick your brain and learn from your expertise. Thank you for always being insightful, energetic, and fun. Your enthusiasm is infectious! Even though I did not do any metabolic engineering during my PhD, I can safely still say that I now understand the field, thanks to you. **Jean-Marc**, thank you for being a dependable head of the research group and for always creating a stimulating working environment with your wealth of knowledge. **Djordje**, thank you for your valuable input on my research and

for being extremely encouraging during the long stretches of failed experiments. Your support helped me keep believing that it would eventually work out. I am excited for all the amazing and innovative research that your group will accomplish in the coming years. Thank you, **Marcel**, for all the fun times as office mates and for the laughs during long growth studies. Thank you for always being extremely thoughtful and supportive. I cannot wait to start working with you, learning and contributing to your amazing research.

Robert and Sophie, my experience with both of you as supervisors during my master's thesis project was instrumental in my decision to pursue a PhD, especially at IMB. Thank you also for welcoming me into your research group meetings (Energetics) at the start of my PhD. They were always stimulating and fostered a positive and inspiring research environment.

I had the opportunity to collaborate with **Daan**, who developed the model for one of the chapters in this thesis. Collaborating with you was a huge learning experience! Thank you, Daan, for your detailed emails, for patiently answering all my questions, for the insightful meetings and for your candour. Thank you also to dsm-firmenich Taste, Texture and Health business group (**Thibaut, Noël, and Ilse**) for your collaboration, which contributed to a chapter in this thesis. Thank you very much for your valuable insights and for hosting me in your facilities.

Marijke, thank you for all your support throughout my PhD. Your resourcefulness and go-getter attitude have been extremely valuable in helping me tackle technical challenges in the lab. You have also been a source of comfort during stressful times. I admire your tireless care for your colleagues. I also enjoyed sharing my culture and experiences with you, and I hope that someday you do make the trip to India about which we've been talking! **Erik**, thank you for all the support in the lab, you have always seemed to have a solution for any problem I brought to you. Thank you also for all the laughs; there is never a dull moment with you around. The Wadlopen trips were a highlight! Although I did not have the opportunity to work with you directly during my PhD, I very much look forward to collaborating soon. Thank you, **Marcel**, for supporting the group and for the lovely conversations. Your genomics carpentry workshop was very valuable! Thank you, **Clara**, for keeping the molecular biology labs running smoothly and for always being available to help. **Christiaan**, I am grateful for your support, especially in coordinating with the BPE group for my final measurements. Thank you, **Flip**, for all your help, particularly during my final experiment—despite difficult personal circumstances, I really appreciate it. Thank you, **Ilja**, for always being so positive and ready to help. And thank you to the MSD ladies, **Apilena, Gea and Jannie**, for all your help, support, and flexibility.

Thank you to all the students who collaborated with me over the course of my PhD — **Linda, Iris, Marius, Nienke, Sam, and Ydo**. I had a wonderful time working with each of you and learned so much from both your contributions and the experience of collaborating with you.

The '**DECO**' weekly/bi-weekly meetings have contributed immensely to my PhD experience. Thank you, Rinke, Djordje, Marcel, Tobias, Tom, Minke, Uros, Thomas, and Michelle, for all the brainstorming, feedback, and valuable suggestions. It has been a pleasure to watch this group develop over the years and to participate in the exciting research that everyone in the group is engaged in.

This PhD journey would not have been the same without my officemates cheering me on and lifting my spirits. **Aafke**, your hard work, perseverance, and ability to run a gazillion bioreactors never ceased to amaze me. Thank you for being so kind and encouraging! I miss all our insightful and silly conversations, and it was a joy to be your paranymph and share part of your PhD journey. **Nicole**, your meticulous experiment planning, and ability to conduct large-scale experiments are inspiring. Thank you for always lending an ear and for all your support. **Marieke**, although you tried to escape, we always ended up in the same office. Thank you for tirelessly listening to me and for being such a great source of inspiration and support. It has been special to have our PhD terms (almost) align. You impress me not only with your incredible knowledge of yeast physiology but also with your talent to assemble IKEA furniture effortlessly! **Michelle**, although you are the newest addition to the office, it is amazing how quickly we found common ground. I am impressed by how easily you have adapted, and by your hard work, organisation, and kindness. Thank you for all your advice, conversations, help, and thoughtful feedback on my research, and for stepping in to help me tremendously during my final year.

I would like to thank **Ewout** for always being open to helping, whether it was through practical advice or scientific discussions. **Denzel**, your positivity, and energy were contagious, and your perseverance was inspiring. Apart from your presence, I also miss your music in the lab and dinners at IKEA! It was wonderful that our PhD journeys aligned, along with **Céline**, and the beer bottling sessions with you both were such fun. **Tobi**, thank you for all the amazing conversations, laughs, and for being such a great support. I am always amazed by your enthusiasm and energy, and it was a pleasure working and learning with you while writing the review paper together. It has been wonderful to watch you grow and conduct such impressive research. And I hope your love for Daal Makhani never dies! **Minke, Iris and Yanfang** thank you for your kindness and for motivating me to keep working out, especially towards the end of my PhD. Signing up for workout classes with you helped me stay focused and get through the final writing phase. **Luca**, I have enjoyed all our small conversations in the hallways and in the lab; you always bring a refreshing perspective. **Maartje and Effie**, I really enjoyed teaching MR with you both; the discussion and evaluation sessions were always such fun. **Uros**, hoi hoi! Thank you for the fun hallway conversations; I am inspired by your stamina during those incredibly long experiments. **Thomas**, I am impressed by your ability to set up so many novel techniques, which require an incredible amount of perseverance. Thank you for always being so kind and helpful. **Tom**, thank you for all the entertaining stories. Apart from your amazing scientific contributions to the group, your work in getting the eLAB journal up and running is hugely appreciated. And thank you to everyone else in **IMB** for fostering such a fun,

collaborative, stimulating, and safe working environment.

Although pursuing a PhD far from home comes with its challenges, but my family away from home made this journey much brighter. **Rosalie**, I feel very lucky that our paths crossed while assisting in teaching MR. If it were not for MR, I might have never grown close to you and your +1 **Miriam**, and this PhD journey would have been extremely dull. Thank you, Miriam, and Rosalie, for all the laughter, silly jokes, trips, countless IKEA dinners, tea breaks, walks around the faculty, celebrations, and conversations. I feel incredibly fortunate that I can count on you, and I am grateful that we got to navigate our PhD journeys together. Thank you also for accepting to be my paranymphs! **Pavithra**, we have been neighbours for most of my PhD and have enjoyed all the perks that came with it — long walks around Delft city centre, warm meals or coffees after long days, comforting conversations, and, of course, lots of laughs. Thank you also for all the incredible trips around Europe, which helped me recharge and create unforgettable memories. **Sanjay**, thank you for tirelessly supporting me, for celebrating even the smallest successes, cooking warm food for me after long experiments, hosting me in Belgium when I needed time off, joining me on incredible trips, and patiently teaching me how to code, use GitHub, and so many other things. I do not think I can thank you enough! My PhD journey would not have been the same without you. I am so excited for you to begin your own PhD, and I am sure you will make all of us very proud. Thank you, **Juan**, for being an incredible housemate during the first year of my PhD! Thank you to **Girish, Rudri, Abhinav, Pooja, Atul, Nagaraj, Vishruth, Shweta, Sumit, Ritika and Nivya** for all the biking trips, dinners, birthday and Indian festival celebrations, badminton games, Bollywood dance parties, game nights, and countless other moments that helped me take my mind off work.

Thank you to all my friends across the globe — **Shruti, Lipika, Samyuktha, Shraddha, Hamsi, Devayani, Jennifer, Deo, Charishma, Nikita, Prathiksha, Satvika, Trisha, and Sanya** — for all the trips, phone calls, texts, and memes that kept my spirits high, and for being incredible sources of inspiration.

Thank you to my family for their unwavering support! **Samrudh**, thank you for being a silent supporter and holding the fort back home. **Amma**, thank you for your blind faith and trust in me, for sending me off to a country we knew little about, to pursue a career that was completely foreign to you. Your bravery in supporting my naïve decisions, even in difficult circumstances, is the reason I could pursue a PhD. **Appa**, your passion for knowledge and your tenacity in pursuing challenging goals have shaped many of my life choices, especially my decision to pursue a PhD. The only explanation I can think of, though not a rational or 'scientific' one, for all the luck and incredible opportunities that have come my way, is that you are up there orchestrating it all.

Curriculum vitae

Sagarika Bangalore Govindaraju was born on 31st May 1995 in Shivamogga, India, and grew up in Bangalore, India. She attended Sophia High School and obtained her pre-university education certificate from Christ Junior College, both located in Bangalore. Upon graduation in 2017, Sagarika obtained her Bachelor of Engineering degree in Biotechnology from the BMS College of Engineering, affiliated with Visvesvaraya Technological University. She finalised her Bachelor of Engineering programme with an internship at String Bio, an early-stage startup, where she helped develop molecular biology tools for a methanotrophic bacterium.

In 2018, she moved to Delft, the Netherlands, to pursue a Master of Science degree in Life Science and Technology at Delft University of Technology. During her MSc studies, she participated in the iGEM competition. As part of the TU Delft team, she contributed to the conceptualisation and development of a platform designed to broaden the range of bacterial species currently used in synthetic biology. She presented the project at the iGEM Grand Jamboree in Boston in 2019, and the team won the 'Foundational Advance' track and was awarded the 'Best Parts Collection' prize. Following the competition, as part of her MSc programme, Sagarika undertook a research project in the Industrial Microbiology section at TU Delft, under the supervision of dr.ir. Sophie de Valk and dr.ir. Robert Mans. The research project focused on engineering proton-coupled sugar transport in *Saccharomyces cerevisiae* to improve ethanol yield from sucrose and on proposing a theoretical strategy to accelerate laboratory evolution in *S. cerevisiae* by leveraging genomic instability in sub-telomeric regions. After obtaining her MSc degree in 2020, she completed a six-month industrial internship at Getinge Life Science in Delft, where she worked in the Cultivation and Application Support team.

In 2021, Sagarika began her PhD project in the Industrial Microbiology section at TU Delft, under the supervision of dr.ir. Rinke van Tatenhove-Pel and prof.dr. Jack Pronk. The research, focused on the application of compartmentalised microbial cultivations to explore applications in biotechnology and microbial ecology, is described in this dissertation.

List of publications

Sagarika B. Govindaraju, Thibaut J. Wenzel, Jack T. Pronk, Rinke J. van Tatenhove-Pel (2025). Development of a high-throughput label-free method for enrichment of antimetabolite-resistant yeast strains using pico-litre agarose beads. Accepted for Publication at Applied Microbiology and Biotechnology (2026).

Sagarika B. Govindaraju, Daan H. de Groot, Rinke J. van Tatenhove-Pel (2025). Deciphering Microbial Interactions Using a Label-Free Microbead Sorting Approach. Manuscript under review at ISME Communications.

Sagarika B. Govindaraju*, Tobias Fecker*, Michelle Rossouw, Jack T. Pronk, Rinke J. van Tatenhove-Pel (2025). Unlocking the potential of defined co-cultures for industrial biotechnology: opportunities and challenges. Published at New Biotechnology (2025) 91:89-99. doi: 10.1016/j.nbt.2025.11.009

*authors contributed equally

Selected conference contributions

Sagarika B. Govindaraju. Deciphering microbial interactions using microbead sorting (oral presentation). MB10.0 Microbial Biotechnology Symposium. November 2024. Delft, The Netherlands.

Sagarika B. Govindaraju and Rinke van Tatenhove-Pel. Deciphering microbial interactions using microbead sorting (oral presentation). Netherlands Integrative Microbial Ecology Initiative Meeting. April 2025. Amsterdam, The Netherlands.

Sagarika B. Govindaraju. Deciphering microbial interactions using microbead sorting (oral presentation). NWOLife. May 2025. Egmond aan Zee, The Netherlands.

Sagarika B. Govindaraju. Deciphering interactions in microbial consortia (poster presentation). Gordon Research Conference on Microbial Population Biology. July 2025. Andover, United States of America.

